Spectroscopic analyses of subluminous B stars: observational constraints for the theory of stellar evolution, pulsation, and diffusion

Den Naturwissenschaftlichen Fakultäten
der Friedrich-Alexander-Universität Erlangen-Nürnberg
zur
Erlangung des Doktorgrades

vorgelegt von
Heinz Edelmann
aus Nürnberg

Als Dissertation genehmigt von den Naturwissenschaftlichen Fakultäten
der Universität Erlangen-Nürnberg

Tag der mündlichen Prüfung:	03.07.2003
Stellvertretender Vositzender der Promotionskommission:	Prof. Dr. H. Kisch
Erstberichterstatter:	Prof. Dr. U. Heber
Zweitberichterstatter:	Prof. Dr. K. Werner

Contents

Zusammenfassung **1**

Abstract **5**

1 Introduction **9**

2 Program stars **13**
2.1 Spectral classification system 13
2.2 Bright sdB stars 15
2.2.1 Selection of the program stars 15
2.2.2 Observations and data reduction 15
2.2.3 Classification of the program stars 17
2.3 sdB stars from the Hamburg Quasar Survey 19
2.3.1 Hamburg Quasar Survey 19
2.3.2 Preselection of the program stars 20
2.3.3 Observations and data reduction 20
2.3.4 Selection and classification of the program stars 21
2.3.5 Completeness 22
2.4 sdB stars from the Hamburg ESO Survey 22
2.4.1 Hamburg ESO Survey 22
2.4.2 Selection of sdB candidates 23
2.4.3 Observations and data reduction 26
2.4.4 Classification of the program stars 28
2.4.5 Completeness 29

3 Atmospheric parameters **31**
3.1 Spectral analysis 31
3.1.1 Model atmospheres and synthetic spectra 31
3.1.2 Fit procedure 32
3.2 Results 35
3.2.1 Bright stars 37
3.2.2 Stars from Hamburg Quasar Survey 38
3.2.3 Stars from Hamburg ESO Survey 38
3.2.4 Comparison with previous results 38
3.3 Constraints on the evolution of sdB stars 41
3.3.1 Evolutionary status 41
3.3.2 Evolutionary scenarios 44

3.4 Constraints on stellar pulsations . . . 45

4 Chemical composition 48
4.1 Spectral analysis . . . 49
4.1.1 Metal abundances . . . 49
4.1.2 Microturbulences . . . 50
4.1.3 Ionisation equilibria . . . 50
4.1.4 Projected rotational velocities . . . 50
4.2 Results for individual objects . . . 53
4.2.1 'Normal' sdB stars . . . 57
4.2.2 Peculiar sdB stars . . . 83
4.2.3 Summary of the results . . . 88
4.3 Trends with atmospheric parameters? . . . 90
4.3.1 Helium abundances . . . 90
4.3.2 Metal abundances . . . 94
4.4 Helium line shifts . . . 99

5 Radial velocity variations 101
5.1 Radial velocity measurements . . . 101
5.2 Radial velocity curves, and the nature of the invisible companions . . . 105
5.2.1 PG 0001+275 . . . 105
5.2.2 PG 1519+640 . . . 107
5.2.3 HD 188112 . . . 107
5.2.4 PB 5333 . . . 109
5.2.5 PG 0133+114 . . . 109
5.2.6 UVO 1735+22 . . . 111
5.2.7 HD 171858 . . . 113
5.2.8 PB 7352 . . . 113
5.2.9 Feige 108 . . . 114
5.3 Summary of the radial velocity curve analyses . . . 115

6 HE 0437−5439 — a main sequence B star leaving the galaxy 117
6.1 Observations and data analysis . . . 117
6.2 Atmospheric parameters and projected rotational velocity . . . 117
6.3 Mass, evolutionary time, radial velocity, and distance . . . 119
6.4 Metal abundances . . . 119
6.5 Discussion . . . 119

7 Conclusions and outlook 120

A Program stars – observing logs 122
A.1 Hamburg Quasar Survey . . . 122
A.2 Hamburg ESO Survey . . . 125
A.3 Bright sdB stars . . . 128
A.3.1 Low-Resolution observations . . . 128
A.3.2 High-Resolution observations . . . 128

B Analyses results **130**
B.1 Hamburg Quasar Survey 130
B.2 Hamburg ESO Survey 133
B.3 Bright sdB stars 136

C Equivalent widths measurements **137**

D Radial velocity measurements **147**

E List of abbreviations **155**

References **159**

Acknowledgements **167**

Lebenslauf **169**

List of Figures

1.1 Illustration of post-EHB evolution 10

2.1 Spectral classification scheme 14
2.2 Binary HQS sdB stars 18
2.3 HQS brightness distribution 22
2.4 Sample of HES finding charts and objective prism spectra 24
2.5 Sample of HES misclassifications 25
2.6 Classification of HES objective prism spectra using model flux distributions . . . 27
2.7 HES brightness distribution 29

3.1 Sample fits for three program sdB stars 32
3.2 Comparison of results determined from spectra with many Balmer lines to those from three Balmer lines 33
3.3 Comparison of results determined from LTE and NLTE model atmospheres . . . 36
3.4 Program stars in the HRD 39
3.5 Plot of numbers of stars versus luminosity 43
3.6 Distribution of $\log(g\theta^4)$ for HQS and HES samples 45
3.7 SdB instability strip 47

4.1 Discrepancy of abundances determined from different multiplets of S II 50
4.2 Sensitivity of the microturbulence 51
4.3 Microturbulence for CD−35° 15910 51
4.4 Determination of $v \sin(i)$ from Mg II doublet 52
4.5 Metal lines within 'normal' sdB stars 54
4.6 Metal lines of peculiar sdB stars 55
4.7 Metal abundances for HD 205805 56
4.8 Metal abundances for PG 0001+275 58
4.9 Metal abundances for HD 4539 60
4.10 Metal abundances for PHL 932 62
4.11 Metal abundances for PG 0133+114 64
4.12 Metal abundances for PG 0342+026 66
4.13 Metal abundances for Feige 65 68
4.14 Metal abundances for UVO 1735+22 70
4.15 Metal abundances for BD+48° 2721 72
4.16 Metal abundances for HD 171858 74
4.17 Metal abundances for LB 1516 76
4.18 Metal abundances for PB 7352 78

4.19 Metal abundances for CD−35° 15910 80
4.20 Metal abundances for UVO 0512−08 82
4.21 Metal abundances for PG 0909+276 84
4.22 Metal abundances for UVO 1758+36 86
4.23 Similarity of metal abundance patterns for 'normal' sdB stars 89
4.24 Plot of the helium abundance versus effective temperature 91
4.25 Plot of the helium abundance versus gravity 92
4.26 Plot of the helium abundance versus luminosity 93
4.27 LTE abundances for C II, C III, N II, and O II versus $T_{\rm eff}$, $\log(g)$, and L/L_e 95
4.28 LTE abundances for Mg II, Al III,Si III, and S II versus $T_{\rm eff}$, $\log(g)$, and L/L_e . . . 96
4.29 LTE abundances for S III, Ar II, and Fe III versus $T_{\rm eff}$, $\log(g)$, and L/L_e 97
4.30 Helium line shifts 100

5.1 RV measurements for three non-variables 103
5.2 RV measurements for two variables, and three absolute high RV stars 104
5.3 RV curve for PG 0001+275 106
5.4 RV curve for PG 1519+640 106
5.5 RV curve for HD 188112 108
5.6 RV curve for PB 5333 108
5.7 RV curve for PG 0133+114 110
5.8 RV curve for UVO 1735+22 110
5.9 RV curve for HD 171858 112
5.10 RV curve for PB 7352 112
5.11 RV curve for Feige 108 114
5.12 Histogram of orbital periods 116

6.1 LTE line fit for HE 0437−5439 for the coadded UVES spectra 118

List of Tables

2.1 Echelle high-resolution observations 16
2.2 Spectral classification of bright program stars compared to literature 17
2.3 HQS follow-up observation runs 19
2.4 Binary HQS sdB stars 20
2.5 Spectral classification of HQS program stars compared to literature 21
2.6 Statistics for visual inspection of sdB candidates from the HES 26
2.7 HES follow-up observation runs 26
2.8 Binary HES sdB stars 28
2.9 Spectral classification of HES program stars compared to literature 30

3.1 Comparison of results determined from different HES runs 34
3.2 Comparison of determined parameters to those from literature 40

4.1 Metal abundances for HD 205805 56
4.2 Metal abundances for PG 0001+275 58
4.3 Metal abundances for HD 4539 60
4.4 Metal abundances for PHL 932 62
4.5 Metal abundances for PG 0133+114 64
4.6 Metal abundances for PG 0342+026 66
4.7 Metal abundances for Feige 65 68
4.8 Metal abundances for UVO 1735+22 70
4.9 Metal abundances for BD+48° 2721 72
4.10 Metal abundances for HD 171858 74
4.11 Metal abundances for LB 1516 76
4.12 Metal abundances for PB 7352 78
4.13 Metal abundances for CD−35° 15910 80
4.14 Metal abundances for UVO 0512−08 82
4.15 Metal abundances for PG 0909+276 84
4.16 Metal abundances for UVO 1758+36 86

5.1 Orbital parameters 115
5.2 Mass functions, and masses of the invisible companions 116

A.1 Classification, Coordinates, B magnitude, observing run, and references for all program HQS stars 122
A.2 Classification, Coordinates, magnitude HES plate and field numbers, and observing run for all program HES stars 125

A.3 Low-resolution observations for the bright program sdB stars 128
A.4 Coordinates, V magnitudes, and RV variability for all bright program sdB stars 129

B.1 Analyses results for the HQS program stars 130
B.2 Analyses results for the HES program stars 133
B.3 Analyses results for the bright program stars 136

C.1 Equivalent width measurements for all 'normal' program stars 137
C.2 Equivalent width measurements for all PG 0909+276 and UVO 0512−08 144

D.1 Radial velovity measurements for all bright program stars 147

Zusammenfassung

Die vorliegende Arbeit beschäftigt sich mit der quantitativen Spektralanalyse von unterleuchtkräftigen B Sternen. Das Hauptziel ist hierbei, mit Hilfe der Beobachtungsdaten vorhandene Sternentwicklungs-, Pulsations- und Diffusionstheorien für diese Sterne besser einzugrenzen.

Unterleuchtkräftige B Sterne, welche auch als Unterzwerge des Spektraltyps B (engl. subdwarf B, oder kurz sdB) bezeichnet werden, sind in vielerlei Hinsicht sehr interessant: Subdwarf B Sterne existieren sowohl innerhalb der Michstraße als auch in Kugelsternhaufen. Durch ihre sehr große Anzahl, welche bei Himmelsdurchmusterungen nach blauen (also heißen) Sterne mit geringer scheinbarer Helligkeit in hohen galaktischen Breiten gefunden wurden, sind sdB Sterne einerseits wichtig um die Struktur und Entwicklung unserer eigenen Galaxie zu verstehen. Andererseits stellen sie aus kosmologischer Hinsicht eine wichtige Gruppe von Sternen dar, weil einige von ihnen als Teil von engen Doppelsternsystemen Vorläufersterne von Supernovae Typ Ia sein können. Auch aus der Sicht der Stellarastrophysik spielen sdB Sterne eine wichtige Rolle: Bei einigen von ihnen wurden nichtradiale Pulsationen entdeckt, mit deren Hilfe man das Innere der Sterne erforschen kann. Darüberhinaus sind unterleuchtkräftige B Sterne auch sehr interessant, weil sie sehr außergewöhnliche Elementhäufigkeitsmuster zeigen, welche vermutlich durch Diffusionsprozesse hervorgerufen werden.

Nach dem heutigen Wissensstand bestehen sdB Sterne aus einem heliumbrennenden Kern mit einer Masse von $0.5 M_{\odot}$, umgeben von einer dünnen wasserstoffreichen Hülle geringer Masse ($< 0.02 M_{\odot}$). Im Hertzsprung-Russell Diagramm bevölkern sie einen sehr kompakten Bereich, welcher auf einer Verlängerung des Horizontalastes (engl. horizontal branch, kurz HB) zum Blauen (also heißen) hin, dem sogenannten 'extreme horizontal branch' (EHB), liegt. Durch ihre sehr dünne, massearme Hülle ist es ihnen unmöglich, nach Erlöschen des zentralen Heliumbrennens ein Wasserstoff-Schalenbrennen auszubilden. Das heißt, der Stern kann nicht wie die anderen Horizontalaststerne, den Asymptotischen Riesenast hinaufwandern um sich zum zweiten Mal zu einem Riesen aufzublähen[1], sondern entwickelt sich direkt zu einem Weißen Zwerg. Die Entwicklung zu einem sdB Stern ist aber nocht nicht vollständig verstanden und verschiedene Szenarien werden diskutiert, denn nach der Standard-Sternentwicklungstheorie sollten sdB Sterne eigentlich überhaupt nicht existieren.

Ziel der vorliegenden Arbeit sollte sein, mit Nachbeobachtungen aus verschiedenen Himmelsdurchmusterungen, die Anzahl der exakt analysierten sdB Sternen zu vergrößern, um aus einem möglichst homogenen Sample Schlüsse auf den Entwicklungszustand zu ziehen. Bei zahlreichen Beobachtungsaufenthalten, welche meist von mir am Deutsch-Spanischen Astronomischen Zentrum auf dem Berg Calar Alto in Spanien, oder an der Europäischen Südsternwarte auf dem Berg La Silla in Chile durchgeführt wurden, konnte eine großen Zahl von sdB Sternen spektroskopiert werden. Es wurden Großteleskope mit Spiegeldurchmessern von 1.5 m bis 8 m und modern-

[1] Die erste Riesenphase haben alle Sterne auf dem Horizontalast schon hinter sich.

ste Langspalt- sowie Echellespektrographen zusammen mit hochempfindlichen CCD Detektoren verwendet, um niedrig- wie auch hochaufgelöste Spektren im optischen Wellenlängenbereich zu gewinnen.

Um die fundamentalen Parameter (Effektivtemperatur, Oberflächenschwerebeschleunigung und photosphärische Heliumhäufigkeit) zu bestimmen, wurden niedrigaufgelöste, optische Langspaltspektren von 146 (mehr als doppelt so viele als bei bisherigen Untersuchungen) unterleuchtkräftigen B Sternen, welche zuvor als Kandidaten aus den Hamburg Quasar und Hamburg ESO Himmelsurchmusterungen für Nachbeobachtungen ausgewählt wurden, analysiert. Die Parameter wurden für jeden Stern aus dem Vergleich der Linienprofile aller vorkommenden Wasserstoff- und Heliumlinien mit berechneten Modellspektren (sowohl im LTE als auch im NLTE) bestimmt. Die erhaltenen Werte zeigen, daß es nur sehr geringe Unterschiede zwischen den Ergebnissen, welche mit Hilfe der LTE- oder NLTE-Modellatmosphären bestimmt wurden, bestehen. Durch Vergleich der Ergebnisse mit Literaturwerten wurden systematische Diskrepanzen bei den Ergebnissen (10% bei der Effektivtemperatur und ~ 0.2 dex bei der Schwerebeschleunigung) festgestellt, welche nicht allein durch NLTE Effekte erklärt werden können. Umfangreiche Untersuchungen, bei denen direkte Vergleiche von Stern zu Stern notwendig sind, könnten vielleicht diese Unterschiede erklären. Dieses Unterfangen würde aber den Rahmen dieser Doktorbeit bei weitem sprengen. Solange die Unterschiede in den Ergebnissen noch nicht verstanden sind, können wir leider keine näheren Aussagen zu der EHB Entwicklung machen.

Erst vor kurzem wurden einige sdB Sterne entdeckt, welche nichtradiale Pulsationen aufweisen. 1999 initiierten wir eine Zusammenarbeit mit zwei Forschergruppen in Norwegen und Italien um nach solchen Pulsatoren in unserer sdB Stichprobe zu suchen. Pro zehn untersuchter Sterne wurde jeweils ein pulsierender sdB Stern entdeckt. Mit dieser Entdeckung konnten wir Anzahl der bekannten sdB Pulsatoren um immerhin 50% steigern.

Die Metallhäufigkeitsmuster von 16 sdB Sternen (fast dreimal so viele als bei bisherigen Untersuchungen zusammen genommen) wurden mit Hilfe von Äquivalentbreitenmessungen der gefundenen Absorptionslinien in hochaufgelösten, optischen Spektren mit hohem S/N, bestimmt. Die Metallinien sind schwach und nicht sehr zahlreich, wie erwartet bei Sternen des Spektraltyps B. Wir entdeckten drei ungewöhnliche sdB Sterne, deren optische Spektren neben den sonst üblichen Absorptionslinien bei sdB Sternen, deutlich mehr Linien aufweisen. Diese Linien konnten den Elementen Kalzium, Scandium, Titan, Vanadium, Mangan und Nickel zugeordnet werden. Solcherlei Elemente wurden in den optischen Spektren von sdB Sternen bisher nie entdeckt. Überraschenderweise zeigen fast alle Programmsterne sehr ähnliche Häufigkeitsmuster: Kohlenstoff, Sauerstoff, Magnesium und Aluminium sind im Vergleich zu den solaren Werten sehr stark abgereichert (~ -1.0 dex). Stickstoff ist fast immer geringfügig untersolar (~ -0.3 dex). Silizium und Schwefel sind abgereichert ($-0.3 \ldots -0.7$ dex). Die Eisenhäufigkeit ist immer ungefähr solar und Argon ist sogar immer angereichert (übersolar, $\sim +0.5$ dex)). Die drei sdB Sterne, bei denen wir die Absorptionslinien von Eisengruppenelementen in den Spektren gefunden haben, zeigen eine enorme Anreicherung dieser Elemente (1 000 bis $\sim$ 32 000 fach denen der solaren Werte). Erstaunlicherweise ist im Gegensatz zu den 'normalen' sdB Sternen, deren Spektren relativ viele Fe III Absorptionslinien zeigen, keinerlei Linien von Eisen in den Spektren der drei Sterne zu entdecken. Desweiteren konnten aus Messungen der Wachstumskurven für fast alle untersuchten Sterne eine mit 0 km/s verträgliche Mikroturbulenz bestimmt werden. Nur zwei Sterne besitzen Werte von 3 ± 1 km/s und 6 ± 1 km/s. Die gemessenen projizierten Rotationsgeschwindigkeiten ergeben, daß alle Sterne nur (sehr) langsam rotieren können.

Zum allererstenmal wurden Element- (speziell Metall-) Häufigkeitsmuster von sdB Sternen mit den atmosphärischen Parametern verglichen, um mögliche Abhängigkeiten zu finden,

welche durch Diffusionsrechnungen vorhergesagt werden. Ein Zusammenhang zwischen den Häufigkeitsmustern und der Effektivtemperatur wurde entdeckt: Je höher die Temperatur des Sterns ist, desto höher ist auch die entsprechende Häufigkeit von Helium, Sauerstoff und Magnesium. Andererseits fällt aber auf, daß die Häufigkeiten von Stickstoff, Silizium, Argon und Eisen immer gleich sind, vollkommen unabhängig von den Sternparametern. Darüber hinaus wurde eine Zweiteilung der untersuchten sdB Sterne entdeckt: Ein kleiner Teil ($\sim 1/6$) besitzt deutlich weniger Helium in seiner Photosphäre bei gleichen Temperaturen, als die Mehrzahl der sdB Sterne. Ähnliches gilt auch für Sauerstoff, Magnesium und Silizium. Darüberhinaus konnte eine Linienverschiebung von einigen Heliumabsorptionslinien in den Spektren von zwei sdB Sternen festgestellt werden. Als Ursache kommt nur eine Isotopverschiebung zugunsten von ^{3}He in Frage. Dies bedeutet, daß in den Atmosphären dieser Sterne ^{3}He überaus stark angereichert ist.

Dadurch, daß in letzter Zeit immer mehr spektroskopische sdB 'Einzelsterne' entdeckt werden, welche eine periodische Schwankungen ihrer Radialgeschwindigkeiten zeigen, verhärtet sich die Ansicht, daß enge Doppelsternentwicklung wohl **die** entscheidende Rolle bei der Entwicklung von subdwarf B Sternen spielt. Aus diesem Grund haben wir ein Programm zur Suche nach solchen radialgeschwindigkeitveränderlichen sdB Sternen begonnen. Dazu untersuchten wir die optischen hochaufgelösten Spektren von 47 hellen, heißen, unterleuchtkräftigen Sternen. Bei neun Sternen konnte keinerlei Schwankung der Radialgeschwindigkeit festgestellt werden. Weder kurzperiodische (Stunden oder Tage) noch langperiodische (Monate oder Jahre) Veränderungen konnten gemessen werden. Für 22 Sterne kann nicht mit absoluter Sicherheit eine kurz- oder langperiodische Variation ausgeschlossen werden. Dazu sind weitere Beobachtungen notwendig. 13 heiße Unterzwerge zeigen indes kurzperiodische Radialgeschwindigkeitsveränderungen. Für neun von ihnen konnten wir die kompletten Radialgeschwindigkeitskurven vermessen. Die daraus bestimmten Perioden liegen zwischen ca. einem halben und fast neun Tagen. Die Halbamplituden betragen zwischen 22 km/s und 188 km/s. Mit Hilfe der Massenfunktion konnten die Massen der unsichtbaren Begleiter ermittelt werden. Untere Grenzen zwischen 0.07 und 0.73 $M_\odot$, sowie statistische Wahrscheinlichkeitswerte zwischen 0.09 und 1.20 $M_\odot$ wurden errechnet. Aus den Werten läßt sich schließen, daß die Begleiter vermutlich entweder massearme Hauptreihensterne oder Weiße Zwerge mit C/O Kern sind. Bei einem Stern kann der Begleiter aber durchaus auch ein Neutronenstern sein.

Als Nebenprodukt unserer Analyse haben wir noch einen vermutlich normalen Hauptreihenstern vom Spektraltyp B gefunden, der, verursacht durch eine konstante horrende Radialgeschwindigkeit von $v_{\rm rad} = 723 \pm 3$ km/s, aus der Milchstraße herausschleudern wird.

Abstract

This thesis deals with quantitative spectroscopic analyses of large samples of subluminous B stars in order to find constraints the theory of stellar evolution, pulsation, and diffusion.

Subluminous B stars, also known as subdwarf B (sdB) stars, are very important in several respects: They dominate the population of faint blue stars in high galactic latitudes, and are found both in the field and in globular clusters. Therefore, sdB stars are important to understand the structure and evolution of our galaxy. From the cosmological point of view, they are candidate progenitors of supernovae of type Ia due to their membership in close binary systems. In the context of stellar astrophysics, subdwarf B stars play an important role because several of them are discovered to show non-radial pulsations, which allows to probe their interior by asteroseismology. Last but not least, sdB stars show very peculiar element abundance patterns, probably caused by diffusion processes.

Subluminous B stars are generally considered to be core helium-burning stars with extremely thin hydrogen envelopes ($< 0.02 M_{\odot}$) and masses around $0.5 M_{\odot}$. In the Hertzsprung-Russell diagram they populate a very narrow area which lies on a blue-ward extension of the horizontal branch (HB), the so called 'Extreme Horizontal Branch' (EHB). Due to their thin hydrogen-rich envelope, they cannot sustain a hydrogen-burning shell. This means that the sdB stars cannot ascend the asymptotic giant branch after the end of the helium-core burning, but should evolve directly to the white dwarf graveyard. However, according to standard stellar evolution theory, subdwarf B stars should not exist. Their evolution is still unclear and several scenarios are under debate. For all these investigations, knowledge of the stellar parameters (effective temperature, gravity and chemical composition) is very important to verify or discard theoretical models and predictions.

Numerous observing runs have been performed mostly by myself at the German-Spanish Astronomical Center on Calar Alto, Spain, and at the European Southern Observatory on La Silla, Chile, in order to perform detailed analyses of large samples of subluminous B stars. To obtain optical spectra with high S/N, 1.5 m to 8 m class telescopes equipped with up-to-date long-slit low-resolution as well as echelle high-resolution spectrographs together with state-of-the-art CCD detectors were used.

Optical low-resolution long-slit spectra of 146 subdwarf B stars (a sample twice as large as that of previous investigations), drawn from follow-up observations of candidates from the Hamburg Quasar and Hamburg ESO surveys have been analyzed to determine their fundamental parameters (effective temperature, gravity, and helium abundance). The parameters are determined by matching synthetic line profiles calculated from LTE and NLTE model atmospheres to all hydrogen and helium absorption lines present in the observed spectra. The results determined from the LTE and NLTE fits show only slight differences. We compared our analysis results with data from the literature. Systematic differences occur at a 10% level in temperatures, and at the level of ~ 0.2 dex in gravity, which cannot be explained by NLTE effects alone. Extensive

investigations on a star by star basis are needed to resolve the cause, which are beyond the scope of this thesis. Due to the remaining uncertainties in the atmospheric parameters we had to refrain from a discussion of the details of EHB evolution. This has to be postponed until the reason for the systematic differences have been clarified.

Recently, several sdB stars have been found to show non-radial pulsations. We initiated a collaboration with two groups in Norway and Italy in 1999 to search for pulsating sdB stars in our sample. About one pulsator within ten observed sdB stars were found. With this discovery we enhanced the number of known pulsating sdB stars by about 50%.

The surface metal abundance patterns of 16 sdB stars have been determined from high resolution, high S/N, optical spectra using equivalent widths measurements. This analysis almost quadruples the number of detailed metal abundance analyses of sdB stars. As typical for early B type stars, the metal lines are few and very weak. Three peculiar sdB stars have been found which show in addition to the absorption lines common in sdB stars many lines due to iron group elements (calcium, scandium, titanium, vanadium, manganese, and nickel) which have never been found before in the optical spectra of sdB stars. Surprisingly, almost all program stars show very similar abundance patterns: carbon, oxygen, magnesium, and aluminum, are strongly depleted (with respect to the solar composition), nitrogen is mostly slightly under-abundant, silicon and sulfur are subsolar, iron is always about solar, and argon is even suprasolar. For the peculiar sdB stars we determine an enormous enrichment of the iron group elements which are found to be 1 000 to $\sim$ 32 000 times the solar values. However, in contrast to the 'normal' sdB stars, no lines due to iron itself occur in the spectra of the peculiar stars. From curve-of-growth measurements we determine vanishing microturbulent velocities for almost all program stars, except for two which have values of 3 ± 1 km/s and 6 ± 1 km/s. The projected rotational velocities determined for all program stars indicate that all are (very) slowly rotating stars.

For the first time, for sdB stars it was possible to correlate element (especially metal) abundance patterns with the atmospheric parameters to search for possible trends, which are predicted by diffusion theory. We discover a correlation for some elements with the effective temperature: the larger the temperature, the larger the abundances for helium, oxygen, and magnesium. On the other hand it is remarkable that the abundances for nitrogen, silicon, aluminum, argon, and iron are constant, irrespective of the stellar parameters. In addition, a separation into two sequences of sdB stars may exist: a minority having much lower helium abundances at the same temperatures than the bulk of the sdB stars. The same possibly holds for oxygen, magnesium, and silicon too. An isotopic anomaly of helium has been found in two sdB stars. In these stars ^{4}He is largely replaced by the isotope ^{3}He which is also due to diffusion processes.

Recently, observational evidence is accumulating that close binary evolution is crucial to understand the origin of sdB stars. Therefore, we embarked on a search program to discover single-lined spectroscopic binaries from radial velocity variations. 47 bright hot subluminous stars have been observed for radial velocity variations from high resolution optical spectra. For nine single lined stars we can definitely rule out them to be RV variable stars. Neither short-term (a few hours), nor long-term (weeks or years) variations could be found. 22 stars remained with unknown status (more observations are necessary). However, for 13 hot subdwarfs short period radial velocity variations have been detected. For nine of them radial velocity curves have been measured. The periods determined range from about half a day up to almost nine days. The radial velocity semi amplitudes found are in the order of 22 km/s to 188 km/s. By use of the mass function, the masses of the unseen companions have been constricted. Lower limits and most probable values of 0.07 up to 0.73 $M_\odot$, and 0.09 up to 1.20 $M_\odot$, respectively, have been

determined. We conclude that the invisible companions are most likely late type main sequence stars, or white dwarfs with a C/O core. However, for one star a neutron star cannot be ruled out as a secondary.

As spin off result, an apparently normal main sequence B star with an enormous absolute radial velocity of $v_{\rm rad} = 723 \pm 3$ km/s has been discovered which will be emitted into the intergalactic space.

Chapter 1

Introduction

Humason & Zwicky (1947) were the first to survey the northern hemisphere for faint blue stars. They aimed at discovering neutron stars, but without success. However, by spectroscopic follow-up observations with the new Palomar 5m telescope, Greenstein (1954) discovered the first hot *subluminous* star (HZ 44) from the sample of Humason & Zwicky. Subluminous stars are less luminous than main-sequence stars of the same spectral type, and are located below the main-sequence within the Hertzsprung-Russell-Diagram (HRD). Main-sequence stars are also called dwarfs, therefore for those new stars the designation *hot subdwarfs* was coined. Further specimens were discovered by similar surveys (e.g. Feige 1958, Slettebak & Brundage 1971). However, the number of known hot subdwarfs remained small until the Palomar Green (PG) survey (Green, Schmidt & Liebert 1986) brought several hundreds of them to light. Green, Schmidt & Liebert (1986) surveyed most of the northern hemisphere for Ultraviolet (UV) excess objects ($B \leq 16\overset{\mathrm{m}}{.}1$). The main goal of the PG survey was to search for quasars in the northern hemisphere. However, quasars account for only 5.4% of the complete survey. Most of the 1874 observed objects were hot stars. Even larger and deeper surveys (Edinburgh-Cape survey, Kilkenny, O'Donoghue & Stobie 1991; Montreal-Cambridge-Tololo survey, Demers et al. 1990; Hamburg Quasar survey, Hagen et al. 1995; Hamburg ESO survey, Wisotzki, Reimers & Wamsteker 1991) have increased the number of hot subluminous stars to more than 2000[1].

This dissertation focuses on the most common subclass among the hot subdwarfs, the *subdwarf B (sdB)* stars. Subdwarf B stars dominate the population of faint blue stars to $16\overset{\mathrm{m}}{.}5$ at high galactic latitudes. For example, within the PG survey sdB stars comprise about 40% of the complete sample, and outnumber the white dwarfs by far. In the HRD, sdB stars populate a very narrow area which lies on a blue-ward extension of the horizontal branch (HB), the so called *extreme horizontal branch* (EHB, Heber et al. 1984, Heber 1986, Saffer et al. 1994). They have hydrogen dominated atmospheres (typically: $n_{\mathrm{He}}/n_{\mathrm{H}} \lesssim 0.01$), with effective temperatures of $20\,000\mathrm{K} \leq T_{\mathrm{eff}} \leq 40\,000\mathrm{K}$ and their logarithmic surface gravities are typically between 5.0 and 6.0 (cgs). SdB stars consist of a helium-burning core with a canonical mass of $M_{\mathrm{core}} \approx 0.5 M_{\odot}$ surrounded by a thin hydrogen-rich envelope ($M_{\mathrm{env}} < 0.02 M_{\odot}$, Heber 1986, Saffer et al. 1994). However, their origin is still unclear. After passing the red-giant stage, these stars must have suffered from such a high mass loss rate that their outer layer was lost almost entirely. The remaining hydrogen-rich envelope has not retained enough mass to sustain a hydrogen-burning shell. This means that the star cannot ascend the Asymptotic Giant Branch (AGB) after the end

[1] An updated version of the catalog of Kilkenny, Heber & Drilling (1988) lists 2313 spectroscopically identified hot subdwarfs.

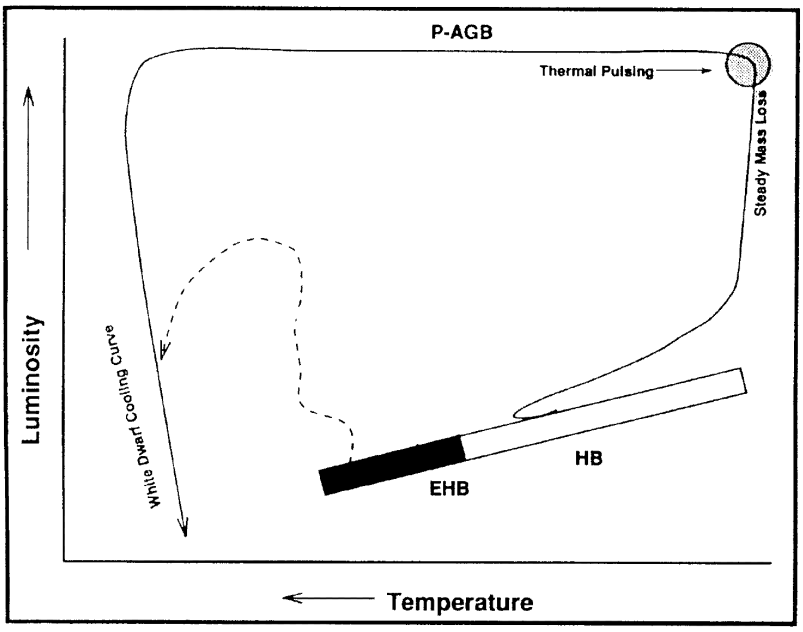

Figure 1.1: Illustration of the different types of post-HB evolution. The HB is characterized by the phase of core helium-burning. The thinner the surrounding hydrogen rich envelope of a star is, the closer lies the star to the left hand side of the HB. SdB stars lie at the extreme left hand side of the HB, the so called EHB (see text).

of the helium-core burning, but should evolve like a $0.5 M_{\odot}$ helium-main-sequence star (Heber et al. 1984, Heber 1986) 'directly' to white dwarfs of low to intermediate masses (see Fig. 1.1). Calculations of Dorman, Rood & O'Connell (1993) support this idea. The reason for very high mass loss at or shortly after the core helium flash is still unclear and several scenarios are discussed. As to the origin of sdB stars, single star evolution scenarios (e.g. stellar wind mass loss near the tip of the first giant branch, D'Cruz et al. 1996, or helium mixing driven by internal rotation, Sweigart 1997), envelope stripping processes (De Marchi & Paresce 1996, Marietta, Burrows & Fryxell 2000), merging of two helium white dwarfs (Iben & Tutukov 1986), as well as close binary evolution scenarios (Mengel, Norris & Gross, 1976, Han et al. 2002, 2003) have been proposed.

Indications that many subdwarf B stars are members of binary systems seem to indicate that binary interaction plays an important part to the evolution of sdB stars. In addition to composite spectrum binaries (Allard et al. 1994, Theissen et al. 1993,1995 and others) several single-lined binary sdB stars have been identified from variable Doppler line shifts resulting from orbital motion (e.g. Maxted et al. 2001, and others). At least two thirds of local disk sdB stars are found to be close binaries with periods shorter than ten days. However, there are also many subdwarf B stars showing no indication of any companion.

SdB stars form an important class of objects in several respects. Due to their large number found in galactic surveys of faint blue stars (e.g. PG survey, Green, Schmidt & Liebert 1986) they are important for our understanding of the structure and evolution of our galaxy. They are the main cause for the UV excess, the so-called *UV upturn*, in elliptical galaxies and galaxy bulges (Brown et al. 1997, Brown et al. 2000b). The reason is that sdB stars spend a long life

time ($\sim 10^8$ years) on the EHB at high temperatures. They are also considered to be useful age indicators for elliptical galaxies (Brown et al. 2000a).

In the cosmological context such stars are important: as members in close binary systems they are candidate progenitors of Supernovae (SN) of type Ia. Such SNe are the best standard candles to measure the large distances of galaxies and to determine the expansion rate of the universe. While the best candidates are double degenerate systems, (see the ESO SN Ia progenitor survey (SPY), Napiwotzki et al. 2001a, 2001b, 2002), sdB + white dwarf systems can also be candidate systems (Maxted, Marsh & North 2000, see also Napiwotzki et al. 2001b).

Subdwarf B stars are also very important in the context of stellar astrophysics. The discovery of several pulsating sdB stars (called sdBV or EC 14026 stars, after the prototype EC 14026−2647, Kilkenny et al. 1997) has rapidly increased the interest in these objects, because of the prospect of probing their structure by asteroseismology.

Furthermore, sdB stars are very important in the study of chemical layering processes in stellar envelopes: gravitational settling, radiative levitation and mass loss. These processes have been invoked to explain abundance peculiarities in a wide range of stars (for a review see Vauclair & Vauclair 1982) including white dwarfs, sdO stars, luminous blue variables, low mass halo stars, Ap and Am stars, and HgMn stars.

Sargent & Searle (1966) were the first, who discovered sdB stars to be helium deficient (down to 1/100th of the solar value). This finding has caused a lot of excitement, because first it was thought that it would disagree with the big-bang theory for nucleosynthesis. One year later, Greenstein, Truran & Cameron (1967) suggested that diffusion processes could cause the helium deficiency observed in sdB stars. In addition to the very low helium abundances, Baschek, Sargent & Searle (1972) discovered that sdB stars show very peculiar metal abundances (some metals are strongly depleted, whereas some are solar, or even enriched). Furthermore, large differences from star to star were found. To understand these puzzling peculiarities observed in the atmospheres of sdB stars, in the 1970s Michaud, Vauclair & Vauclair developed first theoretical models which account for diffusion processes (e.g. Michaud, Vauclair & Vauclair 1983), however, with little success. Up to now, several attempts were performed to describe the atmospheres of sdB stars. Although in some cases diffusion calculations (e.g. Michaud et al. 1989, Bergeron et al. 1988, Ohl et al. 2000, Unglaub & Bues 2001) lead to coincidences between predicted and observed values, it has not been possible to reproduce all abundances simultaneously.

Due to the low number of observations (compared to the large number of known hot subdwarf stars) in order to determine the stellar parameters (effective temperature, gravity, and chemical composition) the theory to model the evolution of sdB stars, as well as the predictions of the atmospheric composition of sdB stars, have still too much degrees of freedom. Like for all scientific investigations, observations are the key to verify or discard theoretical models.

This thesis presents the spectral analyses of large samples of sdB stars, in order to constrain theoretical predictions for their evolution, pulsation, and diffusion processes.

Chapter 2 describes the observations and presents the spectra of the program stars. Chapter 3 deals with the model spectra and procedure used to determine the atmospheric parameters from the observations. The results are presented and compared to values found in the literature. Implications in terms of the evolutionary history are examined. Chapter 4 is dedicated to the determination of the chemical composition of sdB stars. In Chapter 5 radial velocity measurements for our program stars are described. Radial velocity curves measured for nine program

sdB stars allows to estimate masses of the unseen companions. Chapter 6 presents a spin-off result of the analyses: the discovery of an apparently normal main sequence B star which is leaving our galaxy. Chapter 7 summarize the conclusions, and a brief outlook is given.

Chapter 2

Program stars

Some dozens of bright ($B \leq 13\overset{\mathrm{m}}{.}5$) sdB stars are known for several tenths of years (see Introduction). However, due the lack of efficient spectrographs and sensitive detectors, they have not been analyzed in detail. Recently, by use of this up-to-date echelle high-resolution spectrographs and CCD detectors these observations became possible. This allows us to perform a detailed analysis of a large sample of bright sdB stars for the first time.

The interest for quasars leads to numerous surveys for 'faint blue objects'. Especially the Hamburg Quasar survey (HQS, Hagen et al. 1995), and its counterpart the Hamburg ESO survey (HES, Wisotzki, Reimers, & Wamsteker 1991) 'hunted' for quasars. It was expected to find numerous quasars. However, as with the Palomar Green survey (PGS, Green, Schmidt, & Liebert 1986), most of the faint blue objects discovered were hot stars, i.e. white dwarfs and hot subdwarfs. For the first time, the analyses of large samples of hot subdwarfs (> 100 stars) became possible.

With the spectra obtained by the PGS, HQS, or HES, only qualitative statements concerning the type and quantity of the analyzed hot subdwarfs are possible. To determine the atmospheric parameters of the stars, slit-spectra with higher resolution and better S/N are necessary. Therefore, we performed follow-up observations for all objects taken from the HQS and HES. As most of the stars are dimmer ($B \geq 16\overset{\mathrm{m}}{.}0$) by several magnitudes than the bright sdB stars, only fundamental parameters (effective temperature, gravity, and helium abundance) can be determined.

However, beforehand a spectral classification of the program stars is necessary. Before I present the program stars in three sections (Section 2.2 to 2.4) the classification system is explained first.

2.1 Spectral classification system

In the literature at least three different schemes are available to classify the spectra of hot subluminous stars (Green et al. 1986, Moehler et al.1990b, and Jeffery et al. 1997). We use the most common classification system described by Moehler et al. (1990b, see Fig. 2.1): "...

B This designation means main sequence B-type spectra showing Balmer lines and He I absorption with the line at 4388Å being about the same strength as the one at 4471Å.

HBB These stars show Balmer line absorption of moderate gravity accompanied by He I (4471Å) and/or Mg II (4481Å) absorption.

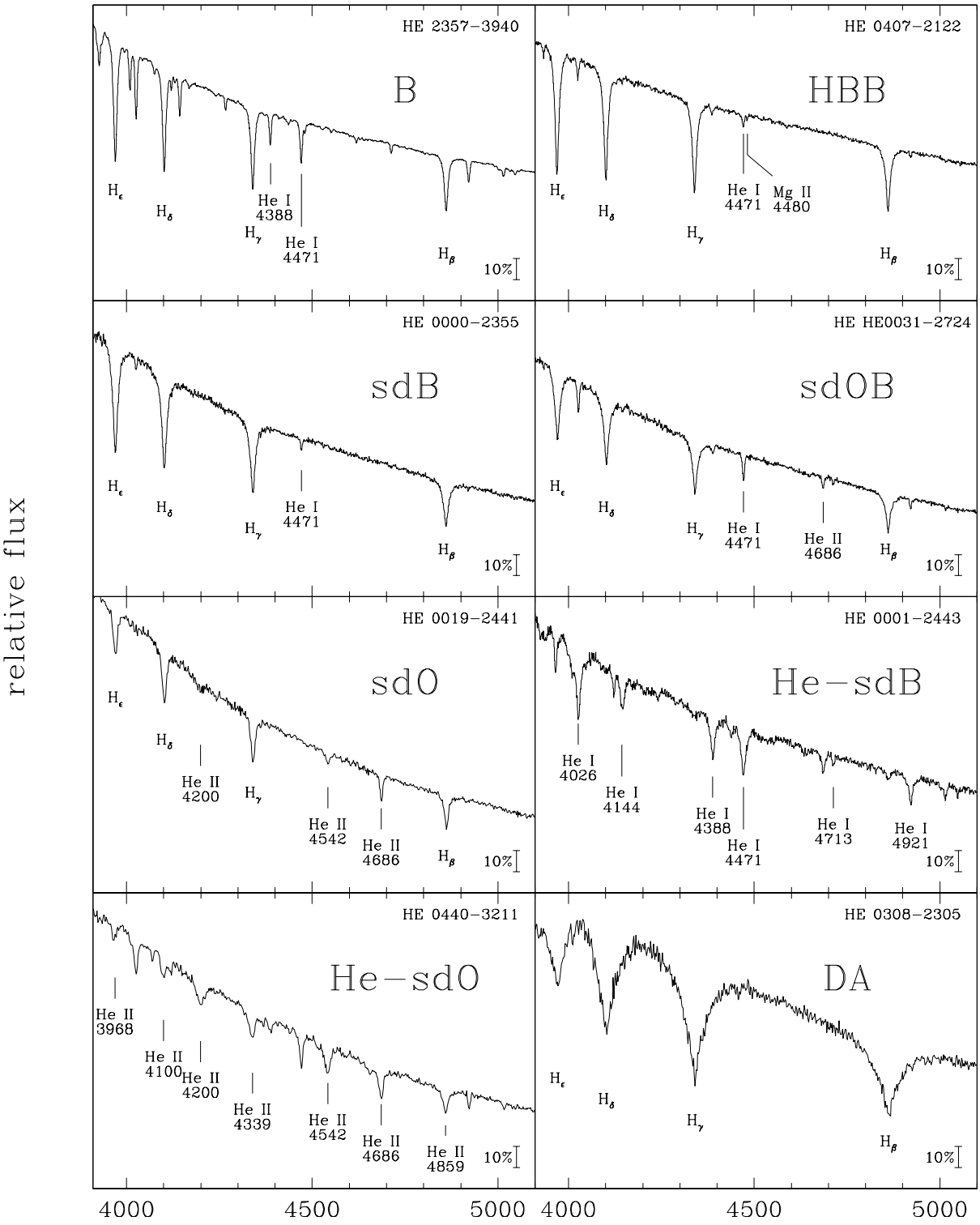

Figure 2.1: Illustration of the spectral classification scheme of Moehler et al. (1990b). Typical representative stars for each class are shown. Characteristic absorption lines for classification are marked.

sdB Subdwarf B stars display strong broad Balmer lines and weak (or no) He I absorption with the line at 4388Å being much weaker than the one at 4471Å.

sdOB This class consists of subdwarfs showing strong broad Balmer lines accompanied by He I (4471Å) and He II (4686Å) absorption (both weak).

sdO This classification denotes spectra with strong broad Balmer lines accompanied by He II absorption.

He-sdB These stars are not "normal" sdB stars but show spectra dominated by strong He I lines accompanied by weak He II lines with no detectable H absorption (identical with the coding sdO(D) of Green et al. 1986).

He-sdO These hotter stars have spectra with strong He II absorption, sometimes also weak He I lines, but no Balmer lines.

DA This abbreviation summarizes all white dwarfs, i.e. stars with extremely broad Balmer lines and no helium lines at all (cf. DA n by Green et al 1986)."

2.2 Bright sdB stars

At first, I would like to present the bright program stars.

2.2.1 Selection of the program stars

All candidates were selected from the *Catalogue of spectroscopically identified hot subdwarf stars* of Kilkenny, Heber & Drilling (1988) except HS 2224+2618, which was included from the HQS sample (see Section 2.3) due to its brightness. We limited ourselves to stars brighter than $V = 13\overset{\text{m}}{.}5$ for which it is possible to measure high resolution spectra with 2m class telescopes.

2.2.2 Observations and data reduction

Optical echelle spectra of 47 sdB stars with high S/N were obtained at two observatories (for the summary of the observing runs performed for all bright program stars see Table 2.1):

Calar Alto

34 sdB stars were observed at the German-Spanish Astronomical Center (DSAZ) on Calar Alto (CA), Spain, with the 2.2m telescope equipped with the Fiber-Optics Cassegrain Echelle Spectrograph (FOCES). We used the Tektronic CCD Chip (1024×1024 pixel) with a pixel size of 24μm, the 200μm entrance aperture and a slit width of 2 arcsecs, resulting in a nominal resolution of $\lambda/\Delta\lambda = 30\,000$. All spectra cover the wavelengths from 3 900Å to 6 900Å.

The spectra were reduced as described in Pfeiffer et al. (1998) using the IDL macros developed by the Munich Group.

The normalization[1] was done for all echelle orders (except those containing the broad Balmer lines) by fitting the continuum with polynomial functions (typically of fourth order). For orders containing the Balmer lines (H_α up to H_γ) the fit functions were interpolated between the

[1]We have normalized the spectra only for those stars included to the measurement of metal abundances (observing runs #1, #2, #3 , and #5, see Section 4).

Table 2.1: Summary of all echelle high-res observations.

run #	date (start of nights)	instrument	observers
1	1998 Sep 09-12	2.2m CA + FOCES	Edelmann/Pfeiffer
2	1999 Jul 19-23	2.2m CA + FOCES	Edelmann/Pfeiffer
3	2000 Jan 28 - Feb 01	2.2m CA + FOCES	Edelmann/Karl
4	2000 Sep 06-09	1.52m ESO + FEROS	Edelmann
5	2001 Aug 27-31	2.2m CA + FOCES	Edelmann/Karl
6	2002 Aug 07-10	1.52m ESO + FEROS	Lisker
7a	2002 Aug 14-21	2.2m CA + FOCES	service-mode
7b	2002 Nov 26	2.2m CA + FOCES	service-mode

adjacent orders, since for the FOCES spectrograph, neighboring orders ($n = \pm 3 \ldots 5$) differ only slightly. Due to the blending of the higher Balmer lines and the low S/N ($\sim 10 \ldots 20$) in the blue part of the spectra, the normalization below ~ 4100Å is difficult and not very reliable.

La Silla

13 sdB stars were observed at the ESO 1.52m telescope equipped with the Fiber-fed Extended Range Optical Spectrograph (FEROS). We used the standard setup (EEV CCD Chip with 2048×4096 pixel, pixel size of 15μm, entrance aperture of 2.7 arcsecs) which results in a nominal resolution of $\lambda/\Delta\lambda = 48\,000$. All spectra cover the wavelengths from 3 600Å to 8 900Å.

The spectra were reduced using the on-line data reduction provided at ESO using the ESO-MIDAS program package (Françoise 1999).

The normalization[2] was done for all echelle orders (except those containing the broad Balmer or Paschen lines) by fitting the continuum with polynomial functions (typically of fourth to fifth order). For orders containing the Balmer lines, I used another strategy. First I selected three bright stars observed during the run, for which the S/N is very good within the entire orders (S/N $\sim$ 100), fitted the orders containing the Balmer lines H_β–H_δ using LTE model atmospheres to obtain (from the resulting effective temperature and gravity) model line distributions for all Balmer and Paschen lines observed. Using these theoretical line profiles, I determined the fit functions for normalization of the orders containing the Balmer and Paschen lines of the bright stars and combined them to one set of fit functions for the individual echelle orders. Using these fit functions I normalized all echelle orders for all stars observed, with the hydrogen Balmer and Paschen absorption lines.

An advantage of the automatical on-line reduction process of the FEROS data, provided at ESO, is that all spectra were automatically corrected for the earth movement to barycentric values, i.e. for radial velocity measurements, no corrections are necessary (see Chapter 5). However, for the normalization, this is a big disadvantage. Because all spectral echelle orders for one star are somewhat shifted compared to another star due to the automatic correction. This means that the fit function for one star is not entirely valid for other stars, especially if the differences of the barycentric corrections are large. Therefore the spectra should be used with caution in order to determine atmospheric parameters using line profile fitting We, therefore, decided to obtain low-resolution spectra as well (see Section 3.2.1). To measure metal abundances, however, the normalization used is sufficient (see Section 4.1.1).

[2]We have normalized the spectra only for those stars included to the measurement of metal abundances (observing run #4, see Section 4).

Table 2.2: Comparison of the spectral classifications of the bright program stars with previous work. Since the PG classification scheme differs from ours, we transfer the PG spectral types into our scheme (Moehler et al. 1990b).

star	this work	other	Ref.	star	this work	other	Ref.
SB 7	sdB+x	sdO+x	H86	PG 1530+212	B	HBB	G86
		sdB+F/G	L00	PG 1607+174	sdB+x	sdB	G86
PG 0001+275	sdB	HBB	G86	LS IV−12 1	sdO	sdO	B95
PG 0011+283	sdB	sd	G86	HD 149382	sdOB	sdB	S94
CD−38° 222	sdB	sdB	B97	PG 1654+138	sdB	HBB	G86
HD 4539	sdB	sdB	S94	PG 1705+537	HBB	HBB	G86, M90
PHL 6783	sdO+x	sdO+G	U98, K88	PG 1710+490	sdB	sdB	G86, B97
SB 395	sdB	sdB	U98	UVO 1735+22	sdOB	sdB	K88
PHL 932	sdOB	sdB	G86	UVO 1758+36	sdB	sdB	S94
		sdOB	N99	BD+48° 2721	sdB	sd	K88
Feige 11	sdB	sdB	G86, S94	HD 171858	sdB	sdB	K88, M03
PG 0116+242	sdB+x	sd	G86, U98	HD 188112	sdB	sdB	K89
PG 0133+114	sdB	sdB	M90, B97	PHL 25	sdB	sdB	U98
CD−24° 731	sdOB	sdB	H84	HD 205805	sdB	sdB	B97
PG 0342+026	sdB	sdB	H86, A01	PG 2151+100	sdB	sd	G86, U98
UVO 0512−08	sdOB	sdOB	K88	PG 2159+051	sdB	sd	G86, U98
PG 0909+276	sdOB	sdB	G86, S94	HS 2224+2618	sdB	-	-
PG 1047+003	sdB	sdB	G86	PHL 382	sdB	sdB	G86
Feige 65	sdB	sdB	G86, S94, A02	PB 7352	sdB	sd/hb	K88
Feige 86	HBB	HBB	A00	LB 1516	sdB	sdB	K88
PG 1336−018	sdB	sdB	G86	PG 2301+259	sdB	sdB	G86
PG 1505+074	sdOB	sdB	G86	Feige 108	sdB	sdB	S94
PG 1519+640	sdB	sdB	G86, B97	PB 5333	sdB	sdB	G86, S94
PG 1524+611	sdB+x	sdB	G86	CD−35° 15910	sdB	sdB	K88
		HBB	M90	PG 2351+198	sdB	HBB	G86

Ref.: A00 = Altmann & de Boer (2000); A01 = Aznar Cuadrado & Jeffery (2001); A02 = Aznar Cuadrado & Jeffery (2002); B95 = Bauer & Husfeld (1995); B97 = de Boer et al. (1997); G86 = Green, Schmidt & Liebert (1986); H84 = Heber et al. (1984); H86 = Heber (1986); K88 = Kilkenny, Heber, & Drilling (1988); K89 = Kilkenny & Muller (1988); L00 = Lamontagne et al. (2000); M90 = Moehler et al. (1990b); M03 = Morales Rueda et al. (2003); N99 = Napiwotzki (1999); S94 = Saffer et al. (1994); U98 = Ulla & Thejll (1998);

2.2.3 Classification of the program stars

We classified all bright program stars using the classification system of Moehler et al. (1990b, see Section 2.1).

This scheme results in 42 (89%) sdB or sdOB stars, 2 (4%) HBB stars, one (2%) main sequence B star (due to the very broad helium lines and Balmer line cores), and two (5%) hotter helium deficient subdwarf O stars.

A closer inspection revealed four sdB, and one sdO program stars to be spectroscopic binaries. All of them show the Mg I triplet at 5167Å, 5173Å, and 5184Å, which is the unmistakably indication of a cool companion, if seen in a high-resolution spectrum of a hot star.

For all of our program stars except one (HS2224+2618, which was included from the HQS sample, see Section 2.3) we found spectral classifications in the literature. As can be seen in Table 2.2 there is a very good agreement with previous classifications.

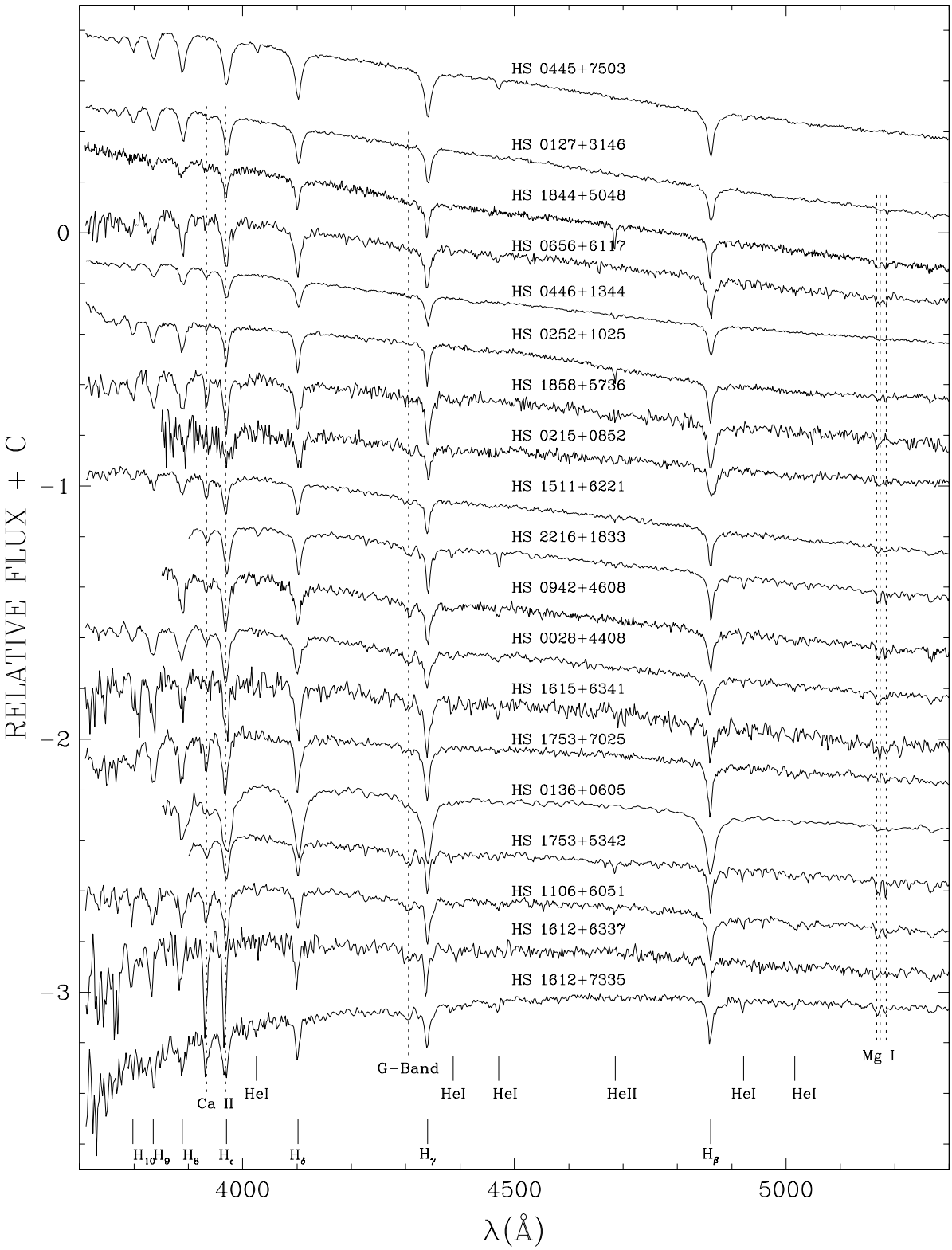

Figure 2.2: Spectra of all HQS stars in our sample which show signs of a cool companion in comparison to a single sdB star (top). The contribution of the companion is increasing from the top to bottom.

Table 2.3: Summary of all HQS follow-up runs for our program stars. A range of spectral resolutions is given for the three runs affected by seeing disk being temporarily smaller than the slit width.

run #	date (start of nights)	instrument	recip. disp. [Å/mm]	spectr. res. [Å]	wavelength coverage [Å]	observers
1	1989 Jan 21-25	3.5m B&C	120	5.0	3850-5650	Heber & Jordan
2	1990 Jan 08-17	3.5m TWIN	144/160	6.5	3550-5550,5570-7030	Jordan & Möller
3	1990 Oct 01-09	3.5m FR	136	7.0	3770-5550	Heber & Dreizler
4	1990 Nov 04-11	3.5m TWIN	144/160	5.5	3430-5550,5560-7030	Jordan & Rauch
5	1991 Jun 19-25	3.5m TWIN	144/160	5.5	3570-5750,5110-9300	Heber & Marten
6	1992 Sep 10-14	3.5m TWIN	144/160	4.5-5.5	3360-5550,5430-9740	Dreizler
7	1993 Mar 07-12	3.5m TWIN	144/160	5.0	3470-5680,5420-9630	Heber
8	1993 Aug 28 - Sep 02	3.5m TWIN	72/72	3.4	3600-5500,5540-7420	Dreizler & Haas
9	1993 Sep 02-05	2.2m CAS	120	4.5-5.5	4010-6720	Haas & Dreizler
10	1994 Sep 21-25	3.5m TWIN	72/72	3.5	3610-5490,5440-7320	Dreizler
11	1995 Jan 23-27	3.5m TWIN	72/72	3.5	3580-5470,5420-7320	Dreizler
12	1996 Aug 16-19	3.5m TWIN	72/72	3.6	3770-5660,5430-7340	Lemke
13	1997 Aug 28-31	3.5m TWIN	72/72	3.5	3300-5450,5300-7550	Edelmann
14	1998 Sep 30 - Oct 04	2.2m CAFOS	100	5.0-8.0	3400-6300	Edelmann

2.3 sdB stars from the Hamburg Quasar Survey

2.3.1 Hamburg Quasar Survey

The Hamburg Quasar Survey (HQS) was carried out, starting in 1980, with the 80cm Schmidt telescope at the German-Spanish Astronomical Center (DSAZ, German: Deutsch-Spanisches Astronomie-Zentrum) on Calar Alto, Spain (Hagen et al. 1995). Although it was primarily initiated as a quasar survey, it is also a very rich source of faint blue stars. Unlike the PG survey (Green, Schmidt, & Liebert 1986), and most other surveys, objective prism spectra (spectral resolution of 45Å FWHM at H_γ) were obtained. Afterwards, the HQS plates were digitized in Hamburg using a PDS micro-densitometer. A search software selects quasar candidates as well as faint blue stars from the 30 000–50 000 spectra per plate in the magnitude range of $13\overset{\mathrm{m}}{.}5 \leq B \leq 18\overset{\mathrm{m}}{.}5$. Selection criteria are blue continua and/or emission lines (Hagen et al. 1995).

In a collaboration between the institutes in Hamburg, Kiel, Tübingen, and Bamberg follow-up observations and analyses of visually selected candidates of hot stars were performed.

The current database of follow-up observations contains well over 400 confirmed stars. The dominant fractions of the list are hot subdwarfs ($\sim 50\%$) and white dwarfs ($\sim 30\%$). A lot of very rare and unusual stars also were found. The discovery of four PG 1159, nine hot DO, and five DAO white dwarfs, so far, are the highlights of the follow-up observations (Heber, Dreizler & Hagen 1996, and references therein). A comprehensive summary of the results from the HQS follow-up observations of hot stars can be found in Heber, Jordan & Weidemann (1991a), Dreizler et al. (1994), Lemke et al. (1997a, sdO stars), and Homeier et al. (1998, 1999, DA white dwarfs).

My goal was to select all sdB stars from the HQS database of stellar objects, in order to analyze them for their atmospheric parameters.

Table 2.4: Spectral signatures of cool companion stars in the spectroscopic binaries of the HQS sample.

binary stars	Ca H+K	G-band	Mg I	flat flux
HS 0028+4407	√	√	√	√
HS 0127+3146	-	√	√	-
HS 0136+0605	-	-	√	√
HS 0215+0852	-	√	√	√
HS 0252+1025	-	√	√	√
HS 0446+1344	-	√	√	√
HS 0656+6117	-	√	√	-
HS 0942+4608	√	√	√	√
HS 1106+6051	√	√	√	√
HS 1511+6221	√	√	√	-
HS 1612+6337	√	√	√	√
HS 1612+7335	√	√	√	√
HS 1615+6341	-	√	√	√
HS 1753+5342	√	√	√	√
HS 1753+7025	√	√	√	√
HS 1844+5048	-	√	√	-
HS 1858+5736	√	-	√	√
HS 2216+1833	√	√	√	√

2.3.2 Preselection of the program stars

Candidate stars were selected from the HQS objective prism plates, first by automatically selecting spectra which are blue compared to the bulk of spectra, and second, by visually classifying them on a graphics display (Hagen et al. 1999). Objects with UV excess emission were either classified directly as hot stars due to the presence of hydrogen Balmer absorption lines or were retained as quasar candidates. Follow-up observations of stellar candidates were mostly made from the hot stars list, and occasionally for objects that were not confirmed as quasars.

2.3.3 Observations and data reduction

Observations

The observations described here were obtained, starting in January 1989, at the DSAZ on Calar Alto, Spain, during various observing runs with different telescopes and instruments. The observational dataset is therefore very inhomogeneous. The spectral resolution ranges from 3.4Å to 8.0Å FWHM (determined from the helium-argon lines in the calibration spectra) and the wavelength coverage also varies between 4010–6720Å and 3360–9740Å. For three observing runs the seeing was sometimes better (smaller) than the slit width, resulting additionally in a varying spectral resolution during these runs. For a detailed overview of the observational material see Table 2.3.

Data reduction

The spectra were extracted from the two-dimensional frames and reduced to linear wavelength and intensity scales using the IDAS package written by G. Jonas in Kiel for the early observations (until 1991) and the ESO-MIDAS package for the data obtained after 1991.

All frames were bias subtracted, flat field corrected, and cosmic ray events were cleaned. The sky background was removed by extracting a stripe on each side of the star's spectrum

Table 2.5: Comparison of the spectral classifications of the HQS program stars with previous work. Since the PG classification scheme differs from ours, we transcribed the PG spectral types into our scheme (Moehler et al. 1990b).

star	this work	other	Ref. & name within
HS 0016+0044	sdB	sdB	T94
HS 0039+4302	sdB	sdB	B91: Balloon 84041013
HS 0048+0026	sdOB	sdB	B91: Balloon 94700002
		sdOB	G86: PG 0048+004
HS 0055+0138	sdB	sdB	B91: Balloon 94700001
		sdB	P86: PG 0055+016
HS 0209+0141	sdB	sdB	G86: PG 0209+0141
HS 0212+1446	sdB	sdB	G86: PG 0212+148
HS 0232+3155	sdOB	sdB	W90: KUV 02324+3156
HS 0941+4649	sdB	sdB	M98: US 909
HS 0942+4608	binary	sdB+G	H89
		sdB	M98: PG 0942+461
HS 1106+6051	binary	sdB	G86: PG 1106+608
HS 1236+4745	sdB	sdB	S94: PG 1236+479
HS 1511+6221	binary	sdB+K5	A94: PG 1511+624
		sdB	A96: FBS 1511+624
HS 1547+6312	sdB	sdB	A96: FBS 1547+632
		sdB	G84: PG 1547+632
HS 1612+7335	binary	sdB+K2.5	A94: PG 1612+735
HS 1641+4601	sdB	sdB	B91: Balloon 83600002
HS 2218+0201	sdB	sdB	U98: PG 2218+020
HS 2233+2332	sdOB	sdB	B91: Balloon 90900003
HS 2240+0136	sdB	sdOB?	K84: PHL 384
HS 2240+1031	sdOB	sdB	G84: PG 2240+105
HS 2246+0158	sdB	sdB	G84: PG 2246+019
HS 2333+3927	sdOB	DAZ	A96: FBS 2333+395

Ref.: A94 = Allard et al. (1994); A96 = Abrahamian & Mickaelian (1996); B91 = Bixler, Bowyer & Laget (1991); G86 = Green, Schmidt & Liebert (1986); H89 = Heber, Jordan & Weidemann (1989); K84 = Kilkenny (1984); M98 = Mitchell (1998); R93 = Rodgers, Roberts & Walker (1993); S94 = Saffer et al. (1994); T94 = Thejll, Theissen & Jimenez (1994); W90 = Wegner, Steven & Swanson (1990).

and subtracting the average of these two stripes from each row of the stellar signal on the CCD. These corrected rows were combined to a one dimensional stellar spectrum. Thereafter a wavelength calibration was performed with calibration spectra recorded immediately after each stellar spectrum. Then all wavelength-calibrated spectra were corrected for atmospheric extinction using the extinction coefficients of La Silla, Chile (Tüg 1977) as these coefficients are not available for the Calar Alto observatory. In the last step for all spectra a relative flux calibration was done using spectra of flux-standard stars (mostly BD+28° 4211, G 191−B2B, or Feige 34, Oke 1990) which were taken each night.

2.3.4 Selection and classification of the program stars

From the list of stellar HQS follow-up observations, we selected here 111 subdwarf B candidates for a detailed analysis, using the classification system of Moehler et al. (1990b). Details of Moehler's classification scheme are given in Section 2.1.

A closer inspection revealed 18 sdB stars of the sample to be spectroscopic binaries. All of them show at least two characteristics of a cool companion star (e.g. flat flux distribution, G-band absorption, Ca H+K, Mg I triplet at 5167Å, 5173Å, and 5184Å) (see Fig. 2.2 and Table 2.4). The spectral classifications for all program stars are listed in Table A.1.

The coordinates were determined on HQS direct plates and are accurate to $\pm 2''$. The B-

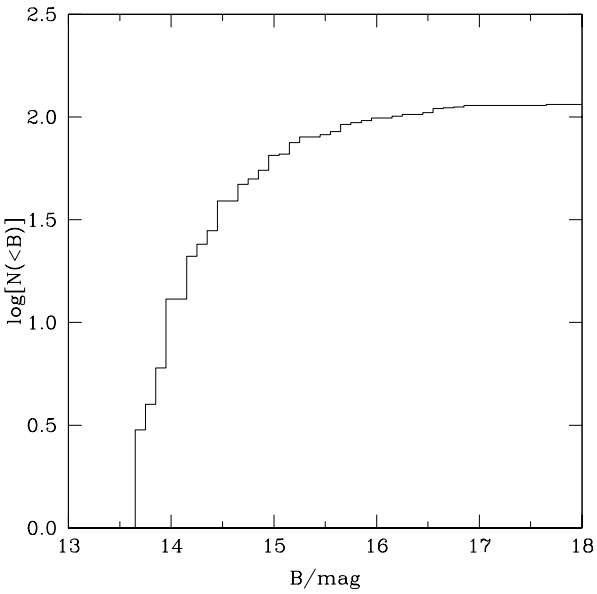

Figure 2.3: Cumulative number density as a function of the B magnitude for the HQS sample.

magnitudes presented in Table A.1 were determined mostly from the objective prism plates and may have an error of up to 0.3 mag.

Several stars were already discovered as UV excess objects independently by various surveys. The references are indicated in Table 2.5. Although 45 of our program stars were already detected in other surveys, we found spectral classifications for only 21 of them in the literature. As can be seen in Table 2.5 there is good agreement with classifications from literature except for HS 2333+3927 which was previously classified as a DAZ white dwarf.

2.3.5 Completeness

In order to test how well our sample represents a complete sample, we construct the cumulative brightness distribution. For a complete sample a linear relation of $\log[(N(< B)]$ versus the B magnitude is expected (see Green, Schmidt, & Liebert 1986). As can be seen from Fig. 2.3, the distribution is quite different from a linear relation. Therefore we conclude, that our HQS sample is not complete for any given brightness interval.

2.4 sdB stars from the Hamburg ESO Survey

2.4.1 Hamburg ESO Survey

The Hamburg ESO survey (HES) was conceived as a twin of the Hamburg Quasar Survey (HQS, see last section). Starting in 1990, objective prism spectra were obtained using the 1.0m Schmidt telescope at the European Southern Observatory (ESO) on La Silla, Chile. Like the HQS, the primarily goal for the HES is the discovery of bright ($B < 17\overset{\mathrm{m}}{.}5$) quasars. However, because its spectral resolution is typically 15Å FWHM at H_γ, it is also possible to search for stellar objects of different types (see e.g. Christlieb et al. 2001).

We started in 1996 a collaboration of the institutes in Hamburg, Bonn, and Bamberg to

observe a large statistically complete (brightness limited) sample of HES sdB stars, in order to determine their atmospheric parameters. We have chosen several sky fields, some of them overlapping with the Slettebak & Brundage (1971) survey. SdB stars from the latter survey have already been studied by Heber (1986).

2.4.2 Selection of sdB candidates

Our aim was to observe all sdB stars with $B \leq 16\overset{\mathrm{m}}{.}0$ from 41 HES fields. We have isolated all sdB candidates in selected South Galactic Pole (SGP) fields down to 16th mag. A second (smaller) sky area at lower latitude ($b_{\mathrm{II}} \approx -40°$) was chosen for comparison and to allow a more efficient observing strategy.

Until the 1997 follow-up observing run, candidates were selected by eye inspection of the prism spectra of stars showing an UV excess ($\rightarrow$ hot star) and showing Balmer lines but no lines of ionized helium. These classifications were sufficient for the brighter stars, where the S/N of the objective prism spectra are pretty good (see e.g Fig. 2.4). However, for the fainter ones this results in two problems: first, we could not identify all sdB stars, so the completeness of the survey was not guaranteed and there are misclassifications (see e.g. Fig. 2.5). So we decided to use a more strict selection process for the following observing runs. Together with Norbert Christlieb from the Hamburg group, I performed the following steps for the classification process:

Step 1: Hot stars are selected automatically by applying a color criterium (Christlieb et al. 1998).
Due to the enormous number of candidates drawn, we decided to concentrate only on those HES fields, where observations have already been performed at the '96 and '97 follow-up runs (41 fields) and enhanced them by 20 new fields which have been digitized so far[3]. This step yielded 1577 candidates.

Step 2: Visual inspection of all candidates selected from step 1.
We used the following criteria to classify the stars:

sdB: Strong Balmer lines, He II lines absent, and strong Balmer jump

unid: Not possible to exclude with certainty that it is an sdB

sdO: He II lines visible, no Balmer lines, and very blue continuum shape

DB: Broad He I lines visible, no Balmer lines

DA: Broad Balmer lines, no Balmer jump

other stellar/interstellar objects: e.g. visibility of emission lines (emis), Ca I lines and/or G-band (star), 'strange' behavior of continuum due to overlap of different spectra (ovl), possibly saturated spectra (sat), or too noisy to decide (nois)

This step was performed independently by Norbert Christlieb and by myself. For the results of the procedure see Table 2.6.

A test with 78 objects already observed in the '96 and '97 follow-up run revealed only one sdB which was not correctly classified neither by Christlieb nor by myself, by selecting the classes "unid" or "sdB" from Christlieb's or my classification. Three sdB stars would have been misclassified by selecting only the class "sdB" from Christlieb's or my classification.

[3]Not all HES survey fields were digitized by that time.

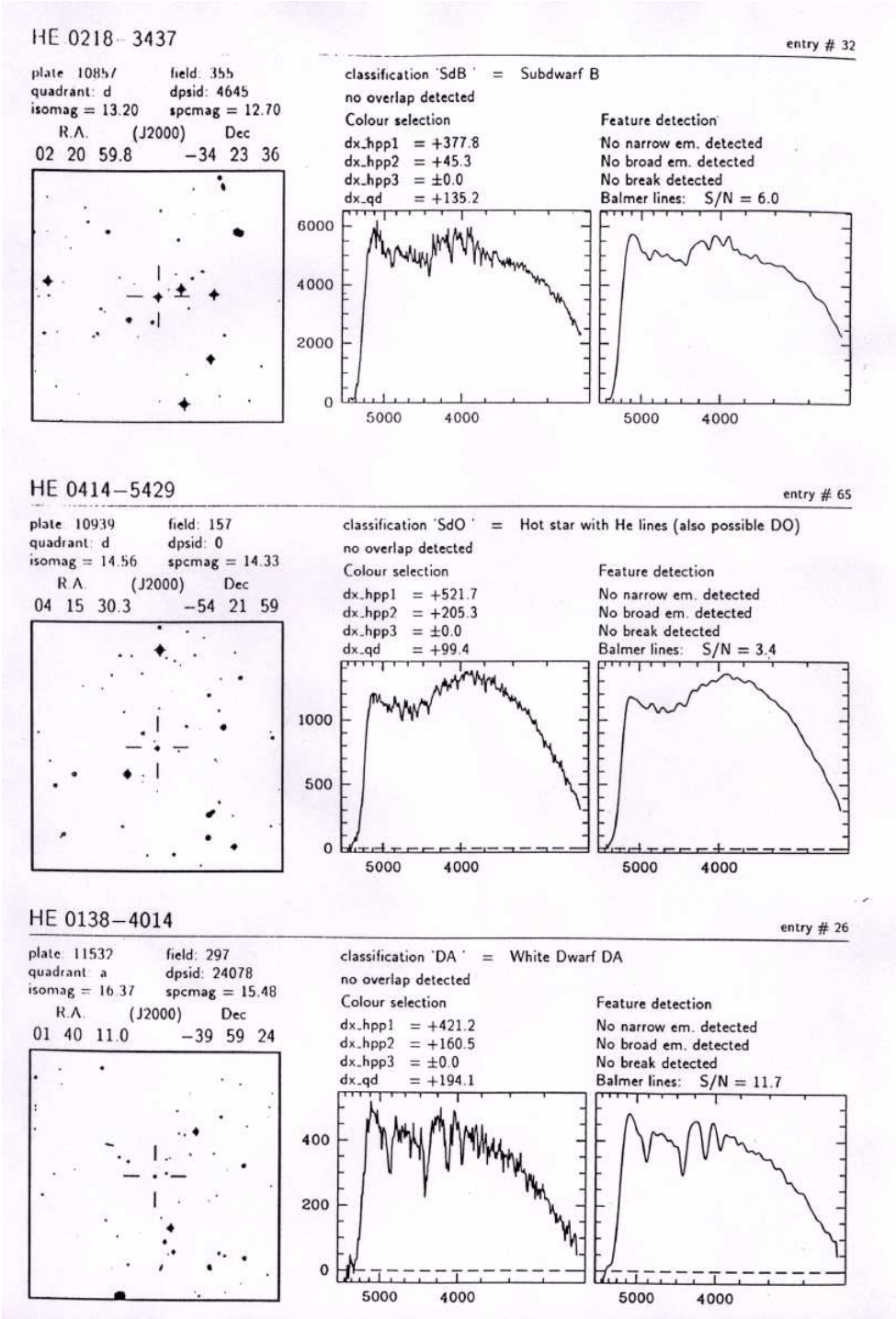

Figure 2.4: HES finding charts and objective prism spectra for three bright UV excess stars. The classification of the spectra was done 'by eye' using the classification scheme of Moehler et al. (1990b, see also Section 2.1). Due to the good S/N of the spectra, the classification is unequivocal.

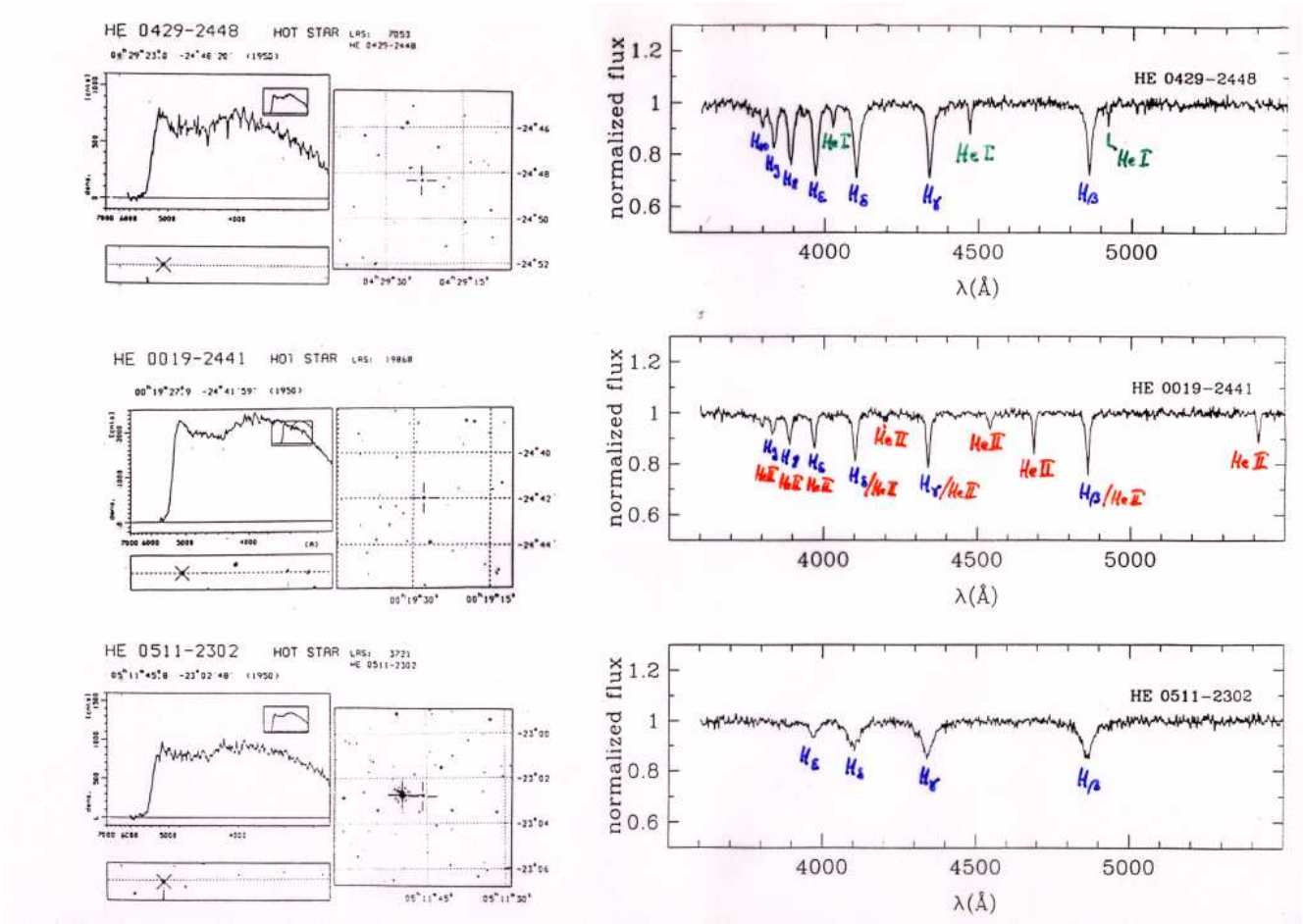

Figure 2.5: Left column: HES finding charts and objective prism spectra for three bright UV excess stars, classified as 'HOT STAR's. Due to the bad S/N of the object prism spectra, a clear classification by eye is not possible.
Right column: Spectra of follow-up observations for the stars on the left panel. Using the classification scheme of Moehler et al. (1990b, see also Section 2.1), a sdB stars (top panel), a sdO star (center panel), and a hot DA white dwarf (lower panel) results.

Table 2.6: Statistics for visually inspection of sdB candidates from the HES (step 2).

class	Edelmann	Christlieb
sdB	140	166
unind	30	45
sdO	65	50
DB	5	7
DA	106	103
emis	73	49
star	46	76
ovl	669	529
sat	94	163
nois	73	66
other	276	323

Table 2.7: Summary of all HES follow-up runs for our program stars.

run #	date (start of nights)	instrument	spectr. res. [Å]	wavelength coverage [Å]	observers
1	1996 Oct 21-25	1.52m ESO + B&C	5.5	3500-7000	Lemke
2	1997 Oct 13-17	1.52m ESO + B&C	?	3500-7000	Edelmann
3	1999 Oct 20-23	1.54m Danish + DFOSC	5.3	2900-5500	Edelmann
4	2001 Nov 16-19	1.54m Danish + DFOSC	4.5	2900-5500	Edelmann

Using the classification either by Christlieb or by myself as "sdB" or "unid" and only stars with a photographic B magnitude brighter than 16, resulting in 150 additional follow-up candidates.

To guarantee the completeness of the sample and to minimize telescope time we use the next and last step:

Step 3: Flux classification.
We used LTE model flux distributions folded with the photographic density curve of the HES photographic plates and compared them with the resulting 150 digitized HES spectra from step 2. All stars within the temperature range of $20\,000\mathrm{K} \lesssim T_{\mathrm{eff}} \lesssim 40\,000\mathrm{K}$ were selected. From the flux distribution it was easy to exclude non-sdB objects (see Fig. 2.6). This step excluded 53 objects. Still, due to the large number of 97 candidates drawn, we decided to concentrate only on the 'old' 41 fields for which observations were already started in the '96 and '97 follow-up runs. Thereby the number of remaining candidates was reduced to 61.

2.4.3 Observations and data reduction

Observations

The observations described here were obtained, starting in August 1996, at the European Southern Observatory (ESO) on La Silla, Chile, during four observing runs at the ESO 1.52m telescope using the Boller & Chivens spectrograph, and at the ESO 1.54m Danish telescope using the Danish Faint Object Spectrograph and Camera (DFOSC) instrument. The observational dataset is relatively homogeneous. For a detailed overview of the observational material see Table 2.7.

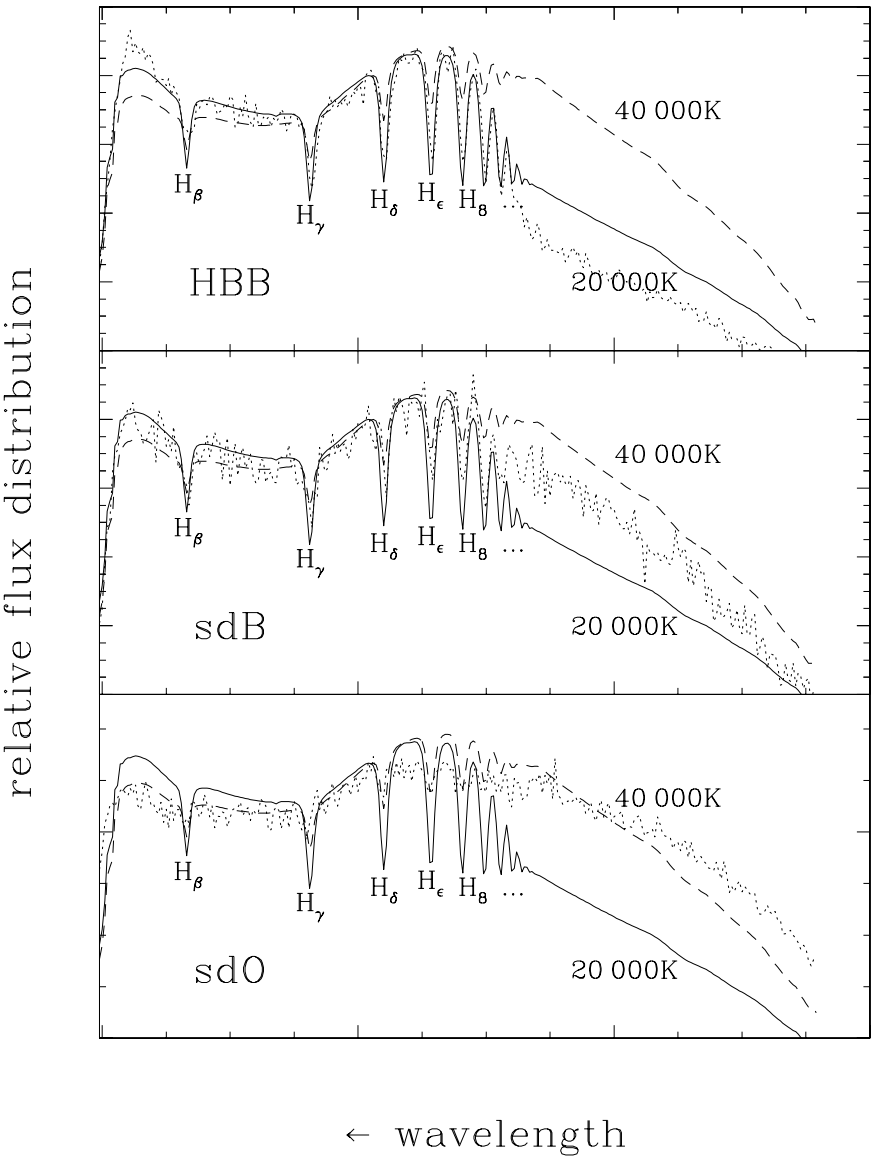

Figure 2.6: LTE model flux distributions folded with the photographic density curve (straight and dashed lines) in comparison to three HES objective prism spectra (dotted lines): a cool HBB star (upper panel), a sdB star (center panel), and a hot sdO star (lower panel). Note the increasing wavelength from the right to the left (see denoted Balmer lines).

Table 2.8: Spectral signatures of cool companion stars in the spectroscopic binaries of the HES sample.

binary stars	Ca H+K	G-band	Mg I	flat flux
HE 2213−2212	-	√	√	-
HE 2226−4005	√	√	√	√
HE 2230−4000	√	√	√	√
HE 2356−2655	√	√	√	√
HE 0226−3639	-	√	√	-
HE 0337−2508	√	√	√	√
HE 0340−2420	-	√	√	-
HE 0430−2457	-	√	√	-
HE 0513−4632	-	√	√	√
HE 0538−5637	√	√	√	

Data reduction

The spectra were extracted from the two-dimensional frames and reduced to linear wavelength and intensity scales using the ESO-MIDAS package. All frames were bias subtracted, flat field corrected, and cosmic ray events were cleaned. The sky background was removed by extracting a stripe on each side of the star's spectrum and subtracting the average of these two stripes from each row of the stellar signal on the CCD. These corrected rows were combined to a one dimensional stellar spectrum. Thereafter a wavelength calibration was performed with calibration spectra recorded immediately after each stellar spectrum.

The spectra of the calibration lamp (He+Rb+Hg, the only one available) show only eight useful emission lines within the used wavelength region. This means that the wavelength calibration should be used with caution (e.g. for radial velocity measurements, see Section 5.1). However, to analyze the spectra for their atmospheric parameters, the calibration is good enough.

Then, all wavelength calibrated spectra were corrected for atmospheric extinction using the extinction coefficients of La Silla, Chile, (Tüg 1977). In the last step all spectra were relatively flux calibrated using spectra of flux-standard stars (mostly Feige 110, LTT 7987, or EG 21, Oke 1990) which were taken each night.

2.4.4 Classification of the program stars

We classified all objects, drawn from our HES follow-up campaign (see Table 2.7) using the classification system of Moehler et al. (1990b, see Section 2.1).

This scheme results in 74 (64%) sdB or sdOB stars, 13 (11%) HBB stars, six (5%) main sequence B stars, six (5%) hotter helium deficient subdwarf O stars, nine (8%) helium rich sdO stars, five (4%) hot DA white dwarfs, 2 (2%) cataclysmic variables, and one (1%) DBA white dwarf. The stars which should be clearly ruled out by our selection scheme (Section 2.4.2), i.e. the hot He-sdO, DA, and DBA stars, are mostly drawn from the '96 observing run, where the stars are selected only by eye inspection of the ESO objective prism spectra.

A closer inspection revealed ten HES sdB program stars to be spectroscopic binaries. They show at least two signatures of a cool companion star (see Table 2.8).

41 of our program stars were already detected in other surveys. However, only for 28 of them we found spectral classifications in the literature. As can be seen in Table 2.9 there is a very good agreement with classifications from literature.

The equatorial coordinates given in Table A.2 were determined from HES direct plates and

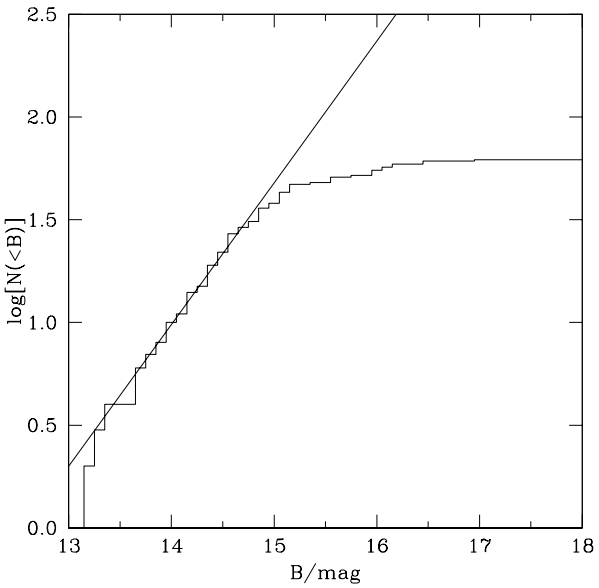

Figure 2.7: Cumulative number density as a function of the B magnitude for the HES sample.

are accurate to $\pm 2''$. The B_J magnitudes given in Table A.2 (two digits given) were determined from the object prism plates and may have an error of up to $0\overset{\mathrm{m}}{.}3$. The V magnitudes (three digits) are directly measured (see Altmann, Edelmann & de Boer 2003) and are accurate to $\sim 0\overset{\mathrm{m}}{.}1$.

2.4.5 Completeness

In order to test how well our sample represents a complete sample, we determined the cumulative brightness distribution. From Fig. 2.7 we conclude that the number density of our HES sample is linearly increasing for $13\overset{\mathrm{m}}{.}3 \lesssim B \lesssim 14\overset{\mathrm{m}}{.}8$, indicating a reasonable degree of completeness for this range of magnitudes. However, the slope of the distribution is much steeper ($\mathrm{d}\log(N)/\mathrm{d}B = 0.69 \pm 0.02$) than the one determined by Green et al. (1986), i.e. 0.32. The reason for this is unclear.

Table 2.9: Comparison of spectral classifications with previous work. The references of other surveys, discovered our program stars as UV excess object, are additionally included.

star	this work	other	Ref. & name within	other Refs.
HE 2135−3749	sdB	sdB	B92: BPS CS 22948−0017	BPS
HE 2151−3043	DA	DA	B92: BPS CS 29493−0071	BPS, MCT
HE 2154−4143	sdB	sdB	B92: BPS CS 22881−0007	BPS
HE 2213−1734	He-sdO	sdO	B92: BPS CS 22892−0051	BPS
HE 2230−4000	sdB+x			BPS
HE 2326−1022	He-sdO			PHL, GD
HE 2337−2944	sdB	sdB	L00: MCT 2337−2944	MCT, BPS, PHL, GD
HE 2340−2806	sdB	sdB+F/G?	L00: MCT 2340−2806	MCT, PHL, GD, TONS
HE 2341−3443	sdB	sdB	L00: MCT 2341−3443	MCT, SB
HE 2343−2944	sdB	sdB	L00: MCT 2343−2944	MCT, BPS, GD
HE 2349−3135	sdB	sdB	L00: MCT 2349−3135	MCT, PHL, GD, TON
HE 2350−2448	DA			PHL
HE 2350−3026	sdOB	sdO	L00: MCT 2350−3026	MCT, SB, GD
HE 2355−3221	sdB	sdB	L00: MCT 2355−3221	MCT, PHL, GD, TONS
HE 2357−3940	B	B5	R01: SB 939	SB, MCT
HE 2359−2844	sdOB	sdO	L00: MCT 2359−2844	MCT, PHL, TON
HE 0000−2355	sdB			BPS
HE 0001−2443	He-sdB	sdO	L00: MCT 0001−2443	MCT, BPS, SB, PHL, TON
HE 0002−2648	sdB	sdB	L00: MCT 0002−2648	MCT, BPS, PHL, TON
HE 0016−3212	He-sdO	sdO	L00: MCT 0016−3212	MCT, PHL, TONS
HE 0019−2441	sdO	sdO	L00: MCT 0019−2441	MCT, BPS, SB, TON, GD
HE 0021−2326	sdB	DA	L00: MCT 0021−2326	MCT, TONS
HE 0023−2317	HBB	HBB	B01: CSI-23-00238	SB, ECS, TONS
HE 0031−2724	sdOB	sdO	L00: MCT 0031−2724	MCT, ECS, TON, GD
HE 0049−2928	sdB	sdB+F/G	L00: MCT 0049−2928	MCT, BPS, PHL
HE 0049−3059	sdB	sdB	L00: MCT 0049−3059	MCT, BPS, PHL
HE 0123−2808	sdB	sdB	L00: MCT 0123−2808	MCT, GD
HE 0136−2758	sdB	sdB	L00: MCT 0136−2758	MCT, PHL, TON, GD
HE 0151−3919	sdB	HBB/B4	B01: CSI-39-01511	ECS, SB
HE 0238−1912	HBB			PHL
HE 0319−5105	HBB			LB
HE 0324−2529	sdB			BPS
HE 0337−2508	sdB+x			PHL, TON
HE 0340−2420	sdB+x			PHL, TON
HE 0341−2449	sdOB			PHL, TON
HE 0343−4748	sdB	B5/HBB	B01: EC 03436−4748	ECS, LB
HE 0405−1719	sdOB			BPS
HE 0407−1956	sdB	sdB	B92: BPS CS 22173−0033	BPS
HE 0430−5341	HBB			ECS, LB
HE 0442−1908	B			ECS
HE 0521−3914	sdB	sdBV	C01: HE 0521−3914	ECS

Ref.: B92 = Beers et al. (1992), B01 = Beers et al. (2001), C01 = Charpinet (2001), L00 = Lamontagne et al. (2000), R01 = Ramspeck et al. (2001); other Refs.: BPS = Beers, Preston, Shectman survey (Beers et al. 1992), ECS = Edinburgh-Cape Survey (Kilkenny, O'Donoghue & Stobie 1991), GD = Giclas Dwarfs (Giclas, Burnham & Thomas 1980), LB = Luyten Blue survey, MCT = Montreal-Cambridge-Tololo survey (Demers et al. 1990), PHL = Palomar Haro Luyten survey (Haro & Luyten 1962), SB = Slettebak & Brundage survey (Sletteback & Brundage 1971), TON = Tonantzintla survey (Iriarte & Chavira 1957),

Chapter 3

Atmospheric parameters

3.1 Spectral analysis

The stellar atmospheric parameters (effective temperature $T_{\rm eff}$, surface gravity $\log(g)$, and photospheric helium abundance $n_{\rm He}/n_{\rm H}$) were determined by matching synthetic line profiles calculated from model atmospheres to all Balmer (mainly H_β up to H_{10}) and helium (mainly He I $\lambda\lambda$ 4026Å, 4471Å, 5015Å, 5876Å, and He II 4686Å) line profiles present in the observed spectra of all program stars.

3.1.1 Model atmospheres and synthetic spectra

Three different sets of models were used:

1. A grid of metal-line blanketed LTE model atmospheres (Heber et al. 2000). The models are plane parallel and chemically homogeneous and consist of hydrogen, helium, and metals (solar abundances). The synthetic spectra were calculated with LINFOR[1].

   For the spectrum synthesis, line profiles were calculated for the Balmer series of neutral hydrogen (n up to 22) with Stark broadening tables of Lemke (1997b) which uses the unified theory of Vidal et al. (1973). Helium lines were calculated using broadening tables of Barnard, Cooper & Smith (1974), Shamey (1969), and Griem (1974) for He I, and Schöning & Butler (1989) for He II. The metal line blanketing was included by the opacity distribution function (ATLAS6) of Kurucz (1979). The grid covers the area for EHB Stars: $T_{\rm eff} = 11\,000{\rm K} \ldots 35\,000{\rm K}$ in steps of $\Delta T_{\rm eff} = 1\,000{\rm K}$ to $2\,500{\rm K}$; $\log(g/{\rm cm\,s^{-2}}) = 3.50 \ldots 6.50$ in steps of $\Delta \log(g) = 0.25$; $n_{\rm He}/n_{\rm H} = 0.0001, 0.001, 0.01, 0.03, 0.10, 0.33$.

2. A grid of partially line blanketed NLTE model atmospheres (Napiwotzki 1997). The models are plane parallel, chemically homogeneous, and consist of hydrogen and helium. The latest version of the NLTE code from Werner (1986) was used which is based on the Accelerated Lambda Iteration (ALI) of Werner & Husfeld (1985). The following grid was used: $T_{\rm eff} = (27, 30, 32, 35, 37, 40, 45, 50, 55, 60) \times 1000{\rm K}$; $\log(g) = 3.50 \ldots 6.50$ in steps of $\Delta \log(g) = 0.25$; $n_{\rm He}/n_{\rm H} = 3 \cdot 10^{-4}, 1 \cdot 10^{-3}, 3 \cdot 10^{-3}, 0.01, 0.03, 0.1, 0.3$.

[1] LINFOR was originally developed by H. Holweger, M. Steffen, and W. Steenbock at Kiel University. It has been enhanced and maintained by M. Lemke, with additional modifications by N. Przybilla. For a description see: `http://www.sternwarte.uni-erlangen.de/~ai26/linfit/linfor.html`

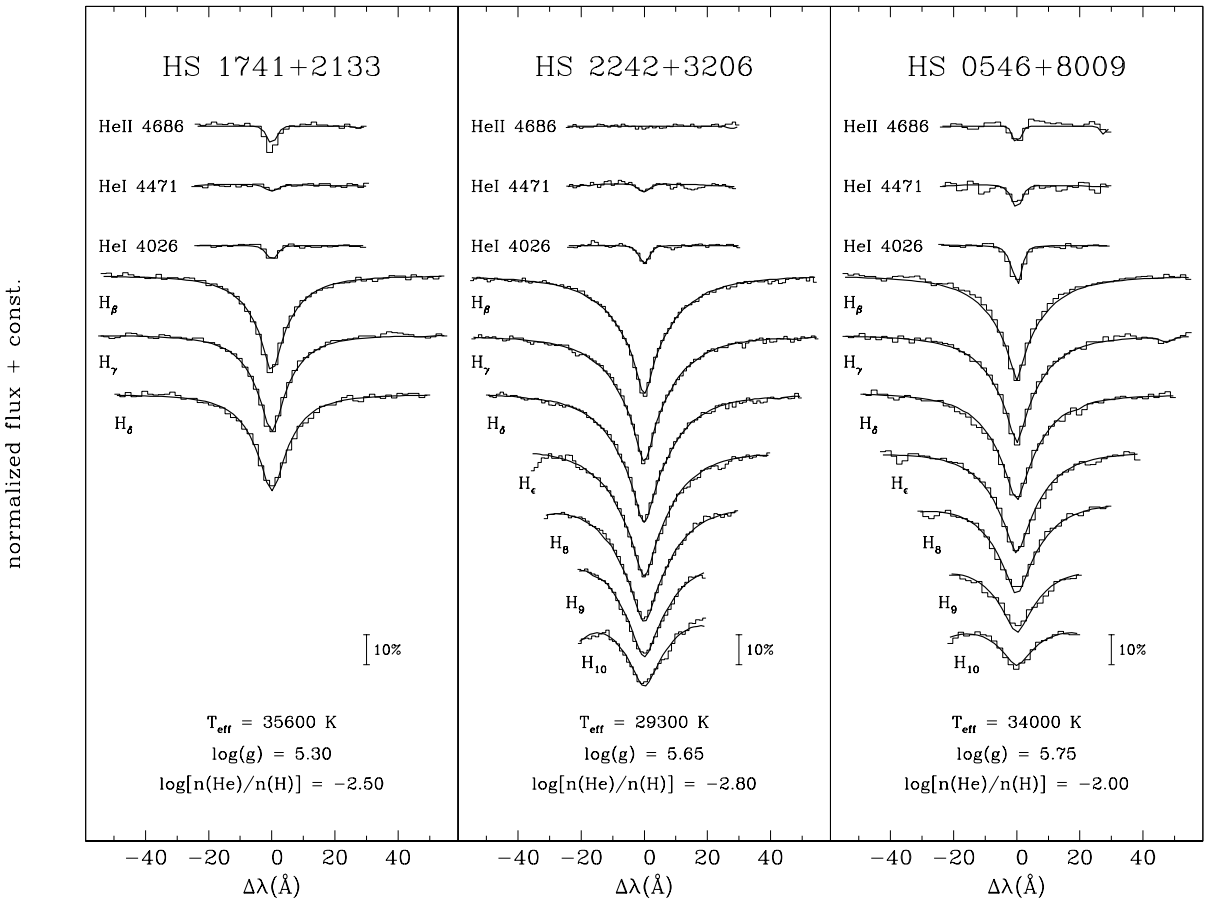

Figure 3.1: Sample fits for three program sdB stars. The observed spectra are plotted as histograms. A detailed discussion of the fit for HS 1741+213 is given in Section 3.1.2.

3. A grid of partially line blanketed NLTE model atmospheres for He-rich ($n_{\rm He}/n_{\rm H} > 0.3$) objects. An extended and updated grid of Dreizler et al. (1990), based on the ALI method, was used. The models are plane parallel and chemically homogeneous and consist of hydrogen and helium. The grid covers: $T_{\rm eff} = (35, 40, 45, 50, 55, 60) \times 1000$K; $\log(g) = 4.0 \ldots 6.5$ in steps of $\Delta \log(g) = 0.5$; $n_{\rm He}/n_{\rm H} = 0.5, 1, 3, 10, 100$.

3.1.2 Fit procedure

The matching of the observed spectra was done by means of a χ^2 fit using an updated procedure of Bergeron et al. (1992) and Saffer et al. (1994) which determines simultaneously the atmospheric parameters. Beforehand all spectra were normalized and the model spectra were folded with the instrumental profile (Gaussians with appropriate width). Rotational broadening was neglected in the fitting procedure for the HQS and HES spectra. Some fit examples are shown in Fig. 3.1.

The numbers of Balmer lines that can be used for the analysis were sometimes limited by insufficient spectral coverage. Hence for several stars spectra are available which cover only three Balmer lines (especially for the HQS stars). In order to check whether the results depend on the number of Balmer lines included in the fit, we compared results based on many Balmer

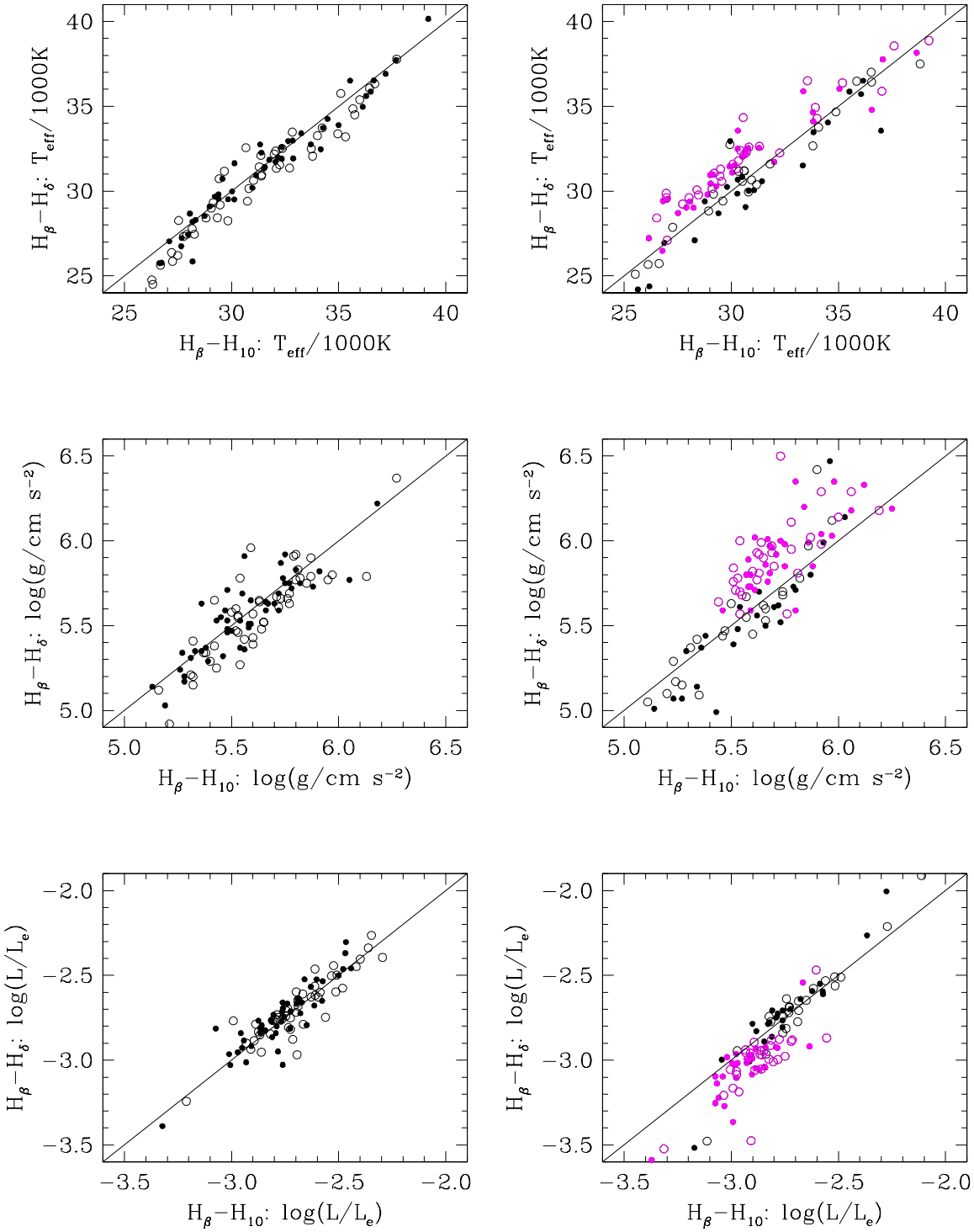

Figure 3.2: Results for $T_{\rm eff}$ (upper panels), $\log(g)$ (mid panels), and $\log(L/L_e)$ (lower panels) based on fits (LTE: filled symbols, NLTE: open symbols) of spectra with many Balmer lines compared to those from three lines for stars with sufficient spectral coverage. The left column represent the results for the HQS stars, the right column for the HES stars (light symbols denote the results of the 1996 run, dark symbols those of the 1999 and 2001 runs).

Table 3.1: Determinations of atmospheric parameters of the sdB stars collected from the 1996 (ESO 1.52m + B&C), 1999 (Danish 1.54m + DFOSC) and 2001 (Danish 1.54m + DFOSC) runs.

	HE 0000−2355				**HE 2341−3443**			
	$T_{\rm eff}$	$\log(g)$	$\log(L/L_e)$	run	$T_{\rm eff}$	$\log(g)$	$\log(L/L_e)$	run
LTE H_β−H_{10}	25 460	5.49	−2.70	1996	28 520	5.49	−2.50	1996
	25 190	5.27	−2.50	1999	26 870	5.36	−2.48	2001
NLTE H_β−H_{10}	25 890	5.46	−2.64	1996	28 790	5.44	−2.44	1996
	25 520	5.24	−2.45	1999	27 260	5.31	−2.40	2001
LTE H_β−H_δ	27 230	5.72	−2.81	1996	29 070	5.57	−2.55	1996
	23 210	5.07	−2.44	1999	26 950	5.37	−2.48	2001
NLTE H_β−H_δ	27 960	5.71	−2.76	1996	29 630	5.56	−2.51	1996
	25 100	5.17	−2.40	1999	27 870	5.37	−2.42	2001

lines to those from three lines for stars with sufficient spectral coverage. For the HQS stars no systematic differences became apparent (cf. Fig 3.2, left column). However, at first glance, for the HES stars the determined $T_{\rm eff}$ and $\log(g)$ are systematically larger for the majority of the spectra using only three Balmer lines (cf. Fig 3.2, right column). A closer inspection revealed that only the results of the data obtained at the 1996 run (ESO 1.52m + B&C) cause this discrepancy (Fig. 3.2, right column, light symbols). The results of the 1999 and 2001 runs (Danish 1.54m + DFOSC) show no dependence of the number of Balmer lines used in the fit process (Fig. 3.2, right column, dark symbols).

Plotting the luminosity (with respect to the Eddington luminosity L_e), derived from gravity and $T_{\rm eff}$:

$$L/L_e = T_{\rm eff}^4/(10^{15.118} \times g) \tag{3.1}$$

(Fig 3.2, lower row) also no dependence of the number of Balmer lines used for fitting became apparent for the HQS stars (Fig. 3.2, lower left plot) and the HES stars of the 1999 and 2001 runs. Again, for the HES stars of the 1996 run (Fig. 3.2, lower right plot), the luminosities determined from the fits including only H_β to H_δ are systematically lower than those obtained from H_β to H_{10}.

A possible reason for the striking behavior of the HES 1996 data could be due to the instrument used. During the spectral analysis the observed line profiles could not be reproduced for the HES data from the 1997 run which was also obtained at the ESO 1.52m telescope equipped with the B&C spectrograph. Inspection of the raw data revealed strange profiles perpendicular to the dispersion direction. The reason could not be identified[2]. However, no such peculiarities in the profiles of the ESO 1996 data became apparent. Two HES stars (HE 2341−3443, and HE 0000−2355) obtained twice at the 1996 run at the ESO 1.52m telescope equipped with the B&C spectrograph, and again later at the Danish 1.54m telescope equipped with the DFOSC instrument, allow a check whether the fit with the lower Balmer lines (H_β to H_δ) or the fit with all available Balmer lines (mostly H_β to H_{10}) is more trustworthy. Table 3.1 compares the results determined for the two stars. As can be seen, the results of the fits using many Balmer lines (H_β to H_{10}) are in considerably better agreement.

Therefore, for the rest of the analysis, we concentrate only on the results of the fits derived from as many Balmer lines as available (mostly H_β to H_{10}).

[2]We excluded all spectra of the HES 1997 observing run of the spectral analysis. Luckily, all stars were re-observed during the 2001 run (see Table A.2).

The fit reproduces the Balmer lines well. For the hottest stars the He I/He II ionisation equilibrium provides an additional temperature indicator. In most cases (e.g. HS 0546+8009, see Fig. 3.1) the fit of the He I and He II lines is consistent with that of the Balmer lines. However, for sdOB stars showing a He II 4686Å line which is comparable or stronger than the He I 4471Å line (i.e. for HS 0048+0026, HS 1051+2933, HS 1741+2133, HS 2156+2215, HS 2333+3927, and HE 2350−3026), the helium ionisation equilibrium indicates a considerably higher effective temperature than from the Balmer lines. The most extreme case is HS 1741+2133 displayed in Fig. 3.1 (left panel). To match the He II line an effective temperature larger by ∼3 000 K would be required. Such a discrepancy has also been observed in the analysis of high resolution spectra of the pulsating sdB star PG 1219+534 (Heber, Reid & Werner 2000). A detailed discussion is given in that paper. In the absence of an explanation for this helium line problem we adopt the parameters from the fit of all lines (H+He).

Our fit process, however, fails in the case of composite spectra. Without knowledge of the flux distributions of the cool companions it is impossible to extract the spectra of the sdB stars. To analyze these binaries, additional spectra and more sophisticated procedures are necessary (see e.g. Aznar Cuadrado & Jeffery 2002).

3.2 Results

Tables B.1, B.2, and B.3 summarize the results of our results for all analyzed program stars.

Statistical errors for the atmospheres which are derived from the fit program are unrealistically small (typically: $\sigma^{\rm fit}_{T_{\rm eff}} \approx 300$K, $\sigma^{\rm fit}_{\log(g)} \approx 0.05$dex, $\sigma^{\rm fit}_{\log(n_{\rm He}/n_{\rm H})} \approx 0.05$dex). The systematic errors that arise from the observations (spectral resolution, S/N), and from the data reduction (flat-field correction, background subtraction, relative flux calibration, and continuum placement) are dominant. The real errors can only be estimated. Individual error estimates for the effective temperatures, the gravities, and helium abundances are given in Tables B.1, B.2, and B.3.

To compare the results determined from LTE and NLTE model atmospheres, I have plotted $T_{\rm eff}$, $\log(g)$, the helium abundance, and the luminosity (calculated from $T_{\rm eff}$ and $\log(g)$, with respect to the Eddington luminosity L_e, see Eq. 3.1). As can be seen from Fig. 3.3, the HQS data (open symbols) has a noticeably larger scatter for all panels, whereas the HES data (filled symbols) is much more consistent with the findings described below. This is probably due to the very inhomogeneous observational HQS dataset (note the large error values for the points lying far outside of the bulk), in contrast to the observational dataset for the HES, which is relatively homogeneous (cf. Sections 2.3.3 and 2.4.3).

- **Effective temperature:**

  For the effective temperature one can see from Fig. 3.3 (top panel):

  - For $30\,000\text{K} \lesssim T_{\rm eff} \lesssim 34\,000\text{K}$:
    There are (almost) no differences between the results determined from LTE or NLTE models. This is in agreement with the results of Napiwotzki (1997) who analyzed the influences of NLTE effects for the analysis of sdB and sdOB stars.
  - For $T_{\rm eff} \gtrsim 34\,000\text{K}$:
    $T_{\rm eff}$ from NLTE models tend to larger values than those from LTE models. This trend is due to increasing NLTE effects with increasing $T_{\rm eff}$, which is also in good agreement with the results of Napiwotzki (1997).

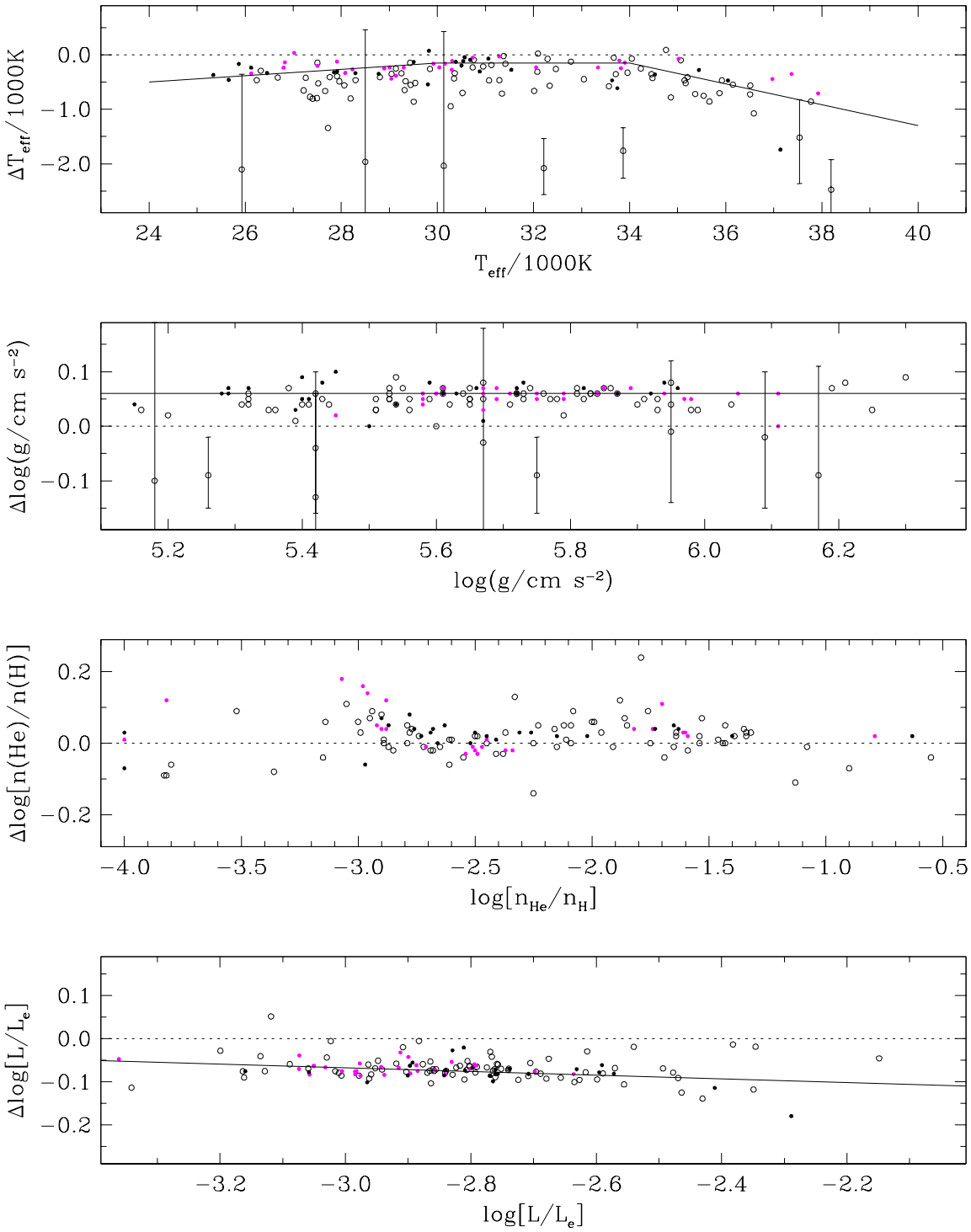

Figure 3.3: Comparison of results determined from LTE and NLTE model atmospheres (LTE−NLTE) for the effective temperature (top panel), the gravity (second panel from the top), the helium abundance (third panel from the top), and the luminosity (lower panel). Open symbols denote the results from the HQS stars, and filled symbols those from HES. The straight lines within the plot for the $T_{\rm eff}$ (top panel) are drawn to guide the eyes of the observer. Whereas, the straight lines drawn for the gravity (second panel from the top), and the luminosity (lower panel) represent the linear regressions to the data. The outliers within all panels are solely from the HQS sample (open symbols) mostly due to bad S/N of the spectra causing large error limits (cf. error bars).

– For $T_{\rm eff} \lesssim 30\,000$K:
$T_{\rm eff}$ from NLTE models are slightly larger than those from LTE models. This is due to the neglect of metal-line-blanketing for the NLTE models used, whereas for the LTE models full metal-line-blanketing is included. However, the effect is negligible compared to the differences of the error estimates (see Tables B.1, B.2, and B.3).

Therefore, we decided to use the results from the NLTE fits for stars with $T_{\rm eff} \geq 35\,000$K. Within the region of $27\,000\text{K} \leq T_{\rm eff} \leq 35\,000$K the mean values of the fits from LTE and NLTE model atmospheres are used. For $T_{\rm eff} \leq 27\,000$K only the results from LTE fits were used.

- **Gravity:**

  For the gravity one can see from Fig. 3.3 (second panel from the top, straight line) that the values determined from LTE fits are systematically larger by 0.06 dex compared to those determined from NLTE fits. We have no clue, what causes this difference.

  The results for the gravities given in Tables B.1, B.2, and B.3) are the mean results of the LTE and NLTE results.

- **Helium abundance:**

  The values drawn from LTE and NLTE models show no systematic differences.

  The results for the helium abundances given in Tables B.1, B.2, and B.3 are the mean results of the LTE and NLTE results

- **Luminosity:**

  For EHB stars the effective temperature and gravity are strongly correlated (cf. Eq. 3.1). Due to the differences discussed above, the luminosity (with respect to the Eddington luminosity L_e) reveals also systematic differences when comparing LTE and NLTE results. On average the difference (LTE−NLTE) is $\Delta \log(L/L_e) = 0.08$ dex, while it is smaller at the low luminosity end (0.05 dex) and larger at the high luminosity end (0.12 dex) (see Fig. 3.3, lower panel, straight line). This is in perfect agreement with the results of Heber, Reid & Werner (2000) who determined a difference of 0.1 dex for their program stars.

- **Metallicity:**

  Another difference between the NLTE and LTE models used is the metal content. NLTE models being metal free and LTE models have solar metal abundances. The influence of metal content on the LTE results was investigated by Heber, Reid & Werner (2000) and found to be quite small at least for the four stars studied. Therefore, we shall assume that the same is true for our program stars.

3.2.1 Bright stars

We have determined the stellar parameters only for those bright stars included in the measurement of metal abundances (see Section 4.1.1).

Due to the problems described in Section 2.2.2 for the normalization process of the echelle spectra, we use exclusively the results of low-resolution spectra, if available. These spectra have been obtained in addition to the high-resolution ones (see Table A.3). For PG 0133+114 and HD 171858 we use the results determined from Morales-Rueda et al. (2003).

However, for PHL 932, HD 205805, LB 1516, and PB 7352 only high-resolution spectra are available to analyze them for their atmospheric parameters. Thus the determined $T_{\rm eff}$ and $\log(g)$ values for these stars should be used with caution.

The stellar parameters are given in Table B.3. Additionally, they are shown in Fig. 3.4 (lower left panel) in a $T_{\rm eff}$–$\log(g)$–diagram. All program stars lie in the region above the ZAEHB with effective temperatures between 20 000K and 40 500K, and logarithmic gravities between 4.8 and 6.0 (cgs). This means that all bright program stars are bona-fide sdB or sdOB stars.

3.2.2 Stars from Hamburg Quasar Survey

The analysis shows that 89 (∼96%) of the 93 selected apparently single HQS stars are bona fide sdB or sdOB stars. One (HS 2229+0910) is considered to be a blue horizontal branch (HBB) star, while three stars (HS 0231+8019, HS 1556+6032, and HS 2131+0349) have atmospheric parameters consistent with those of normal main sequence B stars. One of the sdOB stars (HS 1051+2933) is identified as unusually helium-rich, i.e. exceeding the solar helium abundance. The results for all apparently single program sdB and sdOB stars are shown in Fig. 3.4 (upper left panel) in a $T_{\rm eff}$–$\log(g)$–diagram. As can be seen, within the error limits, all stars lie in a region close to the EHB having temperatures of $20\,000{\rm K} \leq T_{\rm eff} \leq 40\,000{\rm K}$ and gravities of $4.50 \leq \log(g) \leq 6.25$. This means that all apparently single sdB and sdOB stars are consistent with being EHB stars.

3.2.3 Stars from Hamburg ESO Survey

Fig. 3.4 (upper right panel) shows the positions for all apparently single program sdB and sdOB stars, drawn from the HES, in a $T_{\rm eff}$–$\log(g)$–diagram. Due to their position within the diagram, almost all stars can be identified as typically EHB stars. Only one star (HE 0505−2228) lies noticeably below the Zero Age Extended Horizontal Branch (ZAEHB). However, the determined parameters for HE 0505−2228 suffer from very large error limits due to a very bad S/N of the analyzed spectrum (cf. error limits in Table B.2).

3.2.4 Comparison with previous results

Spectroscopic analyses are available in the literature only for five of our HQS program stars, three of our HES, and seven of our bright sdB stars. Table 3.2 compares the parameters determined for our program stars to those collected from literature.

The sample of Bixler, Bowyer & Laget (1991) overlaps with ours for three HQS stars (HS 0039+4302, HS 1641+4601, and HS 2233+2332). Bixler, Bowyer & Laget used a procedure similar to the one described here (fitting of model line profiles to optical spectra) to derive $T_{\rm eff}$ and $\log(g)$. The helium abundance was derived from equivalent widths measurement of the He I 4471Å, 4922Å, and He II 4686Å lines. However, the results given in Bixler, Bowyer & Laget (1991) suffer from very large error limits ($\Delta T_{\rm eff}/T_{\rm eff} \approx 15-20\%$, $\Delta \log(g) \approx 0.4-0.7$dex) probably due to the low resolution and S/N of their spectra, which renders a comparison with our results useless.

One HQS star (HS 0212+1446) overlaps with the sample of Moehler et al. (1990a). The values differ considerably: the effective temperature determined by Moehler et al. is 5 000 K lower and the gravity is 0.9 dex lower than our results. Moehler et al. (1990a) used a three-step-procedure to determine the stellar parameters: The effective temperature has been calculated first from color indices. Keeping the temperature fixed, the surface gravity was obtained by visual

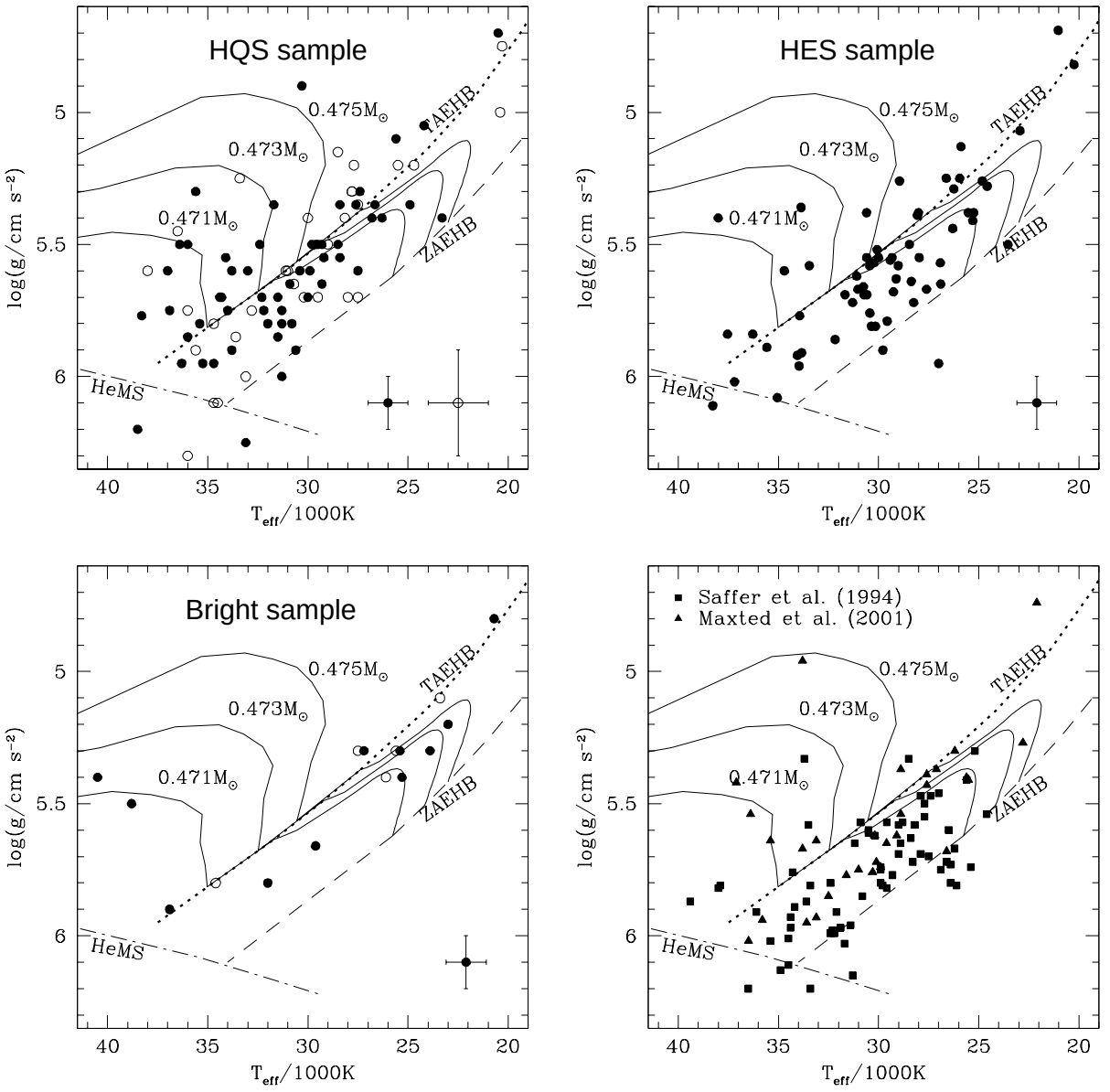

Figure 3.4: Distributions of our HQS (upper left panel), HES (upper right panel), and bright (lower left panel) sdB and sdOB stars in the $T_{\rm eff}$–log(g)–plane. Distribution of the sdB samples of Saffer et al. (1994 filled squares) and Maxted et al. (2001, filled triangles) in the $T_{\rm eff}$–log(g)–plane for comparison purposes (lower right panel, see Section 3.3). HQS stars denoted by open circles have larger uncertainties for the derived temperatures and gravities than the stars denoted by filled circles (see typical error-bars at the lower right side) mostly due to lower S/N and/or spectral resolution. Bright sdB stars denoted by filled circles are drawn from fits of low-res spectra, those denoted by open circles are from fits of high-res spectra. The Helium Main Sequence (HeMS, Paczyński 1972) together with the Zero Age Extended Horizontal Branch for solar metallicity (ZAEHB), the Terminal Age Extended Horizontal Branch for solar metallicity (TAEHB), and evolutionary tracks for extended horizontal branch stars from Dorman, Rood & O'Connell (1993) for three different masses (solar metallicity) are shown for comparison, respectively in all panels.

Table 3.2: Determinations of atmospheric parameters of the sdB stars collected from previous work. The bold face typed values denotes the results presented in this analysis.

star	$T_{\rm eff}$ (1000K)	$\log(g)$ (cgi)	$\log(n_{\rm He}/n_{\rm H})$	Ref & name within
HS 0039+4302	**32.3 ± 0.8**	**5.7 ± 0.1**	**0.005**	
	26.9 ± 4.0	4.9 ± 0.4	0.021	Bi91: Balloon 84041013
HS 0212+1446	**30.6 ± 0.8**	**5.9 ± 0.3**	**0.001**	
	25.0 ± 1.25	5.0 ± 0.2		Mo90: PG 0212+148
HS 1236+4754	**28.4 ± 0.8**	**5.6 ± 0.1**	**0.003**	
	27.9 ± 1.00	5.4 ± 0.2	0.004	Sa94: PG 1236+249
HS 1641+4601	**30.7 ± 0.8**	**5.7 ± 0.2**	**0.022**	
	35.8 ± 6.0	6.2 ± 0.7	0.041	Bi91: Balloon 83600002
HS 2233+2332	**26.6 ± 0.7**	**5.3 ± 0.1**	**0.001**	
	22.4 ± 4.0	5.4 ± 0.5	0.010	Bi91: Balloon 90900003
HE 0000−2355	**25.5 ± 0.4**	**5.4 ± 0.1**	**0.002**	
	25.0 ± 1.3	5.6 ± 0.2	0.005	He86: SB 8
HE 2341−3443	**28.0 ± 0.4**	**5.4 ± 0.1**	**0.001**	
	28.8 ± 1.5	5.4 ± 0.2	0.004	He84: SB 815
HE 2350−3026	**37.5 ± 0.4**	**5.8 ± 0.1**	**0.160**	
	39.8 ± 3.5	6.1 ± 0.4	0.120	Hu81: SB 884
HD 4539	**23.0 ± 0.7**	**5.2 ± 0.1**	**0.005**	
	27.0 ± 1.0	5.5 ± 0.1	0.005	Sa94: PG 0044+097
PHL 932	**34.6 ± 1.5**	**5.8 ± 0.2**	**0.020**	
	35.0 ± 0.9	5.9 ± 0.1	0.030	Na99: PHL 932
PG 0342+026	**25.3 ± 0.7**	**5.4 ± 0.1**	**0.002**	
	26.6 ± 1.0	5.7 ± 0.2	0.004	Sa94: PG0342+026
PG 0909+276	**36.9 ± 0.9**	**5.9 ± 0.1**	**0.158**	
	35.4 ± 1.0	6.0 ± 0.2	0.121	Sa94: PG0909+275
Feige 65	**23.9 ± 0.7**	**5.3 ± 0.1**	**0.002**	
	26.5 ± 1.0	5.6 ± 0.2	0.005	Sa94: PG1233+427
LB 1516	**26.1 ± 1.5**	**5.4 ± 0.2**	**0.002**	
	26.3 ± 1.3	5.7 ± 0.2	0.003	He86: LB1516
CD−35° 15910	**27.5 ± 1.5**	**5.3 ± 0.2**	**0.001**	
	28.8 ± 1.5	5.4 ± 0.2	0.004	He84: SB 815

Ref.: Bi91 = Bixler, Bowyer & Laget (1991); He84 = Heber et al. (1984); He86 = Heber (1986); Hu81 = Hunger et al. (1981); Mo90 = Moehler et al. (1990a); Na99 = Napiwotzki (1999); Sa94 = Saffer et al. (1994).

comparison of model line profiles with optical spectra of one or more Balmer lines (mainly H_γ). Finally, the helium abundance was derived by measuring the equivalent width of the He I 4471Å line. Saffer et al. (1994), who discovered similar differences comparing their results with that of Moehler et al. (1990a), argue that the calibration of the Strömgren colors used by Moehler et al. (1990a) is inappropriate for sdB stars and causes larger systematic errors. This view is supported by investigations of Napiwotzki, Schönberner & Wenske (1993).

The sample of Saffer et al. (1994) shares five program stars (one HQS, and four bright sdB stars) with ours. Saffer et al. used a procedure similar to the one described here (fitting of model line profiles to optical spectra) to derive the atmospheric parameters. As can be seen from Table 3.2, our results for HS 1236+4754, PG 0342+026, and PG 0909+276 are in good agreement with the results of Saffer et al. (within the given error limits). However, the results for the remaining two stars differ noticeably: For HD 4539 Saffer et al. resulted in a $T_{\rm eff}$ 4 000K larger than our value, and a $\log(g)$ which is also 0.3 dex larger than our result. Only the helium abundance is in perfect agreement. For Feige 65 we determined a $T_{\rm eff}$ of $\sim$ 2 500K lower and a $\log(g)$ 0.3 dex lower than the results of Saffer et al.

Four stars (two HES, and 2 bright sdB stars) overlap with the samples of Heber et al. (1984), and Heber (1986). The same procedure to determine the parameters was used by Heber et al. (1984), and Heber (1986): the effective temperature has been determined from FUV flux distributions measured from International Ultraviolet Explorer (IUE) spectra. Afterwards, keeping the temperature fixed, the surface gravity was obtained by visual comparison of model line profiles with optical spectra of one or more Balmer lines (mainly H_β and H_γ). The helium abundance was derived by measuring the equivalent width of the He I 4471Å line. The results for HE 0000−2355, HE 2341−3443, LB 1516[3], and CD−35° 15910 are in very good agreement with ours (within the given error limits).

The sample of Hunger et al. (1981) overlaps with ours for one HES star (HE 2350−3026). Hunger et al. determined the atmospheric parameters using equivalent width measurements of H_γ, He I 4471Å, 4713Å and He II 4686Å using NLTE model atmospheres. Their results are, within the given error limits, in good agreement with ours.

There remains one bright sdOB star of our sample that can be compared with the results of another group. Napiwotzki (1999) determined the stellar parameters for PHL 932 to be in perfect agreement with ours, using the same NLTE models and fit procedures as we do.

3.3 Constraints on the evolution of sdB stars

Due to the still unknown origin of the sdB stars, is it worthwhile to compare the results of our analysis with theoretically predictions of evolutionary models.

But before discussing different models, first we should check the evolutionary status of our program stars.

3.3.1 Evolutionary status

In the gravity versus effective temperature plane (Fig 3.4), our confirmed sdB and sdOB stars lie in a region close to the EHB. However, the HQS and the bright stars seem to have a tendency to

[3]Note that for LB 1516 we compared the values determined from our high-res spectra. The good agreement with the results of Heber (1986) shows, that the normalization process, described in Section 2.2.2, seems to work fine (at least for LB 1516).

cluster near the Terminal Age Extended Horizontal Branch (TAEHB) when the He-core burning diminishes and the phase of helium shell burning starts. But according to the evolutionary life times, most stars should be found closer to the ZAEHB, like the HES stars, or like seen in Heber (1986, Fig. 6), Saffer et al. (1994, Fig. 5), and Maxted et al. (2001, Fig. 2). If we compare our results (Fig 3.4) to that of Saffer et al. (1994) who analyzed 68 EHB stars and/or Maxted et al. (2001) (Fig. 3.4, lower right panel) who analyzed 36 EHB stars for atmospheric parameters, a systematic difference for the HQS and bright stars can be suggested. Saffer et al. (1994) even found some sdB stars (mostly at low temperature, $T_{\rm eff}$ = 25 000 to 27 000K) to lie below the ZAEHB. Because only one HQS star is common to both studies (both sets of parameters agreed very well, see Section 3.2.4), a direct comparison was possible for this case only. We can, however, compare the samples in a global sense using the cumulative luminosity functions. In Fig. 3.5 (upper part) we plot these functions for our samples and those of Saffer et al. (1994) and Maxted et al. (2001). The luminosity is expressed in units of the Eddington luminosity (Eq. 3.1). Additionally the positions of the ZAEHB and the TAEHB are indicated. Since the metallicity of the stars is unknown, we have plotted models for various metallicities ranging from [M/H]=−2.22 to 0.00 (Dorman, Rood & O'Connell 1993). Note that the position of the TAEHB is model-dependent, because poorly understood processes such as semi-convection and convective instabilities (breathing pulses, Castellani et al. 1985) play a role.

As can be seen from Fig. 3.5 (upper part), the overall shape of the cumulative luminosity functions are similar for all five samples when the considerably smaller number of stars for the bright star sample and the sample of Maxted et al. (2001) is taken into account. However, there is an offset of about 0.2 dex in luminosity between the sample of Saffer et al. (1994) and the HQS and bright star samples. On the other hand, the relations for the HES and Maxted et al. (2001) samples are in better agreement. But, remembering the problems concerning the HES 1996 run, we splitt the HES sample into two subsamples. Fig. 3.5 (lower part) shows, that the results drawn from the 1996 run (ESO 1.52m + B&C, which causes a lot of trouble in Section 3.1.2) seem to lie perfectly within the region theory predicts for sdB stars (closer to the ZAEHB), whereas the results from the other runs (Danish 1.54+DFOSC) seem to agree with the results of the HQS sample (closer to the TAEHB). It is striking, that the results for all stars (except the somewhat dubious results from the 1996 ESO run) of our analysis seem to lie closer to the TAEHB, whereas the results of other groups lie closer to the ZAEHB.

Possible reasons for the discrepancy are different observations, the different synthetic spectra used in the analysis, or both. Maxted et al. (2001) and our study is based on the same grid of NLTE models for stars hotter than 27 000K and metal line blanketed LTE models for the cooler ones, whereas Saffer et al. (1994) used metal-free LTE models for all stars. The observations of Maxted et al. (2001) are of considerably higher spectral resolution than that of Saffer et al. (1994) and ours, and on average have a better S/N than our data. In addition, the wavelength coverage of the observations also varies.

From our investigation presented in Section 3.2, we determined the differences in luminosities, using synthetic spectra calculated from different sets of model atmospheres, to be larger for NLTE models by about 0.1 dex than metal line blanketed LTE models. Therefore about half of the observed offset between the cumulative luminosity functions of Saffer et al. (1994) and ours can be traced back to NLTE effects, but an 0.1 dex offset remains unexplained.

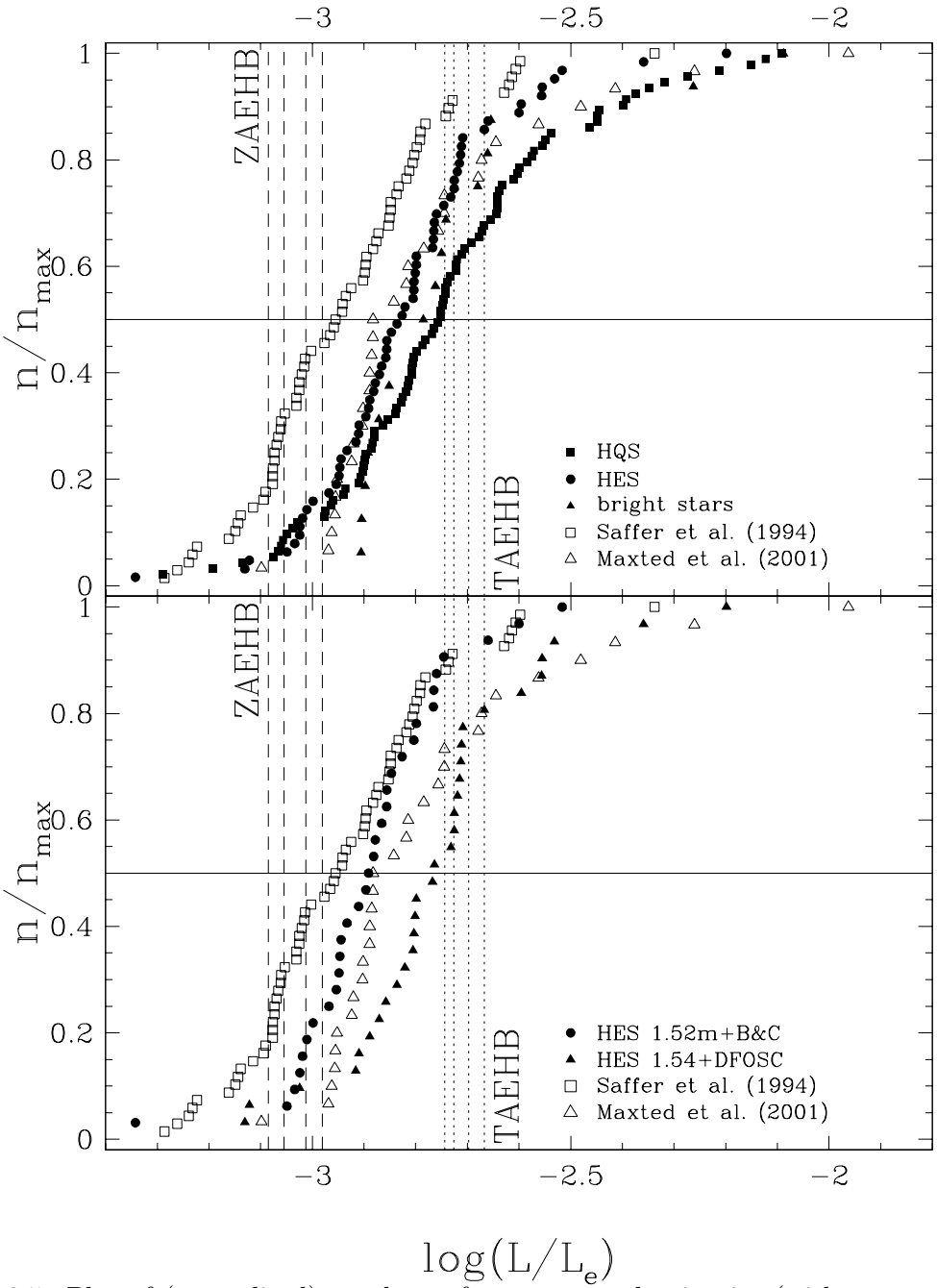

Figure 3.5: Plot of (normalized) numbers of stars versus luminosity (with respect to the Eddington luminosity L_e, see Eq. 3.1).
Upper part: Filled squares denote the results for the HQS stars, filled circles those for the HES stars, and filled triangles the results for the bright sdB stars. Lower part: Filled circles denote the results for the HES stars drawn form observations with the ESO 1.52m telescope equipped with the B&C spectrograph, and filled triangles the results from the Danish 1.54m telescope equipped with the DFOSC instrument.
Additionally are plotted the results of Saffer et al. (1994, open squares), and Maxted et al. (2001, open triangles). The dashed vertical lines denote the ZAEHB, and the dotted vertical lines the TAEHB for metalicities of [M/H]=0.00, −0.47, −1.48, and −2.22, respectively, from the left to the right (Dorman, Rood & O'Connell 1993).

3.3.2 Evolutionary scenarios

We see that sdB stars can be identified with models for the EHB. How stars evolve to the EHB configuration, however, is still under discussion.

Several attempts have been made to explain the processes which lead to a star consisting of a helium-burning core with a canonical mass of $M_{\rm core} \approx 0.5 M_{\odot}$ surrounded by a thin hydrogen-rich envelope ($M_{\rm env} < 0.02 M_{\odot}$, i.e. EHB star, Heber 1986, Saffer et al. 1994).

Single star evolution

- D'Cruz (1996) suggests a strong stellar wind near the tip of the first giant branch. Blowing away the envelope of a red giant, a star with a helium core surrounded by a thin hydrogen rich envelope remains. If the helium ignites within the core, a single sdB star results.
- De Marchi & Paresce (1996) proposed the formation of a sdB star due to envelope stripping of a red giant star by close encounters in densely populated stellar environments.
- Sweigart (1997) has studied the evolution of globular-cluster stars. Internal rotation of a star can lead to helium mixing processes, which can substantially increase the helium abundance in the envelope. As a consequence, enhanced mass loss along the first giant branch may produce a single sdB.

Close binary evolution

However, a significant fraction of sdB stars are known to have composite spectra (e.g. Ferguson, Green & Liebert 1984, Allard et al. 1994, Theissen et al. 1993, 1995, Jeffery & Pollacco 1998, and others), leading to suggestions of a binary fraction between 50% and 100%. In addition, several single-lined binary sdB stars have been identified from variable Doppler line shifts resulting from orbital motion (Saffer, Livio & Yungelson 1998, Maxted, Marsh & North 2000, Maxted et al. 2001, and Green, Liebert & Saffer 2001, see also Chapter 5). Maxted et al. (2001) estimated from their sample that at least 2/3rd of all local single sdB stars are close binaries, with periods of hours up to days.

The channels that can produce sdB stars from close binary systems recently have been elucidated in detail by Han et al. (2002, 2003):

- The first channel is the *common envelope (CE) ejection channel* which can be divided into two others. The *first CE ejection channel*, in which the initially more massive star of the binary experiences mass transfer when it is on the red giant branch. This results in the formation of a CE, both stars are spiral in and consequently the ejection of the CE leading to the formation of a very close binary. If the core of the giant star still ignites helium it becomes a sdB. The final result is therefore a sdB star in a short period binary with a main sequence (MS) companion. In the *second CE ejection channel*, the companion to the giant star is already a white dwarf (WD). This channel can lead to shorter orbital periods because a WD has a smaller radius than a MS star and can penetrate deeper into the CE without merging. SdB stars that form through this second channel have a wider range of orbital periods and their companions are WDs.
- The second channel is the *stable Roche lobe overflow (RLOF) channel* and involves stable mass transfer where a low-mass giant fills its Roche lobe on the red giant branch and loses most of its envelope as a result of stable RLOF.

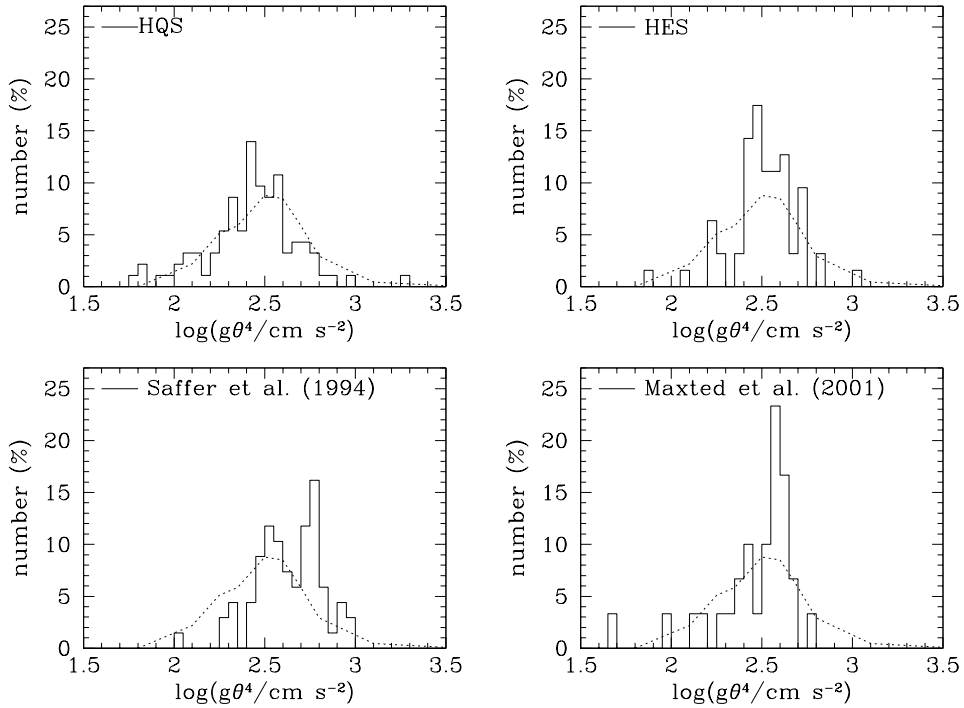

Figure 3.6: Distributions of $\log(g\theta^4)$ (g is the surface gravity, and $\theta = 5040\mathrm{K}/T_{\mathrm{eff}}$) for our HQS, and HES samples. Additionally are plotted the samples of Saffer et al. (1994), and Maxted et al. (2001). The dotted curve denotes evolution calculations from Han et al. (2003, best fit model including GK selection effect).

- The third channel is the *merger channel*, i.e. sdB stars can be formed by the merger of two helium WDs if the mass is sufficient to burn helium in the core. Consequently the resulting sdB should not have a companion and be non-RV variable.

In Fig. 3.6 we compare our results for the HQS and HES sdB stars to the calculations of Han (2003). As can be seen, the simulation set #2 of Han (2003, best fit model for the data of Maxted et al. 2001, and Morales-Rueda et al. (2002, 2003) including the GK selection effect) matches our distributions of $\log(g\theta^4)$ ($\theta = 5040\mathrm{K}/T_{\mathrm{eff}}$) for the HQS and HES sdB stars well.

However, we could not decide whether the close binary evolution scenario is the key to understand the origin of sdB stars. Further observations for all apparently single sdB program stars are important to search for possible companion stars (see e.g. Chapter 5).

3.4 Constraints on stellar pulsations

Recently, several sdB stars have been found to be pulsating (termed EC 14026 stars, see Koen et al. 1998 for a review), defining a new instability strip in the HR-diagram. The study of these pulsators offers the exciting possibility of exploiting the full power of asteroseismology to investigate the sdB phase of stellar evolution. The existence of pulsating sdB stars was predicted theoretically by Charpinet et al. (1996), who uncovered an efficient driving mechanism due to an opacity bump associated with iron ionization in such models. However, in order to drive the pulsations, iron needed to be enhanced in the appropriate subphotospheric depths.

Diffusion could result possibly the required iron enhancement. In a subsequent study, Charpinet et al. (1997) calculated iron abundances from the equilibrium between gravitational settling and radiative levitation and found that, indeed, iron is enriched in the driving regions. Even more encouraging was the agreement of the observed and predicted instability strip. The prediction of Charpinet et al. (1997) that sdB stars in the temperature range of 29 000K $\leq T_{\rm eff} \leq$ 36 000K should pulsate is very well confirmed by subsequent spectroscopical analyses of the EC 14026 stars (Heber, Reid & Werner 2000, Østensen et al. 2000a, 2001b, Dreizler et al. 2002, Silvotti et al. 2002). However, in view of the He puzzle it remains to be shown that the equilibrium calculations reproduce the iron abundances correctly.

A puzzle in understanding the EC 14026 stars is the fact that, as suspected by Billères et al. (1997), now demonstrated unquestionably by Koen et al. (1999), the region of the $T_{\rm eff}$–$\log(g)$ plane occupied by the pulsators also includes non-pulsators. Fontaine & Chayer (1997) suggest: "... two stars with similar values of $\log(g)$ and $T_{\rm eff}$ may suffer from mass loss at different rates. In that case, one star (with enough iron in its reservoir) could pulsate, while the other (with a depleted reservoir) could be stable."

First attempts to find more pulsating sdB stars included all known sdB stars, most of them without determination of the atmospheric parameters, especially the effective temperature. Due to the large number of stars needed to be observed, and for which in addition the effective temperature was not known for most of them, the chance to detect a pulsating sdB star is low. Therefore, only few EC 14026 stars were found.

A more successful strategy would have been to determine the atmosheric parameters of a large numer of sdB stars first, and afterwards select all stars lying within the instability strip predicted by Charpinet et al. (1997) to investigate them for pulsations. We used this strategy. The majority of our program stars lie in the temperature range where non-radial pulsations occur. We initiated a collaboration with two groups in Norway and Italy in 1999 to search for pulsating sdB stars in our sample. All of our HQS sdB stars will be observed for light variations. Up to June 2002, about 70 HQS sdB stars had been observed and nine (HS 0039+4302, HS 0444+0408, HS 0702+6043, HS 0815+4243, HS 1824+5745, HS 2149+0847, HS 2151+0857, HS 2201+2610, and HS 2303+0152) were found to be pulsating (Østensen et al. 2000a, 2001b, Dreizler et al. 2002, Silvotti et al. 2002). This represents about one pulsator within ten sdB stars. It also means that about one third of all known sdBV stars discovered so far have been drawn from our investigation presented here.

However most of all sdB stars lying within the sdB instability strip do not pulsate (see Fig. 3.7). A possible reason is the different metal content in the atmospheres of pulsating sdB stars, compared to non-pulsators. This suggestion will be discussed in Section 4.3.2.

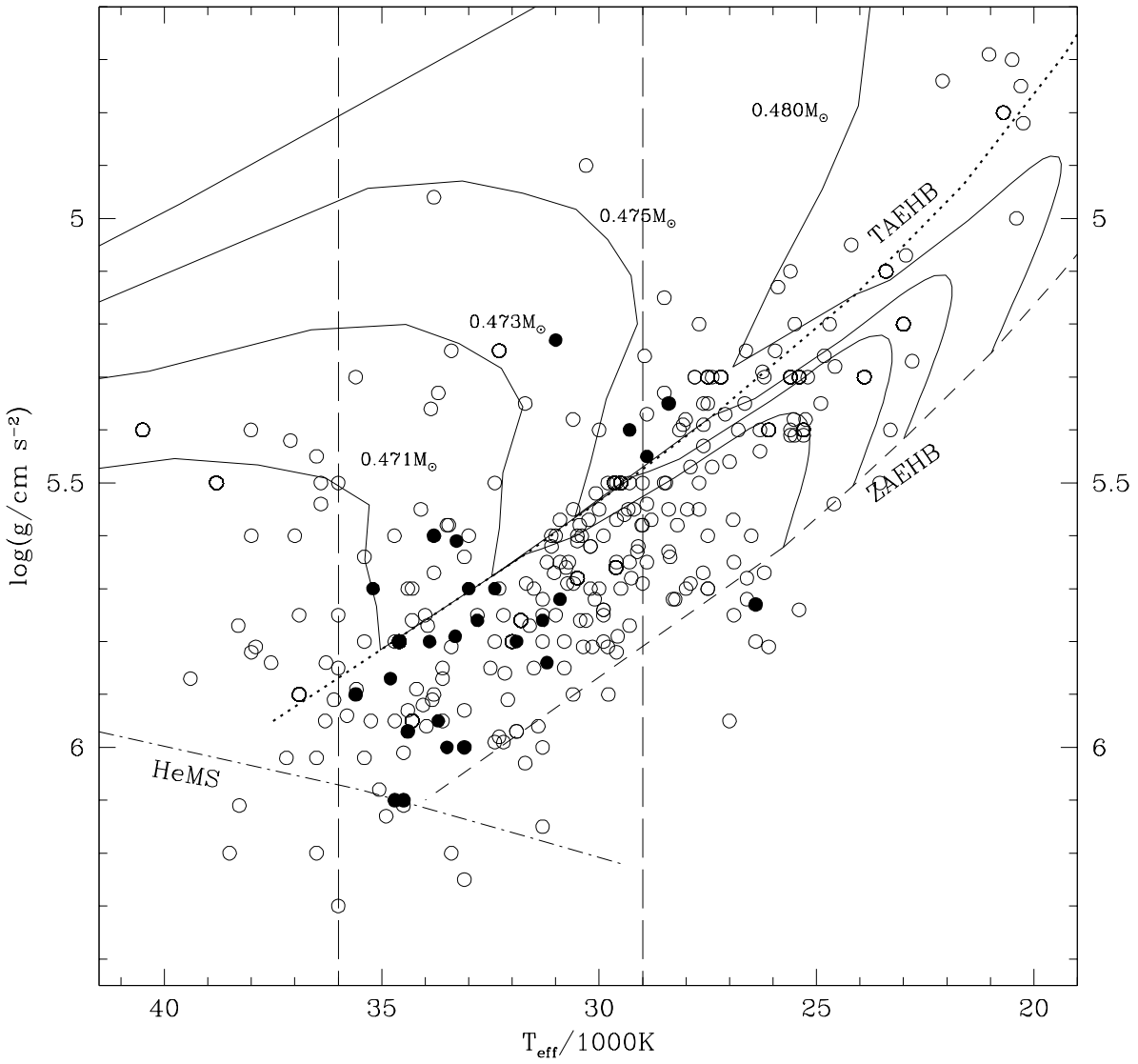

Figure 3.7: Distribution of our HQS, HES, and bright sdB sample together with the results of Saffer et al. (1994) and those of Maxted et al. (2001) in the $T_{\rm eff}$–log(g)–plane (open symbols). The filled symbols denote the position of all known pulsating sdB stars. The Helium Main Sequence (HeMS, Paczyński 1972) together with the Zero Age Extended Horizontal Branch for solar metallicity (ZAEHB), the Terminal Age Extended Horizontal Branch for solar metallicity (TAEHB), and evolutionary tracks for extended horizontal branch stars from Dorman, Rood & O'Connell (1993) for four different masses (solar metallicity) are shown for comparison. The region bracketed by the vertical long dashed lines, denotes the instability strip, predicted by Charpinet et al. (1997).

Chapter 4

Chemical composition

Helium abundances

Spectral analyses revealed that for sdB stars helium (He) is typically deficient by more than one order of magnitude, but there is a wide spread from solar $n_{\rm He}/n_{\rm H}$ to stars with $n_{\rm He}/n_{\rm H} < 10^{-4}$. No obvious correlation between He abundance and the effective temperature or gravity have been found before. These He abundances are still much too large to be accounted for by diffusion (the balance between radiative levitation and gravitational settling, Michaud et al. 1989) which predicts He abundances **lower** by two orders of magnitudes than the average observed He abundance of $n_{\rm He}/n_{\rm H} \approx 10^{-2}$ (see Fontaine & Chayer 1997). Since the diffusion time-scale is small (10^4 yrs) compared to the EHB lifetime (10^8 yrs), **no** He should be visible in the radiative atmospheres: the puzzle here is not so much the low helium abundance but an excess in the sdB atmospheres. An explanation invoking a stellar wind has frequently been suggested. Realistic calculations have been carried out by Fontaine & Chayer (1997) and Unglaub & Bues (2001). They can explain the observed He abundances if a mass loss rate of 10^{-14} to 10^{-12} $M_\odot$/yr is adopted.

We will present the helium abundances for all program sdB stars in Section 4.3.1. A detailed discussion can be found in that section.

At first, we will concentrate on the metal abundances.

Metal abundances

Our knowledge about metal abundances of subdwarf B stars is poor. Early studies were mostly based on IUE UV spectra and restricted to C, N, and Si abundances (e.g. Lamontagne et al. 1985, 1987, see also Heber 1991b for a review). More complete studies for a few stars have been reported recently, based on optical spectra (Edelmann et al. 1999, Heber, Reid & Werner 1999, 2000) and FUSE FUV spectra (Ohl, Chayer & Moos 2000). The resulting abundance patterns are puzzling and large differences from star to star were found; e.g. carbon is strongly deficient in Ton S-227 (by a factor of 20 000 with respect to the sun), while it is depleted by only a factor of 16 in Feige 65 (Lamontagne et al. 1985).

There is now general consensus, that the peculiar abundance patterns are due to diffusion. Although in some cases diffusion calculations (e.g. Michaud et al. 1989, Bergeron et al. 1988, Ohl et al. 2000, Unglaub & Bues 2001) lead to coincidences between predicted and observed values, it has not been possible to reproduce all abundances simultaneously. In addition, the available sample of stars with well determined abundances is far too small to confine diffusion

theory.

4.1 Spectral analysis

We present here the analysis for 16 EHB stars drawn from four observing runs obtained in September 1998, July 1999, and Jan/Feb 2000 with the 2.2m telescope equipped with the FOCES instrument at the DSAZ on Calar Alto, Spain (PG 0001+275, HD 4539, PHL 932, PG 0133+114, PG 0342+026, UVO 0512−08, PG 0909+276, Feige 65, UVO 1735+22, UVO 1758+36, and BD+48° 2721), and in September 2000 with the ESO 1.52m telescope equipped with the FEROS instrument at ESO on La Silla, Chile (HD 171858, HD 205805, LB 1516, PB 7352, and CD−35° 15910).

For the summary of the observations and reduction of the spectra see Section 2.1. We coadded all spectra obtained for each stars after shifting them to laboratory wavelengths to enhance the S/N for the analysis.

4.1.1 Metal abundances

LTE abundances were derived for all metals from measured equivalent widths using the classical curve-of-growth method.

The equivalent widths were measured employing nonlinear least-squares Gaussian fitting routines in ESO-MIDAS with the central wavelength, the central intensity, and the full-width-at-half-maximum as adjustable parameters. For metal lines located in the wings of Balmer or helium lines an additional Lorentzian function is used to describe the line wings of the latter. The resulting equivalent widths measured for all stars are given in Table C. Thereafter, we generated model atmospheres, using the atmospheric parameters determined in Section 3.2.1, and solar metal abundances with the ATLAS9 code of Kurucz (1992). From these models we calculated curves-of-growth for the observed metal lines, from which abundances were derived. Blends from different ions were omitted from the analysis. Finally, the abundances were determined from a detailed spectrum synthesis (using LINFOR, see Section 3.1.1) for all lines measured before. The atomic data for the analysis were taken from the list of Wiese et al. (1996) for the CNO elements, from Kurucz (1992) and Ekberg (1993) for Fe, and for all other elements from the table of Hirata & Horaguchi (1995).

We found that for some multiplets of a given ion (e.g. S II multiplet #14 and #15, see Section C) the results differ for large amounts ($\sim$ 0.6 dex) from those determined for other multiplets (see Fig. 4.1). This may be due to wrong data taken from the literature ($\log(gf)$ values, cf. Section C), or due to NLTE effects which are not accounted for in our analysis. Therefore, we discarded those multiplets from the analysis.

The abundances (and errors) given in Tables 4.1 to 4.16, and plotted in Figs. 4.7 to 4.22 (with respect to solar values) are mean (statistical rms) values, determined from all lines measured (except the discarded multiplets, see above) for all individual ions, respectively.

However, for some elements (e.g. Mg II) only one spectral line for a given ion can be identified. Due to trustworthy atomic data (especially for Mg II) we use the resulting abundance and adopt an error of ±0.2 dex for the 'normal' sdB stars. For the peculiar sdB stars we adopt an error of ±0.5 dex.

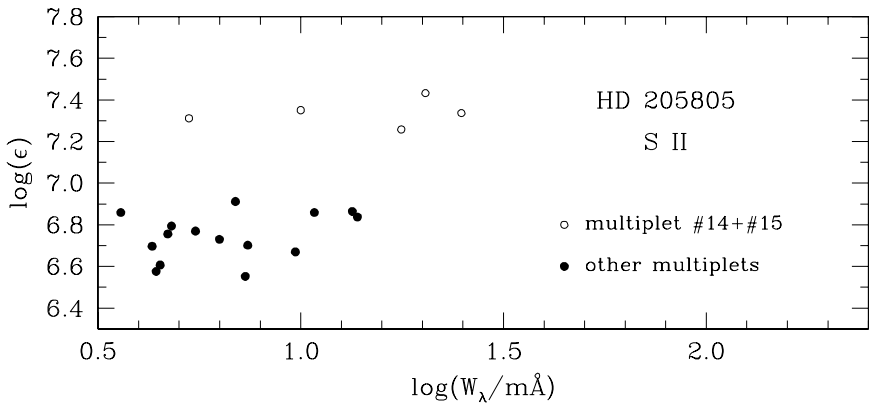

Figure 4.1: Sulfur abundance determined from individual S II lines for HD 205805. Note the discrepancy of the abundances determined from the multiplets #14, and #15 to those of other multiplets.

4.1.2 Microturbulences

The determination of metal abundances is closely connected to measurements of microscopically turbulences within the atmosphere of a star. This microturbulence ξ broadens the spectral lines due to the Doppler effect, and can be derived if a sufficient number of lines of one ion is measured over a wide range of line strengths. Lines, which are on the flat part of the curve-of-growth, are very sensitive to a change of ξ. The microturbulence is, besides the effective temperature and the gravity, a free parameter used for calculating the curve-of-growth for all ions. By varying this parameter, a different slope of the linear regression fitted to the determined abundances of the individual lines versus the equivalent widths results.

Fig. 4.2 exemplarily demonstrates the sensitivity of ξ for a change from 0 to 5 km/s for the N II lines of HD 205805. A vanishing slope of the linear regression is the aim, to determine the value of ξ (cf. Figs. 4.2 and 4.3).

In our program stars N II, O II, and Fe III lines are most suitable to determine ξ, since the numerically dominant metal lines are from these ions (see Section 4.2.1). The resulting microturbulences are generally low, in line with previous analyses of sdB stars.

4.1.3 Ionisation equilibria

In some of the stars some chemical elements are detected in different states of ionisation (mostly S II and S III). This allows an independent check of the effective temperature derived in Section 3.1 from Balmer and helium lines.

4.1.4 Projected rotational velocities

The rotation of a star causes a broadening of the spectral lines due to the Doppler effect. Because the rotational axis of a star in most cases is not perpendicular to the line of sight, we can only measure the projected rotational velocity $v \sin(i)$, with the unknown inclination angle i. The projected rotational velocity can be measured by comparing synthetic line profiles, calculated for the given atmospheric parameters ($T_{\rm eff}$, $\log(g)$, element abundance) of a star folded with

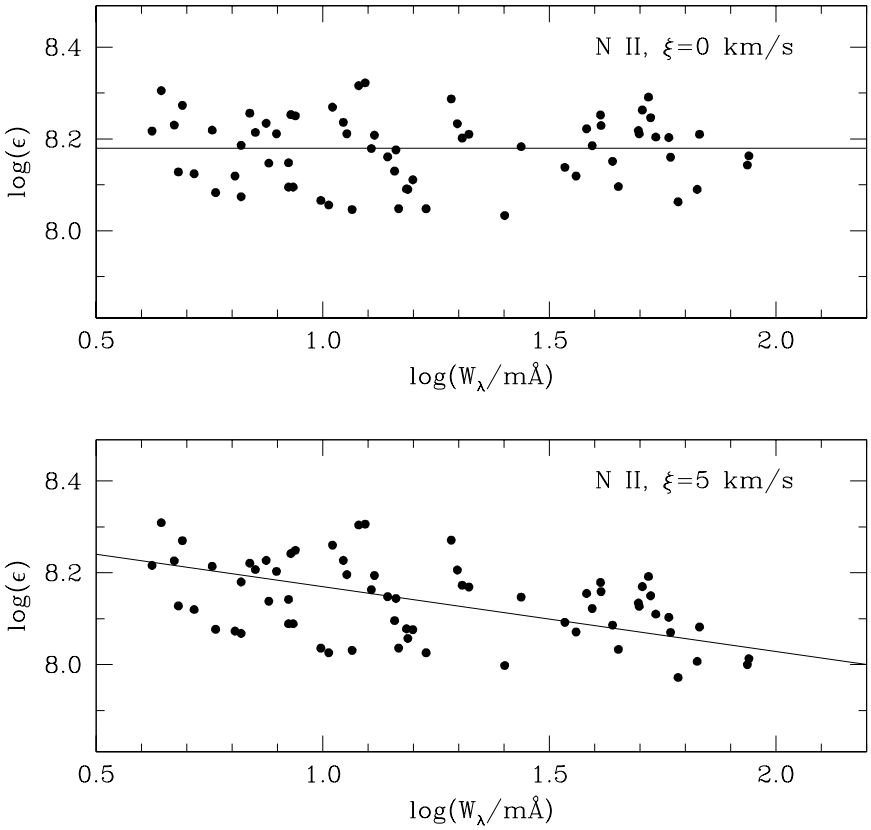

Figure 4.2: Determination of the microturbulence ξ for HD 205805. Value of $\xi = 0$ km/s (upper part), and $\xi = 5$ km/s (lower part) are applied. For $\xi = 0$ km/s the slope of the regression line vanishes as expected if the choice of ξ is correct.

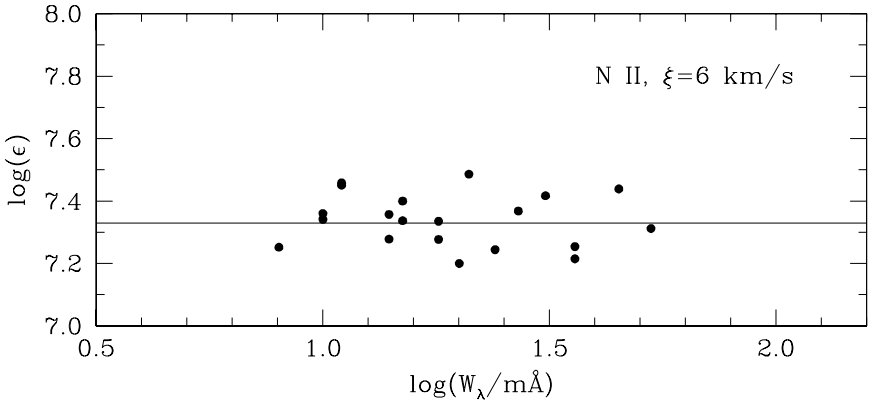

Figure 4.3: Determination of the microturbulence ξ for CD$-35°$ 15910. A value of $\xi = 6$ km/s is applied.

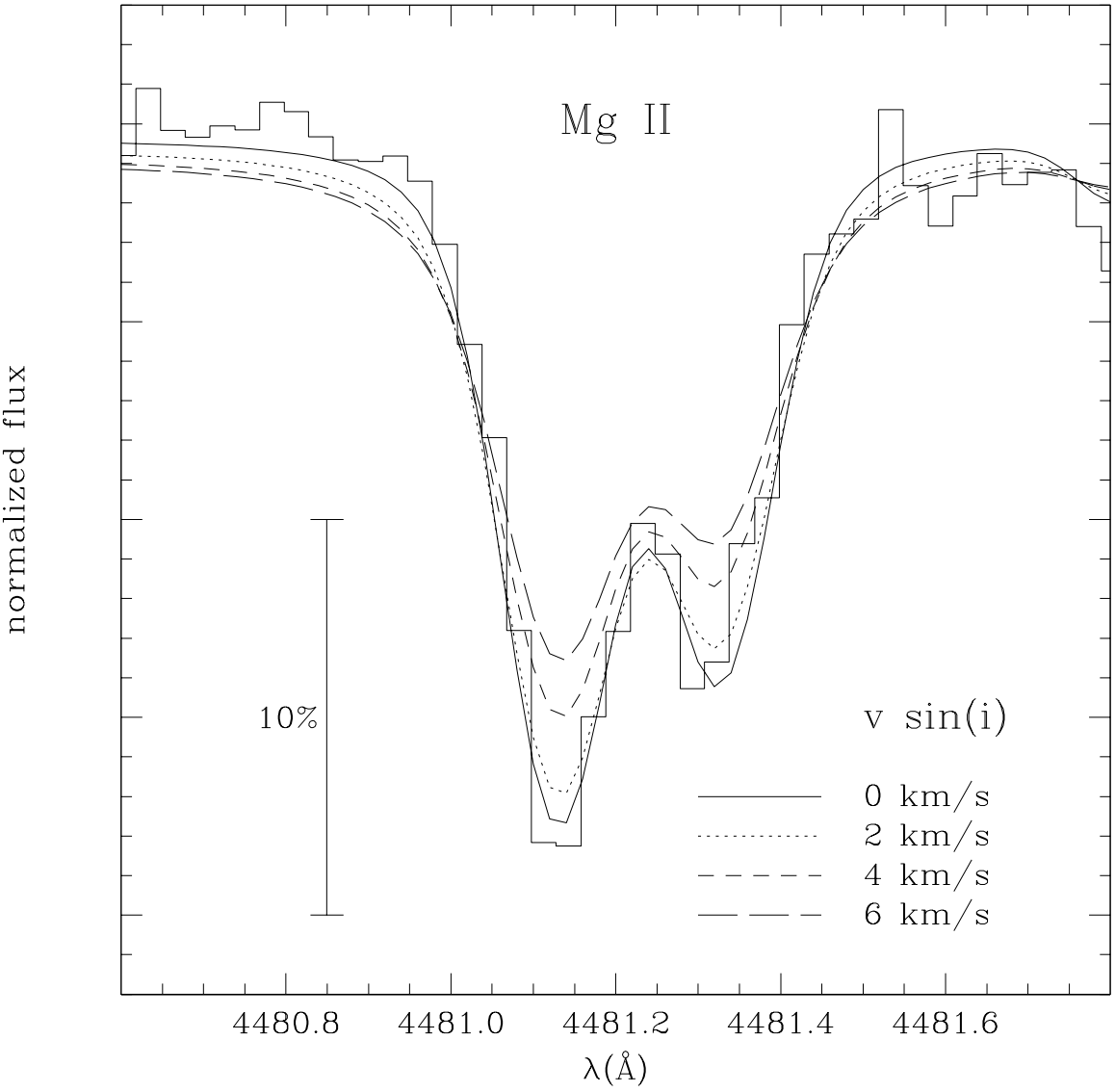

Figure 4.4: Mg II doublet at 4481.13Å, and 4481.33Å calculated for four different projected rotational velocities of $v \sin(i) = 0$, 2, 4, and 6 km/s (straight line, dotted line, dashed line, long dashed line, respectively), compared to the observed line profile of HD 205805 (histogram).

an adopted rotational velocity, with the observed line profiles. The Mg II doublet at 4481.13Å, and 4481.33Å, is most suitable for this purpose. The lines are very narrow, and therefore very sensitive to rotational broadening (see Fig. 4.4). If the doublet is resolved into two components, the star is likely to be a slow rotator. A few program stars, however, do not show the magnesium doublet. In these cases $v \sin(i)$ is determined mostly from lines of N II and O II because for those the quality of the atomic data is excellent and these lines are best reproduced by the model spectrum calculated with the abundances derived.

4.2 Results for individual objects

From the spectra, we can identify two distinct groups:

- 'normal' sdB stars

  Most of our program stars show, as typical for early type B stars, few and very weak metal lines in their spectra, mostly due to ions of carbon, nitrogen, oxygen, magnesium, aluminum, silicon, sulfur, argon, and iron (see e.g. Fig. 4.5).

- peculiar sdB stars

  Three stars, however, show many more lines than the other ones. First of all, the additional lines could not be assigned to elements, which are common in sdB stars. Further investigations show, that most of them are due to Ca III, Sc III, Ti III, Ti IV, V III, V IV, Mn III, and Ni III. These lines have never been found before in the optical spectra of sdB stars. But many of the lines in each star remained unidentified. (see e.g. Fig. 4.6).

In the following we discuss the results for all individual objects.

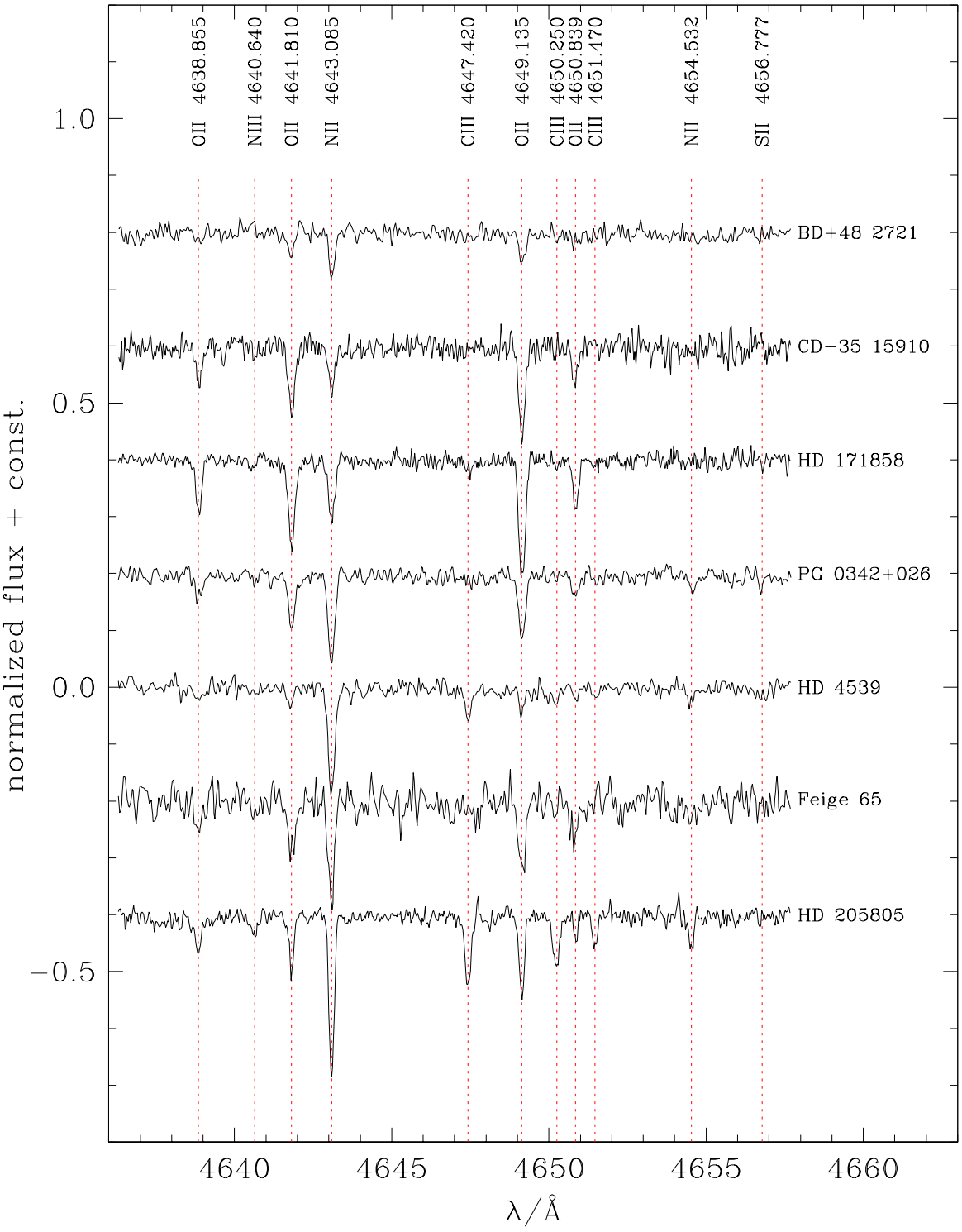

Figure 4.5: Sample plot of identified metal lines within the spectra of all normal sdB stars.

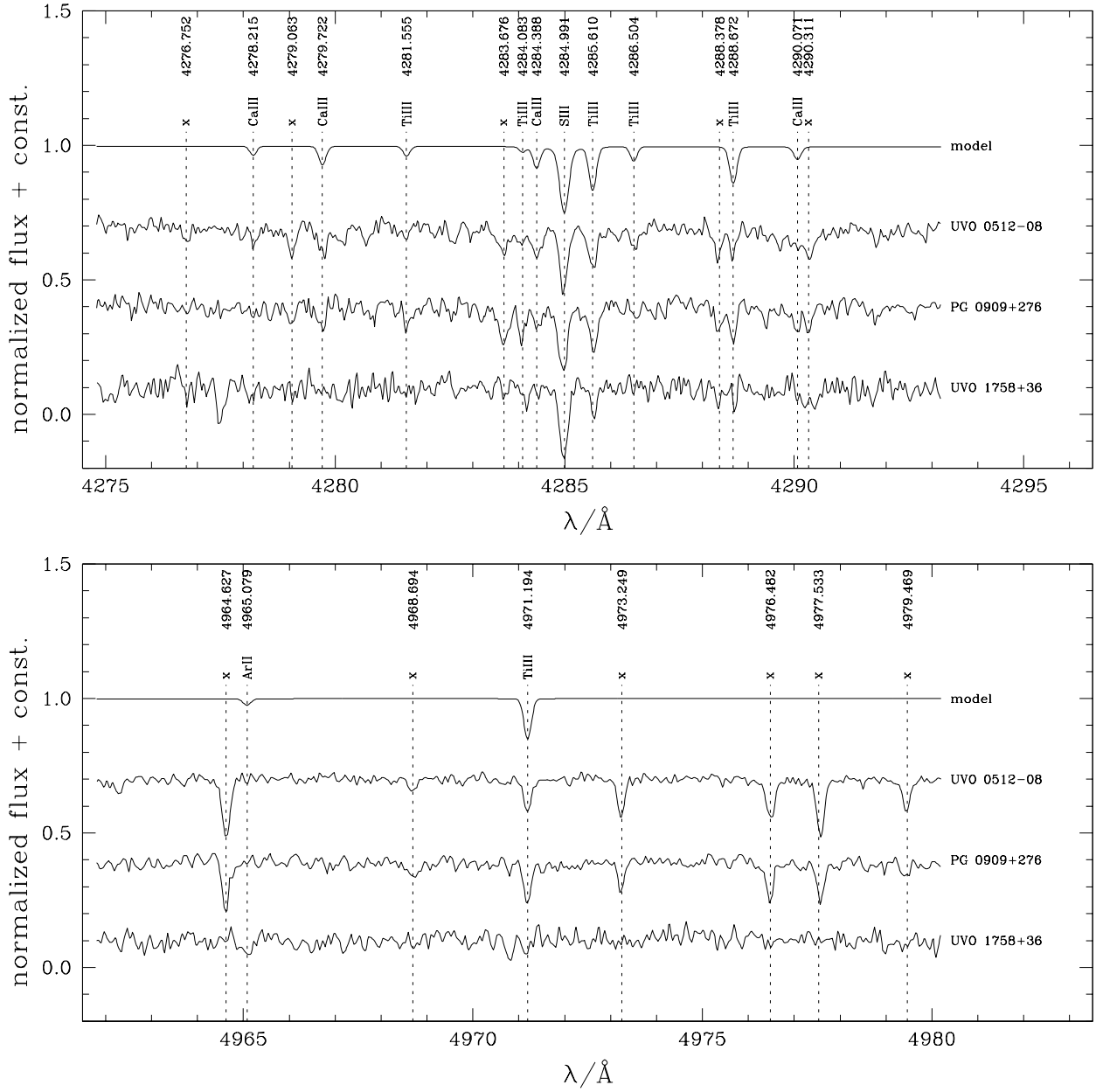

Figure 4.6: Sample plot of identified metal lines within the spectra of all peculiar sdB stars. Additionally, a LTE model plot, consistent with the parameters of UVO 0512−08, is shown. The absorption lines denoted by "x" remained unidentified.

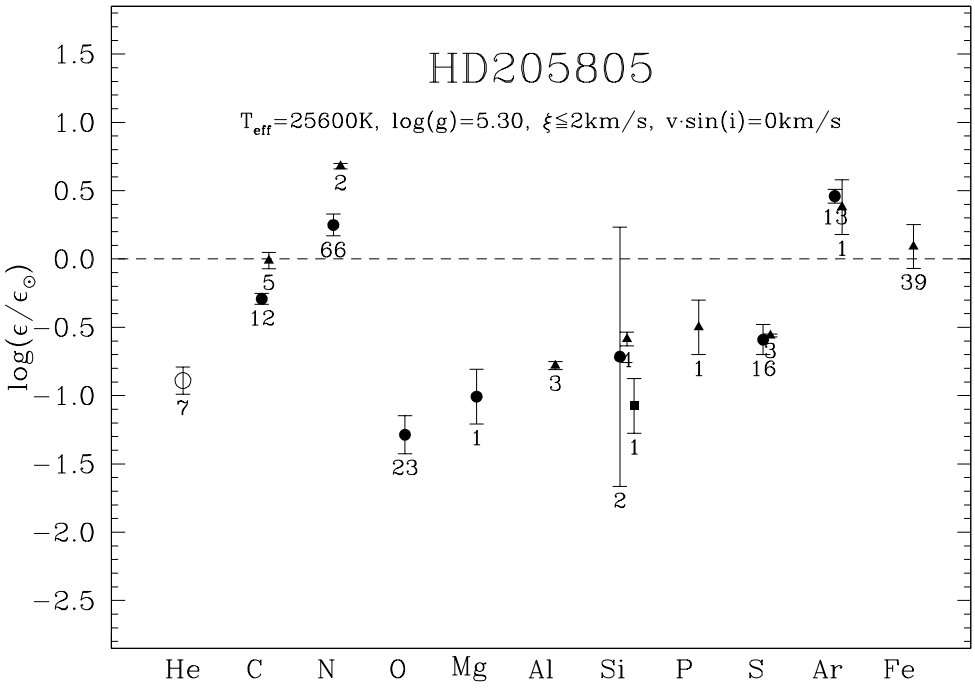

Figure 4.7: LTE abundances with error bars for HD 205805 relative to the solar values (dashed horizontal line). Abundances derived from neutral elements are shown as open circles, from singly ionized ones as filled circles, and from doubly ionized ones as filled triangles. The numbers indicate the number of lines per ion used.

Table 4.1: LTE metal abundances for HD 205805 compared to solar composition; n is the number of spectral lines per ion used for the analysis.

ion	n	$\log(\varepsilon)$	$\log(\varepsilon_\odot)$
He I	7	10.04 ± 0.10	10.930
C II	12	8.30 ± 0.04	8.592
C III	5	8.58 ± 0.06	8.592
N II	66	8.18 ± 0.08	7.931
N III	2	8.61 ± 0.02	7.931
O II	23	7.45 ± 0.14	8.736
Mg II	1	6.53	7.538
Al III	3	5.69 ± 0.03	6.470
Si II	2	6.82 ± 0.95	7.536
Si III	4	6.95 ± 0.05	7.536
Si IV	1	6.46 ± 0.20	7.536
P III	1	4.95	5.450
S II	16	6.74 ± 0.11	7.330
S III	3	6.77 ± 0.01	7.330
Ar II	13	6.86 ± 0.05	6.400
Ar III	1	6.78 ± 0.20	6.400
Fe III	39	7.54 ± 0.16	7.448

4.2.1 'Normal' sdB stars

HD 205805

The spectrum of HD 205805 (sdB, $T_{\rm eff}$ = 25 600K, $\log(g)$ = 5.3), coadded from two spectra obtained in September 2000 at ESO, shows plenty of absorption lines (520 identified lines) of the species C II, C III, N II, N III, O II, Mg II, Al III, Si II, Si III, Si IV, P III, S II, S III, Ar II, Ar III, and Fe III. Due to the excellent S/N of the spectrum almost all lines of every multiplet for these ions are detected, making HD 205805 a perfect reference sdB star for comparison purposes.

From the numerous equivalent widths measured, the abundances for all elements could be determined very precisely. Also, the abundances determined for different ionisation levels are consistent for silicon, sulfur, and argon (within the given error limits). Only for carbon and nitrogen, the abundances determined for the doubly ionized elements, are somewhat larger by about +0.3, and +0.4 dex, respectively. However, only five lines of C III, and two lines of N III are used for the analysis in comparison to 12 lines for C II, and 66 (!!) for N II, (cf. Fig. 4.7).

Oxygen, magnesium, aluminum, silicon, phosphorus, and sulfur are consistent with sub-solar values (−1.2, −1.0, −0.8, −0.6, −0.5, and −0.5 dex, respectively). The carbon abundance is close to solar (−0.2 dex, mean value of C II, and C III), and iron is solar (within the error limit). Furthermore, we determined the abundances of nitrogen and argon to be even enriched (+0.3, and +0.5 dex, compared to the solar value).

The abundances for all metals are given in Table 4.1. Additionally, the values are plotted, with respect to the solar abundances, in Fig. 4.7.

A microturbulence of $\xi \leq 2$ km/s is derived from the curve-of-growths for the C II, N II, O II, S II, Ar II, and Fe III lines (see Fig. 4.2).

From the Mg II doublet, we determined a vanishing projected rotational velocity ($v \sin(i)$ = 0 km/s, see Fig. 4.4). We conclude that HD 205805 is a very slowly rotating star, if not seen pole-on.

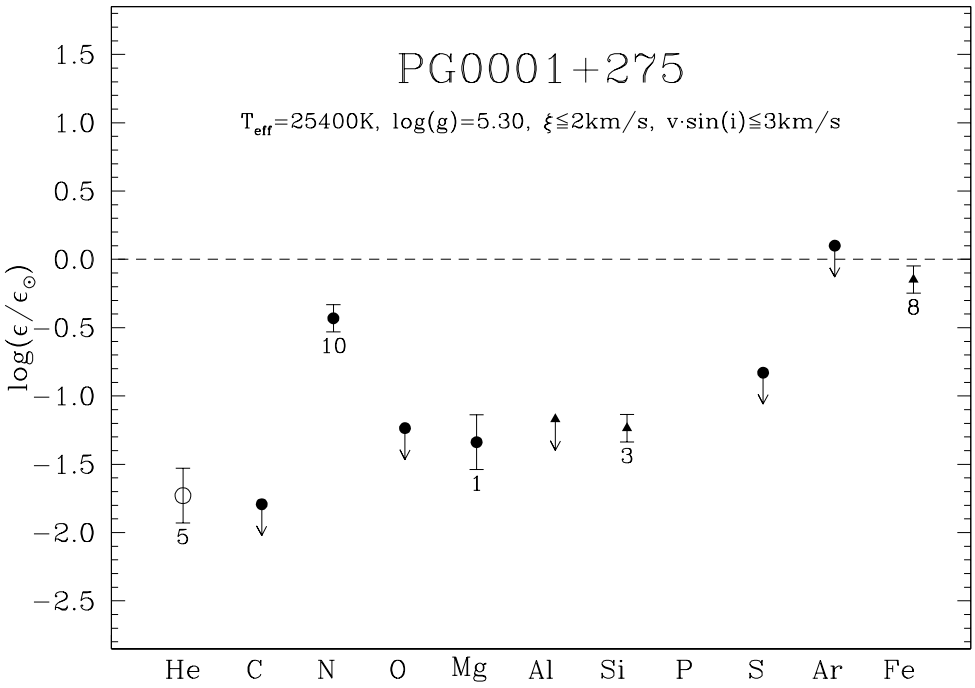

Figure 4.8: LTE abundances with error bars for PG 0001+275 relative to the solar values (dashed horizontal line). Abundances derived from neutral elements are shown as open circles, from singly ionized ones as filled circles, and from doubly ionized ones as filled triangles. The numbers indicate the number of lines per ion used.

Table 4.2: LTE metal abundances for PG 0001+275 compared to solar composition; n is the number of spectral lines per ion used for the analysis.

ion	n	$\log(\varepsilon)$	$\log(\varepsilon_\odot)$
He I	5	9.2 ± 0.2	10.930
C II	0	<6.8	8.592
N II	10	7.5 ± 0.1	7.931
O II	0	<7.5	8.736
Mg II	1	6.2	7.538
Al III	0	<5.3	6.470
Si III	3	6.3 ± 0.1	7.536
S II	0	<6.5	7.330
Ar II	0	<6.5	6.400
Fe III	8	7.3 ± 0.1	7.448

PG 0001+275

The spectrum of the radial velocity variable sdB star PG 0001+275 ($T_{\rm eff}$ = 25 400K, $\log(g) = 5.3$, see also Section 5.2.1), coadded from 16 observations obtained in July 1999, August 2001, and September 2001, at the DSAZ, shows only spectral lines of the species N II, Mg II, Si III, and Fe III. We determine a subsolar nitrogen abundance of 0.5 dex below the solar content, magnesium and silicon to be strongly depleted (-1.3, and -1.2 dex, respectively, compared to the solar value), and an iron content which is almost solar (-0.1 dex).

For carbon, oxygen, aluminum, sulfur, and argon, we could only estimate upper limits: almost all of these elements are strongly depleted (-0.8 to -1.7 dex, compared to the solar values). Only the upper limit of the argon abundance is almost solar ($+0.1$ dex).

The abundances (or upper limits) for all metals are given in Table 4.2. Additionally, the values are plotted, with respect to the solar abundances, in Fig. 4.8.

A sufficient number of nitrogen lines has been measured to allow to determine the microturbulence, $\xi \leq 2$ km/s was found.

From the Mg II doublet at 4481.13Å, and 4481.33Å, and N II lines we conclude that PG 0001+275 is a very slowly rotating star ($v \sin(i) \leq 3$ km/s[1]), unless seen pole-on.

[1]Due to the bad S/N even for the coadded spectrum, the projected rotational velocity is uncertain. The Mg II doublet is not clearly solved, however, the magnesium doublet and the N II lines match best the model using a $v \sin(i) \leq 3$ km/s.

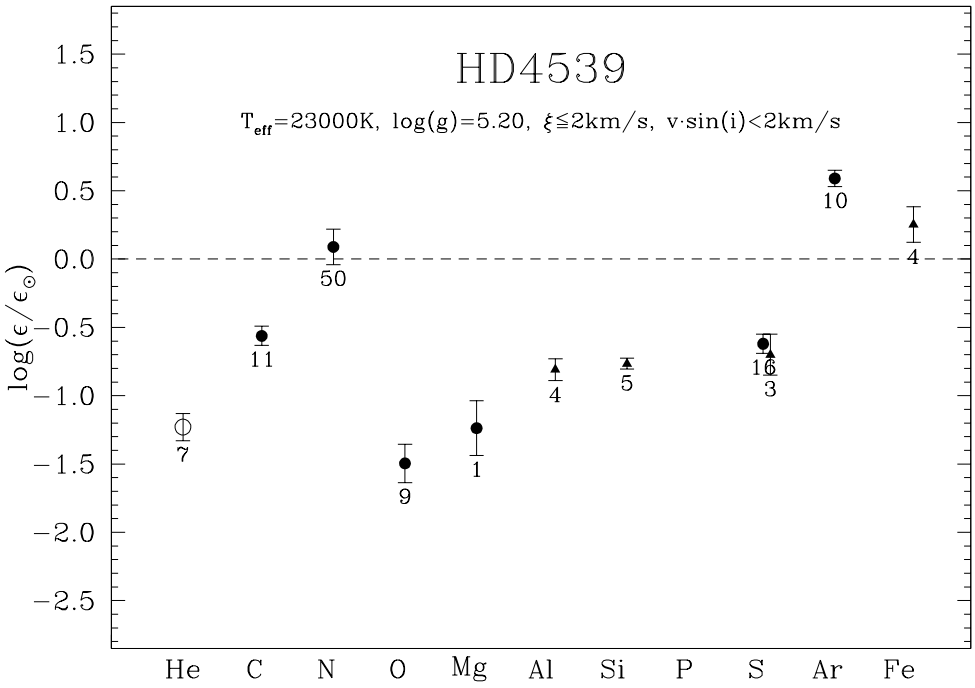

Figure 4.9: LTE abundances with error bars for HD 4539 relative to the solar values (dashed horizontal line). Abundances derived from neutral elements are shown as open circles, from singly ionized ones as filled circles, and from doubly ionized ones as filled triangles. The numbers indicate the number of lines per ion used.

Table 4.3: LTE metal abundances for HD 4539 compared to solar composition; n is the number of spectral lines per ion used for the analysis.

ion	n	$\log(\varepsilon)$	$\log(\varepsilon_\odot)$
He I	7	9.70 ± 0.10	10.930
C II	11	8.03 ± 0.07	8.592
N II	50	8.02 ± 0.12	7.931
O II	9	7.24 ± 0.15	8.736
Mg II	1	6.30	7.538
Al III	4	5.66 ± 0.08	6.470
Si III	5	6.77 ± 0.04	7.536
S II	16	6.71 ± 0.07	7.330
S III	3	6.63 ± 0.14	7.330
Ar II	10	6.99 ± 0.06	6.400
Fe III	4	7.70 ± 0.12	7.448

HD 4539

We identified spectral lines of the species C II, C III, N II, N III, O II, Mg II, Al III, Si III, S II, S III, Ar II, and Fe III within the spectrum of HD 4539 (sdB, $T_{\rm eff} = 23\,000$K, $\log(g) = 5.2$), coadded from three spectra obtained in September 1998 at the DSAZ.

Oxygen and magnesium are determined to be strongly depleted (-1.5, and -1.2 dex, respectively, compared to the solar values).The abundances of carbon, aluminum, silicon, and sulfur are subsolar (-0.5, -0.8, -0.8, and -0.6 dex, respectively). To within error limits nitrogen, and iron are about solar ($+0.1$, and $+0.3$ dex, respectively). Argon is even suprasolar ($+0.6$ dex).

The abundances for all metals are given in Table 4.3. Additionally, the values are plotted, with respect to the solar abundances, in Fig. 4.9. Note the very good consistency for the result drawn from the S II and S III lines.

The curve-of-growth for the nitrogen lines is consistent with a vanishing microturbulence ($\xi \leq 2$ km/s).

Due to the very sharp metal lines, together with the separation of the Mg II doublet at 4481.13Å, and 4481.33Å, we could determine an upper limit of the projected rotational velocity of $v \sin(i) < 2$ km/s. Therefore, HD 4539 is rotating very slowly, unless seen pole-on.

Baschek, Sergent & Searle (1972) already analysed photographic optical and near UV spectra. They determined $T_{\rm eff} = 25\,000 \pm 2\,000$ K and a $\log(g) = 5.4 \pm 0.2$ dex, higher than our results by 2 000 K and 0.2 dex, respectively. They were unable to determine the microturbulence and therefore derived metal abundances for C II, N II, O II, Mg II, Al III, Si II, Si II, S III, and Fe III for two choices of ξ (0 and 5 km/s, we found $\xi \leq 2$ km/s). Comparing their results for $\xi = 0$ km/s to ours, one can see that their results are at least $+0.4$ dex (up to $+0.9$ dex) larger. For $\xi = 5$ km/s, their abundances for helium, oxygen, and iron agree very well with ours, but the remaining abundances differ still ($+0.4$ to 0.7 dex). The remaining differences can be partly explained by lower temperature and gravity, and the use of fully line blanketed model atmospheres in our analysis.

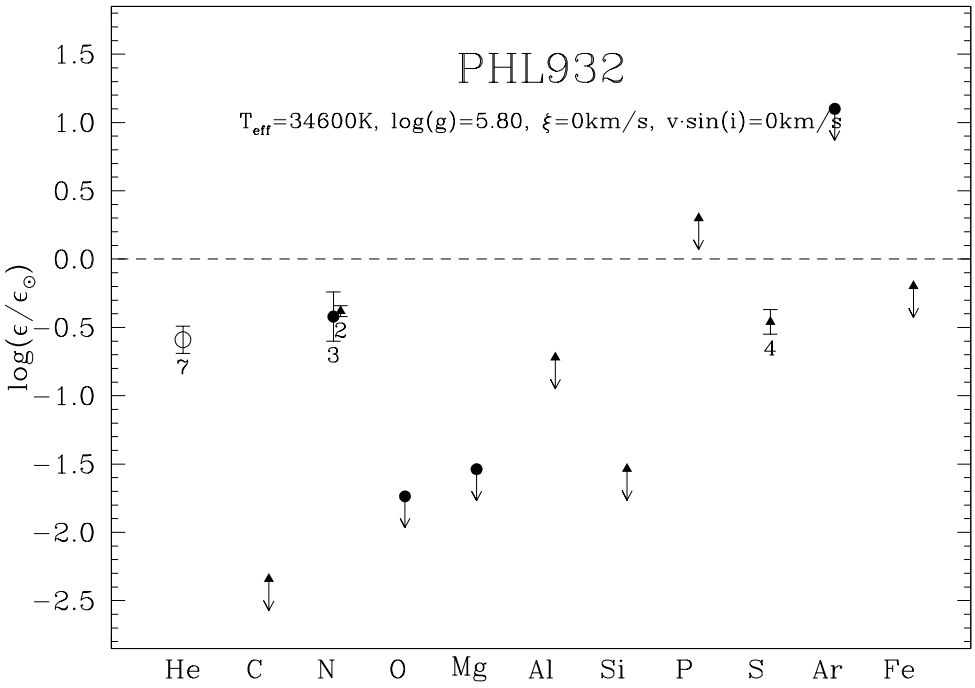

Figure 4.10: LTE abundances with error bars for PHL 932 relative to the solar values (dashed horizontal line). Abundances derived from neutral elements are shown as open circles, from singly ionized ones as filled circles, and from doubly ionized ones as filled triangles. The numbers indicate the number of lines per ion used.

Table 4.4: LTE metal abundances for PHL 932 compared to solar composition; n is the number of spectral lines per ion used for the analysis.

ion	n	$\log(\varepsilon)$	$\log(\varepsilon_\odot)$
He I+II	7	10.34 ± 0.10	10.930
C III	0	<6.25	8.592
N II	3	7.51 ± 0.18	7.931
N III	2	7.55 ± 0.04	7.931
O II	0	<7.00	8.736
Mg II	0	<6.00	7.538
Al III	0	<5.75	6.470
Si III	0	<6.00	7.536
P III	0	<5.75	5.450
S III	4	6.87 ± 0.09	7.330
Ar II	0	<7.50	6.400
Fe III	0	<7.25	7.448

PHL 932

We coadded four spectra of PHL 932 (sdOB, $T_{\rm eff} = 34\,600$K, $\log(g) = 5.8$) obtained in August 1999 at the DSAZ. From this spectrum, we identified only lines of the species N II, N III, and S III. Their abundances are all subsolar (-0.4 dex). Note the remarkably good consistency of the abundances drawn from the N II, and N III lines.

Upper limits for carbon, oxygen, magnesium, aluminum, silicon, phosphorus, argon, and iron are estimated: the abundances of carbon, oxygen, magnesium, and silicon are strongly depleted (at least -2.3, -1.7, -1.5, and -1.5 dex, respectively, compared to the solar values). aluminum is subsolar (-0.7 dex); upper limits for phosphorus, iron, and argon are inconclusive, allowing their abundances to be as high as the solar one, or higher (argon).

The abundances (or upper limits) for all metals are given in Table 4.4. Additionally, the values are plotted, with respect to the solar abundances, in Fig. 4.10.

Due to the very small number of metal lines found, no microturbulence coud be determined. For the analysis we used a value of $\xi = 0$ km/s.

A projected rotational velocity of $v \sin(i) < 5$ km/s is consistent with the the sharp metal lines seen.

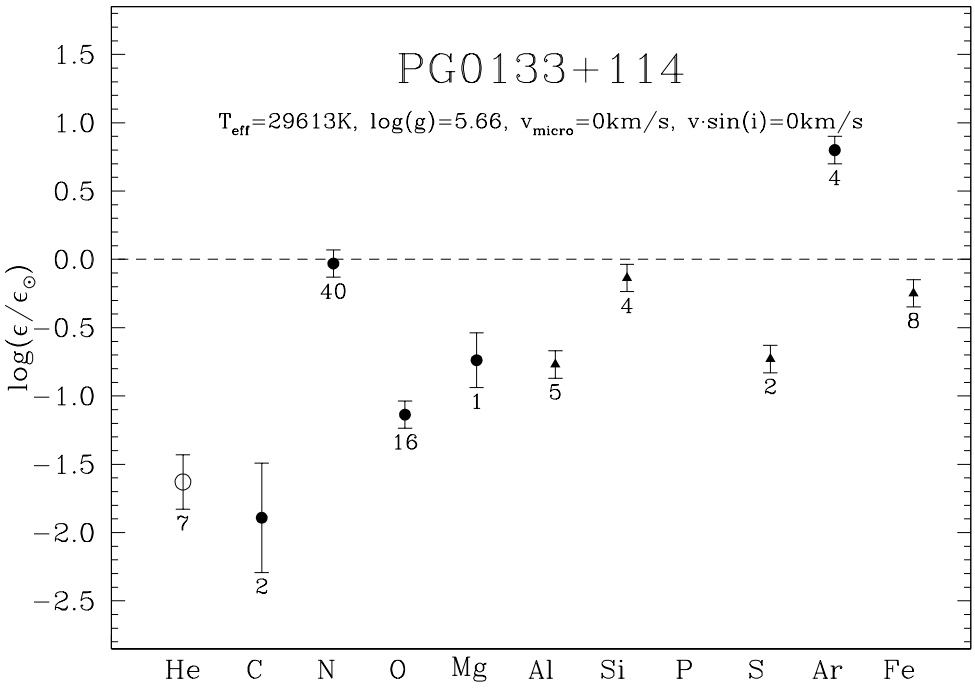

Figure 4.11: LTE abundances with error bars for PG 0133+114 relative to the solar values (dashed horizontal line). Abundances derived from neutral elements are shown as open circles, from singly ionized ones as filled circles, and from doubly ionized ones as filled triangles. The numbers indicate the number of lines per ion used.

Table 4.5: LTE metal abundances for PG 0133+114 compared to solar composition; n is the number of spectral lines per ion used for the analysis.

ion	n	$\log(\varepsilon)$	$\log(\varepsilon_\odot)$
He I	7	9.3 ± 0.2	10.930
C II	2	6.7 ± 0.4	8.592
N II	40	7.9 ± 0.1	7.931
O II	16	7.6 ± 0.1	8.736
Mg II	1	6.8	7.538
Al III	5	5.7 ± 0.1	6.470
Si III	4	7.4 ± 0.1	7.536
S III	2	6.6 ± 0.1	7.330
Ar II	4	7.2 ± 0.1	6.400
Fe III	8	7.2 ± 0.1	7.448

PG 0133+114

The spectrum of the radial velocity variable sdB star PG 0133+114 ($T_{\rm eff}$ = 29 613K, $\log(g)$ = 5.66, see also Section 5.2.5), coadded from 22 observations obtained in July 1999 and August 2001 at the DSAZ, shows spectral lines of the species C II, N II, O II, Mg II, Al III, Si III, S II, S III, Ar II, and Fe III.

We determined carbon to be strongly subsolar (−1.9, dex). The abundances of oxygen, magnesium, aluminum, and sulfur are depleted (−1.1, −0.7, −0.8, −0.7 dex, respectively, compared to the solar value). Nitrogen is solar, silicon, and iron are almost solar (−0.1, and −0.2 dex, respectively), and argon is suprasolar (+0.8 dex).

The abundances for all metals are given in Table 4.5. Additionally, the values are plotted, with respect to the solar abundances, in Fig. 4.11.

From the nitrogen and oxygen lines we are able to determine a vanishing microturbulence ($\xi \leq 2$ km/s).

The metal lines are all very sharp. Due to the separated Mg II doublet at 4481.13Å, and 4481.33Å, we could measure that PG 0133+114 is likely to be a very slowly rotating star ($v \sin(i) < 2$ km/s), unless seen pole-on.

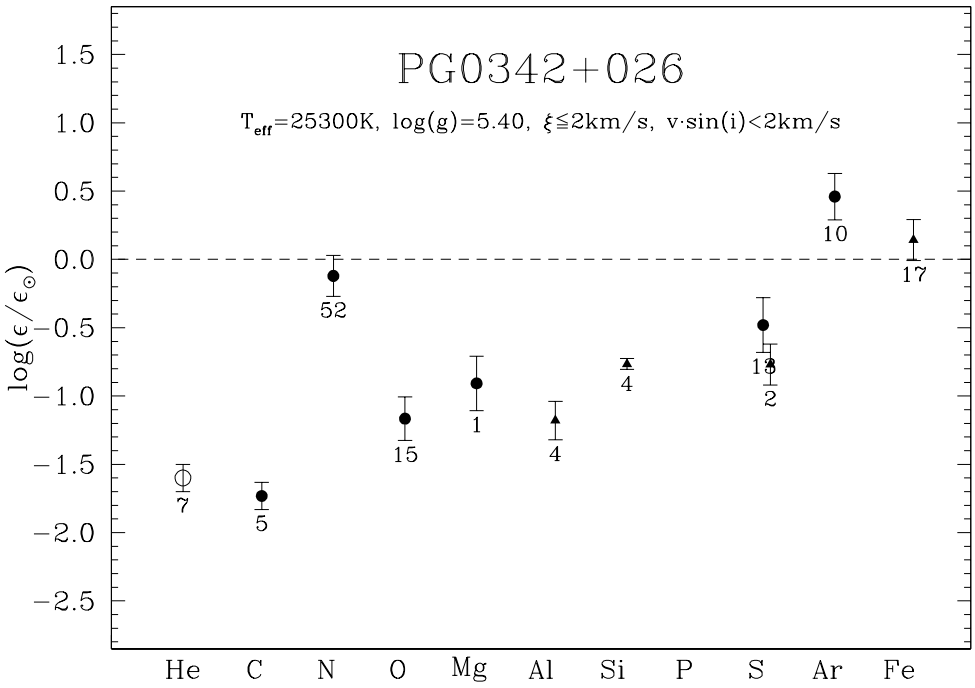

Figure 4.12: LTE abundances with error bars for PG 0342+026 relative to the solar values (dashed horizontal line). Abundances derived from neutral elements are shown as open circles, from singly ionized ones as filled circles, and from doubly ionized ones as filled triangles. The numbers indicate the number of lines per ion used.

Table 4.6: LTE metal abundances for PG 0342+026 compared to solar composition; n is the number of spectral lines per ion used for the analysis.

ion	n	$\log(\varepsilon)$	$\log(\varepsilon_\odot)$
He I	7	9.33 ± 0.10	10.930
C II	5	6.86 ± 0.10	8.592
N II	52	7.81 ± 0.15	7.931
O II	15	7.57 ± 0.16	8.736
Mg II	1	6.63	7.538
Al III	4	5.29 ± 0.14	6.470
Si III	4	6.77 ± 0.04	7.536
S II	13	6.85 ± 0.20	7.330
S III	2	6.56 ± 0.08	7.330
Ar II	10	6.86 ± 0.17	6.400
Fe III	17	7.59 ± 0.15	7.448

PG 0342+026

We identified spectral lines of the species C II, C III, N II, N III, O II, Mg II, Al III, Si III, S II, S III, Ar II, and Fe III within the spectrum of PG 0342+026 (sdB, $T_{\rm eff} = 25\,300$K, $\log(g) = 5.4$), coadded from three spectra obtained in September 1998 at the DSAZ.

We determined carbon, oxygen, magnesium, aluminum, and silicon, to be strongly depleted (-1.7, -1.1, -0.9, -1.1, and -0.8 dex, respectively, compared to the solar values). The abundance of sulfur is mildly depleted (-0.4 dex). Note the consistency of the results determined for S II, and S III (within the given error limits). Nitrogen, and iron are about solar (-0.1, and $+0.1$ dex, respectively). Argon is even suprasolar ($+0.5$ dex).

The curve-of-growths for the nitrogen, and oxygen lines are consistent with a vanishing microturbulence ($\xi \leq 2$ km/s).

Due to the very sharp metal lines, together with the separation of the Mg II doublet at 4481.13Å, and 4481.33Å, we could determine a projected rotational velocity of $v \sin(i) < 2$ km/s. Therefore, PG 0342+026 is rotating very slowly, unless seen pole-on.

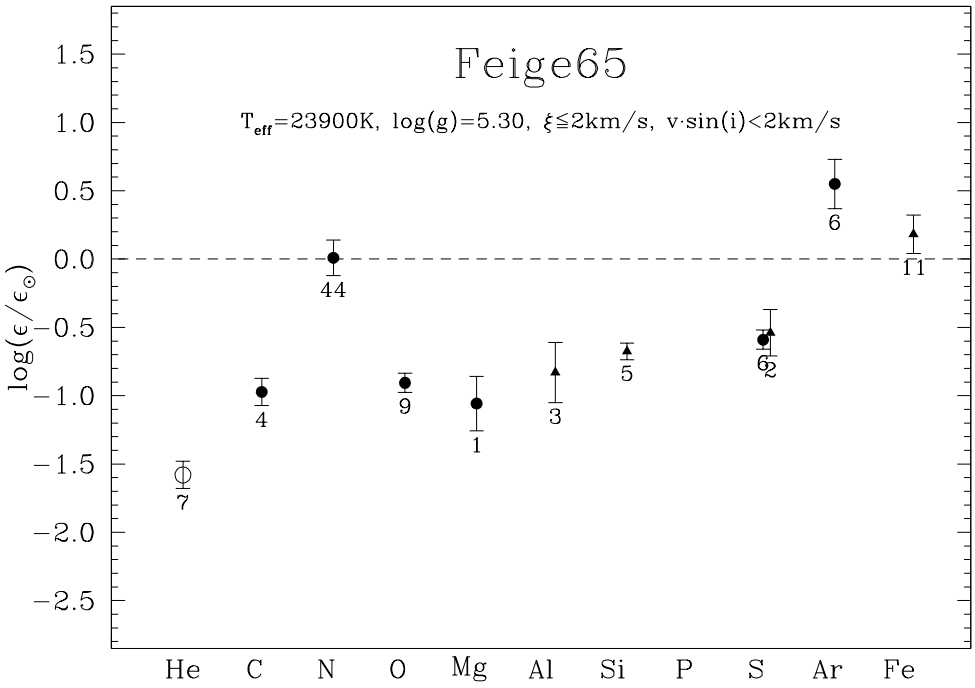

Figure 4.13: LTE abundances with error bars for Feige 65 relative to the solar values (dashed horizontal line). Abundances derived from neutral elements are shown as open circles, from singly ionized ones as filled circles, and from doubly ionized ones as filled triangles. The numbers indicate the number of lines per ion used.

Table 4.7: LTE metal abundances for Feige 65 compared to solar composition; n is the number of spectral lines per ion used for the analysis.

ion	n	$\log(\varepsilon)$	$\log(\varepsilon_\odot)$
He I	7	9.35 ± 0.10	10.930
C II	4	7.62 ± 0.10	8.592
N II	44	7.94 ± 0.13	7.931
O II	9	7.83 ± 0.07	8.736
Mg II	1	6.48	7.538
Al III	3	5.64 ± 0.22	6.470
Si III	5	6.86 ± 0.06	7.536
S II	6	6.74 ± 0.07	7.330
S III	2	6.79 ± 0.17	7.330
Ar II	6	6.95 ± 0.18	6.400
Fe III	11	7.63 ± 0.14	7.448

Feige 65

We coadded two spectra of Feige 65 (sdB, $T_{\rm eff}$ = 23 900K, $\log(g) = 5.3$) obtained in January 2000 at the DSAZ. From this spectrum, we identified lines of the species C II, C III, N II, N III, O II, Mg II, Al III, Si II, Si III, S II, S III, Ar II, and Fe III.

The abundances of carbon, oxygen, magnesium, aluminum, silicon, and sulfur are found to be depleted (-1.0, -0.9, -1.0, -0.7, and -0.5 dex, respectively, compared to the solar values). Nitrogen and iron are, within their error limits, consistent with the solar values. The abundance of argon is enriched ($+0.5$ dex, compared to the solar value).

The abundances for all metals are given in Table 4.7. Additionally, the values are plotted, with respect to the solar abundances, in Fig. 4.13. Note the remarkably consistency for the abundances drawn from the S II and S III lines.

A microturbulence of $\xi \leq 2$ km/s is derived from the curve-of-growth for the N II lines.

From the Mg II doublet, both components are clearly resolved, we determined an upper limit of $v \sin(i) < 2$ km/s for the projected rotational velocity. We conclude that Feige 65 is a very slowly rotating star, if not seen pole-on.

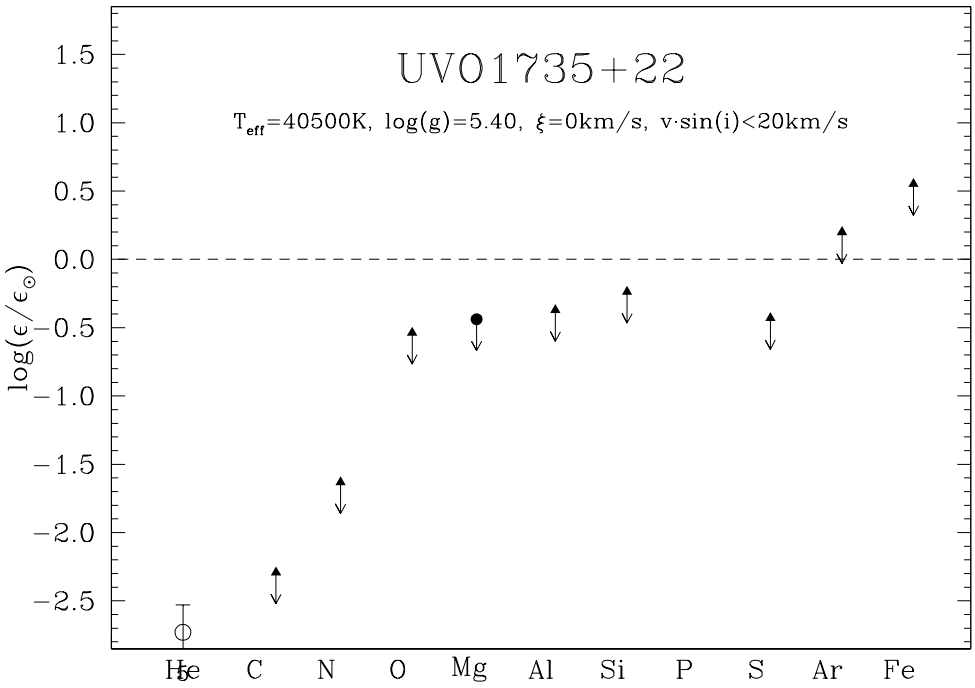

Figure 4.14: LTE abundances with error bars for UVO 1735+22 relative to the solar values (dashed horizontal line). Abundances derived from neutral elements are shown as open circles, from singly ionized ones as filled circles, and from doubly ionized ones as filled triangles. The numbers indicate the number of lines per ion used.

Table 4.8: LTE metal abundances for UVO 1735+22 compared to solar composition; n is the number of spectral lines per ion used for the analysis.

ion	n	$\log(\varepsilon)$	$\log(\varepsilon_\odot)$
He I+II	5	8.2 ± 0.2	10.930
C III	0	<6.3	8.592
N III	0	<6.3	7.931
O III	0	<8.2	8.736
Mg II	0	<7.1	7.538
Al III	0	<6.1	6.470
Si III	0	<7.3	7.536
S III	0	<6.9	7.330
Ar III	0	<6.6	6.400
Fe III	0	<8.0	7.448

UVO 1735+22

The radial velocity variable sdOB star UVO 1735+22 ($T_{\rm eff}$ = 40 500K, $\log(g)$ = 5.4, see also Section 5.2.6) shows no metal lines at all in his spectrum (coadded from three spectra obtained in August 1999 at the DSAZ).

We can only estimate upper limits for all metals which are common in sdOB stars: carbon and nitrogen are strongly depleted (by at least −2.2, and −1.6 dex, respectively, compared to the solar values). For oxygen, magnesium, aluminum, silicon, and sulfur, the upper limits are subsolar (−0.5, −0.4, −0.4, −0.2, and −0.4 dex, respectively). The estimated upper limits of the abundances for argon and iron are inconclusive allowing their abundances to be as high as +0.2, and +0.5 dex, respectively.

The upper limits for all metals are given in Table 4.8. Additionally, the values are plotted, with respect to the solar abundances, in Fig. 4.14.

Due to the lack of metal lines found, we are not able to determine a microturbulent velocity. For the calculations, we used $\xi = 0$ km/s.

A projected rotational velocity of $v \sin(i) < 20$ km/s results from the fit of the helium lines. Therefore, unless seen pole-on, UVO 1735+22 is probably slowly rotating.

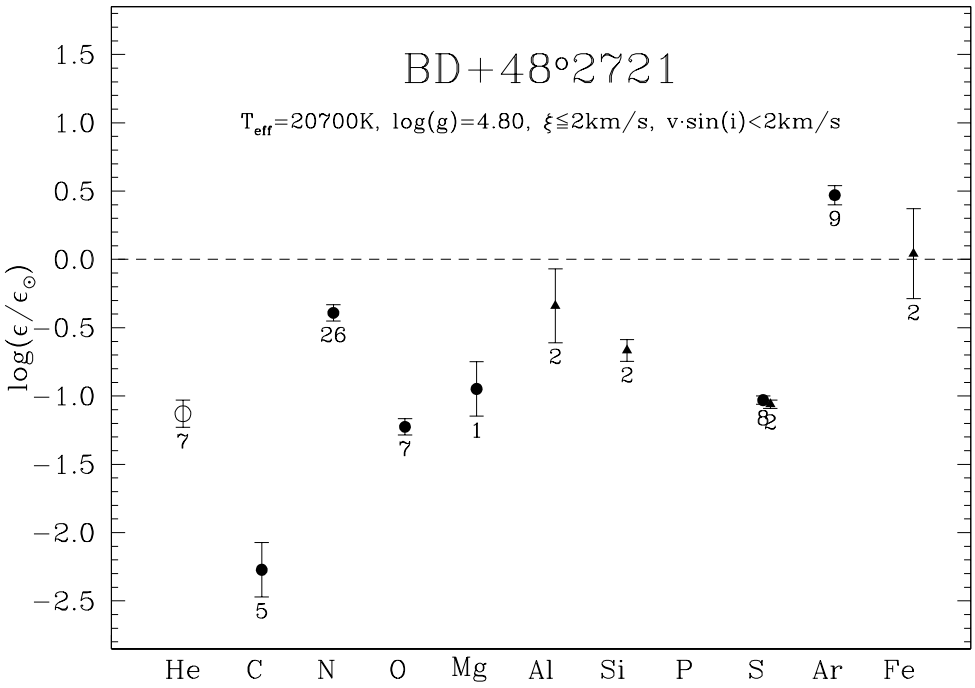

Figure 4.15: LTE abundances with error bars for BD+48° 2721 relative to the solar values (dashed horizontal line). Abundances derived from neutral elements are shown as open circles, from singly ionized ones as filled circles, and from doubly ionized ones as filled triangles. The numbers indicate the number of lines per ion used.

Table 4.9: LTE metal abundances for BD+48° 2721 compared to solar composition; n is the number of spectral lines per ion used for the analysis.

ion	n	$\log(\varepsilon)$	$\log(\varepsilon_\odot)$
He I	7	9.80 ± 0.10	10.930
C II	5	6.32 ± 0.20	8.592
N II	26	7.54 ± 0.06	7.931
O II	7	7.51 ± 0.06	8.736
Mg II	1	6.59	7.538
Al III	2	6.13 ± 0.27	6.470
Si III	2	6.87 ± 0.08	7.536
S II	8	6.30 ± 0.03	7.330
S III	2	6.27 ± 0.03	7.330
Ar II	9	6.87 ± 0.07	6.400
Fe III	2	7.49 ± 0.33	7.448

BD+48° 2721

We identified spectral lines of the species C II, C III, N II, N III, O II, Mg II, Al III, Si II, Si III, S II, S III, Ar II, and Fe III in the spectrum of BD+48° 2721 (sdB, $T_{\rm eff} = 20\,700$K, $\log(g) = 4.8$), coadded from two spectra obtained in September 1998 at the DSAZ.

We determined carbon to be strongly depleted (−2.3 dex, compared to the solar value). The abundances of nitrogen, oxygen, magnesium, aluminum, silicon, and sulfur are consistent with subsolar values (−0.4, −1.2, −1.0, −0.4, −0.7, and −1.0 dex, respectively). The results determined for S II, and S III are remarkably consistent. Iron is solar, and argon is even suprasolar (+0.5 dex).

The curve-of-growths for the nitrogen, and oxygen lines are consistent with a vanishing microturbulence ($\xi \leq 2$ km/s).

Due to the very sharp metal lines, together with the separation of the Mg II doublet at 4481.13Å, and 4481.33Å, we could determine a limit to the projected rotational velocity of $v \sin(i) < 2$ km/s. We conclude that BD+48° 2721 is a very slow rotating star, unless seen pole-on.

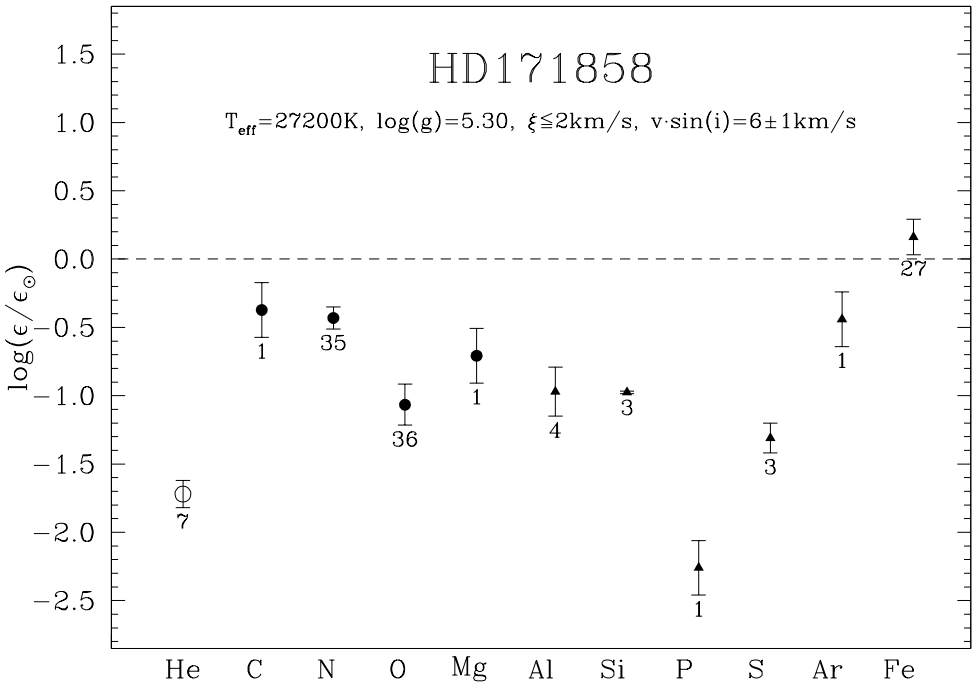

Figure 4.16: LTE abundances with error bars for HD 171858 relative to the solar values (dashed horizontal line). Abundances derived from neutral elements are shown as open circles, from singly ionized ones as filled circles, and from doubly ionized ones as filled triangles. The numbers indicate the number of lines per ion used.

Table 4.10: LTE metal abundances for HD 171858 compared to solar composition; n is the number of spectral lines per ion used for the analysis.

ion	n	$\log(\varepsilon)$	$\log(\varepsilon_\odot)$
He I	7	9.21 ± 0.10	10.930
C II	1	8.22	8.592
N II	35	7.50 ± 0.08	7.931
O II	36	7.67 ± 0.15	8.736
Mg II	1	6.83	7.538
Al III	4	5.50 ± 0.18	6.470
Si III	3	6.56 ± 0.01	7.536
P III	1	3.19	5.450
S III	3	6.02 ± 0.11	7.330
Ar III	1	5.96	6.400
Fe III	27	7.61 ± 0.13	7.448

HD 171858

From the spectrum of the radial velocity variable sdB star HD 171858 ($T_{\rm eff} = 27\,200$K, $\log(g) = 5.3$, see also Section 5.2.7), coadded from two spectra obtained in September 2000 at ESO, we identified lines of the species C II, N II, O II, Mg II, Al III, Si III, P III, S II, S III, Ar II, and Fe III.

The abundances of all elements, except for iron which is close to solar (+0.2 dex), are found to be depleted: carbon −0.4 dex, nitrogen −0.4 dex, oxygen −0.5 dex, magnesium −0.7 dex, aluminum −1.0 dex, silicon −1.0 dex, phosphorus −2.3 dex, sulfur −1.3 dex, and argon −0.4 dex (compared to the solar value, respectively).

The abundances for all metals are given in Table 4.10. Additionally, the values are plotted, with respect to the solar abundances, in Fig. 4.16.

A microturbulence of $\xi \leq 2$ km/s is derived from the curve-of-growths for the N II, O II, and Fe III lines.

From the Mg II doublet, N II, and O II lines we could measure a projected rotational velocity of $v \sin(i) = 6 \pm 1$ km/s, making HD 171858 the only program star for which we coud determine a non-vanishing value.

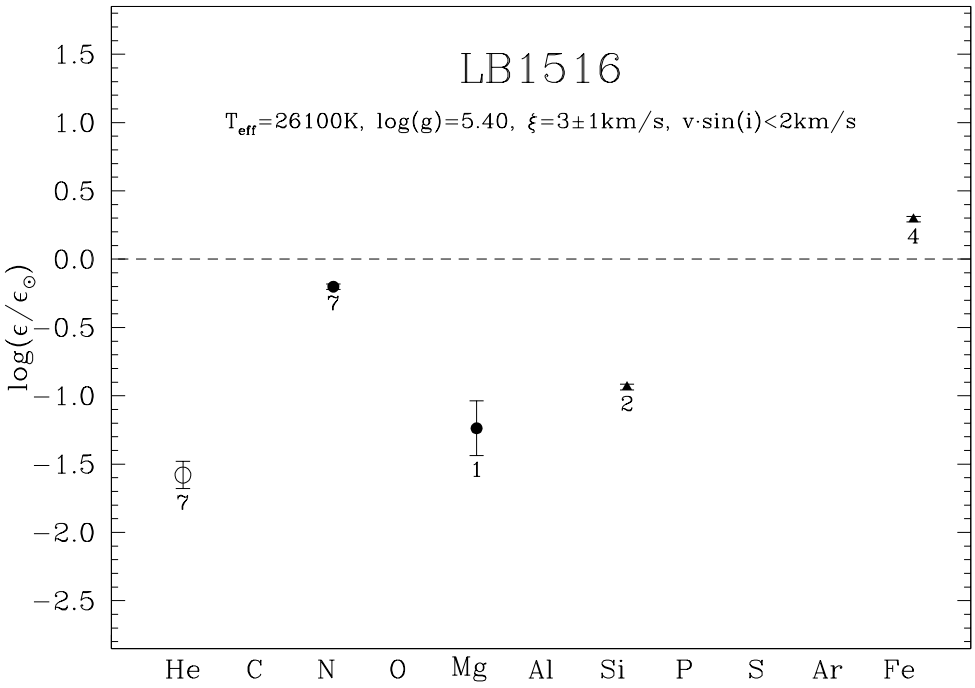

Figure 4.17: LTE abundances with error bars for LB 1516 relative to the solar values (dashed horizontal line). Abundances derived from neutral elements are shown as open circles, from singly ionized ones as filled circles, and from doubly ionized ones as filled triangles. The numbers indicate the number of lines per ion used.

Table 4.11: LTE metal abundances for LB 1516 compared to solar composition; n is the number of spectral lines per ion used for the analysis.

ion	n	$\log(\varepsilon)$	$\log(\varepsilon_\odot)$
He I	7	9.35 ± 0.10	10.930
N II	7	7.73 ± 0.02	7.931
Mg II	1	6.30	7.538
Si III	2	6.60 ± 0.02	7.536
Fe III	4	7.74 ± 0.02	7.448

LB 1516

We coadded two spectra of LB 1516 (sdB, $T_{\rm eff} = 26\,100$K, $\log(g) = 5.4$) obtained in September 2000 at ESO. From this spectrum, we identified only lines of the species N II, Mg II, Si III, and Fe III.

The abundances of magnesium and silicon are found to be depleted (-1.2, and -0.9 dex, respectively, compared to the solar values), nitrogen is almost solar (-0.2 dex), and the abundance of iron is mildly enriched ($+0.3$ dex, compared to the solar value).

The abundances for all metals are given in Table 4.11. Additionally, the values are plotted, with respect to the solar abundances, in Fig. 4.17.

A microturbulence of $\xi = 3 \pm 1$ km/s is derived from the curve-of-growth for the N II lines, making LB 1516, besides CD-35° 15910, one of two program sdB stars in our sample which show a non-vanishing microturbulence.

A vanishing projected rotational velocity ($v \sin(i) < 2$) is determined from the Mg II doublet, which is clearly separated. Therefore, unless seen pole-on, LB 1516 is probably very slowly rotating.

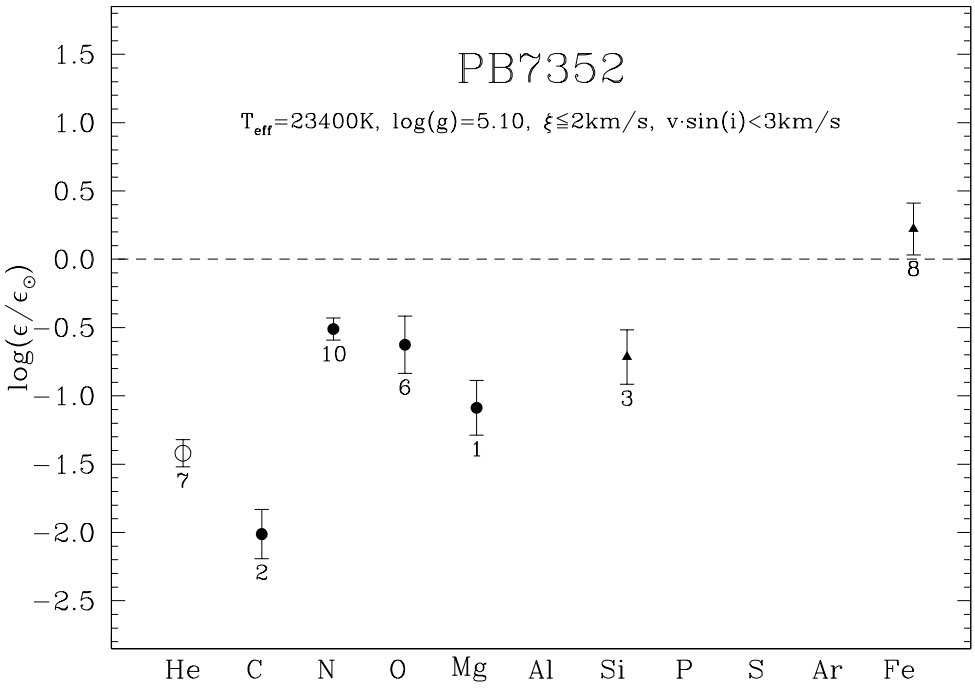

Figure 4.18: LTE abundances with error bars for PB 7352 relative to the solar values (dashed horizontal line). Abundances derived from neutral elements are shown as open circles, from singly ionized ones as filled circles, and from doubly ionized ones as filled triangles. The numbers indicate the number of lines per ion used.

Table 4.12: LTE metal abundances for PB 7352 compared to solar composition; n is the number of spectral lines per ion used for the analysis.

ion	n	$\log(\varepsilon)$	$\log(\varepsilon_\odot)$
He I	7	9.51 ± 0.10	10.930
C II	2	6.58 ± 0.18	8.592
N II	10	7.42 ± 0.08	7.931
O II	6	8.11 ± 0.21	8.736
Mg II	1	6.45	7.538
Si III	3	6.82 ± 0.20	7.536
Fe III	8	7.67 ± 0.19	7.448

PB 7352

We coadded two spectra of the radial velocity variable sdB star PB 7352 ($T_{\rm eff}$ = 23 400K, $\log(g) = 5.1$, see also Section 5.2.8) obtained in September 2000 at ESO. From this spectrum, we identified ion lines of the species C II, N II, O II, Mg II, Si III, S II, and Fe III

We found carbon to be strongly subsolar (−2.0 dex). Nitrogen, oxygen, magnesium, and silicon are depleted (−0.5, −0.6, −1.1, and −0.7 dex, respectively, with respect to the solar values). The abundances determined for iron is very close to the solar one (+0.2 dex).

The abundances for all metals are given in Table 4.12. Additionally, the values are plotted, with respect to the solar abundances, in Fig. 4.18.

From the N II lines, we were able to estimate a vanishing microturbulent velocity ($\xi \leq$ 2 km/s).

The Mg II doublet is clearly resolved, resulting in a projected rotational velocity of $v \sin(i) <$ 3 km/s. We concluded PB 7352 to be a slowly rotator, except seen pole-on.

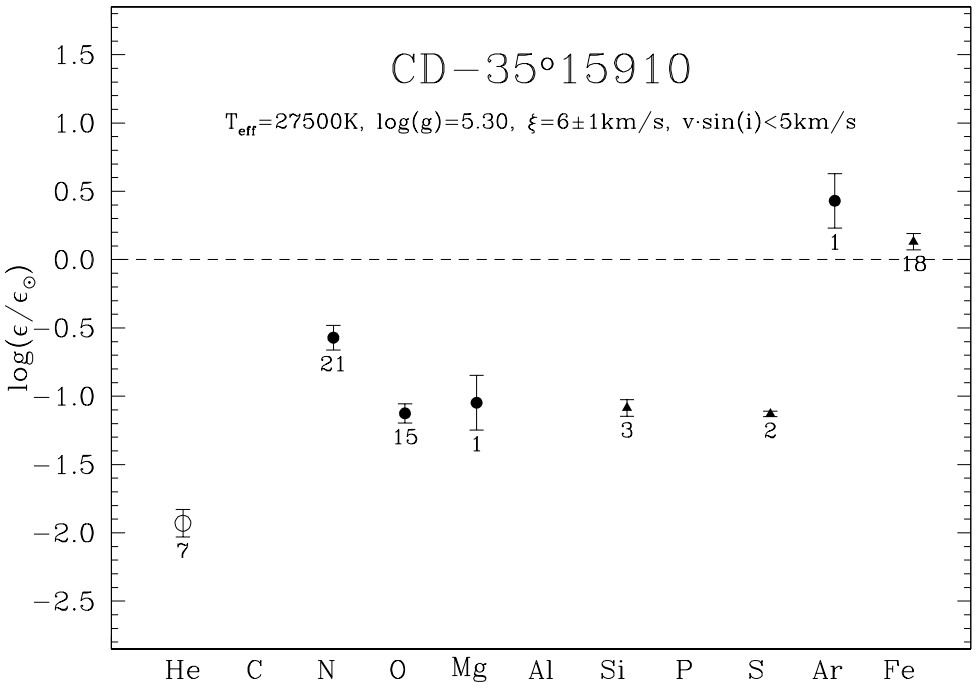

Figure 4.19: LTE abundances with error bars for CD−35° 15910 relative to the solar values (dashed horizontal line). Abundances derived from neutral elements are shown as open circles, from singly ionized ones as filled circles, and from doubly ionized ones as filled triangles. The numbers indicate the number of lines per ion used.

Table 4.13: LTE metal abundances for CD−35° 15910 compared to solar composition; n is the number of spectral lines per ion used for the analysis.

ion	n	$\log(\varepsilon)$	$\log(\varepsilon_\odot)$
He I	7	9.00 ± 0.10	10.930
N II	21	7.36 ± 0.09	7.931
O II	15	7.61 ± 0.07	8.736
Mg II	1	6.49	7.538
Si III	3	6.45 ± 0.06	7.536
S III	2	6.20 ± 0.02	7.330
Ar II	1	6.83	6.400
Fe III	18	7.58 ± 0.06	7.448

CD−35° 15910

We identified spectral lines of the species N II, O II, Mg II, Si III, S II, S III, Ar II, and Fe III in the spectrum of CD−35° 15910 (sdB, $T_{\rm eff} = 27\,500$K, $\log(g) = 5.3$), coadded from three spectra obtained in September 2000 at ESO.

We determined nitrogen, oxygen, magnesium, silicon, and sulfur to be depleted (−0.6, −1.1, −1.0, −1.1, and −1.1 dex, respectively, compared to the solar values). The abundance of iron is about solar (+0.1 dex). For argon we derive an enriched value of +0.4 dex (compared to the solar one).

The abundances for all metals are given in Table 4.13. Additionally, the values are plotted, with respect to the solar abundances, in Fig. 4.19.

The curve-of-growths for the nitrogen, and oxygen lines are consistent with a microturbulence of $\xi = 6 \pm 1$ km/s. CD−35° 15910 is the second program star, besides LB 1516, showing a non-vanishing microturbulence.

A projected rotational velocity of $v \sin(i) < 5$ km/s is consistent with the the Mg II doublet at 4481.13Å, and 4481.33Å and N II lines. We conclude that CD−35° 15910 is a very slowly rotating star, unless seen pole-on.

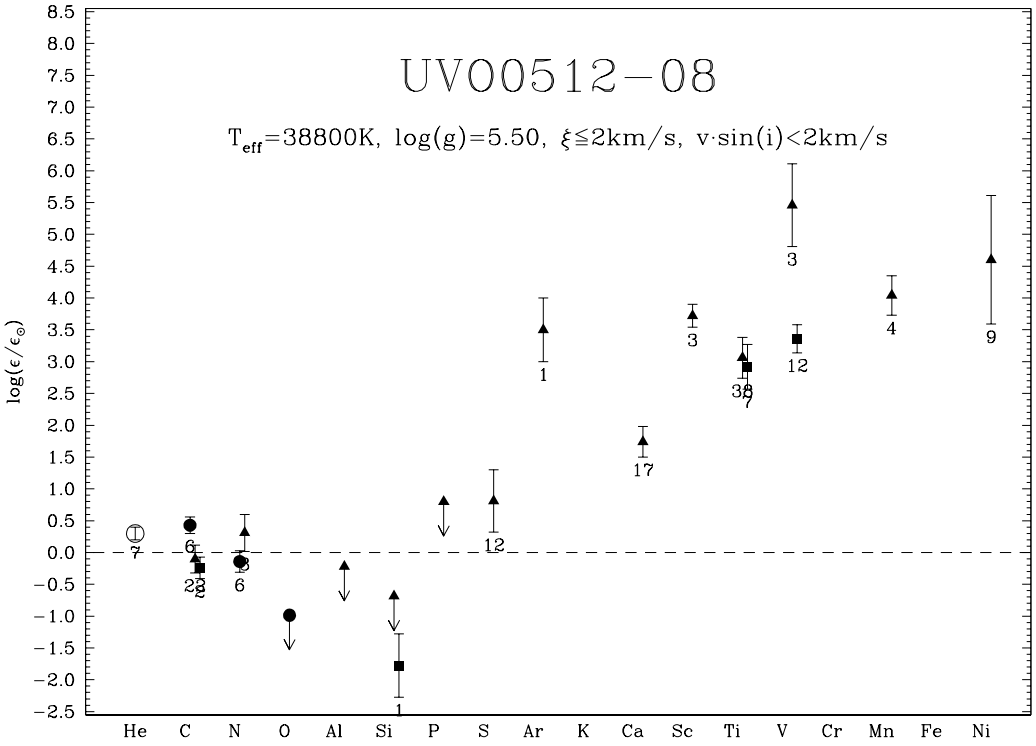

Figure 4.20: LTE abundances with error bars for UVO 0512−08 relative to the solar values (dashed horizontal line). Abundances derived from neutral elements are shown as open circles, from singly ionized ones as filled circles, from doubly ionized ones as filled triangles, and from triply ionized ones as filled squares. The numbers indicate the number of lines per ion used.

Table 4.14: LTE metal abundances for UVO 0512−08 compared to solar composition; n is the number of spectral lines per ion used for the analysis.

ion	n	$\log(\varepsilon)$	$\log(\varepsilon_\odot)$	ion	n	$\log(\varepsilon)$	$\log(\varepsilon_\odot)$
He I+II	7	11.23 ± 0.10	10.930	S III	12	8.14 ± 0.49	7.330
C II	6	9.02 ± 0.13	8.592	Ar III	1	9.90	6.400
C III	22	8.49 ± 0.22	8.592	Ca III	17	8.10 ± 0.24	6.360
C IV	2	8.35 ± 0.17	8.592	Sc III	3	6.89 ± 0.18	3.170
N II	6	7.79 ± 0.17	7.931	Ti III	38	8.08 ± 0.32	5.020
N III	3	8.24 ± 0.29	7.931	Ti IV	7	7.94 ± 0.35	5.020
O II	0	<7.75	8.736	V III	3	9.46 ± 0.65	4.000
Al III	0	<6.25	6.470	V IV	12	7.36 ± 0.22	4.000
Si III	0	<6.85	7.536	Mn III	4	9.43 ± 0.31	5.390
Si IV	1	5.76	7.536	Ni III	9	10.85 ± 1.01	6.250
P III	0	<6.25	5.450				

4.2.2 Peculiar sdB stars

UVO 0512−08

The spectrum of UVO 0512−08 (sdOB, $T_{\rm eff} = 38\,800$K, $\log(g) = 5.5$), coadded from two spectra obtained in January and February 2000 at the DSAZ, shows a lot more (~ 500) spectral lines than the spectra of 'normal' sdB stars described in Section 4.2.1. First of all, the additional lines could not be assigned to ions which are common in sdB stars (e.g. comparing to HD 205805). Further investigations show, that most of them are due to Ca III, Sc III, Ti III, Ti IV, V III, V IV, Mn III and Ni III. These lines have never been found before in the optical spectra of sdB stars. However, 129 ($\sim 23\%$) of the lines remained unidentified.

Beside the peculiar lines found, we identified additionally lines due to 'normal' ions of the type C II, C III, C IV, N II, N III, Si IV, S III, and Ar III. It is remarkable, that we cannot identify any lines due to iron, whereas, all 'normal' sdB stars do show many Fe III lines.

The abundances of carbon and nitrogen are about solar, i.e. compared to the 'normal' sdB stars carbon is slightly enriched. We determined upper limits for oxygen, aluminum, silicon, and phosphorus to be mostly subsolar (oxygen −1.0 dex, aluminum −0.2 dex, and silicon ~ -1.5 dex). For phosphorous we derived an upper limit which is inconclusive because it is suprasolar (+0.8 dex). The abundance for sulfur is determined to be enriched (+0.7 dex, with respect to the solar value).

However, the iron group elements together with argon are enormously enriched: argon +3.5 dex, calcium +1.7 dex, scandium +3.7 dex, titanium +3.0 dex, vanadium ~ 3.3 dex, manganese +4.0 dex, and nickel +4.6 dex, compared to the solar values. The abundance of vanadium is uncertain: the abundance of V III (+5.5 dex) is inconsistent with that of V IV (+3.4 dex). The abundance of V III, however, rests on three lines only, while those of V IV is based on twelve lines. We, therefore, discard the V III abundance.

The abundances (and upper limits) for all metals are given in Table 4.14. Additionally, the values are plotted, with respect to the solar abundances, in Fig. 4.20. Note the very good agreement of the results drawn from different ionization levels for carbon (except for C II, the reason is unclear), and titanium (within the given error limits).

The curve-of-growths for the C III, Ca III, Ti III, and V IV lines are consistent with a vanishing microturbulence ($\xi \leq 2$ km/s).

Due to the very sharp metal lines we could determine a projected rotational velocity of $v \sin(i) < 2$ km/s. We conclude that UVO 0512−08 is a very slowly rotating star, unless seen pole-on.

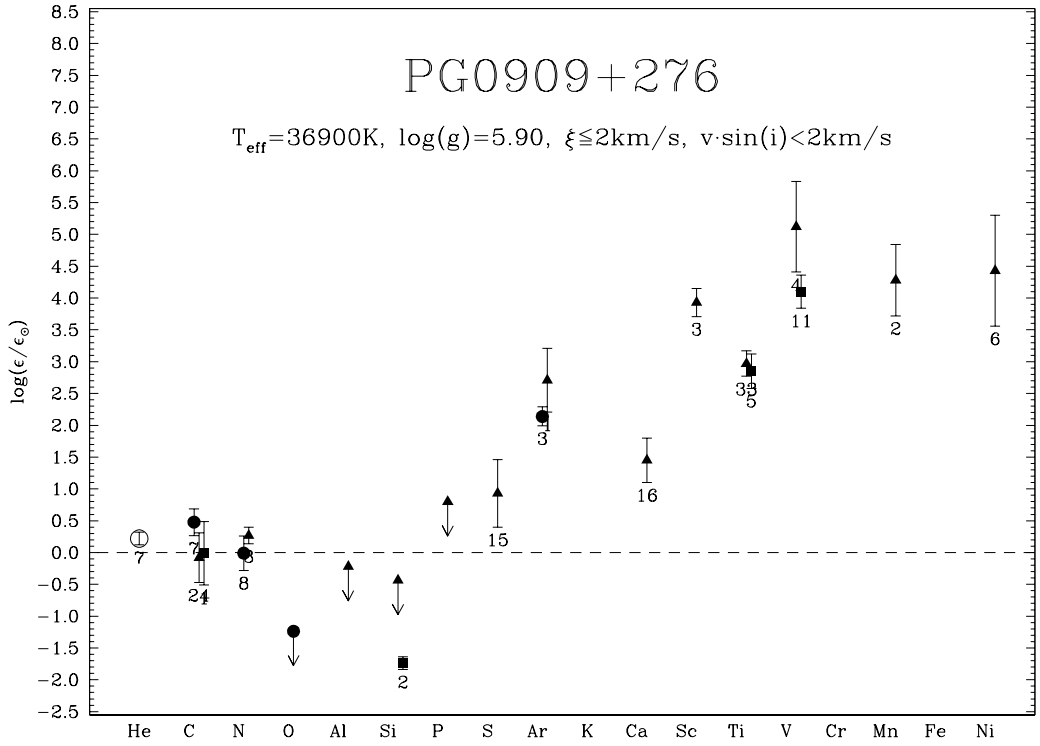

Figure 4.21: LTE abundances with error bars for PG 0909+276 relative to the solar values (dashed horizontal line). Abundances derived from neutral elements are shown as open circles, from singly ionized ones as filled circles, from doubly ionized ones as filled triangles, and from triply ionized ones as filled squares. The numbers indicate the number of lines per ion used.

Table 4.15: LTE metal abundances for PG 0909+276 compared to solar composition; n is the number of spectral lines per ion used for the analysis.

ion	n	$\log(\varepsilon)$	$\log(\varepsilon_\odot)$	ion	n	$\log(\varepsilon)$	$\log(\varepsilon_\odot)$
He I+II	7	11.15 ± 0.10	10.930	Ar II	3	8.54 ± 0.15	6.400
C II	7	9.07 ± 0.21	8.592	Ar III	1	9.11	6.400
C III	24	8.51 ± 0.39	8.592	Ca III	16	7.81 ± 0.35	6.360
C IV	1	8.58	8.592	Sc III	3	7.10 ± 0.22	3.170
N II	8	7.92 ± 0.27	7.931	Ti III	33	7.99 ± 0.20	5.020
N III	3	8.20 ± 0.13	7.931	Ti IV	5	7.87 ± 0.27	5.020
O II	0	<7.50	8.736	V III	4	9.12 ± 0.71	4.000
Al III	0	<6.25	6.470	V IV	11	8.10 ± 0.26	4.000
Si III	0	<7.10	7.536	Mn III	2	9.67 ± 0.56	5.390
Si IV	2	5.80 ± 0.10	7.536	Ni III	6	10.68 ± 0.87	6.250
P III	0	<6.25	5.450				
S III	15	8.26 ± 0.53	7.330				

PG 0909+276

For the metal abundance analysis of PG 0909+276 (sdOB, $T_{\rm eff} = 36\,900$K, $\log(g) = 5.9$) we used a spectrum coadded from three observations obtained in January 2000 at the DSAZ.

Like in the case of UVO 0512−08, we identified lines of of the type Ca III, Sc III, Ti III, Ti IV, V III, V IV, Mn III and Ni III beside the 'normal' ion lines (C II, C III, C IV, N II, N III, Si IV, S III, Ar II, and Ar III) However, 125 ($\sim 23\%$) of the lines remained unidentified. Again, we found no lines due to iron.

The abundances determined for carbon, and nitrogen are, like PG 0909+276, consistent with solar values. Upper limits for oxygen, and aluminum indicate that these elements are depleted (−1.2 dex, and −0.2, respectively, compared to the solar values), while that of phosphorus is suprasolar (+0.8 dex). For silicon we determined a strongly depleted value (−1.7 dex), those for sulfur is enriched (+1.3 dex).

Again, like UVO 0512−08, the iron group elements together with argon are enormously enriched: argon +2.1 dex, calcium +1.5 dex, scandium +4.0 dex, titanium +3.0 dex, vanadium +4.1 dex, manganese +4.3 dex, and nickel +4.4 dex, compared to the solar values.

The abundances determined for different ionization levels are consistent for carbon, nitrogen, argon, and titanium (within the given error limits). Only for vanadium the abundance determined for the doubly ionized element is larger by about +1.9 dex than the triply ionized. However, only four lines of V III are used for the analysis (in comparison to eleven lines for V IV).

The abundances (and upper limits) for all metals are given in Table 4.15. Additionally, the values are plotted, with respect to the solar abundances, in Fig. 4.21.

A sufficient number of carbon, sulfur, calcium, and titanium lines has been measured to allow to determine the microturbulence, $\xi \leq 2$ km/s was found.

A projected rotational velocity of $v \sin(i) < 2$ results from the fit of the carbon, and nitrogen lines. Therefore, if not seen pole-on, PG 0909+276 is probably very slowly rotating.

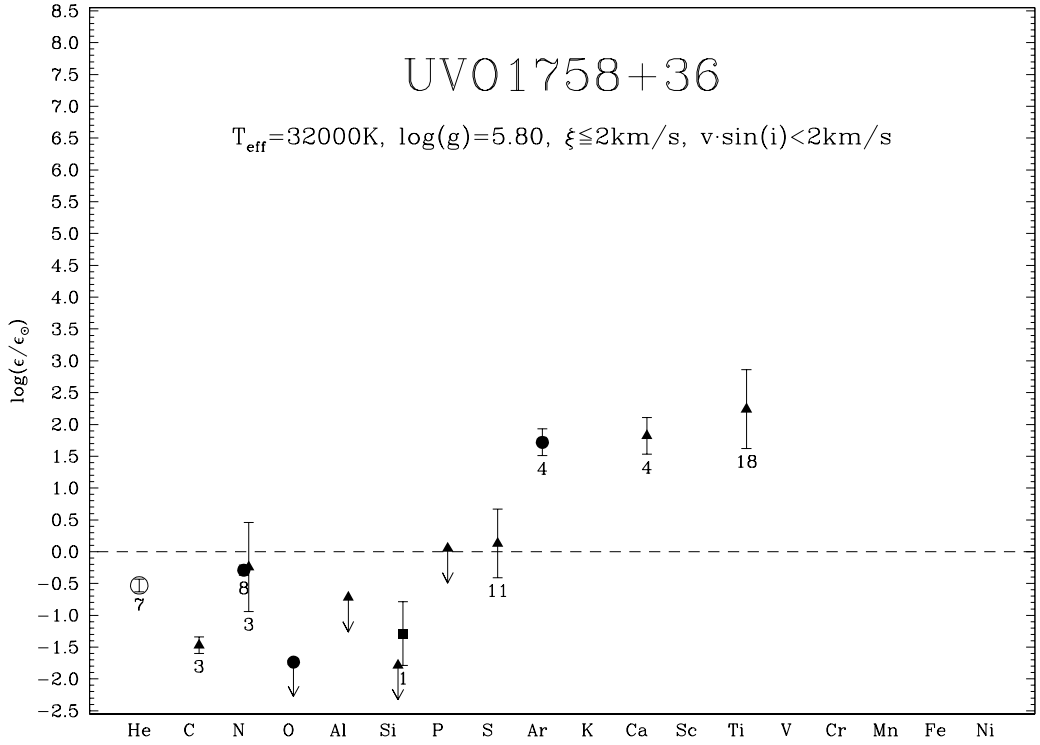

Figure 4.22: LTE abundances with error bars for UVO 1758+36 relative to the solar values (dashed horizontal line). Abundances derived from neutral elements are shown as open circles, from singly ionized ones as filled circles, from doubly ionized ones as filled triangles, and from triply ionized ones as filled squares. The numbers indicate the number of lines per ion used.

Table 4.16: LTE metal abundances for UVO 1758+36 compared to solar composition; n is the number of spectral lines per ion used for the analysis.

ion	n	$\log(\varepsilon)$	$\log(\varepsilon_\odot)$	ion	n	$\log(\varepsilon)$	$\log(\varepsilon_\odot)$
He I+II	7	10.40 ± 0.10	10.930	Si IV	1	6.25	7.536
C III	3	7.12 ± 0.13	8.592	P III	0	<5.50	5.450
N II	8	7.64 ± 0.08	7.931	S III	11	7.46 ± 0.54	7.330
N III	3	7.69 ± 0.70	7.931	Ar II	4	8.12 ± 0.21	6.400
O II	0	<7.00	8.736	Ca III	4	8.18 ± 0.29	6.360
Al III	0	<5.75	6.470	Ti III	18	7.26 ± 0.62	5.020
Si III	0	<5.75	7.536				

UVO 1758+36

We coadded three spectra of UVO 1758+36 (sdB, $T_{\rm eff}$ = 32 000K, $\log(g)$ = 5.8) obtained in September 1998 at the DSAZ. From this spectrum, we identified metal lines of the species C III, N II, N III, Si IIV, S II, S III, Ar II Ca III, and Ti III. Again, as for UVO 0512−08 and PG 0909+276, many lines remained unidentified, and no line due to iron was found.

The light elements show a similar abundance pattern as seen in the 'normal' sdB stars: carbon is strongly depleted (−1.7 dex), nitrogen is almost solar (−0.2 dex), and upper limits for oxygen, aluminum, and silicon are consistent with subsolar values (−1.7, −0.7, and −1.8 dex, respectively), while the abundances determined for argon, calcium, and titanium are again strongly enriched (+1.7, +1.7, and +2.3 dex, respectively, compared to the solar values). These enrichments, however, are smaller than in UVO 0512−08 and PG 0909+276, making UVO 1758+36 an intermediate object between the 'normal' and peculiar sdB stars.

The abundances (and upper limits) for all metals are given in Table 4.16. Additionally, the values are plotted, with respect to the solar abundances, in Fig. 4.22.

From the Ti III lines we are able to determine a microturbulence of $\xi \leq 2$ km/s.

The metal lines are all very sharp. From the nitrogen lines we could measure that UVO 1758+36 is likely to be a very slow rotator ($v \sin(i) < 2$ km/s), unless seen pole-on.

4.2.3 Summary of the results

Spectral lines of the species C II, C III, C IV, N II, N III, O II, O III, Mg II, Al III, Si II, Si III, Si IV, P III, S II, S III, Ar II, Ar III and Fe III can be identified in almost all program stars (see Table C). Noteable exceptions are PHL 932 and UVO 1735+22. For PHL 932 only a few N II, N III, and S III lines could be identified. UVO 1735+22 displays no metal lines at all. The numerically dominant (more than 20 lines/ion) metal lines in ten stars are mostly from N II, O II and Fe III.

Three sdB stars (UVO 0512−08, PG 0909+276, and UVO 1758+36) show many more lines than the other ones. Most of them are due to Ca III, Sc III, Ti III, Ti IV, V III, V IV, Mn III, and Ni III, which have never been found before in the optical spectra of sdB stars. However, $\sim 1/4$th of the lines found in each star remained unidentified. The most numerous metal lines here are (in contrast to the 'normal' sdB stars) from Ca III and Ti III. It is remarkably that no lines due to iron are found within the spectra of UVO 0512−08, PG 0909+276, and UVO 1758+36, whereas all 'normal' sdB stars do show many Fe III lines.

From curve-of-growth measurements, mostly for N II, O II, and Fe III, we determined microturbulent velocities of $\xi \leq 2$ km/s for all stars, except for CD−35° 15910 ($\xi = 6 \pm 1$ km/s), and LB 1516 ($\xi = 3 \pm 1$ km/s).

We determined projected rotational velocities of $v \sin(i) < 3$ km/s for almost all program stars. The only exceptions are HD 171858, for which we yielded a value of 6 ± 1 km/s, and UVO 1735+22, for which we estimates a $v \sin(i) < 20$ km/s from the helium lines, due to lack of metal lines. Nevertheless, all stars are (very) slowly rotating stars, because it is very unlikely that all are observed pole-on.

'Normal' sdB stars

Surprisingly, almost all program stars show very similar abundance patterns (see e.g. Fig. 4.23). Carbon, oxygen, magnesium, and aluminum are always strongly depleted ($\sim$ -1.0 dex, with respect to the solar composition). Nitrogen is mainly slightly underabundant (~ -0.3 dex). Silicon and sulfur are subsolar ($-0.3 \ldots -0.7$ dex). Iron is always about solar and argon is even suprasolar ($\sim +0.5$ dex) for all analysed stars.

The remarkable consistence of the abundances determined for different ionization levels in almost all stars shows the accuracy of our method to determine the effective temperature using Balmer and helium line fitting procedures (see Section3.1.2). Because the ionization equilibrium of a given element is a method to determine the effective temperature very precisely.

Three peculiar sdB stars

UVO 0512−08, PG 0909+276, and UVO 1758+36 show very peculiar metal abundances (see Figs. 4.20, 4.22, and 4.21). Carbon and nitrogen are about solar, i.e. compared to the 'normal' sdB stars carbon is slightly enriched. Silicon is depleted (≈ -2 dex); sulfur and calcium are suprasolar (+1 to +2 dex). But the iron group elements (Sc, Ti, V, Mn, and Ni) together with argon are enormously enriched by a factor of 1 000 to $\sim$ 32 000 times, with respect to the solar values.

A similar behaviour is observed in Ap stars, where strong magnetic fields are the reason for the enrichment (Strittmatter & Norris 1971). However, no direct evidence for magnetic fields was found in the spectra. Spectropolarimetric observations are needed to measure the magnetic field strengths.

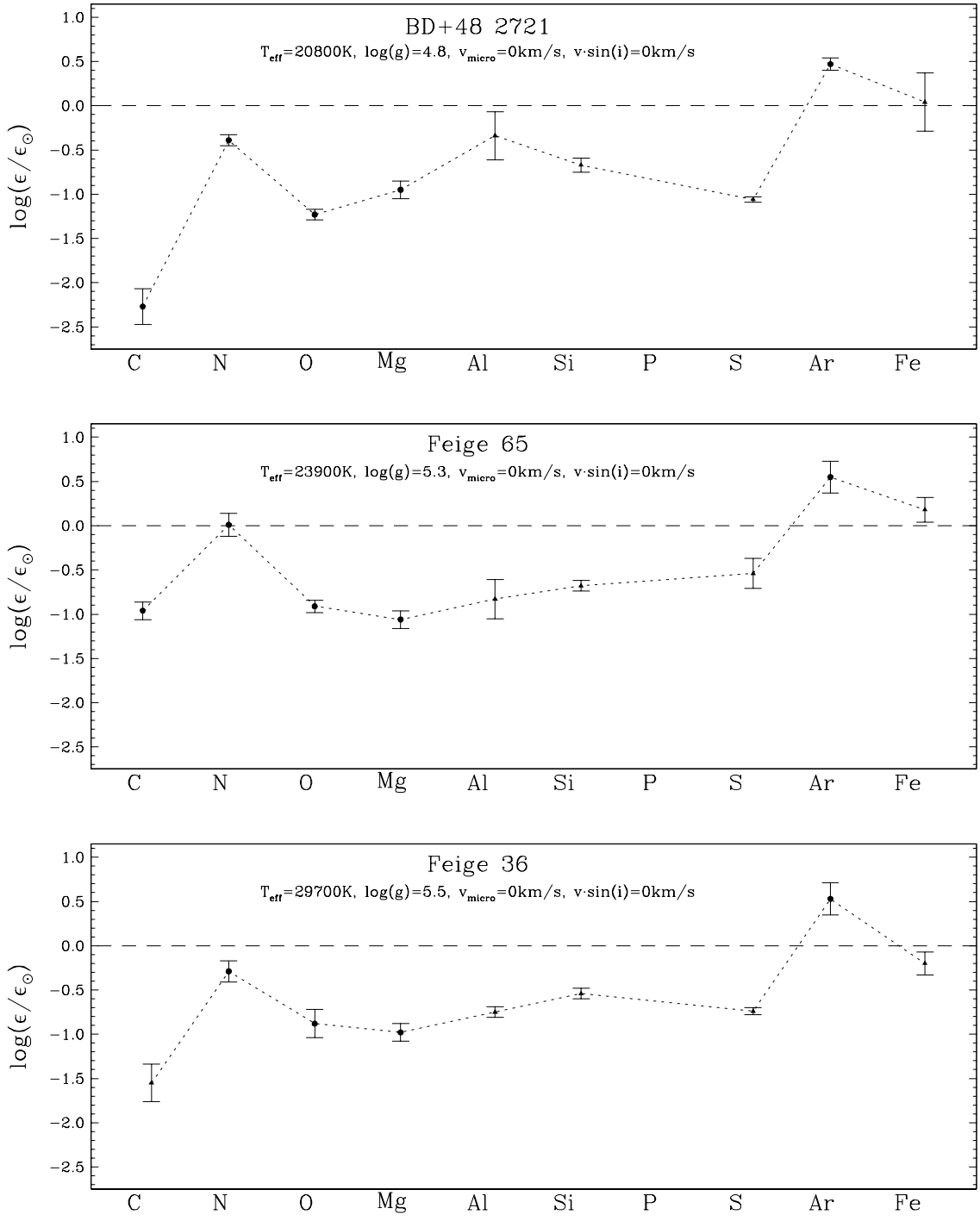

Figure 4.23: LTE abundances with error bars for three program stars relative to the solar values (dashed horizontal lines). Abundances derived from neutral elements are shown as open circles, from singly ionized ones as filled circles, from doubly ionized ones as filled triangles, and from triply ionized ones as filled squares. Note the very similar abundance patterns for all three sdB stars (the abundance values are connected to guide the eyes of the reader).

Again, a remarkable consistency of the abundances determined for different ionization levels in all stars should be noted.

4.3 Trends with atmospheric parameters?

The chemical abundances observed in the atmospheres of sdB stars are very puzzling. There is now general consensus, that the peculiar abundance patterns are due to *diffusion*. Diffusion denotes the interplay between radiative acceleration (directly proportional to $T_{\rm eff}$) which levitates particels into upper regions, and the gravity which settles particels into lower regions inside the atmospheres of stars. Therefore, we tried to find possible trends of the chemical composition with $T_{\rm eff}$ and $\log(g)$ for our program stars.

4.3.1 Helium abundances

At first, we compare the derived helium abundances[2] with the measured stellar parameters $T_{\rm eff}$, $\log(g)$, and luminosity[3] for all apparently single EHB program stars in Figs. 4.24, 4.25, and 4.26.

First of all, we discovered a clear correlation between the helium abundance and the effective temperature: The larger the temperature, the larger the helium content (cf. Fig. 4.24). Furthermore, there seems to be a separation into two sequences of sdB stars in the $T_{\rm eff}$ – helium abundance plane. A fraction of our analysed sdB stars (about 1/6th, indicated with filled symbols) have much lower helium abundances at the same temperatures than the bulk of the sdB stars.

Fig. 4.25 may indicate a connection between the helium abundance and the gravity. However, for sdB stars the gravity is not independent of the effective temperature (see Eq. 3.1) since the horizontal branch is a sequence of nearly constant luminosity. The stars that seperate from the main bulk (filled circles) in Fig. 4.24 lie somewhat below the main bulk in Fig. 4.25 as well, but do not separate as clearly as in the former diagram.

The luminosity as derived from gravity and $T_{\rm eff}$ (see Eq. 3.1). is plotted in Fig. 4.26. No correlation is detectable. However, for the peculiar sdB stars (indicated with filled symbols) there is a slight tendency for a correlation to occur at higher luminosities.

To verify our discoveries, we added the results of Saffer et al. (1994, squares) and Maxted et al. (2001, triangles) (see Section 3.3) to ours in Figs. 4.24 to 4.26. The correlation between the helium abundance and the effective temperature is confirmed. Furthermore, the suggested separation into two sequences (cf. Fig. 4.24) is reinforced.

A linear regression for the bulk of sdB stars (open symbols) gives:

$$\log(n_{\rm He}/n_{\rm H}) = -3.53 + 1.35 \cdot \left(\frac{T_{\rm eff}}{10^4{\rm K}} - 2.00 \right) \tag{4.1}$$

For the other sequence (filled symbols, except the upper limit values indicated by downward arrows) we get:

$$\log(n_{\rm He}/n_{\rm H}) = -4.79 + 1.26 \cdot \left(\frac{T_{\rm eff}}{10^4{\rm K}} - 2.00 \right) \tag{4.2}$$

[2]For the determination of the helium abundances, see Section 3.1.2

[3]We express the luminosity in terms of the Eddington Luminosity L_e (for electron scattering, see Eq. 3.1).

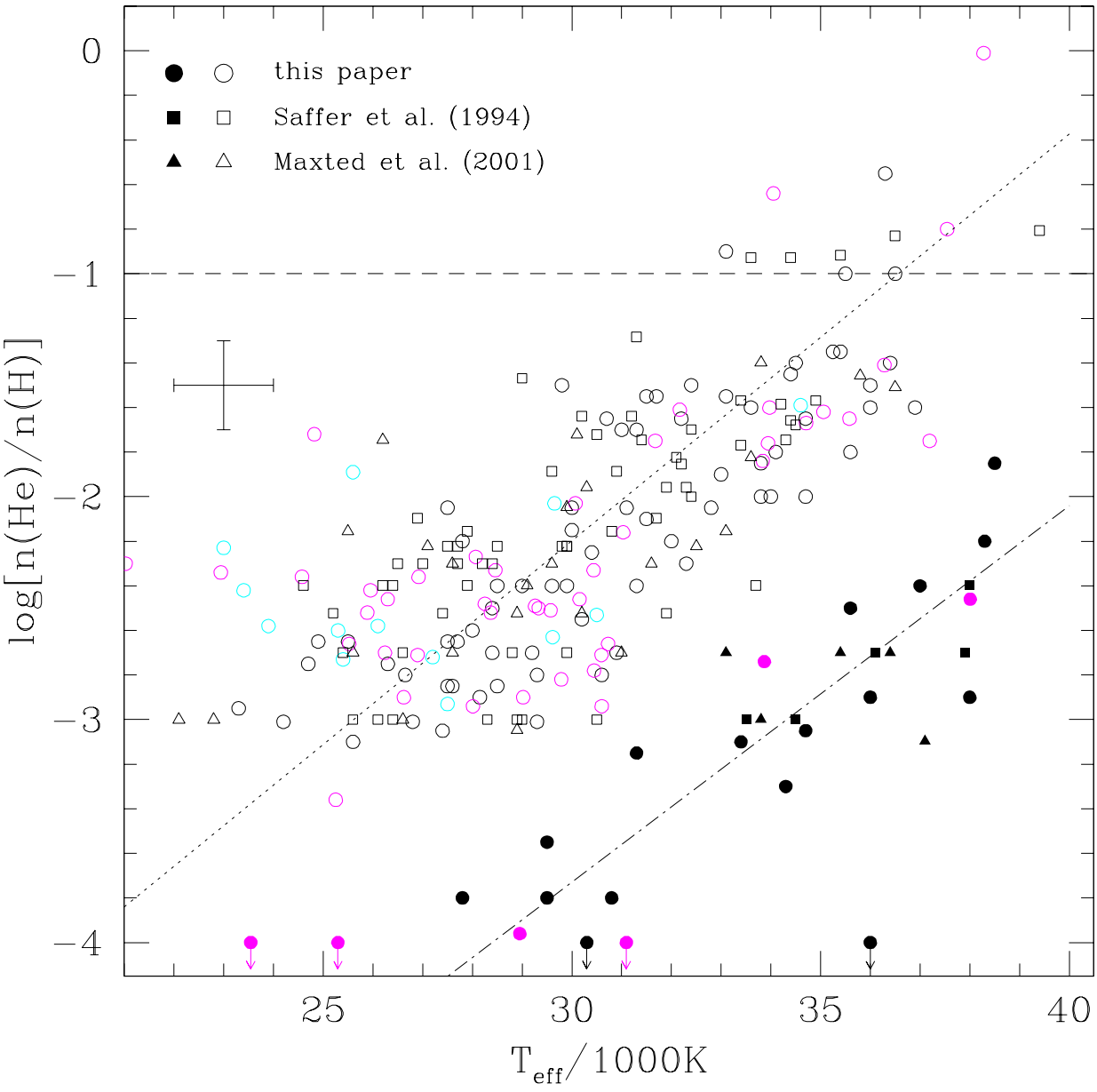

Figure 4.24: Plot of the helium abundance versus effective temperature for all HQS, HES (1999 and 2001 runs), and bright sdB stars. Additionally the results of Saffer et al. (1994, squares) and Maxted et al. (2001, triangles) are plotted. The dotted line indicates the linear regression (Eq. 4.1) for the bulk of the sdB stars (open symbols) and the dashed-dotted line shows the linear regression (Eq. 4.2) for the peculiar sdB stars (filled symbols). The dashed horizontal line denotes the solar helium abundance.

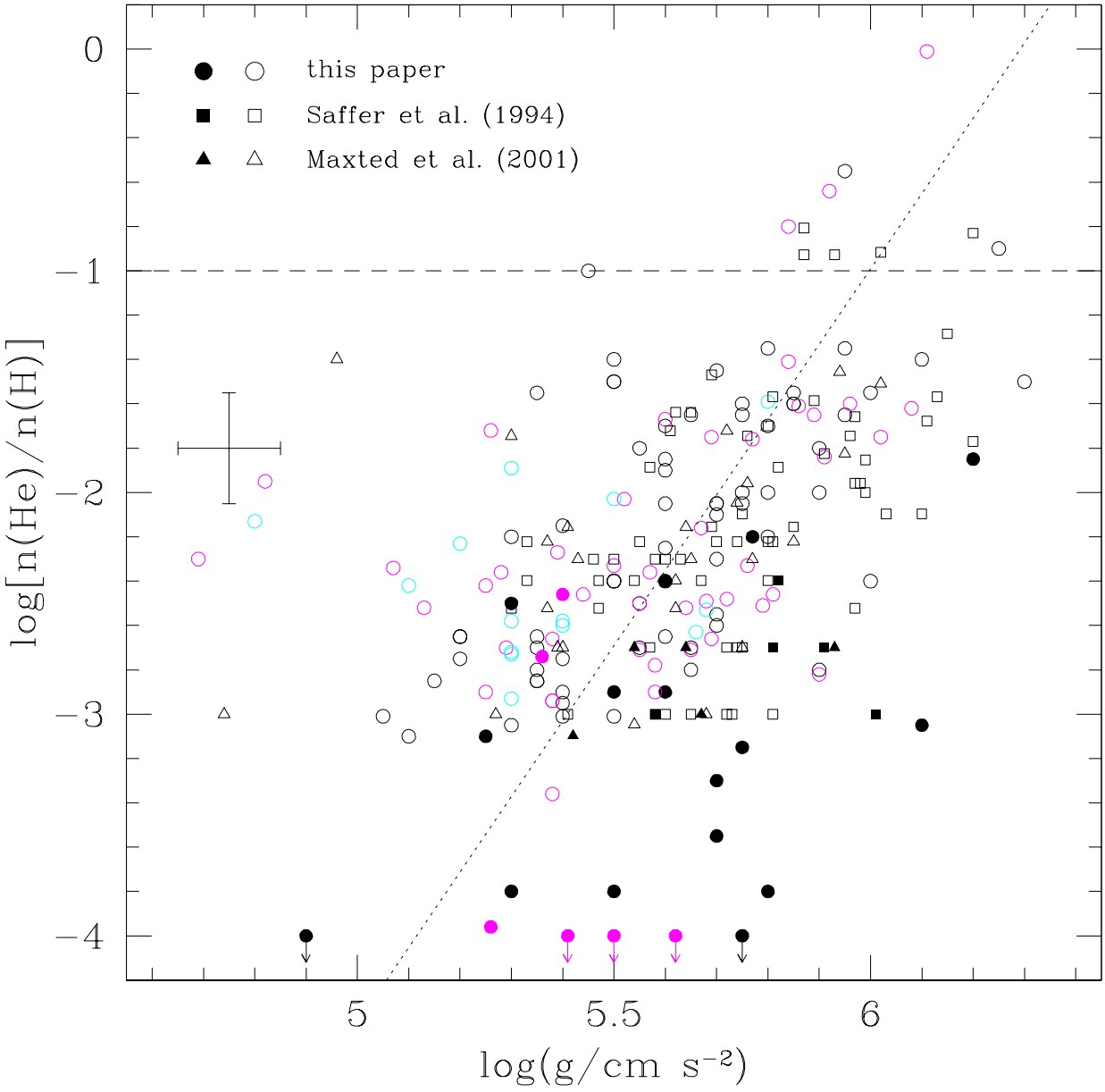

Figure 4.25: Plot of the helium abundance versus gravity for all HQS, HES (1999 and 2001 runs), and bright sdB stars. Additionally the results of Saffer et al. (1994, squares) and Maxted et al. (2001, triangles) are plotted. The dashed horizontal line denotes the solar helium abundance. For the filled symbols cf. Fig. 4.24. The dotted line is the linear regression for the bulk of the sdB stars (open symbols).

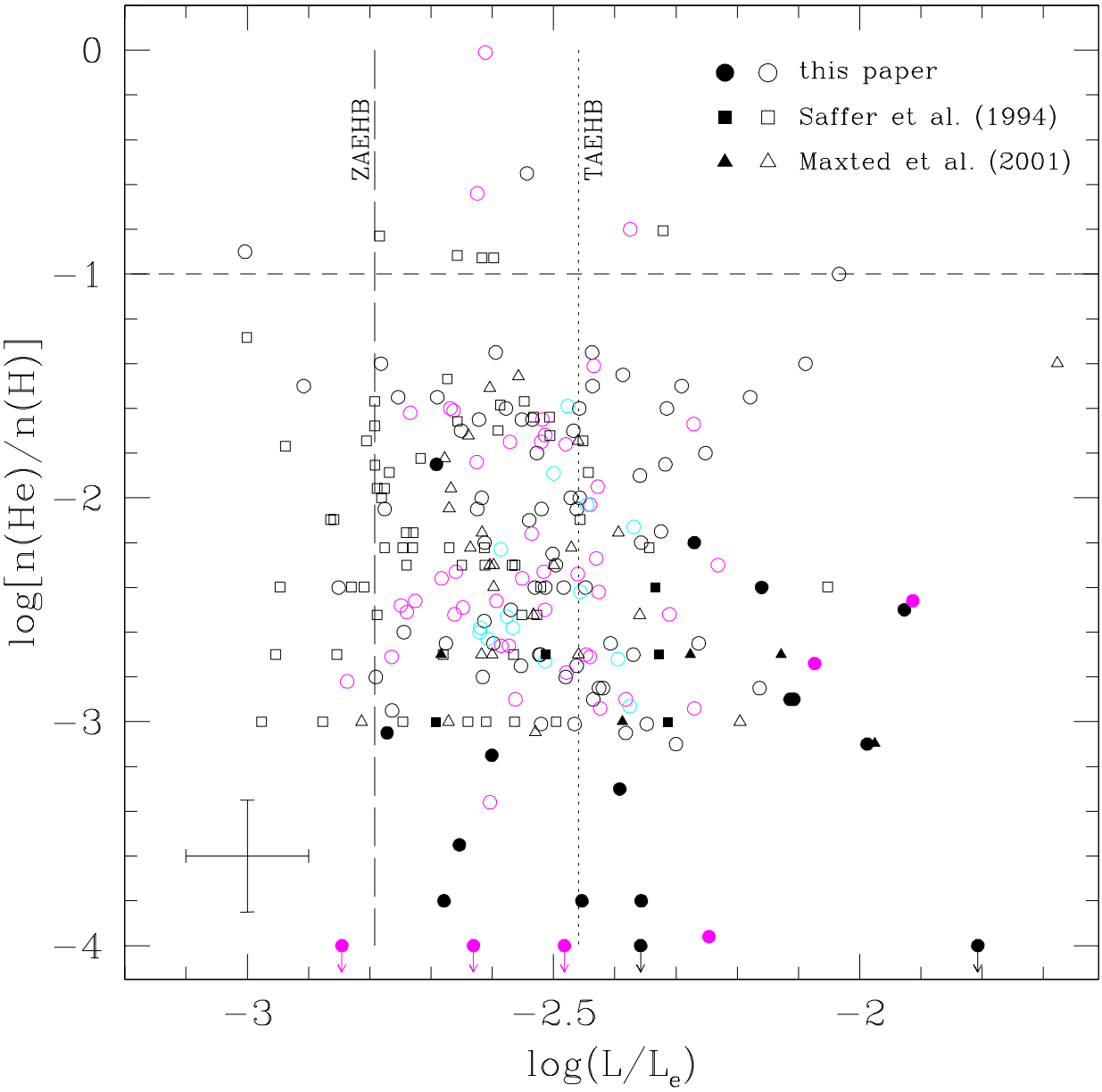

Figure 4.26: Plot of the helium abundance versus luminosity (with respect to the Eddington luminosity L_e, see Eq. 3.1) for all HQS, HES (1999 and 2001 runs), and bright sdB stars. Additionally the results of Saffer et al. (1994, squares) and Maxted et al. (2001, triangles) are plotted. The dashed horizontal line denotes the solar helium abundance, the long dashed vertical line denotes the ZAEHB, and the dotted vertical line the TAEHB. For the filled symbols cf. Fig. 4.24.

4.3.2 Metal abundances

We tried to find correlations between the element abundances for the analyzed sdB stars and the atmospheric parameters (effective temperature or gravity) or any combination of them (e.g. luminosity, see Eq. 3.1).

Additionally, we included the results of metal abundance analyses for six sdB stars from literature, with spectral coverage, resolution and analysis methods comparable to ours. In detail: Four pulsating sdB stars (PG 1605+072, Heber, Reid & Werner 1999; Feige 48, KPD 2109+4401 and PG 1219+534, Heber, Reid & Werner 2000) and two sdB stars, which are part of a binary system (sdB+WD, Feige 36, Edelmann et al. 1999, and HE 1047-0436, Napiwotzki et al. 2001b).

Figs. 4.27 to 4.29 show the results for all analyzed metals. We use different symbols to distinguish apparently single, non-pulsating, stars (filled circles), radial velocity variables (filled triangles), pulsating sdB stars (open circles), and apparently peculiar stars (asterisks).

- **C** II

  The abundances determined from C II show a large scatter all over the parameter space. No clear trend can be found.

  The results drawn from the RV variable, and apparently single non-pulsators show no differences. However, a bimodality can be assumed. About one half show a strong depletion (~ -2.0 dex), whereas the others are only moderate sub-solar (-1.0 to -0.3 dex).

  The peculiar sdB stars show a noticeably larger abundance (+0.5 dex, with respect to the solar value) than the others.

- **C** III (only detectable in the hotter stars)

  The scatter of the abundances determined from C III is even larger than from C II. We can find no trend.

  There are no obvious differences between the different groups of sdB stars.

- **N** II

  The abundances drawn from N II lines are almost perfectly constant all over the parameter space.

  No differences became apparent for the different groups of sdB stars, i.e. all analyzed sdB stars do have a nitrogen content of -0.2 ± 0.4 dex (with respect to the solar value).

- **O** II

  A trend for the O II abundance with the effective temperature seems to exist: The larger the temperature, the larger is the oxygen content for the bulk of the analyzed stars. In addition, as seen for helium (cf. Section 4.3.1), there might be a group of stars (six stars (30%) in the lower right corner of the $T_{\rm eff}$–abundance–plane) which have a lower oxygen content than the bulk of stars at the same temperature. A separation into two groups can also be assumed in the abundance versus gravity plane: All stars with gravities of $\log(g) \geq \sim 5.65$ dex have lower oxygen abundances than the ones with lower gravities. No trend nor any separation into different groups is found in the abundance versus luminosity plane.

  There are no obvious differences between the different groups of sdB stars.

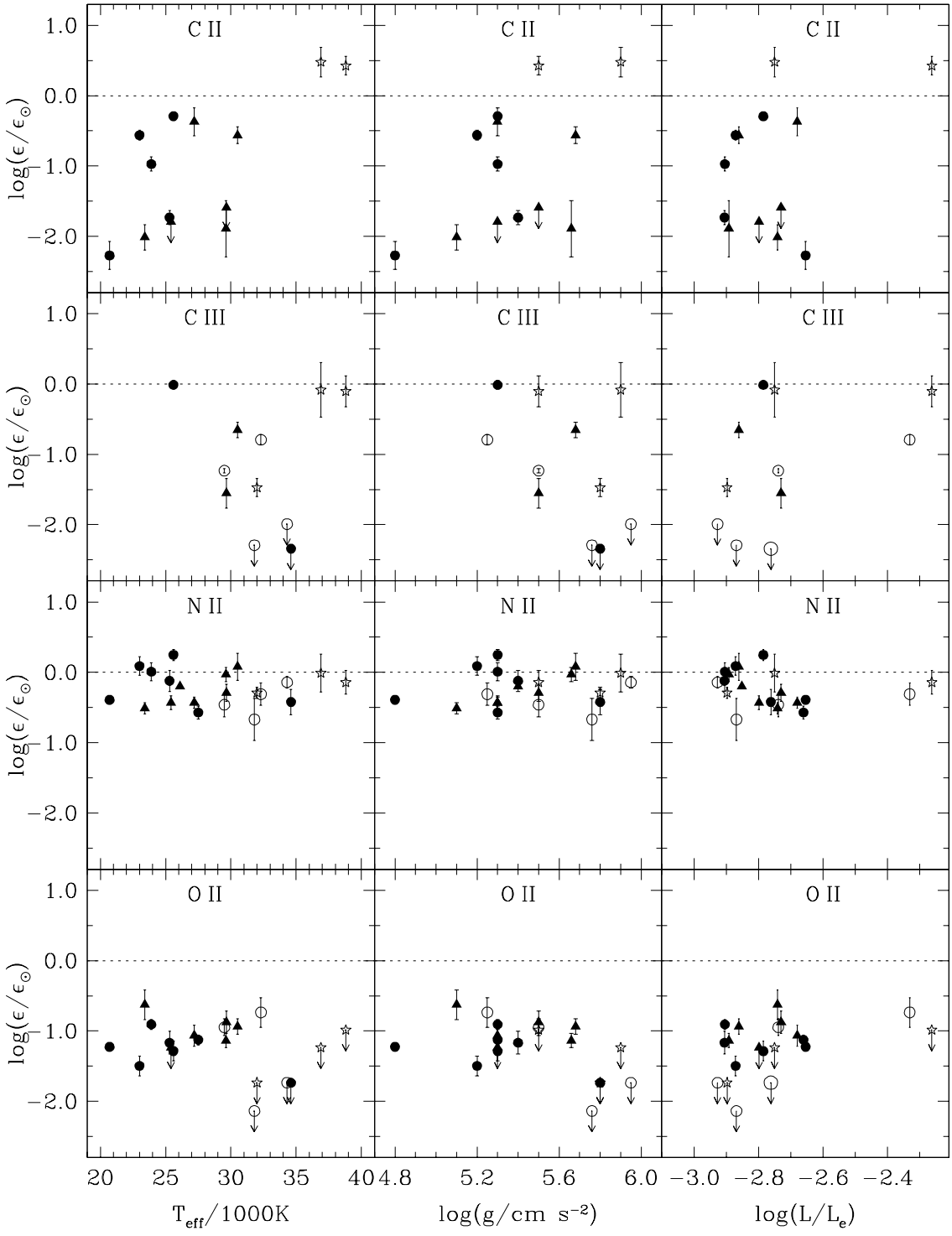

Figure 4.27: LTE abundances for C II, C III, N II, and O II with error bars for all analyzed stars. Pulsating stars are plotted as open circles, RV variable stars are plotted as filled triangles, apparently single non pulsators are plotted as filled circles, and the peculiar sdB stars are plotted as asterisks.

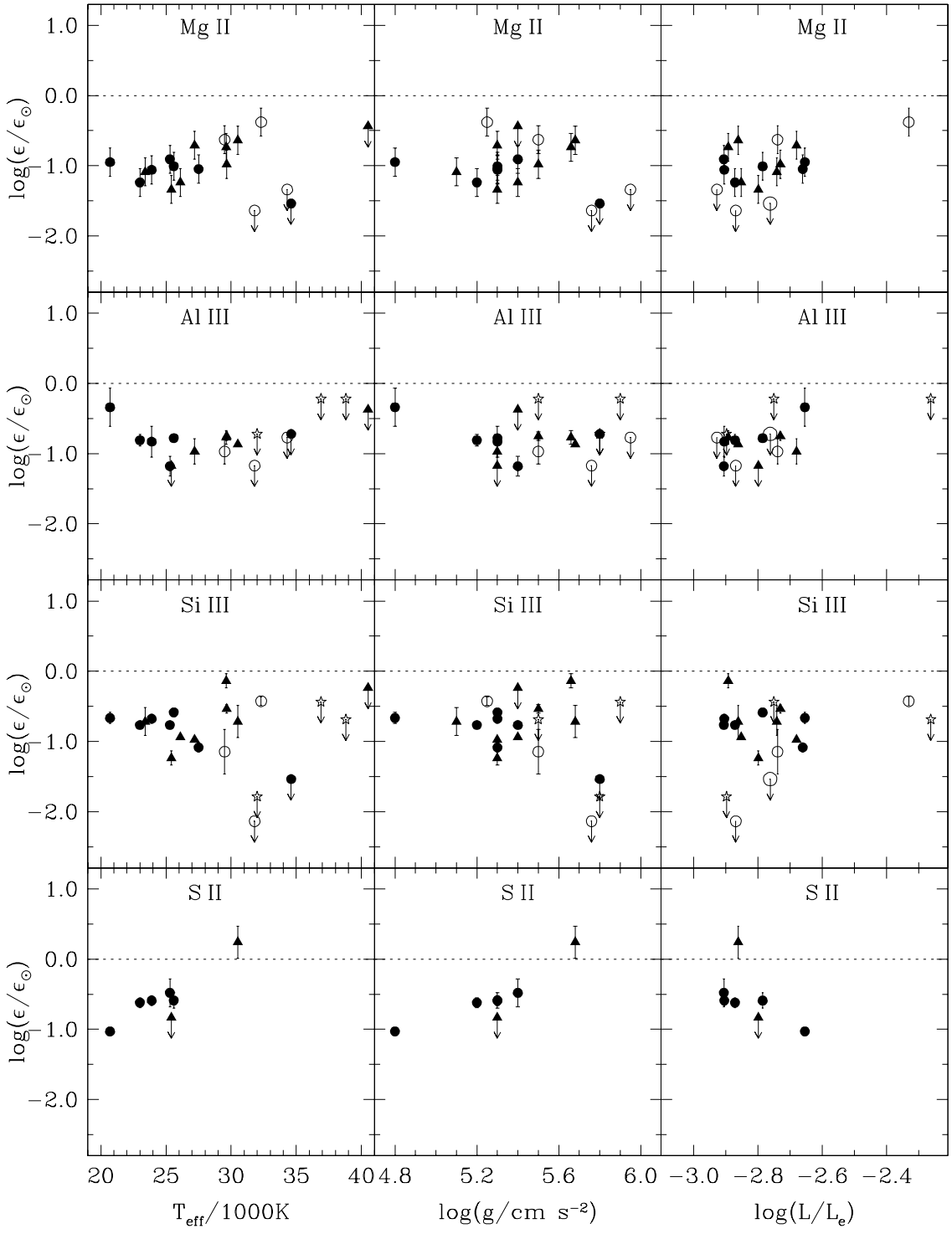

Figure 4.28: LTE abundances for Mg II, Al III,Si III, and S II with error bars for all analyzed stars. Pulsating stars are plotted as open circles, RV variable stars are plotted as filled triangles, apparently single non pulsators are plotted as filled circles, and the peculiar sdB stars are plotted as asterisks.

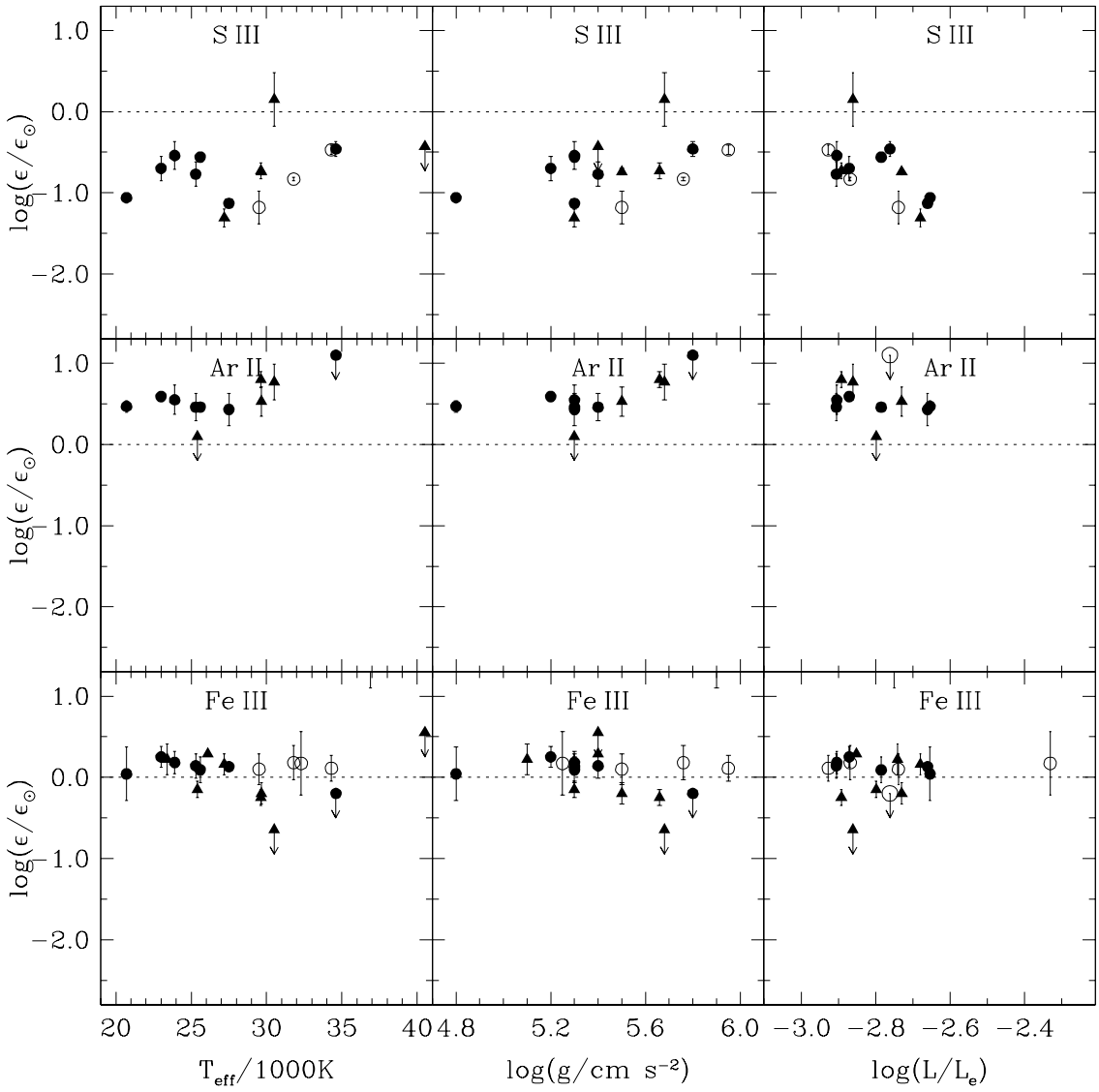

Figure 4.29: LTE abundances for S III, Ar II, and Fe III with error bars for all analyzed stars. Pulsating stars are plotted as open circles, RV variable stars are plotted as filled triangles, apparently single non pulsators are plotted as filled circles, and the peculiar sdB stars are plotted as asterisks.

- **Mg** II

  Similar to O II, a slight correlation for the Mg II abundance with the effective temperature might exist: The larger the temperature, the larger is the magnesium content for the bulk of the analyzed sdB stars (except the one with the coolest temperature, and for all those with upper limit results).

  A separation into two groups, the bulk showing larger abundances at lower temperatures, and some at higher temperatures with lower abundances (upper limits), can be also suggested. Again, as seen for O II, all stars with gravities $\log(g) \geq 5.65$ have lower magnesium abundances, than those with lower gravities. No trend nor any separation into different groups is found in the abundance versus luminosity plane.

  No obvious differences between the groups of sdB stars can be detected all over the parameter space.

- **Al** III

  All stars are consistent with an aluminum abundance of -0.9 ± 0.3 dex (with respect to the solar value).

  There are no obvious differences between all groups of sdB stars.

- **Si** III

  The abundances determined from Si III show a large scatter all over the parameter space. No clear trend can be found.

  No obvious differences between the groups of sdB stars can be detected all over the parameter space.

- **S** II

  A trend of the S II abundance with the effective temperature and/or gravity seems to exist: the larger the effective temperature and/or gravity, the larger the S II abundance. However, there are only few of our program stars showing S II lines at all.

  No differences between the RV variable and non-variable sdB stars became apparent.

- **S** III

  The abundances drawn from S III lines are almost constant all over the parameter space. Discarding the RV variable star HE 1047−0436 showing a solar value (within the given error limit), all stars are consistent with a S III abundance of -0.9 ± 0.4 dex (with respect to the solar value).

  There are no differences between the different groups of sdB stars.

- **Ar** II

  All stars are consistent with an supra-solar argon abundance of $+0.6 \pm 0.2$ dex. Only one RV variable sdB star (PG 0001+275) has an upper limit of about the solar content.

  No obvious differences between the groups of sdB stars can be detected all over the parameter space.

- **Fe** III

  Discarding the RV variable star HE 1047−0436 which shows an upper limit of −0.6 dex (comparing to the solar value), all stars are consistent with a solar Fe III abundance (0.0 ± 0.3 dex).

  There are no differences between the different groups of sdB stars.

Summarizing the findings described above:

1. The abundances determined for almost all elements are constant all over the parameter space. Only for singly ionized carbon, oxygen, magnesium, and sulfur a trend for the abundance with one or two atmospheric parameter seem to exist: the larger the temperature, the larger the abundance for C II, O II, Mg II, and S II, and the larger the gravity, the larger the abundance for C II, S II. However, more sdB stars need to be analyzed for their metal abundances, to proof or discard our suggested trends.

2. No obvious differences for the abundances determined for pulsating or non-pulsating, and RV variable or non-variable sdB stars became apparent.

4.4 Helium line shifts

After Doppler-correction of all spectra to laboratory wavelength positions we discovered that for BD+48° 2721, and PG 0133+114 the He I 4921Å and 6678Å lines are still shifted somewhat to higher wavelength positions, whereas the other He I lines were unshifted. For all other spectra all He I lines show no line shifts.

This phenomenon can possibly be explained, assuming an isotopic line shift for ^{3}He, i.e. ^{3}He is strongly enriched in the atmospheres of BD+48° 2721, and PG 0133+114. Laboratory measurements of Fred et al. (1951) show that, within our observational wavelength coverage, the lines of He I 4921Å and 6678Å should have the largest isotopic line shifts, He I 5015Å should be shifted a small amount, and the lines of He I $\lambda\lambda$ 4471Å, 4713Å, and 5876Å should show almost no line shifts. This is perfectly consistent with the behavior of the He I lines for BD+48° 2721, and PG 0133+114 (see Fig 4.30).

With this discovery, we double the number of known sdB stars showing a ^{3}He isotopic line shift (besides SB 290, Heber 1991b and Feige 36, Edelmann 1999).

Diffusion is the likely cause for the ^{3}He enrichment, since the lighter isotope will float atop the heavier one. However, the time-scale for the process is of the same order as the evolutionary time scale ($\approx 10^8$yrs, Vauclair 1975). This makes the ^{3}He/^{4}He ratio a potential age indicator when new diffusion calculations that allow for the influence of a stellar wind become available.

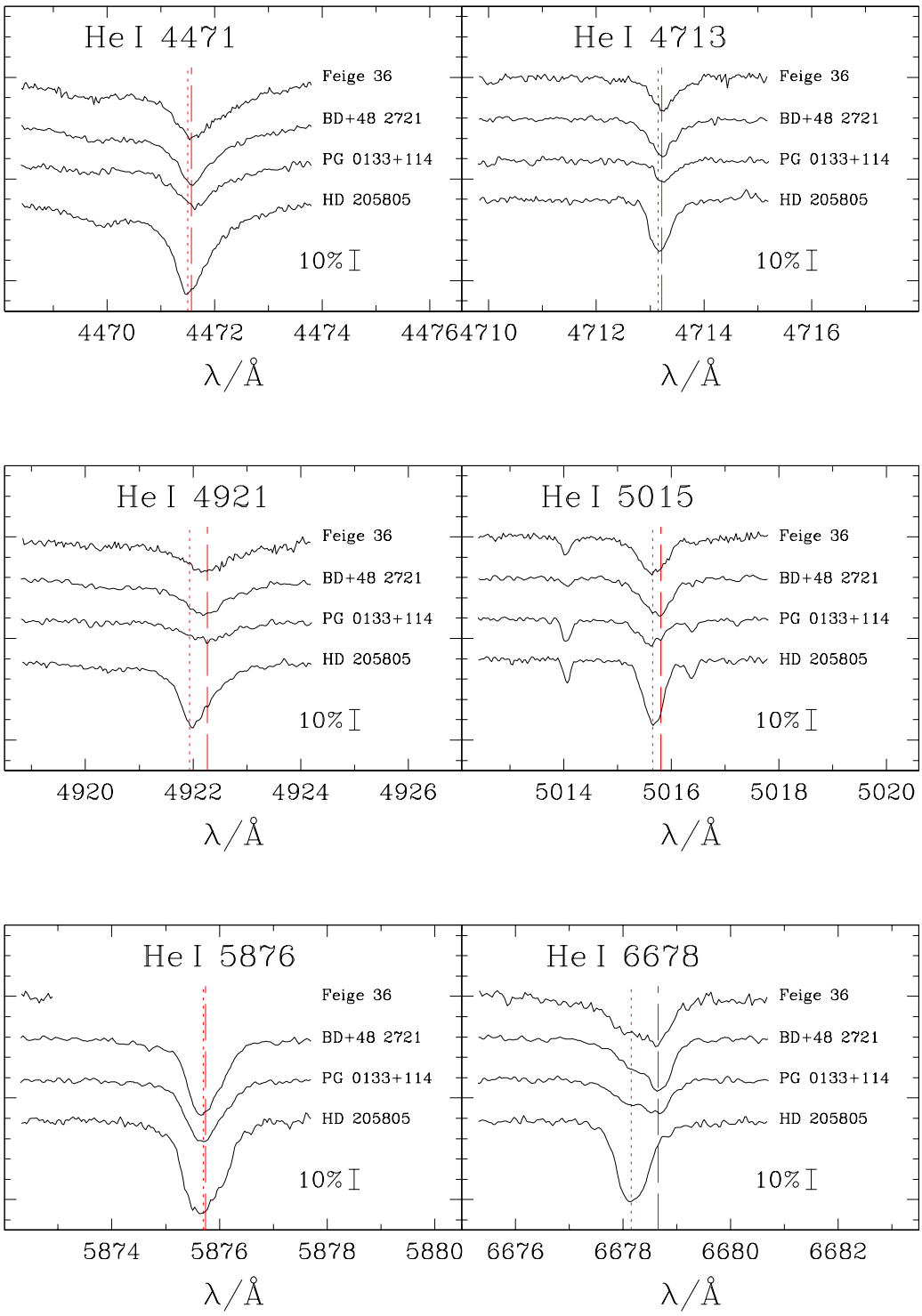

Figure 4.30: Observed line profiles of He I 4471Å and 4713Å (top panel), He I 4921Å and 5015Å (center panel), and He I 5876Å and 6876Å (lower panel) of BD+48° 2721 and PG 0133+114 in comparison to the known ^{3}He sdB star Feige 36 (Edelmann et al. 1999) and the 'normal' program sdB star HD 205805 (the He I 5876Å line of Feige 36 is lying in a gap in between two echelle orders). The laboratory line positions for ^{3}He (dotted line) and ^{4}He (dashed line) are indicated. Note that one can even see BD+48° 2721 having the largest enrichment of ^{3}He in its atmosphere.

Chapter 5

Radial velocity variations

While the evolutionary status of sdB stars as extreme horizontal branch stars is well established, their origin has been under discussion for years. Recent analyses have shown that close binary evolution is fundamental to the origin of sdB stars (Heber et al. 2002). 2/3rd of all sdB stars appear to be radial velocity variable with periods shorter than ten days (Maxted et al. 2001). However, the periods and amplitudes still have to be determined. The unseen companions can only be white dwarfs or low mass main sequence stars. Some of such systems may qualify as type Ia Supernova progenitors as exemplified by the subdwarf B star KPD 1930+2752, for which Maxted, Marsh & North (2000) found a massive WD companion ($M \geq 0.95 M_{\odot}$) and the system mass to exceed the Chandrasekhar mass limit. The typical mass for WD's is about 0.6 $M_{\odot}$, thus it is not very likely to find a system like KPD 1930+2752, i.e. exceeding the mass limit. Nevertheless, in the context of evolutionary theory for close binaries, systems with lower masses are also very interesting, because they went through a common envelope phase (or two such phases if the companion is a white dwarf). The physics of common envelope evolution is still unclear (efficiency parameter α), but very important for the future evolution of the system.

Up to now, radial velocity curves for only 38 sdB binaries are measured (Morales-Rueda et al. 2003, and references therein). Clearly, the sample size has to be increased to constrain evolutionary models.

Previous studies were based on sdB stars drawn from surveys for UV excess objects (e.g. Palomar Green, PG or Kitt Peak Downes, KPD). These stars are mostly rather faint ($B > 13$ mag). Surprisingly some bright sdB stars ($B = 10$ to 12 mag) have been overlooked, because they are not listed in the PG catalog or misidentified due to saturation effects. Serendipitously we discovered three bright sdB stars to be radial velocity (RV) variable in a project to determine metal abundances, rotation velocities, and the isotopic abundance ratio for helium (see last Chapter). The companions are invisible. Therefore we embarked a project to search for RV variation among all program stars.

5.1 Radial velocity measurements

The radial velocities are determined by calculating the shifts of the measured wavelengths of Balmer H_{α}, He I 5876Å and all clearly identified metal lines to laboratory wavelengths. We used the ESO MIDAS software package to fit Gaussian curves to the absorption lines in order to determine their central wavelengths. After the measurement, they were corrected to barycentric[1]

[1]Correction for the orbital velocity of the earth to the barycenter of the solar system.

values.

For our program stars, drawn from the HQS, we decided to determine the RV's only for spectra with spectral resolutions equal to or better than 3.6Å, because the error margins for the spectra of lower resolution are too large to yield meaningful results. The resulting values are accurate to about ±30 km/s and can be found in Table B.1. Out of four stars which were observed twice at different dates, only one sdB star (HS 2333+3927) is found to be a RV variable. Follow-up observations showed this star to be a sdB+M star system with a period of $P = 4^{\rm h}7^{\rm m}24^{\rm s} = 0.171803$ days (Heber et al., in prep.).

Due to the low spectral resolution ($\geq$ 4.5Å) and the uncertain wavelength calibration of the HES spectra (cf. Section 2.4.3) we were worried, whether the measured line shifts are reliable. When comparing our RV's to those measured from high-resolution echelle spectra (kindly provided by R. Napiwotzki, C. Karl, and T. Lisker, priv. comm.), differences of up to $\Delta v_{\rm rad} \approx 100$km/s became apparent. Therefore, we decided not to trust the RV measurement from our HES sample. However, for one star (HE 0437−5439) classified as main sequence B star we determined a RV of $v_{\rm rad} \approx +700$km/s!!! Even, if we consider an error of ±100km/s, this star should be a very high RV object. We will investigate this star in more detail in Chapter 6.

The resulting RV's for the bright sdB stars together with the individual error values are denoted in Table D.1. All together, we took 322 spectra of 47 bright stars for RV measurements. Our aim was to find short term (hours up to days) as well as long term (years) RV variations.

- RV non-variable stars:

  For nine stars (PG 0011+283, HD 4539, PHL 932, PG 0342+026, UVO 0512−08, UVO 1758+36, BD+48° 2721, HD 205805, and CD−35° 15910) we can definitely rule out them to be RV variable stars. Neither short-term (a few hours), nor long-term (weeks or years) variations could be found. All of them have been observed at least four times. Mostly two times one after another in one night, again at least one or a few days later, and again at least one or a few years later (see e.g. Fig. 5.1). The result for PHL 932, to be non RV variable, is consistent with the results of Wade (2001).

- Stars with uncertain status:

  - short-term constant (within a few hours):

    Due to observations taken directly one after another, for three stars we can only rule out them to be short-term RV variable, i.e. RV variable with a period of a few hours. However, they could be RV variable with periods of $P \gtrsim 1$ day.

  - short-term and intermediate-term ($P \lesssim 10$ days) constant:

    Four stars (PG 0909+276, PG 1047+003, LS IV−12 1, and HD 149382) have been observed at least three times, mostly two times one after another in one night, and again at least one or a few nights later. These stars are not RV variable with periods of $P \lesssim 10$ days. However, longer periods cannot be ruled out.

  - intermediate-term constant (within $\sim$ 10 days):

    16 stars were observed at least two times, with a separation of at least one night, but all within one week. All are RV constant during $\sim$ 10 days (see e.g. Fig. 5.2, lower panels). They could, however, be short-term (a few hours, which is unlikely but possible) or long-term (longer than $\sim$10 days) RV variable.

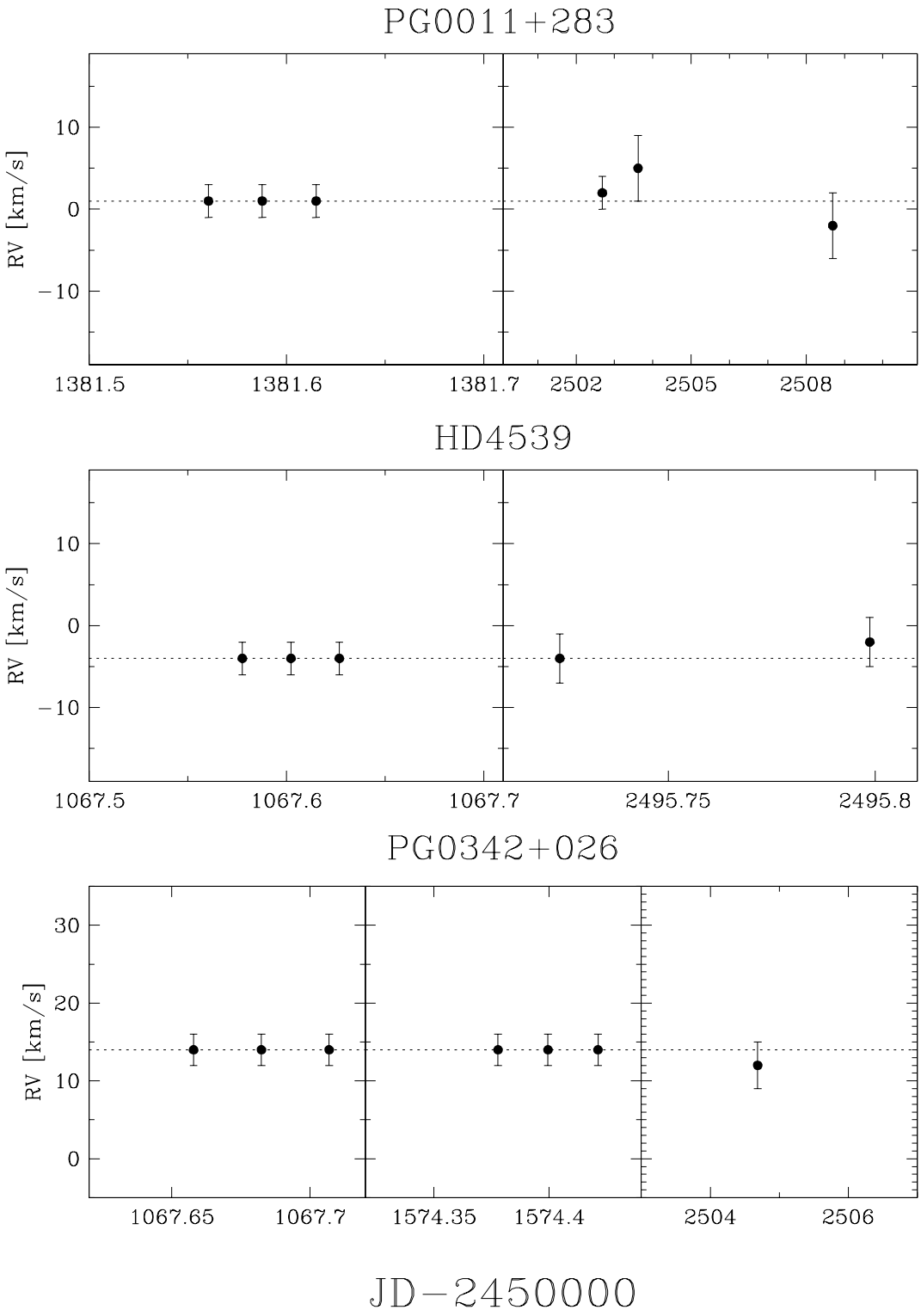

Figure 5.1: Radial velocity measurements for three bright program stars. All stars are neither short-term (within a few hours), nor long-term (weeks or years) variable.

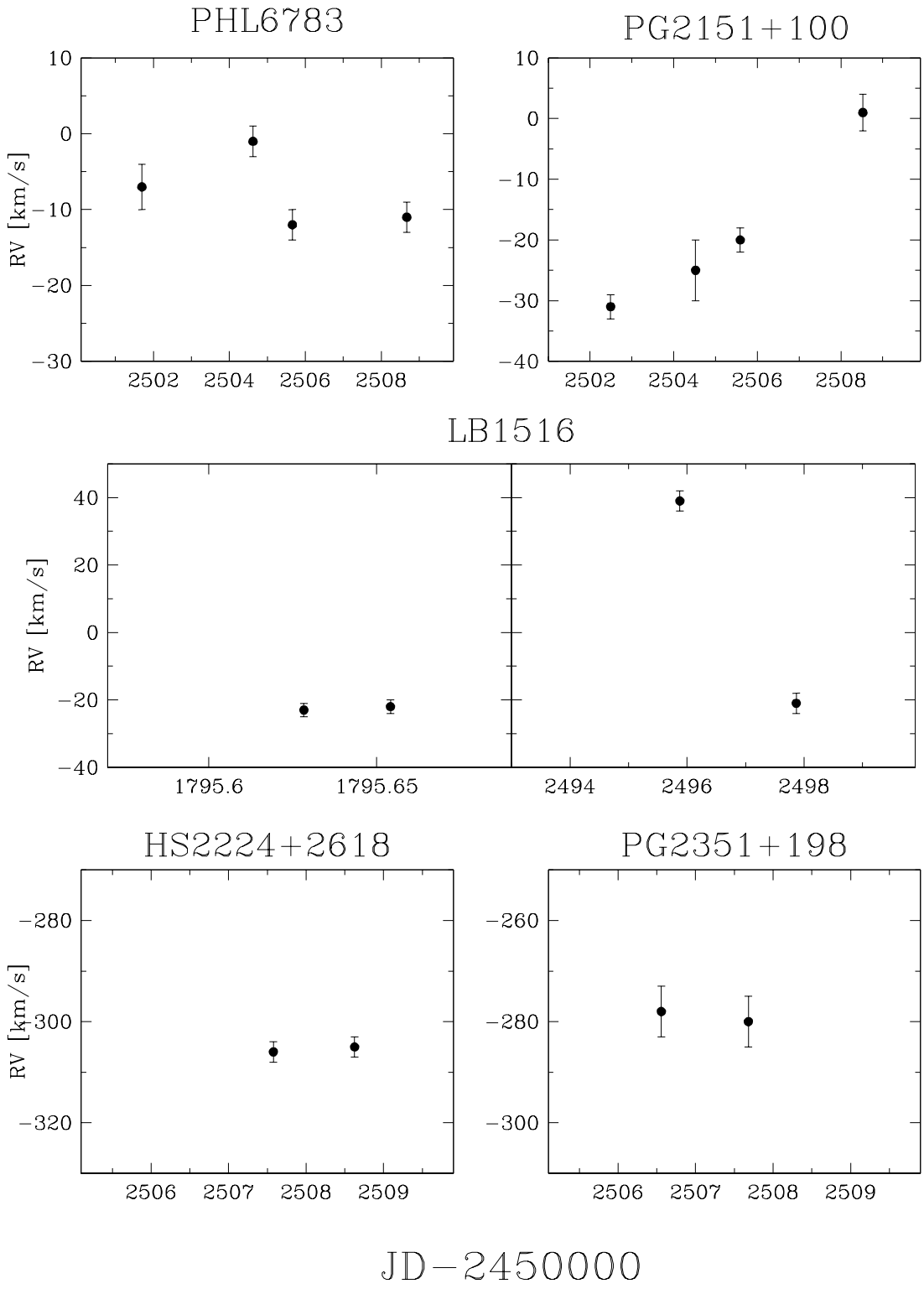

Figure 5.2: Measured RVs for five bright program stars. Three stars (PHL 6783, PG 2151+100, and LB 1516) are found to be RV variable. Two stars (HS 2224+2618 and PG 2351+198) show very large absolute radial velocities. However, they do not show RV variations from one night to the next.

  - long-term constant (within tree months):

    For two stars (SB 395, and PG 2301+259) only two observations with a separation of three months, respectively, are available. The derived RV's do not vary within the error limits, i.e. they are not long-term variable. However, we can not rule out them to be short-term variable.

  For all of them, more observations are desirable.

- RV variable stars:

  We discovered 13 bright sdB stars to be RV variable (see next Section, and Fig. 5.2, top and center panels). Three of them have been discovered independently to be RV variable by Moran et al. (1999, Feige 11), and Morales-Rueda et al. (2003, PG 0133+114, and HD 171858). E. M. Green reported her measurements of PG 1519+620, PB 5333, and Feige 108 to us. Combining her measurements with ours allowed us to determine the radial velocity curves.

In Table A.4, all observed bright stars are indicated, either as RV variable or RV constant (short term, long term, or both).

5.2 Radial velocity curves, and the nature of the invisible companions

For nine of the thirteen sdB stars, discovered to be RV variable, we could determine their orbital parameters.

The period search was carried out by means of a periodogram analysis based on the *Singular Value Decomposition* (SVD) method. A sine-shaped RV curve is fit to the observations for a multitude of phases, which are calculated as a function of period (see Napiwotzki et al. 2001b). The difference between the observed radial velocities and the best fitting theoretical RV curve for each phase set is evaluated in terms of the logarithm of the sum of squared residuals (χ^2) as a function of period, yielding the power spectrum of the data set, which allows to determine the most probable period of variability (see e.g. Lorenz et al. 1998).

Since the stars are single-lined binaries, we can only derive the mass function

$$f_m = \frac{M_{\rm comp.}^3 \sin^3(i)}{(M_{\rm sdB} + M_{\rm comp.})^2} = \frac{PK^3}{2\pi G}. \tag{5.1}$$

Using the mass function, the masses of the unseen companions can be constricted. However, due to the unknown inclination angle i, we can only determine lower limits ($i = 90°$), or most probable masses ($i = 52°$) for the invisible secondaries.

5.2.1 PG 0001+275

We discovered PG 0001+275, to be RV variable during our second observing run (July 1999) at the DSAZ on Calar Alto, Spain, with the 2.2m telescope equipped with the FOCES instrument (see Table 2.1, and D.1) to measure ^{3}He, metal abundances and rotation of sdB stars (see also the last Chapter). For three observations performed within ~ 2 hours the RV differs by $\Delta v_{\rm rad} \approx$ 60 km/s. Additional high-resolution observations were made during August and September 2001

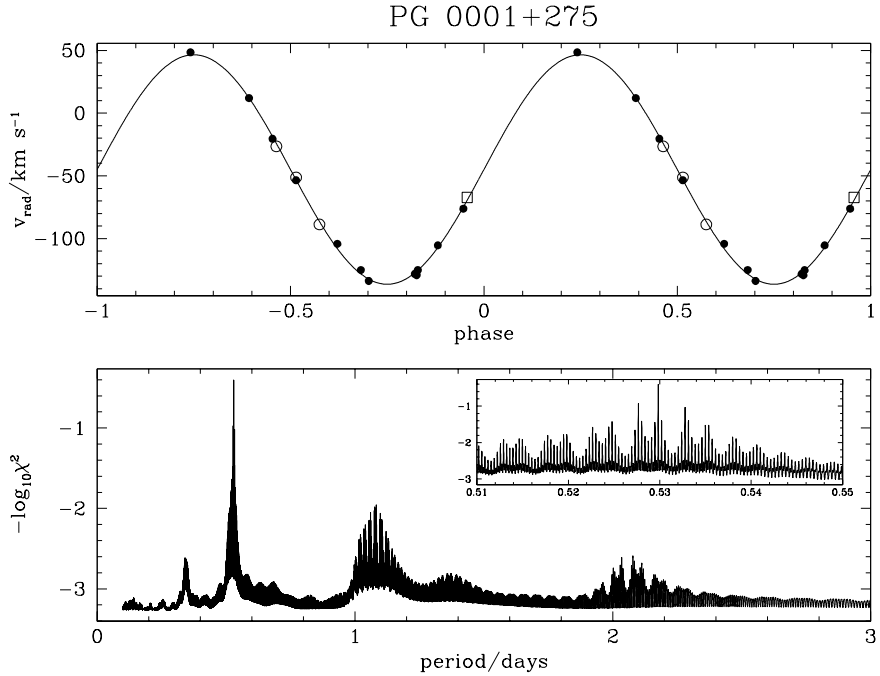

Figure 5.3: Upper part: Measured RV's as a function of orbital phase and fitted sine curve for PG 0001+275. Filled circles indicate 2001 FOCES observations, open circles 1999 discovery FOCES observations and the open square TWIN measurements. Lower part: Power spectrum of the PG 0001+275 measurements. The inset shows details of the region around the main peak.

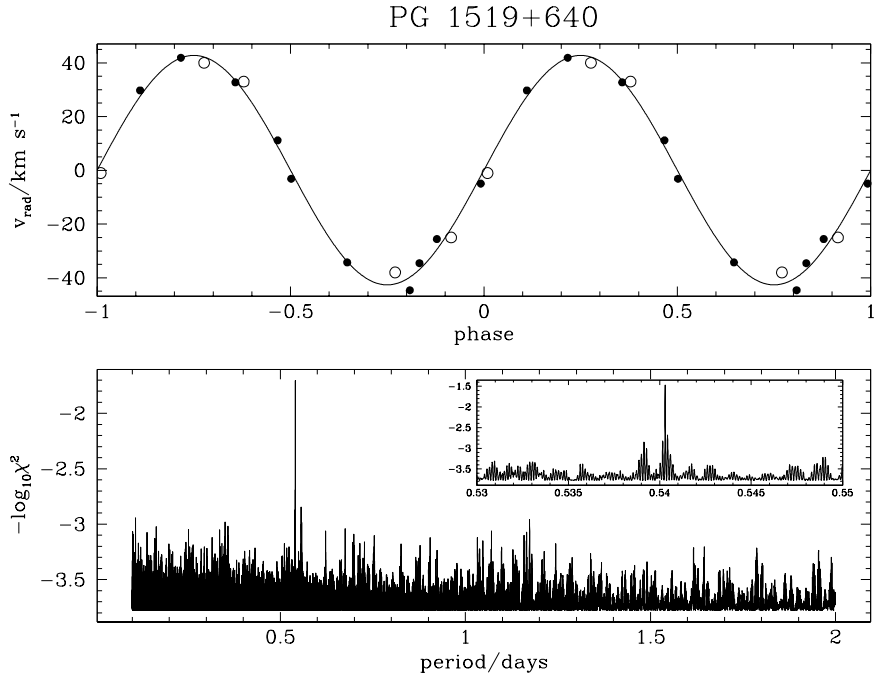

Figure 5.4: Upper part: Measured RV's as a function of orbital phase and fitted sine curve for PG 1519+640. Open circles indicate FOCES observations, and filled circles measurements of E. M. Green (priv. comm.). Lower part: Power spectrum of the PG 1519+640 measurements. The inset shows details of the region around the main peak.

to determine the orbital parameters. Fig. 5.3 shows the resulting power spectrum and best fit RV curve. We derived a period of $P = 12^{\rm h}42^{\rm m}58^{\rm s}$, a system velocity of $\gamma_0 = -44.9 \pm 1.0$ km/s, and a RV semi amplitude of $K = 91.5 \pm 1.4$ km/s for PG 0001+275.

The ephemeris for the time T_0, defined as the conjunction time at which the star moves from the blue side to the red side of the RV curve (cf. Fig. 5.3, upper part) is

$$\mathrm{BC.JD}(T_0) = 2\,452\,152.202437 \pm 0.52984098 \times E.$$

Two aliases exist, which differ by $-4^{\rm m}13^{\rm s}$ and $+3^{\rm m}8^{\rm s}$, but they can be ruled out at a high confidence level (cf. inset of Fig. 5.3, lower part)).

From an optical low-resolution spectrum (see Section 3.2.1) we determined the atmospheric parameters to be $T_{\rm eff} = 25\,400 \pm 700$K, $\log(g) = 5.3 \pm 0.1$, and $\log(n_{\rm He}/n_{\rm H}) = -2.8 \pm 0.2$. Using evolutionary calculations (cf. Fig. 3.4, lower left panel), we estimated a mass of $0.47M_\odot$ for the sdB primary. The mass function (Eq. 5.2, $f_m = 0.042M_\odot$) yields a lower limit of $0.29M_\odot$ (for an inclination of $i = 90°$), and a most probable mass of $0.40M_\odot$ (assuming average $i = 52°$) for the invisible companion. We conclude that the sdB companion is probably a white dwarf with a C/O core or a late type main sequence star.

5.2.2 PG 1519+640

PG 1519+640 was discovered by E. M. Green to be RV variable (priv. comm.). However, her measurements results in too many aliases for the period. Therefore, we included this star in our August 2002 run at the DSAZ. Five additional observations could be obtained (see Table D.1).

Adding our RV's to those determined by E. M. Green, an unequivocal period of $P = 12^{\rm h}58^{\rm m}01^{\rm s}$, a system velocity of $\gamma_0 = +0.1 \pm 0.4$ km/s, and a RV semi amplitude of $K = 42.7 \pm 0.6$ km/s was derived from the analysis (see Fig. 5.4 for resulting power spectra and best RV curve).

The ephemeris for PG 1519+640 is

$$\mathrm{BC.JD}(T_0) = 2\,452\,153.603215 \pm 0.540291403 \times E.$$

Using the canonical mass of $0.5M_\odot$ for the sdB primary (yet, we have not determined the atmospheric parameters) the mass function ($f_m = 0.004M_\odot$) yields a lower limit of $0.12M_\odot$ (for an inclination of $i = 90°$), and a most probable mass of $0.15M_\odot$ (assuming average $i = 52°$) for the invisible companion. Therefore, we conclude that the sdB secondary is most probably a M dwarf.

5.2.3 HD 188112

During our investigation of sdB stars at ESO with FEROS at the 1.5m telescope in order to determine atmospheric parameters, metal and isotope abundances, and rotational velocities (September 2000, see Table 2.1), we discovered that one of the brightest sdB stars, HD 188112 ($V = 10\overset{\rm m}{.}2$) has a gravity higher than typical sdB stars and therefore cannot be an extreme horizontal branch star but a progenitor of a helium core white dwarf (Heber et al., in prep.). Moreover the star was found to be RV variable. Four radial velocity measurements revealed a huge change of 360 km/s within 2 days (see Table D.1). Therefore, we obtained more observations in August 2002 at ESO and at the DSAZ resulting in an excellent phase coverage. Fig. 5.5 shows the resulting power spectrum and best fit RV curve. We derived a period of $P = 14^{\rm h}33^{\rm m}29^{\rm s}$, a system velocity of $\gamma_0 = +26.6 \pm 0.3$ km/s, and a RV semi amplitude of $K = 188.3 \pm 0.5$ km/s.

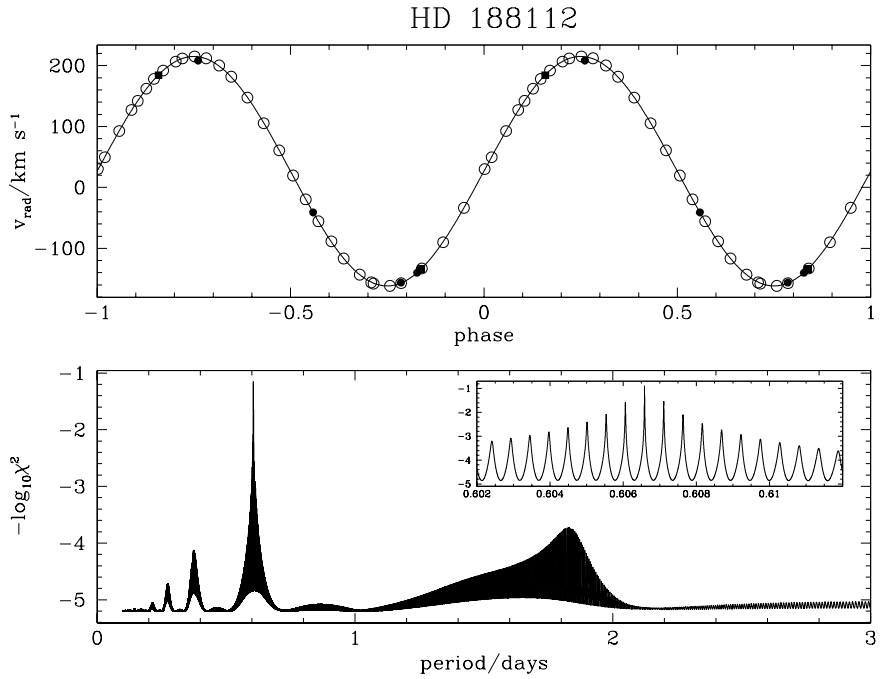

Figure 5.5: Upper part: Measured RV's as a function of orbital phase and fitted sine curve for HD 188112. Open circles indicate the 2002 FEROS observations, filled circles 2000 discovery FEROS observations and filled square 2002 FOCES measurements. Lower part: Power spectrum of the HD 188112 measurements. The inset shows details of the region around the main peak.

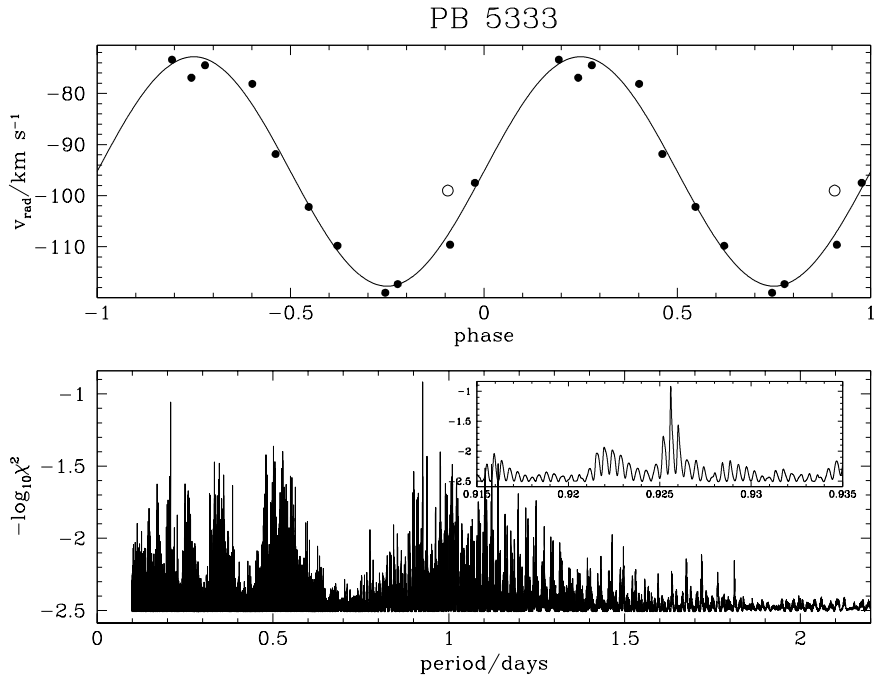

Figure 5.6: Upper part: Measured RV's as a function of orbital phase and fitted sine curve for PB 5333. Open circles indicate 2002 FOCES observations, and filled circles measurements of E. M. Green (priv. comm.). Lower part: Power spectrum of the PB 5333 measurements. The inset shows details of the region around the main peak.

The ephemeris for HD 188112 is

$$\mathrm{BC.JD}(T_0) = 2\,452\,151.936050 \pm 0.606584658 \times E.$$

A spectral analysis of the hydrogen and helium lines resulted in $T_{\rm eff} = 21\,700 \pm 500$K, $\log(g) = 5.68 \pm 0.05$, and $\log(n_{\rm He}/n_{\rm H}) = -5.0$. Using evolutionary calculations of Driebe et al. (1998), a mass of $M = 0.23^{+0.15}_{-0.09} M_\odot$ could be determined for the sdB primary (Heber et al., in prep.).

The mass function ($f_m = 0.4175 M_\odot$) yielded a lower limit of $0.73 M_\odot$ (for an inclination of $i = 90°$), and a most probable mass of $1.20 M_\odot$ (assuming average $i = 52°$) for the invisible companion. Heber et al. concluded that the sdB secondary must be a compact object, most likely a white dwarf. However, a neutron star cannot be ruled out.

5.2.4 PB 5333

As in the case of PG 1519+640, also PB 5333 was discovered by E. M. Green to be RV variable (priv. comm.). We obtained two spectra within our August 2002 run at the DSAZ. However, only one could be used for RV measurements, due to very bad S/N of the second spectrum.

Including our RV point to the data of E. M. Green, we can estimate a most probable period of $P = 22^{\rm h}12^{\rm m}52^{\rm s}$, a system velocity of $\gamma_0 = -95.3 \pm 1.3$ km/s, and a RV semi amplitude of $K = 22.4 \pm 0.8$ km/s was derived from the analysis (see Fig. 5.4 for resulting power spectra and best RV curve). However, an alias period of $P = 6^{\rm h}\ 11^{\rm m}\ 22^{\rm s}$ cannot be ruled out. This period has almost the same probability. (cf. inset of Fig. 5.6, lower part). More observations are necessary to decide which one is real.

Using the period of $P \approx 22$ hours, the ephemeris for PB 5333 is

$$\mathrm{BC.JD}(T_0) = 2\,452\,159.429518 \pm 0.92560306 \times E.$$

For the period of $P \approx 6$ hours, the ephemerides would be

$$\mathrm{BC.JD}(T_0) = 2\,452\,159.431074 \pm 0.257893518 \times E.$$

Using the canonical mass of $0.5 M_\odot$ for the sdB primary (our spectra are too noisy to determine the atmospheric parameters) the mass function for the period of $P \approx 22$ hours ($f_m = 0.001 M_\odot$) yields a lower limit of $0.07 M_\odot$ (for an inclination of $i = 90°$), and a most probable mass of $0.09 M_\odot$ (assuming average $i = 52°$) for the invisible companion. For $P \approx 6$ hours the mass function ($f_m = 0.0001 M_\odot$) yields a lower limit of $0.04 M_\odot$, and a most probable mass of $0.05 M_\odot$ for the sdB secondary. We conclude that the invisible companion is most probably a brown dwarf or a very low mass main sequence star.

5.2.5 PG 0133+114

PG 0133+114 was included in our July 1999 run to measure ^{3}He, metal abundances and rotation of sdB stars (see also last chapter). Serendipitously, we discovered that PG 0133+114 is RV variable[2].

[2]We took four spectra with the intention to maximize the S/N by coadding the spectra afterwards, and to minimize cosmic ray events. Three observations have been made directly one after another, and one, during the next night. If we had not taken the last spectrum, we would not have noticed PG 0133+114 to be RV variable, because the first three observations were obtained almost exactly within the minimum of the RV curve (see Fig. 5.7). Sometimes, luck is the essential ingredient of science!

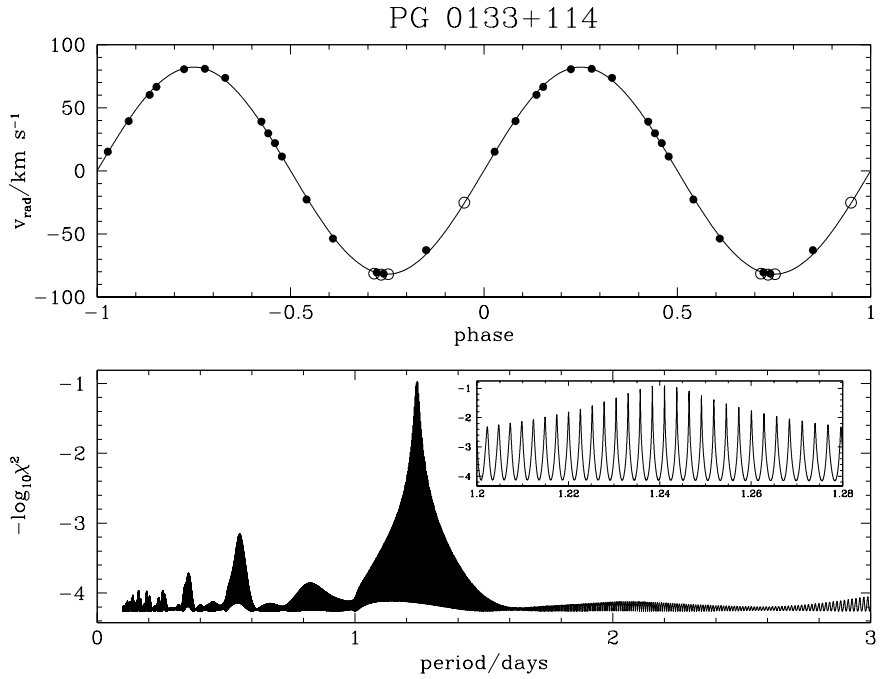

Figure 5.7: Upper part: Measured RV's as a function of orbital phase and fitted sine curve for PG 0133+114. Filled circles indicate 2001 FOCES observations and open circles 2000 discovery FOCES measurements. Lower part: Power spectrum of the PG 0133+114 measurements. The inset shows details of the region around the main peak.

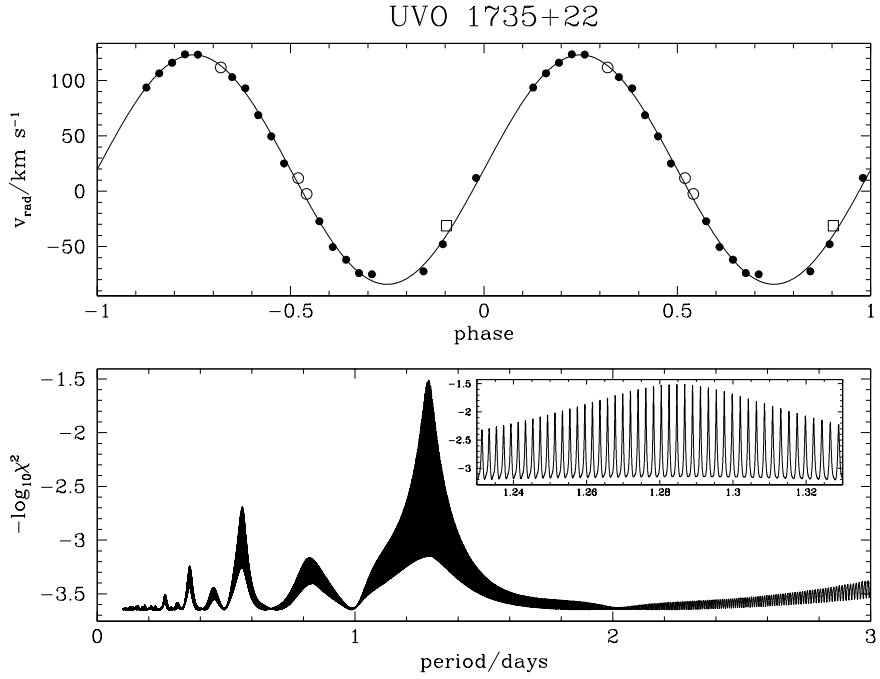

Figure 5.8: Upper part: Measured RV's as a function of orbital phase and fitted sine curve for UVO 1735+22. Filled circles indicate measurements of E. M. Green (priv. comm.), open circles 2002 FOCES observations, and the open square 1999 TWIN measurements. Lower part: Power spectrum of the UVO 1735+22 measurements. The inset shows details of the region around the main peak.

Additional high-resolution observations have been made at the end of August 2001 at the DSAZ to determine the orbital parameters. Fig. 5.7 shows the resulting power spectrum and best fit RV curve. The power spectrum is not perfectly unequivocal. Many alias periods of $\Delta P = 3^{\rm m}30^{\rm s}$, equal to an error of about $0.002 \times P$, exists (cf. inset of Fig. 5.7, lower part). In order to determine the mass of the unseen companion, however, we do not need a period with extremely high accuracy.

A period of $P = 29^{\rm h}45^{\rm m}30^{\rm s} \pm 15^{\rm m}$ results. Additionally, a system velocity of $\gamma_0 = +0.2 \pm 0.5$ km/s, and a RV semi amplitude of $K = 82.1 \pm 0.6$ km/s was derived for PG 0133+114.

The ephemeris is

$$\mathrm{BC.JD}(T_0) \approx 2\,452\,151.2656 \pm 1.24 \times E.$$

Due to the lack of a low-resolution spectrum for PG 0133+114, we adopt the atmospheric parameters from Morales-Rueda et al. (2003): $T_{\rm eff} = 29\,613$K, $\log(g) = 5.66$, and $\log(n_{\rm He}/n_{\rm H}) = -2.3$. A mass of $0.47 M_\odot$ for the sdB primary is derived. The mass function ($f_m = 0.071 M_\odot$) yields a lower limit of $0.37 M_\odot$ (for an inclination of $i = 90°$), and a most probable mass of $0.52 M_\odot$ (assuming average $i = 52°$) for the invisible companion. Therefore, we conclude that it is probably a white dwarf with a C/O core, or a late type main sequence star.

Morales-Rueda et al. (2003) discovered independently PG 0133+114 being RV variable. They determined a period of $P = 1.238390$ days which is in perfect agreement with our result. Their system velocity of $\gamma_0 = +5.1 \pm 0.6$ km/s, and RV semi amplitude of $K = 83.5 \pm 0.6$ km/s are also consistent with our values. A lower limit of $M = 0.389 M_\odot$, determined by Morales-Rueda et al. (2003) for the companion, agrees furthermore with our result.

5.2.6 UVO 1735+22

We discovered UVO 1735+22 to be RV variable, like most of the other RV variable stars for which we could obtain complete RV curves, during our July 1999 run at the DSAZ. From three observations (two made one after another, and the third, one night thereafter) we measured a RV variation of $\Delta v_{\rm rad} \approx 110$ km/s.

Again, additional high-resolution observations have been made end of August 2001 at the DSAZ to determine the orbital parameters. Fig. 5.7 shows the resulting power spectrum and best fit RV curve. The power spectrum is, as for PG 0133+114, not perfectly unequivocal. Many alias periods of $\Delta P \approx 3^{\rm m}$, equal to an error of about $0.0016 \times P$, exists (cf. inset of Fig. 5.7, lower part). However, for our purposes, a "perfect" determination of the period is desirable but not necessary. We derive a period of $P = 30^{\rm h}50^{\rm m} \pm 15^{\rm m}$, a system velocity of $\gamma_0 = +0.2 \pm 0.5$ km/s, and a RV semi amplitude of $K = 82.1 \pm 0.6$ km/s.

The ephemeris is

$$\mathrm{BC.JD}(T_0) \approx 2\,452\,152.1685 \pm 1.285 \times E.$$

From an optical low-resolution spectrum (see Section 3.2.1) we determined the atmospheric parameters for UVO 1735+22 to be $T_{\rm eff} = 40\,500 \pm 1\,000$K, $\log(g) = 5.4 \pm 0.1$, and $\log(n_{\rm He}/n_{\rm H}) = -3.8 \pm 0.2$, consistent with a mass of $0.47 M_\odot$ for the sdB primary. The mass function ($f_m = 0.148 M_\odot$) yields a lower limit of $0.53 M_\odot$ (for an inclination of $i = 90°$), and a most probable mass of $0.78 M_\odot$ (assuming average $i = 52°$) for the secondary. We conclude that the invisible companion must be a compact star, most likely a C/O white dwarf.

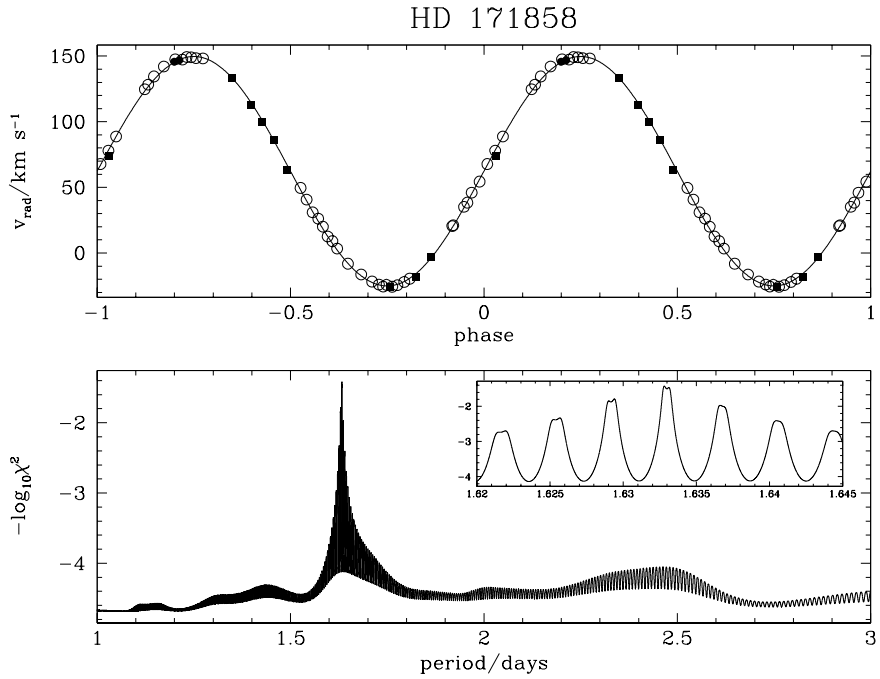

Figure 5.9: Upper part: Measured RV's as a function of orbital phase and fitted sine curve for HD 171858. Open circles indicate 2002 FEROS observations, filled circles 2000 FEROS observations and filled squares 2002 FOCES measurements. Lower part: Power spectrum of the HD 171858 measurements. The inset shows details of the region around the main peak.

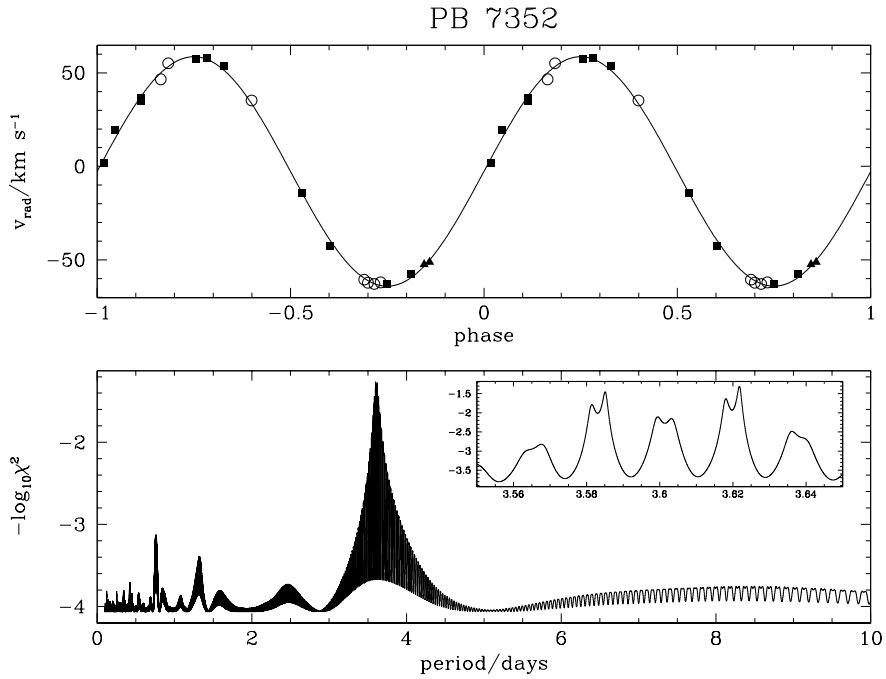

Figure 5.10: Upper part: Measured RV's as a function of orbital phase and fitted sine curve for PB 7352. Filled triangles indicate 2000 FEROS observations, filled circles 2002 FEROS observations and filled squares 2002 FOCES measurements. Lower part: Power spectrum of the PB 7352 measurements. The inset shows details of the region around the main peak.

5.2.7 HD 171858

HD 171858 was first detected by Morales-Rueda et al. (2003) to show RV variations. Our observations, made in September 2000 at ESO, consists of two spectra, taken one after another, and, as in the case of PG 0133+114, turned out to be at an extremum of the RV curve, however, in this case at maximum. Therefore we missed the discovery of RV variation. During our latest run in August 2002 at ESO, to measure the RV curve for HD 188112 presented before, we decided to observe HD 171858 independently, due to the poor phase coverage of Morales-Rueda et al. (2003). Additionally, at the August 2002 run at the DSAZ, we obtained again some spectra to perfectly sample the RV curve.

Fig. 5.9 shows the resulting power spectrum and best fit RV curve. We derived a period of $P = 39^{\rm h}11^{\rm m}15^{\rm s}$, a system velocity of $\gamma_0 = +62.3 \pm 0.3$ km/s, and a RV semi amplitude of $K = 87.4 \pm 0.4$ km/s. An alias of $\Delta P = +28^{\rm s}$, however, cannot be ruled out, corresponding to an error for the period of 0.002%.

The ephemeris for HD 171858 is

$$\mathrm{BC.JD}(T_0) = 2\,452\,153.368254 \pm 1.63281378 \times E.$$

As for PG 0133+114, we adopt the atmospheric parameters for HD 171858 from Morales-Rueda et al. (2003): $T_{\rm eff} = 27\,700$K, $\log(g) = 5.25$, and $\log(n_{\rm He}/n_{\rm H}) = -2.9$. A mass of $0.46 M_{\odot}$ is estimated for the sdB primary, using the evolutionary calculations of Dorman, Rood, & O'Connell (1993).

From this, the mass function ($f_m = 0.112 M_{\odot}$) a lower limit of $0.48 M_{\odot}$ (for an inclination of $i = 90°$), and a most probable mass of $0.67 M_{\odot}$ (assuming average $i = 52°$) for the invisible companion. The secondary is therefore, probably, a white dwarf with a C/O core.

Morales-Rueda et al. (2003) determined a period for HD 171858 of $P = 1.529$ days, a $\gamma_0 = +73.8 \pm 0.8$ km/s, and a $K = 93.6 \pm 0.7$ km/s, which differs somewhat from our values. However, due to their poor phase coverage, the values can be regarded as consistent with ours. Therefore, their estimate of the minimum mass for the invisible companion of $0.51 M_{\odot}$ is, again, in good agreement with our result.

5.2.8 PB 7352

We observed PB 7352 two times during our September 2000 run at ESO. Because the spectra were taken directly one after another, we did not detect the existing RV variability. These became apparent only later on when we re-observed the star in August 2002 at ESO. Almost the full amplitude of $\Delta v_{\rm rad} \approx 62$ km/s was already detected from seven observations in three nights (see Table 2.1, see also Fig. 5.10, upper part). Additional RV points were obtained from observations in August and November 2002 at the DSAZ.

Fig. 5.10 shows the resulting power spectrum and best fit RV curve. We derived a period of $P = 86^{\rm h}55^{\rm m}22^{\rm s}$, a system velocity of $\gamma_0 = -2.7 \pm 0.5$ km/s, and a RV semi amplitude of $K = 61.3 \pm 0.6$ km/s.

However, an alias of $\Delta P = -52^{\rm m}52^{\rm s}$ with almost the same probability, and two with $\Delta P = -5^{\rm m}19^{\rm s}$, and $-1^{\rm h}17^{\rm m}59^{\rm s}$ cannot be ruled out.

The ephemeris for HD 171858 is

$$\mathrm{BC.JD}(T_0) = 2\,452\,151.175245 \pm 3.62178218 \times E.$$

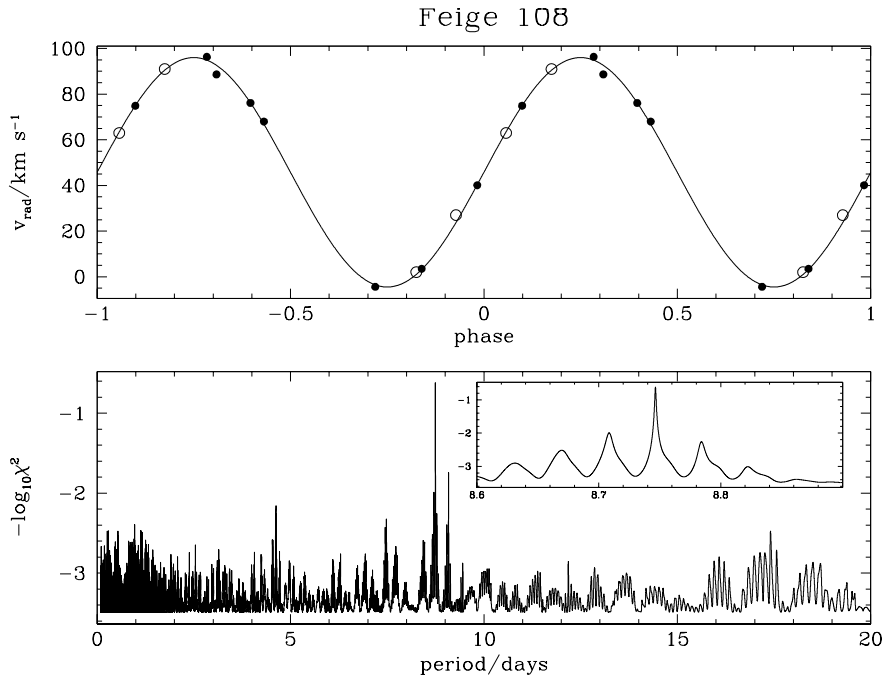

Figure 5.11: Upper part: Measured RV's as a function of orbital phase and fitted sine curve for Feige 108. Open circles indicate 2002 FEROS observations, and filled circles measurements of E. M. Green (priv. comm.). Lower part: Power spectrum of the Feige 108 measurements. The inset shows details of the region around the main peak.

From the high-resolution spectrum (see Section 3.2.1) we determined the atmospheric parameters for PB 7352 to be $T_{\rm eff} = 23\,400 \pm 1\,500$K, $\log(g) = 5.1 \pm 0.2$, and $\log(n_{\rm He}/n_{\rm H}) = -2.5 \pm 0.2$, consistent with a mass of $0.48 M_{\odot}$ for the sdB primary. The mass function ($f_m = 0.086 M_{\odot}$) yields a lower limit of $0.40 M_{\odot}$ (for an inclination of $i = 90°$), and a most probable mass of $0.58 M_{\odot}$ (assuming average $i = 52°$) for the invisible companion. We conclude that the invisible companion is likely to be a white dwarf with a C/O core.

5.2.9 Feige 108

Like PG 1519+640, and PB 5333, Feige 108 was discovered by E. M. Green being RV variable (priv. comm.). Again, her measurements resulted in too many aliases for the period. Therefore, we included this star in our August 2002 run at the DSAZ. Four additional observations could be obtained (see Table D.1, and Fig. 5.11, upper part).

Using our RV measurements together with the data of E. M. Green, a period of $P = 209^{\rm h}54^{\rm m}58^{\rm s}$, the longest period in our sdB binary sample, a system velocity of $\gamma_0 = +45.8 \pm 0.6$ km/s, and a RV semi amplitude of $K = 50.2 \pm 1.0$ km/s resulted from the analysis (see Fig. 5.4 for resulting power spectra and best RV curve). All aliases could be ruled out at a very high confidence level.

The ephemeris for Feige 108 is

$$\mathrm{BC.JD}(T_0) = 2\,452\,156.228358 \pm 8.74650465 \times E.$$

Using the canonical mass of $0.5 M_{\odot}$ for the sdB primary (we have not determined the atmospheric

Table 5.1: Orbital parameters (given are the periods P, the barycentric ephemeris for the time T_0 defined as the conjunction time at which the stars moves from the blue side to the red side of the RV curve, the system velocities γ_0 and the RV semi-amplitudes K), for our program bright radial velocity variable stars.

star	P	BJD(T_0) $-2\,450\,000$	γ_0 [km/s]	K [km/s]
PG 0001+275	$12^{\rm h}\ 42^{\rm m}\ 58^{\rm s}$	2152.202437	-44.9 ± 1.0	91.5 ± 1.4
PG 1519+640	$12^{\rm h}\ 58^{\rm m}\ 01^{\rm s}$	2153.603215	$+0.1 \pm 0.4$	42.7 ± 0.6
HD 188112	$14^{\rm h}\ 33^{\rm m}\ 29^{\rm s}$	2151.936050	$+26.6 \pm 0.3$	188.3 ± 0.5
PB 5333	$22^{\rm h}\ 12^{\rm m}\ 52^{\rm s}$	2159.429518	-95.3 ± 1.3	22.4 ± 0.8
PG 0133+114	$29^{\rm h}\ 45^{\rm m}\ 36^{\rm s}$	2151.265599	$+0.2 \pm 0.5$	82.1 ± 0.6
UVO 1735+22	$30^{\rm h}\ 49^{\rm m}\ 58^{\rm s}$	2152.168534	$+19.6 \pm 0.7$	103.7 ± 0.9
HD 171858	$39^{\rm h}\ 11^{\rm m}\ 15^{\rm s}$	2153.368254	$+62.3 \pm 0.3$	87.4 ± 0.4
PB 7352	$86^{\rm h}\ 55^{\rm m}\ 22^{\rm s}$	2151.175245	-2.7 ± 0.5	61.3 ± 0.6
Feige 108	$209^{\rm h}\ 54^{\rm m}\ 58^{\rm s}$	2156.228358	$+45.8 \pm 0.6$	50.2 ± 1.0

for Feige 108 yet) the mass function ($f_m = 0.116 M_\odot$) yields a lower limit of $0.47 M_\odot$ (for an inclination of $i = 90°$), and a most probable mass of $0.70 M_\odot$ (assuming average $i = 52°$) for the invisible companion. Again, we conclude the secondary star to be a white dwarf with a C/O core, or a late type main sequence star.

5.3 Summary of the radial velocity curve analyses

Table 5.1 summarizes the orbital parameters for all analyzed RV variable sdB stars. Additionally, we plotted a histogram of all periods known for RV variable sdB stars in Fig. 5.12. The dotted line denotes the published periods (review of Morales-Rueda et al. 2003) and the solid line represents the published values including our new results. One can see that most of the RV variable sdB stars have periods of about one day. However, there is a sharp peak around 0.1 day which is separated from the bulk. The gap between the bulk and the "secondary peak" is quite similar to the well known period-gap of the cataclysmic variable stars.

Table 5.2 summarizes the mass functions, and masses for the sdB primaries and secondaries for all analyzed stars. Assuming the most probable masses for the unseen companions, one of them is likely to be a brown dwarf or low mass main sequence star (PB 5553), one a late type main sequence star (PG 1519+640), and the masses of the remaining stars are mostly consistent with those of white dwarfs, or late type main sequence stars.

However, further investigations are necessary to clarify the nature of all companions, in particular infrared measurements are required to possibly detect flux from the companions.

Table 5.2: Mass functions f_m, masses of the sdB stars $M_{\rm sdB}$, the minimum $M_{\rm comp.}^{i=90^\circ}$, and most probable masses $M_{\rm comp.}^{i=52^\circ}$ for the companions of our program bright radial velocity variable stars.

star	f_m [$M_\odot$]	$M_{\rm sdB}$ [$M_\odot$]	$M_{\rm comp.}^{i=90^\circ}$ [$M_\odot$]	$M_{\rm comp.}^{i=52^\circ}$ [$M_\odot$]
PG 0001+275	0.042	0.47	0.29	0.40
PG 1519+640	0.004	0.50	0.12	0.15
HD 188112	0.420	0.23*	0.73	1.20
PB 5333	0.001	0.50	0.07	0.09
PG 0133+114	0.071	0.47	0.37	0.52
UVO 1735+22	0.148	0.47	0.53	0.78
HD 171858	0.112	0.48	0.46	0.67
PB 7352	0.086	0.48	0.40	0.58
Feige 108	0.116	0.50	0.47	0.70

*: HD 188112 is not an EHB star but a progenitor of a helium core white dwarf. This mass estimate is derived from parallax and gravity (Heber et al., in prep.).

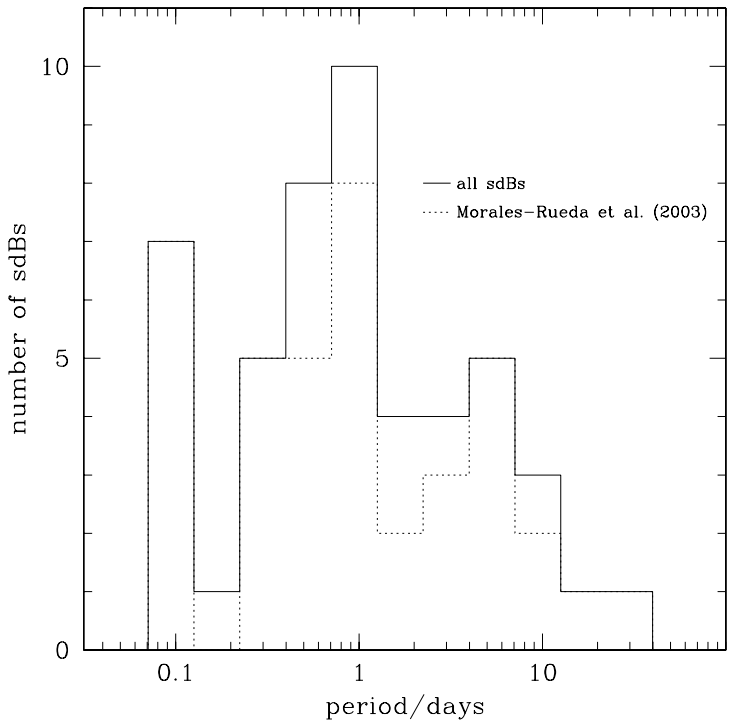

Figure 5.12: Histogram of orbital periods for all binary sdB stars known up to now.

Chapter 6

HE 0437−5439 — a main sequence B star leaving the galaxy

Our observations confirmed earlier classifications of stars in the literature or from objective. prism (Schmidt) spectra in most cases. Amongst the few exceptions, there is a remarkable case, HE 0437−5439, which we shall discuss in this chapter in some detail.

6.1 Observations and data analysis

HE 0437−5439 (α_{2000}=$04^{\rm h}38^{\rm m}12\overset{\rm s}{.}8$, $\delta_{2000} = -54°33'12''$, $B = 16\overset{\rm m}{.}2$) was discovered 2001 by our campaign to search for sdB stars within several Hamburg ESO survey fields (see Section 2.4.1) as a normal main sequence B star, showing a very large radial velocity (RV). This came very much to our surprise. However, due to a quite unreliable wavelength calibration, we could only estimate $v_{\rm rad} \approx +700$km/s. But even if considering an error of ±100km/s, this star must be an extremely interesting object. Regretfully, we had only one spectrum. To verify our discovery we needed more observations. I could persuade R. Napiwotzki, to include HE 0437−5439 into his observing run in November 2002 at the ESO Paranal observatory using the VLT UT2 8m telescope (Kueyen) equipped with the UVES high-resolution echelle spectrograph. He obtained two spectra of the star.

The nominal resolution of the two spectra with the 2.1" slit used is $\lambda/\Delta\lambda = 19\,000$. Details on the observational set-up of the UVES instrument can be found in Koester et al. (2001).

The spectra were reduced using the "Bamberg" pipeline reduction (Karl, Lisker, Napiwotzki, priv. comm.).

6.2 Atmospheric parameters and projected rotational velocity

From the coadded high-res spectra we determined the atmospheric parameters to be $T_{\rm eff} = 20\,200 \pm 200$K, $\log(g) = 3.8 \pm 0.1$ (cgs), and $\log(n_{\rm He}/n_{\rm H}) = -0.94 \pm 0.05$, using the same procedures, as described in Section 3.1, except that now we included also the rotational velocities into the fit process (i.e. convolving the theoretical spectra with rotational profiles).

A velocity of $v\sin(i) = 60 \pm 5$km/s matches best the data (for the fit see Fig. 6.1). The derived parameters for the high-resolution spectrum are in good agreement with the results drawn from the low-resolution spectrum ($T_{\rm eff} = 19,800 \pm 400$K, $\log(g) = 3.6 \pm 0.2$ (cgs), and $\log(n_{\rm He}/n_{\rm H}) = -0.9 \pm 0.2$).

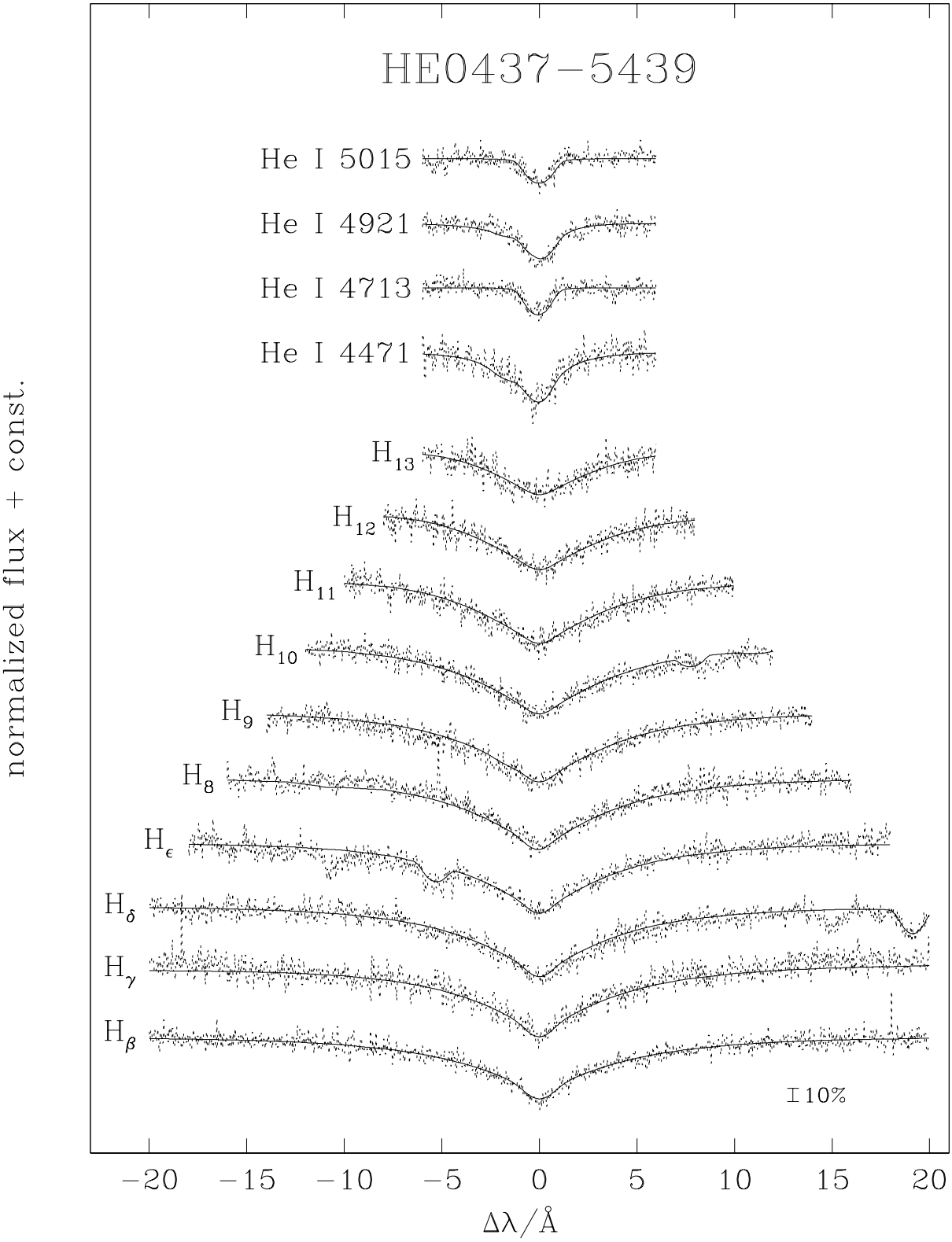

Figure 6.1: LTE line fit for HE 0437−5439 for the coadded UVES spectrum.

6.3 Mass, evolutionary time, radial velocity, and distance

Assuming the star to be a main sequence B star of solar metallicity, we estimate a mass of $8M_{\odot}$ and an evolutionary time of $T_{\rm evol} \approx 25$Myr for HE 0437−5439, using evolutionary tracks calculated by Schaller et al. (1992).

The radial velocities were derived from the line-shift of the Balmer and helium lines and corrected to barycentric values. From the two high-resolution spectra we measure a constant RV of 723 ± 3km/s, which is in agreement with the RV drawn from the low-res spectrum.

Using the mass, effective temperature, gravity and apparent magnitude, given above, we determine a distance of

$$d = 1.11\sqrt{\frac{M_* F_V}{g} 10^{0.4\mathrm{V}_0}} = 65 \pm 5\mathrm{kpc} \tag{6.1}$$

(M_* is the stellar mass in $M_{\odot}$, g is the gravity in cm/s^2, F_V is the model atmosphere flux at the stellar surface in units of 10^8 erg cm^{-2} s^{-1} Å^{-1} and V_0 is the de-reddened apparent visual magnitude) for HE 0437−5439, as described by Ramspeck, Heber, & Edelmann (2001).

6.4 Metal abundances

No metal lines can be clearly identified in the coadded high-resolution spectrum. This is possibly due to the the high projected rotational velocity of $v \sin(i) = 60 \pm 5$km/s, the bad S/N of the high-resolution spectra (even if coadded), or both. Nevertheless, the Si III triplet at $\lambda\lambda$ 45512.61Å, 4567.82Å, and 4574.76Å should be seen, if the silicon abundance were solar. Regretfully they lie within a gap of the blue and lower red part of the UVES echelle orders[1].

However, by comparing synthetic LTE model line distributions for the derived atmospheric parameters and different metal abundances with the coadded spectrum of HE 0437−5439, we can estimate an upper limit of the metal content. A solar metallicity, or lower, is consistent with the data. A higher metallicity can clearly be ruled out.

6.5 Discussion

The atmospheric parameters together with the high rotational velocity, derived for HE 0437−5439, favors a relatively young massive star. However, this star lies far out in the halo of our galaxy, and its space velocity is probably larger than the escape velocity from the Milky Way galaxy. Hence HE 0437−5439 will be emitted into intergalactic space.

[1] Murphy's law is omnipresent!

Chapter 7

Conclusions and outlook

In principle the evolutionary state of sdB stars is known. The results by several authors have shown that they populate a very narrow area which lies on a blue-ward extension of the HB, the so called EHB. However, for individual objects rather discrepant results can be found in the literature and we are not in a position to investigate details of EHB star evolution. We aimed to determine the atmospheric parameters of large samples of sdB stars with a precision of at most 5% in $T_{\rm eff}$, and 0.2 dex in $\log(g)$. Comparison of our results with those of other groups (Saffer et al. 1994, Maxted et al. 2001), however, revealed systematic differences, i.e. places our sdB stars closer to the TAEHB whereas the bulk of sdB stars from the other groups prefer them to lie closer to the ZAEHB. These differences are probably due to different observations, different models used for the analysis, or both. We are unable to resolve the relative importance of the latter. A direct comparison on a star by star basis of different observations, using different analysis methods, and model atmospheres, which is mandatory for a detailed comparison with theory, has to be done before the details of EHB evolution can be tested.

The processes which form sdB stars, however, are less clear. Single star as well as binary star evolution has been proposed, but have met with little success. The discovery of more and more close binaries among them may indicate that interaction with a secondary star is the key to understand the evolution of sdB stars. Recent theoretical work (Han et al. 2002, 2003), elucidates the channels by which sdB stars can form within a binary system: the common envelope ejection, stable Roche lobe overflow, and the merger channel. A comparison of our results with the favored model by Han et al. (2003), reveals no striking differences. Their 'best choice model' was selected by Han et al. (2003) by a subjective judgment, because they had to match the 'cloud of model points' to less than 40 observations. We have increased the number of systems with known periods by more than 20%. However, analyses of many more systems are urgently needed in order to better constrain the theoretical predictions of Han et al.

Until now, only a handful of sdB stars have been analyzed for their metal abundance patterns. With our work, this number has almost been quadrupled. We have selected stars for the abundance analysis covering a wide range of parameter space, which for the first time allowed us to search for trends of the metal abundances with these parameters. We discovered that the abundances of some elements (helium, oxygen, and magnesium) correlate with the effective temperature by a subjective judgment. On the other hand it is remarkable that the abundances for the majority of elements, which are common in the atmospheres of sdB stars (nitrogen, silicon,

aluminum, argon, and iron), are constant all over the parameter space. In addition, a possible separation into two sequences of sdB stars, a minority having much lower helium (possibly also oxygen, magnesium, and silicon) abundances at the same temperatures than the bulk of the sdB stars, was found. In addition, a very exciting result of this work is that no obvious differences for the abundances determined for pulsating or non-pulsating, and RV variable or non-variable sdB stars became apparent. Furthermore, the discovery of three peculiar sdB stars which show an enormous enrichment for the iron group elements (Sc, Ti, V, Mn, and Ni together with argon) by factors of 1 000 to $\sim$ 32 000 times is without an explanation. Theoreticians are challenged to interpret these results.

One can see, that a lot of work, both from theoretical and observational point of view, still needs to be done to understand the subluminous B stars.

Appendix A

Program stars – observing logs

A.1 Hamburg Quasar Survey

Table A.1: Classification, Coordinates, B magnitude, observing run, and references for all program HQS stars.

star	spectral type	α (1950)	δ (1950)	l_{II} (1950)	b_{II} (1950)	B mag	run #	Ref.
HS 0016+0044	sdB	$00^h16^m09\overset{s}{.}7$	$+00°44'45''$	$106\overset{\circ}{.}05$	$-60\overset{\circ}{.}67$	14.6	6	-
HS 0023+3049	sdB	$00^h23^m24\overset{s}{.}5$	$+30°49'44''$	$116\overset{\circ}{.}57$	$-31\overset{\circ}{.}35$	14.6	9	-
HS 0025+3423	sdOB	$00^h25^m08\overset{s}{.}8$	$+34°23'51''$	$117\overset{\circ}{.}44$	$-27\overset{\circ}{.}85$	15.4	8	-
HS 0028+4407	binary	$00^h28^m01\overset{s}{.}5$	$+44°07'59''$	$119\overset{\circ}{.}04$	$-18\overset{\circ}{.}21$	15.1	14	-
HS 0035+3034	sdOB	$00^h35^m58\overset{s}{.}6$	$+30°34'14''$	$119\overset{\circ}{.}70$	$-31\overset{\circ}{.}85$	15.8	8	-
HS 0039+4302	sdB	$00^h39^m57\overset{s}{.}3$	$+43°02'34''$	$121\overset{\circ}{.}25$	$-19\overset{\circ}{.}43$	15.1	14	BB,FBS
HS 0040+4417	sdB	$00^h40^m35\overset{s}{.}4$	$+44°17'57''$	$121\overset{\circ}{.}42$	$-18\overset{\circ}{.}18$	15.6	14	FBS
HS 0048+0026	sdOB	$00^h48^m33\overset{s}{.}1$	$+00°26'17''$	$122\overset{\circ}{.}76$	$-62\overset{\circ}{.}06$	15.6	6	PG,PHL,BB
HS 0055+0138	sdB	$00^h55^m50\overset{s}{.}3$	$+01°38'25''$	$126\overset{\circ}{.}51$	$-60\overset{\circ}{.}81$	15.1	6	PG,BB
HS 0127+3146	binary	$01^h27^m03\overset{s}{.}2$	$+31°46'42''$	$132\overset{\circ}{.}34$	$-30\overset{\circ}{.}03$	14.4	14	-
HS 0136+0605	binary	$01^h36^m41\overset{s}{.}2$	$+06°05'59''$	$143\overset{\circ}{.}70$	$-54\overset{\circ}{.}48$	14.1	3	-
HS 0209+0141	sdB	$02^h09^m51\overset{s}{.}6$	$+01°41'14''$	$159\overset{\circ}{.}95$	$-54\overset{\circ}{.}93$	13.6	6	PG,PB
HS 0212+1446	sdB	$02^h12^m27\overset{s}{.}5$	$+14°46'03''$	$151\overset{\circ}{.}16$	$-43\overset{\circ}{.}14$	14.6	3	PG
HS 0213+2329	sdOB	$02^h13^m05\overset{s}{.}6$	$+23°29'20''$	$146\overset{\circ}{.}72$	$-35\overset{\circ}{.}12$	14.6	10	-
HS 0215+0852	binary	$02^h15^m12\overset{s}{.}7$	$+08°52'12''$	$155\overset{\circ}{.}90$	$-48\overset{\circ}{.}07$	14.9	3	-
HS 0231+8019	B	$02^h31^m40\overset{s}{.}8$	$+80°19'16''$	$127\overset{\circ}{.}41$	$+18\overset{\circ}{.}71$	15.1	14	-
HS 0232+3155	sdOB	$02^h32^m21\overset{s}{.}0$	$+31°55'54''$	$147\overset{\circ}{.}23$	$-25\overset{\circ}{.}68$	15.1	11	KUV
HS 0233+3037	sdB	$02^h33^m49\overset{s}{.}6$	$+30°37'57''$	$148\overset{\circ}{.}17$	$-26\overset{\circ}{.}71$	14.1	11	KUV
HS 0252+1025	binary	$02^h52^m51\overset{s}{.}0$	$+10°25'18''$	$165\overset{\circ}{.}62$	$-41\overset{\circ}{.}65$	13.8	10	-
HS 0338+2946	sdB	$03^h38^m32\overset{s}{.}5$	$+29°46'47''$	$161\overset{\circ}{.}46$	$-19\overset{\circ}{.}84$	15.1	14	-
HS 0349+0700	sdB	$03^h49^m02\overset{s}{.}3$	$+07°00'29''$	$181\overset{\circ}{.}38$	$-34\overset{\circ}{.}48$	14.4	3	-
HS 0352+1019	sdB	$03^h52^m30\overset{s}{.}0$	$+10°19'29''$	$179\overset{\circ}{.}06$	$-31\overset{\circ}{.}65$	13.9	14	KUV
HS 0357+0133	sdB	$03^h57^m16\overset{s}{.}8$	$+01°33'43''$	$188\overset{\circ}{.}18$	$-36\overset{\circ}{.}25$	14.9	8	-
HS 0430+7712	sdB	$04^h30^m04\overset{s}{.}0$	$+77°12'00''$	$134\overset{\circ}{.}16$	$+19\overset{\circ}{.}77$	13.7	14	FBS
HS 0444+0458	sdB	$04^h44^m39\overset{s}{.}3$	$+04°58'16''$	$192\overset{\circ}{.}77$	$-24\overset{\circ}{.}60$	15.2	*	-
HS 0445+7503	sdB	$04^h45^m12\overset{s}{.}7$	$+75°03'38''$	$136\overset{\circ}{.}54$	$+19\overset{\circ}{.}18$	14.2	14	-
HS 0446+1344	binary	$04^h46^m18\overset{s}{.}9$	$+13°44'49''$	$185\overset{\circ}{.}25$	$-19\overset{\circ}{.}26$	14.8	14	-

continued on next page

*: see Østensen et al. (2001b)

continued from last page

star	spectral type	α (1950)	δ (1950)	l_{II} (1950)	b_{II} (1950)	B mag	run #	Ref.
HS 0447+7545	sdB	$04^h47^m37\overset{s}{.}9$	$+75°45'48''$	$136\overset{\circ}{.}03$	$+19\overset{\circ}{.}72$	15.7	14	-
HS 0457+0907	sdOB	$04^h57^m34\overset{s}{.}8$	$+09°07'41''$	$190\overset{\circ}{.}94$	$-19\overset{\circ}{.}63$	14.1	14	-
HS 0546+8009	sdOB	$05^h46^m27\overset{s}{.}5$	$+80°09'56''$	$133\overset{\circ}{.}41$	$+24\overset{\circ}{.}46$	13.9	11	FBS
HS 0600+6602	sdOB	$06^h00^m21\overset{s}{.}7$	$+66°02'31''$	$148\overset{\circ}{.}03$	$+20\overset{\circ}{.}25$	16.1	1	-
HS 0656+6117	binary	$06^h56^m02\overset{s}{.}0$	$+61°17'25''$	$154\overset{\circ}{.}91$	$+24\overset{\circ}{.}71$	16.2	4	-
HS 0702+6043	sdB	$07^h02^m41\overset{s}{.}7$	$+60°43'31''$	$155\overset{\circ}{.}70$	$+25\overset{\circ}{.}38$	14.8	3	-
HS 0705+6700	sdB	$07^h05^m38\overset{s}{.}2$	$+67°00'37''$	$148\overset{\circ}{.}86$	$+26\overset{\circ}{.}76$	14.2	2	FBS
HS 0707+8225	sdB	$07^h07^m55\overset{s}{.}7$	$+82°25'18''$	$131\overset{\circ}{.}55$	$+27\overset{\circ}{.}86$	14.9	7	FBS
HS 0740+3734	sdB	$07^h40^m38\overset{s}{.}3$	$+37°34'40''$	$182\overset{\circ}{.}27$	$+26\overset{\circ}{.}02$	14.4	7	FBS
HS 0741+3818	sdB	$07^h41^m47\overset{s}{.}0$	$+38°18'23''$	$181\overset{\circ}{.}56$	$+26\overset{\circ}{.}43$	14.4	7	FBS
HS 0815+4243	sdOB	$08^h15^m53\overset{s}{.}2$	$+42°43'04''$	$178\overset{\circ}{.}10$	$+33\overset{\circ}{.}67$	16.4	11	KUV,FBS
HS 0941+4649	sdB	$09^h41^m31\overset{s}{.}7$	$+46°49'21''$	$172\overset{\circ}{.}21$	$+48\overset{\circ}{.}74$	16.7	1	US,SA
HS 0942+4608	binary	$09^h42^m02\overset{s}{.}5$	$+46°08'35''$	$173\overset{\circ}{.}20$	$+48\overset{\circ}{.}95$	14.4	1	PG
HS 1051+2933	sdOB	$10^h51^m28\overset{s}{.}0$	$+29°33'11''$	$201\overset{\circ}{.}41$	$+64\overset{\circ}{.}17$	16.1	11	TON,CSO
HS 1106+6051	binary	$11^h06^m31\overset{s}{.}5$	$+60°51'18''$	$143\overset{\circ}{.}21$	$+52\overset{\circ}{.}45$	14.9	7	PG,LB,SBSS
HS 1236+4754	sdB	$12^h36^m43\overset{s}{.}4$	$+47°54'19''$	$128\overset{\circ}{.}87$	$+69\overset{\circ}{.}46$	15.5	1	PG,TON,
HS 1320+2622	sdB	$13^h20^m16\overset{s}{.}1$	$+26°22'36''$	$25\overset{\circ}{.}63$	$+82\overset{\circ}{.}94$	16.5	11	-
HS 1511+6221	binary	$15^h11^m26\overset{s}{.}8$	$+62°21'15''$	$99\overset{\circ}{.}16$	$+48\overset{\circ}{.}04$	14.3	7	PG,FBS
HS 1547+6312	sdB	$15^h47^m28\overset{s}{.}4$	$+63°12'14''$	$96\overset{\circ}{.}80$	$+44\overset{\circ}{.}17$	14.8	5	PG,FBS
HS 1552+6333	sdB	$15^h52^m29\overset{s}{.}5$	$+63°33'28''$	$96\overset{\circ}{.}85$	$+43\overset{\circ}{.}51$	16.4	5	FBS
HS 1556+6032	B	$15^h56^m01\overset{s}{.}1$	$+60°32'51''$	$92\overset{\circ}{.}86$	$+44\overset{\circ}{.}50$	15.9	5	SBSS
HS 1612+6337	binary	$16^h12^m29\overset{s}{.}5$	$+63°37'21''$	$95\overset{\circ}{.}61$	$+41\overset{\circ}{.}48$	16.8	5	-
HS 1612+7335	binary	$16^h12^m54\overset{s}{.}0$	$+73°35'29''$	$107\overset{\circ}{.}07$	$+36\overset{\circ}{.}92$	14.7	5	PG
HS 1615+6341	binary	$16^h15^m37\overset{s}{.}6$	$+63°41'56''$	$95\overset{\circ}{.}52$	$+41\overset{\circ}{.}13$	15.9	5	FBS
HS 1641+4601	sdB	$16^h41^m27\overset{s}{.}7$	$+46°01'34''$	$71\overset{\circ}{.}50$	$+41\overset{\circ}{.}12$	14.6	†	BB
HS 1717+6042	sdB	$17^h17^m21\overset{s}{.}6$	$+60°42'24''$	$89\overset{\circ}{.}68$	$+34\overset{\circ}{.}87$	14.4	6	PG
HS 1736+8001	sdB	$17^h36^m06\overset{s}{.}5$	$+80°01'16''$	$112\overset{\circ}{.}02$	$+30\overset{\circ}{.}19$	14.8	5	FBS,LB
HS 1739+5244	sdB	$17^h39^m19\overset{s}{.}6$	$+52°44'35''$	$80\overset{\circ}{.}13$	$+31\overset{\circ}{.}89$	14.6	10	-
HS 1741+2133	sdOB	$17^h41^m11\overset{s}{.}6$	$+21°33'54''$	$45\overset{\circ}{.}72$	$+24\overset{\circ}{.}22$	14.1	12	-
HS 1747+6924	sdB	$17^h47^m28\overset{s}{.}4$	$+69°24'13''$	$99\overset{\circ}{.}69$	$+31\overset{\circ}{.}00$	15.1	9	-
HS 1747+8014	sdB	$17^h47^m02\overset{s}{.}4$	$+80°14'10''$	$112\overset{\circ}{.}16$	$+29\overset{\circ}{.}69$	16.2	5	-
HS 1753+5342	binary	$17^h53^m00\overset{s}{.}6$	$+53°42'03''$	$81\overset{\circ}{.}48$	$+29\overset{\circ}{.}94$	14.9	12	-
HS 1753+7025	binary	$17^h53^m54\overset{s}{.}9$	$+70°26'00''$	$100\overset{\circ}{.}83$	$+30\overset{\circ}{.}39$	15.6	5	-
HS 1756+7056	sdB	$17^h56^m49\overset{s}{.}5$	$+70°56'46''$	$101\overset{\circ}{.}43$	$+30\overset{\circ}{.}12$	15.6	5	-
HS 1806+5024	sdOB	$18^h06^m25\overset{s}{.}9$	$+50°24'41''$	$78\overset{\circ}{.}13$	$+27\overset{\circ}{.}40$	16.8	13	-
HS 1813+7247	sdB	$18^h13^m09\overset{s}{.}2$	$+72°47'47''$	$103\overset{\circ}{.}52$	$+28\overset{\circ}{.}81$	15.2	5	-
HS 1824+5745	sdOB	$18^h24^m04\overset{s}{.}0$	$+57°45'37''$	$86\overset{\circ}{.}76$	$+26\overset{\circ}{.}23$	15.6	9	-
HS 1831+6432	sdOB	$18^h31^m12\overset{s}{.}5$	$+64°32'25''$	$94\overset{\circ}{.}38$	$+26\overset{\circ}{.}52$	14.9	6	FBS
HS 1831+7647	sdB	$18^h31^m12\overset{s}{.}0$	$+76°47'54''$	$108\overset{\circ}{.}09$	$+27\overset{\circ}{.}73$	14.4	14	-
HS 1832+7009	sdB	$18^h32^m10\overset{s}{.}4$	$+70°09'32''$	$100\overset{\circ}{.}64$	$+27\overset{\circ}{.}16$	14.4	5	-
HS 1839+7951	sdB	$18^h39^m45\overset{s}{.}7$	$+79°51'22''$	$111\overset{\circ}{.}56$	$+27\overset{\circ}{.}44$	17.6	5	-
HS 1842+6557	sdB	$18^h42^m18\overset{s}{.}6$	$+65°57'36''$	$96\overset{\circ}{.}16$	$+25\overset{\circ}{.}61$	15.2	9	KUV
HS 1843+6953	sdB	$18^h43^m10\overset{s}{.}7$	$+69°53'13''$	$100\overset{\circ}{.}47$	$+26\overset{\circ}{.}19$	15.0	14	-
HS 1844+5048	binary	$18^h44^m42\overset{s}{.}4$	$+50°48'02''$	$80\overset{\circ}{.}18$	$+21\overset{\circ}{.}61$	16.5	13	-
HS 1846+8149	sdB	$18^h46^m24\overset{s}{.}7$	$+81°49'16''$	$113\overset{\circ}{.}79$	$+27\overset{\circ}{.}29$	14.4	14	FBS
HS 1858+5736	binary	$18^h58^m55\overset{s}{.}1$	$+57°36'15''$	$87\overset{\circ}{.}83$	$+21\overset{\circ}{.}67$	14.5	9,14	-

continued on next page

†: T. Rauch (priv. comm.): obs. date: 1994 Jun, instr.: 3.5m TWIN,
recip. disp.: 36/36 Å/mm, spectr. res.: 1.5 Å, wavelength cov.: 4070-4940Å,5790-6650Å

continued from last page

star	spectral type	α (1950)	δ (1950)	l_{II} (1950)	b_{II} (1950)	B mag	run #	Ref.
HS 1859+6219	sdB	$18^h59^m35\overset{s}{.}4$	$+62°19'37''$	$92\overset{\circ}{.}75$	$+22\overset{\circ}{.}95$	14.9	6	-
HS 2100+1710	sdOB	$21^h00^m46\overset{s}{.}1$	$+17°10'39''$	$65\overset{\circ}{.}04$	$-18\overset{\circ}{.}93$	14.9	8	-
HS 2126+8320	sdB	$21^h26^m57\overset{s}{.}1$	$+83°20'50''$	$117\overset{\circ}{.}42$	$+23\overset{\circ}{.}16$	13.9	5	-
HS 2131+0349	B	$21^h31^m01\overset{s}{.}8$	$+03°49'40''$	$58\overset{\circ}{.}29$	$-32\overset{\circ}{.}96$	14.3	9	-
HS 2143+8157	sdB	$21^h43^m51\overset{s}{.}2$	$+81°57'48''$	$116\overset{\circ}{.}75$	$+21\overset{\circ}{.}81$	15.4	5	-
HS 2149+0847	sdOB	$21^h49^m26\overset{s}{.}2$	$+08°47'14''$	$66\overset{\circ}{.}34$	$-33\overset{\circ}{.}40$	16.5	9	-
HS 2149+1428	sdB	$21^h49^m29\overset{s}{.}9$	$+14°28'03''$	$71\overset{\circ}{.}24$	$-29\overset{\circ}{.}56$	14.4	3	-
HS 2151+0214	sdB	$21^h51^m24\overset{s}{.}7$	$+02°14'15''$	$60\overset{\circ}{.}52$	$-37\overset{\circ}{.}97$	16.5	6	-
HS 2151+0857	sdOB	$21^h51^m50\overset{s}{.}5$	$+08°57'31''$	$66\overset{\circ}{.}96$	$-33\overset{\circ}{.}73$	16.5	9	PG
HS 2156+2215	sdOB	$21^h56^m21\overset{s}{.}2$	$+22°15'30''$	$78\overset{\circ}{.}65$	$-25\overset{\circ}{.}08$	15.1	12	-
HS 2156+2517	sdB	$21^h56^m34\overset{s}{.}9$	$+25°17'41''$	$80\overset{\circ}{.}90$	$-22\overset{\circ}{.}84$	14.1	14	-
HS 2158+2137	sdB	$21^h58^m25\overset{s}{.}7$	$+21°37'39''$	$78\overset{\circ}{.}58$	$-25\overset{\circ}{.}87$	14.1	14	-
HS 2201+2610	sdB	$22^h01^m54\overset{s}{.}4$	$+26°10'33''$	$82\overset{\circ}{.}51$	$-22\overset{\circ}{.}95$	13.6	13	-
HS 2206+2847	sdB	$22^h06^m05\overset{s}{.}1$	$+28°47'57''$	$85\overset{\circ}{.}08$	$-21\overset{\circ}{.}51$	14.2	13	-
HS 2208+2718	sdB	$22^h08^m19\overset{s}{.}2$	$+27°18'04''$	$84\overset{\circ}{.}49$	$-22\overset{\circ}{.}99$	14.1	13	-
HS 2209+2840	sdB	$22^h09^m47\overset{s}{.}0$	$+28°40'25''$	$85\overset{\circ}{.}68$	$-22\overset{\circ}{.}11$	14.7	13	-
HS 2213+1336	sdB	$22^h13^m51\overset{s}{.}4$	$+13°36'22''$	$75\overset{\circ}{.}53$	$-34\overset{\circ}{.}29$	15.8	4	-
HS 2216+1833	binary	$22^h16^m06\overset{s}{.}6$	$+18°33'06''$	$79\overset{\circ}{.}87$	$-30\overset{\circ}{.}91$	13.9	12	-
HS 2218+0201	sdB	$22^h18^m52\overset{s}{.}1$	$+02°01'10''$	$66\overset{\circ}{.}12$	$-43\overset{\circ}{.}37$	13.9	6	PG,PHL
HS 2224+2618	sdB	$22^h24^m56\overset{s}{.}8$	$+26°18'09''$	$87\overset{\circ}{.}09$	$-26\overset{\circ}{.}01$	12.8	14	-
HS 2225+2220	sdB	$22^h25^m09\overset{s}{.}8$	$+22°20'51''$	$84\overset{\circ}{.}51$	$-29\overset{\circ}{.}24$	15.5	13	-
HS 2229+0910	sdOB	$22^h29^m55\overset{s}{.}3$	$+09°10'24''$	$75\overset{\circ}{.}50$	$-40\overset{\circ}{.}22$	15.9	3	-
HS 2229+2628	HBB	$22^h29^m02\overset{s}{.}5$	$+26°28'39''$	$88\overset{\circ}{.}04$	$-26\overset{\circ}{.}40$	13.9	14	-
HS 2231+2441	sdB	$22^h31^m59\overset{s}{.}1$	$+24°41'27''$	$87\overset{\circ}{.}51$	$-28\overset{\circ}{.}25$	14.1	14	-
HS 2233+1418	sdOB	$22^h33^m04\overset{s}{.}1$	$+14°18'26''$	$80\overset{\circ}{.}46$	$-36\overset{\circ}{.}77$	13.8	3	-
HS 2233+2332	sdB	$22^h33^m24\overset{s}{.}0$	$+23°32'06''$	$87\overset{\circ}{.}07$	$-29\overset{\circ}{.}38$	14.3	10	BB
HS 2240+0136	sdB	$22^h40^m19\overset{s}{.}4$	$+01°36'38''$	$70\overset{\circ}{.}99$	$-47\overset{\circ}{.}52$	14.4	8	PHL,PB
HS 2240+1031	sdOB	$22^h40^m59\overset{s}{.}6$	$+10°31'09''$	$79\overset{\circ}{.}39$	$-40\overset{\circ}{.}94$	14.8	4	PG
HS 2242+3206	sdB	$22^h42^m43\overset{s}{.}5$	$+32°06'04''$	$94\overset{\circ}{.}14$	$-23\overset{\circ}{.}25$	14.7	13	-
HS 2246+0158	sdB	$22^h46^m54\overset{s}{.}0$	$+01°58'40''$	$73\overset{\circ}{.}14$	$-48\overset{\circ}{.}39$	15.6	6	PG
HS 2333+3927	sdOB	$23^h33^m14\overset{s}{.}8$	$+39°27'51''$	$107\overset{\circ}{.}46$	$-20\overset{\circ}{.}75$	14.6	8	FBS

Ref.:

BB = Balloon-Born survey (Bixler et al. 1991);
FBS = First Byurakan Sky survey (Abrahamian et al. 1990);
PG = Palomar Green survey (Green, Schmidt & Liebert 1986);
KUV = Kiso UV survey (Noguchi, Maehara & Kondo 1980);
TON = Tonantzintla survey (Iriarte & Chavira 1957);
US = Usher Survey (Usher 1981);
PB = Palomar Berger survey (Berger & Fringant 1977);
PHL = Palomar Haro Luyten survey (Haro & Luyten 1962);
HZ = Humason & Zwicky survey (Humason & Zwicky 1947);
CSO = Case low-dispersion northern sky survey of Stellar-like Objects (Pesch & Sanduleak 1983);
SA = Durchmusterung of Selected Areas (Pickering & Kapteyn 1918);
LB = Luyten Blue survey, and SBSS = Second Biurakan Spectral Sky survey (Markarian & Stepanian 1983).

A.2 Hamburg ESO Survey

Table A.2: Classification, Coordinates, V or B_J magnitude (V: all values for sdB and sdOB stars, Altmann 2002, priv. comm.; B_J: all values for non-sdB stars from the HES plates, if known), HES plate and field numbers, and observing run for all program HES stars.

star	spectral type	α (2000)	δ (2000)	l_{II} (2000)	b_{II} (2000)	V,B_J mag	HES plate	HES field	run #
HE 2134−4119	HBB	$21^h37^m59\overset{s}{.}9$	$-41°06'13''$	$0\overset{\circ}{.}54$	$-48\overset{\circ}{.}18$	14.62	1530	343	3
HE 2135−3749	sdB	$21^h38^m44\overset{s}{.}1$	$-37°36'15''$	$5\overset{\circ}{.}79$	$-48\overset{\circ}{.}45$	13.926	1530	343	2,4
HE 2137−4221	HBB	$21^h40^m09\overset{s}{.}6$	$-42°08'19''$	$358\overset{\circ}{.}94$	$-48\overset{\circ}{.}50$	14.23	1530	343	3
HE 2151−2844	sdO	$21^h54^m24\overset{s}{.}1$	$-28°30'29''$	$20\overset{\circ}{.}23$	$-51\overset{\circ}{.}06$	15.70	0096	466	1
HE 2151−3043	DA	$21^h54^m53\overset{s}{.}3$	$-30°29'18''$	$17\overset{\circ}{.}11$	$-51\overset{\circ}{.}42$		0096	466	1
HE 2154−4143	sdB	$21^h58^m02\overset{s}{.}0$	$-41°28'50''$	$359\overset{\circ}{.}34$	$-51\overset{\circ}{.}89$	15.173	1543	344	2,4
HE 2155−1724	sdB	$21^h58^m19\overset{s}{.}6$	$-17°10'16''$	$37\overset{\circ}{.}65$	$-48\overset{\circ}{.}92$	15.042	0718	601	1
HE 2156−1732	sdB	$21^h59^m30\overset{s}{.}2$	$-17°18'22''$	$37\overset{\circ}{.}61$	$-49\overset{\circ}{.}23$	15.064	0718	601	1
HE 2156−3927	sdB	$21^h59^m35\overset{s}{.}5$	$-39°13'15''$	$2\overset{\circ}{.}94$	$-52\overset{\circ}{.}45$	14.448	1543	344	2,4
HE 2159−1747	p-AGB	$22^h02^m16\overset{s}{.}2$	$-17°33'15''$	$37\overset{\circ}{.}63$	$-49\overset{\circ}{.}94$	12.46	0718	601	3
HE 2200−2154	sdO	$22^h03^m15\overset{s}{.}3$	$-21°39'52''$	$31\overset{\circ}{.}62$	$-51\overset{\circ}{.}50$	15.59	0718	601	1
HE 2200−4047	sdB	$22^h03^m55\overset{s}{.}9$	$-40°32'28''$	$0\overset{\circ}{.}61$	$-53\overset{\circ}{.}12$	16.47	1543	344	4
HE 2201−2113	sdB	$22^h04^m06\overset{s}{.}7$	$-20°59'09''$	$32\overset{\circ}{.}75$	$-51\overset{\circ}{.}49$	15.903	0718	601	1
HE 2203−2210	He-sdO	$22^h06^m29\overset{s}{.}4$	$-21°55'60''$	$31\overset{\circ}{.}54$	$-52\overset{\circ}{.}30$	15.04	0718	601	1
HE 2203−3740	HBB	$22^h06^m27\overset{s}{.}4$	$-37°26'12''$	$5\overset{\circ}{.}71$	$-53\overset{\circ}{.}95$	13.31	1543	344	3
HE 2204−2136	B	$22^h07^m12\overset{s}{.}3$	$-21°21'20''$	$32\overset{\circ}{.}53$	$-52\overset{\circ}{.}29$	13.30	0718	601	3
HE 2205−1952	sdB	$22^h08^m41\overset{s}{.}3$	$-19°37'39''$	$35\overset{\circ}{.}38$	$-52\overset{\circ}{.}08$	14.591	0718	601	1
HE 2210−1801	sdO	$22^h12^m57\overset{s}{.}8$	$-17°46'22''$	$38\overset{\circ}{.}80$	$-52\overset{\circ}{.}39$	14.63	0092	601,602	1
HE 2211−2021	sdB	$22^h14^m25\overset{s}{.}3$	$-20°06'60''$	$35\overset{\circ}{.}34$	$-53\overset{\circ}{.}52$	14.54	0718	601	1
HE 2213−1734	He-sdO	$22^h16^m04\overset{s}{.}5$	$-17°19'48''$	$39\overset{\circ}{.}93$	$-52\overset{\circ}{.}91$	14.41	0092	601,602	1
HE 2213−2212	sdB+x	$22^h16^m23\overset{s}{.}5$	$-21°57'26''$	$32\overset{\circ}{.}59$	$-54\overset{\circ}{.}51$	13.97	0718	601,602	1
HE 2213−4158	sdB	$22^h16^m17\overset{s}{.}6$	$-41°43'22''$	$357\overset{\circ}{.}92$	$-55\overset{\circ}{.}20$	16.153	1543	344	4
HE 2222−3738	sdB	$22^h24^m56\overset{s}{.}4$	$-37°23'32''$	$5\overset{\circ}{.}10$	$-57\overset{\circ}{.}60$	14.889	1415	345	2,4
HE 2226−4005	sdB+x	$22^h29^m23\overset{s}{.}9$	$-39°49'55''$	$0\overset{\circ}{.}30$	$-58\overset{\circ}{.}03$	14.70	1415	345	3
HE 2230−4000	sdB+x	$22^h33^m10\overset{s}{.}8$	$-39°44'41''$	$0\overset{\circ}{.}16$	$-58\overset{\circ}{.}76$	14.86	1415	345	2
HE 2316−0909	sdB	$23^h19^m24\overset{s}{.}4$	$-08°52'38''$	$68\overset{\circ}{.}58$	$-61\overset{\circ}{.}63$	13.14	0835	749	2,4
HE 2326−1022	He-sdO	$23^h29^m09\overset{s}{.}8$	$-10°06'05''$	$70\overset{\circ}{.}26$	$-64\overset{\circ}{.}22$	13.21	0835	749	4
HE 2337−2944	sdB	$23^h40^m15\overset{s}{.}3$	$-29°27'60''$	$20\overset{\circ}{.}16$	$-74\overset{\circ}{.}18$	14.452	0719	471	2,4
HE 2340−2806	sdB	$23^h42^m41\overset{s}{.}5$	$-27°50'02''$	$26\overset{\circ}{.}20$	$-74\overset{\circ}{.}75$	14.996	0719	471	1
HE 2341−3443	sdB	$23^h44^m21\overset{s}{.}8$	$-34°27'01''$	$1\overset{\circ}{.}74$	$-73\overset{\circ}{.}86$	10.89	0839	408	1,2,4
HE 2343−2944	sdB	$23^h46^m17\overset{s}{.}8$	$-29°27'50''$	$19\overset{\circ}{.}74$	$-75\overset{\circ}{.}49$	15.041	0719	471	1
HE 2349−3135	sdB	$23^h51^m43\overset{s}{.}6$	$-31°18'53''$	$11\overset{\circ}{.}43$	$-76\overset{\circ}{.}33$	15.908	0719	409,471	1

continued on next page

continued from last page

star	spectral type	α (2000)	δ (2000)	l_{II} (2000)	b_{II} (2000)	V,B$_J$ mag	HES plate	HES field	run #
HE 2350−2448	DA	$23^h53^m03\overset{s}{.}9$	$-24°32'02''$	$40\overset{\circ}{.}73$	$-76\overset{\circ}{.}63$		0723	472	1
HE 2350−3026	sdOB	$23^h52^m36\overset{s}{.}0$	$-30°10'08''$	$16\overset{\circ}{.}08$	$-76\overset{\circ}{.}75$	12.10	0719	409,471	1
HE 2355−3221	sdB	$23^h58^m22\overset{s}{.}5$	$-32°04'39''$	$6\overset{\circ}{.}38$	$-77\overset{\circ}{.}46$	15.181	0827	409	1
HE 2356−2655	sdB+x	$23^h59^m07\overset{s}{.}1$	$-26°38'39''$	$32\overset{\circ}{.}19$	$-78\overset{\circ}{.}34$	13.42	0723	472,537	3
HE 2357−3940	B	$00^h00^m20\overset{s}{.}1$	$-39°23'56''$	$340\overset{\circ}{.}53$	$-73\overset{\circ}{.}75$	9.96	1417	348	3
HE 2359−2844	sdOB	$00^h01^m38\overset{s}{.}5$	$-28°27'43''$	$22\overset{\circ}{.}99$	$-78\overset{\circ}{.}92$	16.440	0827	409	1
HE 0000−2355	sdB	$00^h03^m22\overset{s}{.}0$	$-23°38'58''$	$47\overset{\circ}{.}92$	$-78\overset{\circ}{.}62$	13.293	0723	472,537	1,3
HE 0001−2443	He-sdB	$00^h04^m31\overset{s}{.}0$	$-24°26'21''$	$44\overset{\circ}{.}47$	$-79\overset{\circ}{.}12$	13.66	0723	472	3
HE 0002−2648	sdB	$00^h05^m09\overset{s}{.}6$	$-26°31'48''$	$33\overset{\circ}{.}46$	$-79\overset{\circ}{.}67$	14.31	0723	472	4
HE 0004−2737	sdOB	$00^h06^m46\overset{s}{.}3$	$-27°20'53''$	$28\overset{\circ}{.}94$	$-80\overset{\circ}{.}08$	13.967	0827	409	1
HE 0016−3212	He-sdO	$00^h18^m53\overset{s}{.}2$	$-31°56'03''$	$356\overset{\circ}{.}62$	$-81\overset{\circ}{.}44$	14.26	0809	410	1
HE 0019−2441	sdO	$00^h21^m58\overset{s}{.}6$	$-24°25'20''$	$53\overset{\circ}{.}30$	$-82\overset{\circ}{.}86$	14.20	0727	473	1
HE 0021−2326	sdB	$00^h23^m59\overset{s}{.}3$	$-23°09'54''$	$63\overset{\circ}{.}81$	$-82\overset{\circ}{.}66$	15.942	0727	473	1
HE 0023−2317	HBB	$00^h26^m14\overset{s}{.}5$	$-23°00'36''$	$67\overset{\circ}{.}22$	$-82\overset{\circ}{.}99$	14.44	0727	437	3
HE 0031−2724	sdOB	$00^h33^m53\overset{s}{.}9$	$-27°08'24''$	$31\overset{\circ}{.}34$	$-86\overset{\circ}{.}11$	14.229	0809	410	3
HE 0049−2928	sdB	$00^h51^m57\overset{s}{.}7$	$-29°12'08''$	$299\overset{\circ}{.}59$	$-87\overset{\circ}{.}89$	15.781	0836	411	1
HE 0049−3059	sdB	$00^h51^m37\overset{s}{.}6$	$-30°42'57''$	$302\overset{\circ}{.}16$	$-86\overset{\circ}{.}38$	14.413	0836	411	1
HE 0123−2808	sdB	$01^h25^m33\overset{s}{.}4$	$-27°53'04''$	$220\overset{\circ}{.}80$	$-82\overset{\circ}{.}39$	16.089	0720	413	1
HE 0127−4325	sdB	$01^h29^m11\overset{s}{.}4$	$-43°10'28''$	$279\overset{\circ}{.}89$	$-72\overset{\circ}{.}19$	14.597	1419	244	2,4
HE 0128−4311	HBB	$01^h30^m28\overset{s}{.}9$	$-42°55'54''$	$278\overset{\circ}{.}82$	$-72\overset{\circ}{.}29$	14.33	1419	244	3
HE 0136−2758	sdB	$01^h39^m14\overset{s}{.}4$	$-27°43'22''$	$219\overset{\circ}{.}03$	$-79\overset{\circ}{.}37$	16.173	0720	413	1
HE 0151−3919	sdB	$01^h53^m11\overset{s}{.}2$	$-39°04'17''$	$259\overset{\circ}{.}72$	$-72\overset{\circ}{.}42$	14.311	1532	297	2,4
HE 0218−3437	sdB	$02^h20^m59\overset{s}{.}8$	$-34°23'36''$	$239\overset{\circ}{.}21$	$-69\overset{\circ}{.}47$	13.391	0857	355	2,4
HE 0218−4447	sdO	$02^h20^m24\overset{s}{.}3$	$-44°33'29''$	$263\overset{\circ}{.}15$	$-65\overset{\circ}{.}05$	15.56	0828	246	2
HE 0221−3250	sdB	$02^h23^m58\overset{s}{.}2$	$-32°36'34''$	$233\overset{\circ}{.}89$	$-69\overset{\circ}{.}23$	14.700	0857	355	2,4
HE 0222−3641	sdO	$02^h24^m12\overset{s}{.}7$	$-36°28'27''$	$244\overset{\circ}{.}20$	$-68\overset{\circ}{.}24$	15.47	0857	355	3
HE 0225−4007	HBB	$02^h27^m29\overset{s}{.}1$	$-39°53'38''$	$251\overset{\circ}{.}79$	$-66\overset{\circ}{.}35$	12.22	1482	299	3
HE 0226−3639	sdB+x	$02^h28^m36\overset{s}{.}8$	$-36°25'46''$	$243\overset{\circ}{.}36$	$-67\overset{\circ}{.}41$	13.51	0857	355	4
HE 0227−4012	CV	$02^h29^m16\overset{s}{.}8$	$-39°59'03''$	$251\overset{\circ}{.}63$	$-66\overset{\circ}{.}00$	13.51	1482	299	2
HE 0230−4323	sdB	$02^h32^m54\overset{s}{.}6$	$-43°10'28''$	$257\overset{\circ}{.}59$	$-63\overset{\circ}{.}93$	13.779	0828	246	2,4
HE 0231−3441	sdB	$02^h34^m00\overset{s}{.}3$	$-34°28'56''$	$237\overset{\circ}{.}80$	$-66\overset{\circ}{.}84$	14.828	0857	355	2,4
HE 0238−1912	HBB	$02^h41^m03\overset{s}{.}9$	$-19°00'11''$	$200\overset{\circ}{.}93$	$-63\overset{\circ}{.}57$	12.57	0415	546	3
HE 0255−1814	HBB	$02^h57^m57\overset{s}{.}2$	$-18°02'08''$	$202\overset{\circ}{.}34$	$-59\overset{\circ}{.}51$	13.72	0415	546	3
HE 0258−2158	sdB	$03^h00^m17\overset{s}{.}7$	$-21°46'30''$	$209\overset{\circ}{.}73$	$-60\overset{\circ}{.}27$	14.645	0415	546	1
HE 0307−4554	sdB	$03^h09^m25\overset{s}{.}9$	$-45°43'32''$	$256\overset{\circ}{.}42$	$-56\overset{\circ}{.}96$	15.063	1587	248	2,4
HE 0308−2305	DA	$03^h11^m07\overset{s}{.}1$	$-22°54'05''$	$213\overset{\circ}{.}18$	$-58\overset{\circ}{.}17$		8351	481	1
HE 0315−4244	sdB	$03^h17^m47\overset{s}{.}0$	$-42°33'41''$	$250\overset{\circ}{.}07$	$-56\overset{\circ}{.}57$	16.918	1587	248	3
HE 0319−5105	HBB	$03^h21^m21\overset{s}{.}7$	$-50°55'16''$	$263\overset{\circ}{.}28$	$-53\overset{\circ}{.}03$	13.30	0146	200	1
HE 0324−2529	sdB	$03^h26^m15\overset{s}{.}0$	$-25°18'37''$	$218\overset{\circ}{.}90$	$-55\overset{\circ}{.}36$	14.624	8351	481	1
HE 0337−2508	sdB+x	$03^h39^m47\overset{s}{.}9$	$-24°59'14''$	$219\overset{\circ}{.}46$	$-52\overset{\circ}{.}29$	13.98	8361	482	1
HE 0340−2420	sdB+x	$03^h42^m30\overset{s}{.}5$	$-24°11'16''$	$218\overset{\circ}{.}43$	$-51\overset{\circ}{.}51$	14.67	8361	482	4
HE 0340−3820	sdB	$03^h42^m47\overset{s}{.}1$	$-38°11'27''$	$241\overset{\circ}{.}23$	$-52\overset{\circ}{.}62$	14.771	0858	302	2,4
HE 0341−2449	sdOB	$03^h43^m36\overset{s}{.}3$	$-24°39'47''$	$219\overset{\circ}{.}26$	$-51\overset{\circ}{.}38$	14.889	8361	482	1
HE 0343−4748	sdB	$03^h45^m09\overset{s}{.}4$	$-47°38'54''$	$256\overset{\circ}{.}12$	$-50\overset{\circ}{.}54$	14.193	0146	200	1
HE 0343−4933	DA	$03^h45^m17\overset{s}{.}0$	$-49°24'13''$	$258\overset{\circ}{.}75$	$-50\overset{\circ}{.}02$	15.28	0146	200	1
HE 0351−3536	sdB	$03^h53^m51\overset{s}{.}2$	$-35°27'35''$	$236\overset{\circ}{.}73$	$-50\overset{\circ}{.}49$	14.107	9124	359	1
HE 0405−1719	sdOB	$04^h07^m27\overset{s}{.}5$	$-17°11'17''$	$211\overset{\circ}{.}15$	$-43\overset{\circ}{.}82$	14.003	0433	550	1

continued on next page

continued from last page

star	spectral type	α (2000)	δ (2000)	l_{II} (2000)	b_{II} (2000)	V,B$_J$ mag	HES plate	HES field	run #
HE 0405−3859	sdB	$04^h07^m02\overset{s}{.}8$	$-38°51'47''$	$241\overset{\circ}{.}93$	$-47\overset{\circ}{.}85$	14.392	0858	302	2,4
HE 0407−1956	sdB	$04^h10^m11\overset{s}{.}3$	$-19°48'54''$	$214\overset{\circ}{.}88$	$-44\overset{\circ}{.}12$	13.610	0433	550	3
HE 0407−2122	HBB	$04^h09^m11\overset{s}{.}7$	$-21°14'37''$	$216\overset{\circ}{.}68$	$-44\overset{\circ}{.}79$	12.57	0433	550	3
HE 0410−4901	sdB	$04^h11^m30\overset{s}{.}1$	$-48°53'48''$	$256\overset{\circ}{.}44$	$-45\overset{\circ}{.}99$	14.508	0844	201	2,4
HE 0414−5429	He-sdO	$04^h15^m30\overset{s}{.}2$	$-54°21'59''$	$263\overset{\circ}{.}78$	$-44\overset{\circ}{.}14$	14.58	0939	157	4
HE 0419−2538	sdB	$04^h22^m04\overset{s}{.}2$	$-25°31'01''$	$223\overset{\circ}{.}51$	$-43\overset{\circ}{.}11$	13.666	8363	484	3
HE 0420−1806	HBB	$04^h22^m25\overset{s}{.}1$	$-17°59'20''$	$213\overset{\circ}{.}88$	$-40\overset{\circ}{.}78$	14.02	0433	550	3
HE 0421−5415	He-sdO	$04^h22^m37\overset{s}{.}3$	$-54°08'50''$	$263\overset{\circ}{.}13$	$-43\overset{\circ}{.}19$	13.91	0939	157	4
HE 0429−2448	sdOB	$04^h31^m28\overset{s}{.}3$	$-24°41'57''$	$223\overset{\circ}{.}18$	$-40\overset{\circ}{.}85$	15.301	8363	484	1
HE 0430−2457	sdB+x	$04^h33^m03\overset{s}{.}8$	$-24°51'20''$	$223\overset{\circ}{.}50$	$-40\overset{\circ}{.}54$	14.15	8363	484	1
HE 0430−5341	HBB	$04^h31^m11\overset{s}{.}0$	$-53°35'27''$	$262\overset{\circ}{.}03$	$-42\overset{\circ}{.}07$	13.59	0939	157	4
HE 0437−5439	B	$04^h38^m12\overset{s}{.}8$	$-54°33'12''$	$263\overset{\circ}{.}04$	$-40\overset{\circ}{.}88$	16.21	0939	157	4
HE 0439−1826	He-sdO	$04^h42^m08\overset{s}{.}2$	$-18°20'55''$	$216\overset{\circ}{.}42$	$-36\overset{\circ}{.}52$	14.12	0416	551	1
HE 0440−3211	He-sdO	$04^h42^m25\overset{s}{.}9$	$-32°05'59''$	$233\overset{\circ}{.}37$	$-40\overset{\circ}{.}12$		8403	361	1
HE 0442−1746	sdOB	$04^h44^m34\overset{s}{.}8$	$-17°40'44''$	$215\overset{\circ}{.}91$	$-35\overset{\circ}{.}74$	15.150	0416	551	1
HE 0442−1908	B	$04^h44^m16\overset{s}{.}3$	$-19°02'42''$	$217\overset{\circ}{.}45$	$-36\overset{\circ}{.}29$	13.08	0416	551	3
HE 0442−3523	DBA	$04^h44^m27\overset{s}{.}4$	$-35°17'43''$	$237\overset{\circ}{.}59$	$-40\overset{\circ}{.}20$	15.80	8400	361	1
HE 0444−4945	sdB	$04^h46^m14\overset{s}{.}1$	$-49°40'11''$	$256\overset{\circ}{.}45$	$-40\overset{\circ}{.}28$	15.113	0841	203	2,4
HE 0447−3654	sdB	$04^h49^m15\overset{s}{.}6$	$-36°49'28''$	$239\overset{\circ}{.}72$	$-39\overset{\circ}{.}43$	14.552	8400	361	1
HE 0451−3706	He-sdO	$04^h53^m32\overset{s}{.}1$	$-37°01'43''$	$240\overset{\circ}{.}12$	$-38\overset{\circ}{.}60$	15.69	8400	361	4
HE 0452−3654	sdB	$04^h53^m52\overset{s}{.}6$	$-36°49'15''$	$239\overset{\circ}{.}87$	$-38\overset{\circ}{.}51$	13.836	8400	361	1
HE 0500−3518	sdB	$05^h02^m31\overset{s}{.}6$	$-35°14'20''$	$238\overset{\circ}{.}23$	$-36\overset{\circ}{.}54$	15.044	8401	362	1
HE 0504−2041	sdB	$05^h06^m39\overset{s}{.}7$	$-20°37'38''$	$221\overset{\circ}{.}42$	$-31\overset{\circ}{.}88$	14.959	0423	552	1
HE 0505−2228	sdB	$05^h07^m47\overset{s}{.}5$	$-22°24'28''$	$223\overset{\circ}{.}50$	$-32\overset{\circ}{.}22$	15.547	8348	486	1
HE 0505−3833	sdB	$05^h06^m58\overset{s}{.}8$	$-38°29'16''$	$242\overset{\circ}{.}39$	$-36\overset{\circ}{.}17$	14.185	8397	305	1
HE 0510−4023	sdB	$05^h12^m18\overset{s}{.}1$	$-40°19'35''$	$244\overset{\circ}{.}80$	$-35\overset{\circ}{.}39$	14.837	8397	305	1
HE 0511−2302	DA	$05^h13^m51\overset{s}{.}8$	$-22°59'19''$	$224\overset{\circ}{.}68$	$-31\overset{\circ}{.}08$		8364	486	1
HE 0513−4632	sdB+x	$05^h14^m45\overset{s}{.}9$	$-46°29'15''$	$252\overset{\circ}{.}38$	$-35\overset{\circ}{.}54$	15.56	0934	252	2
HE 0516−2311	sdB	$05^h18^m06\overset{s}{.}9$	$-23°08'46''$	$225\overset{\circ}{.}22$	$-30\overset{\circ}{.}21$	15.57	8348	486	3
HE 0519−3512	HBB	$05^h20^m48\overset{s}{.}5$	$-35°09'31''$	$238\overset{\circ}{.}99$	$-32\overset{\circ}{.}86$	13.20	8401	362	1
HE 0521−3914	sdB	$05^h23^m25\overset{s}{.}5$	$-39°11'55''$	$243\overset{\circ}{.}84$	$-33\overset{\circ}{.}11$	15.550	8397	305	3
HE 0522−2055	CV	$05^h25^m08\overset{s}{.}5$	$-20°52'24''$	$223\overset{\circ}{.}40$	$-27\overset{\circ}{.}91$	13.77	0434	553	3
HE 0523−1831	sdB	$05^h25^m31\overset{s}{.}2$	$-18°29'09''$	$220\overset{\circ}{.}93$	$-26\overset{\circ}{.}97$	14.307	0434	553	2,4
HE 0528−5431	B	$05^h29^m54\overset{s}{.}6$	$-54°29'17''$	$262\overset{\circ}{.}19$	$-33\overset{\circ}{.}42$	11.30	0388	159	4
HE 0532−4503	sdB	$05^h33^m40\overset{s}{.}5$	$-45°01'35''$	$251\overset{\circ}{.}02$	$-32\overset{\circ}{.}11$	16.056	0417	253	2,4
HE 0538−5637	sdB+x	$05^h39^m08\overset{s}{.}3$	$-56°35'56''$	$264\overset{\circ}{.}73$	$-32\overset{\circ}{.}16$	14.82	0388	159	2
HE 0539−4246	sdB	$05^h41^m06\overset{s}{.}7$	$-42°45'33''$	$248\overset{\circ}{.}64$	$-30\overset{\circ}{.}44$	14.804	0417	253	3

A.3 Bright sdB stars

A.3.1 Low-Resolution observations

Table A.3: Summary of all low-resolution observations for the bright program sdB stars.

name	date	instrument	spectral res. [Å]	wavelength coverage [Å]	observers
PG 0001+275	Jul 08, 2001	CA 3.5m TWIN	1.3/1.5	3910–5000/5970–7070	N & K
HD 4539	Sep 30, 1998	CA 2.2m CAFOS	4.5	3300–6300	E
PG 0342+026	Feb 10, 2003	CA 2.2m CAFOS	5.0	3200–5700	P
PG 0909+276	Feb 10, 2003	CA 2.2m CAFOS	5.0	3200–5700	P
Feige 65	Mar 11, 2001	CA 3.5m TWIN	1.3/1.5	3920–5020/5960–7070	N
UVO 1735+22	Jul 17, 1999	CA 3.5m TWIN	2.9/3.0	3450–5600/5550–7550	W & F
UVO 1758+36	Jul 17, 1999	CA 3.5m TWIN	2.9/3.0	3450–5600/5550–7550	W & F
BD+48° 2721	Jul 17, 1999	CA 3.5m TWIN	2.9/3.0	3450–5600/5550–7550	W & F
CD−35° 15910	Nov 20, 2001	ESO 1.54m DFOSC	4.5	3500-5500	E

Observers: E=Edelmann, F=Furlan, K=Karl, N=Napiwotzki, W=Werner

A.3.2 High-Resolution observations

Table A.4: Coordinates and V magnitudes for all bright program sdB stars. Additionally is indicated, if the stars are RV variable (– (s): constant short time, i.e. hours; – (i) constant intermediate time, i.e. a few days; – (l): constant long time, i.e. longer than a few weeks).

star	type	α (2000)	δ (2000)	V (mag)	run #	RVV
SB 7	sdOB+x	$00^h03^m24^s.5$	$-16°21'05''$	12.6	7a	– (i)
PG 0001+275	sdB	$00^h03^m55^s.7$	$+27°48'37''$	12.8	2, 5	$\surd$
PG 0011+283	sdB	$00^h14^m22^s.3$	$+28°36'56''$	12.2	2, 7a	– (s+i+l)
CD−38° 222	sdB	$00^h42^m58^s.3$	$-38°07'37''$	10.5	6	– (s)
HD 4539	sdB	$00^h47^m29^s.2$	$+09°58'56''$	10.3	1, 6	– (s+i+l)
PHL 6783	sdO+x	$00^h52^m15^s.1$	$-10°39'46''$	11.1	7a, 7b	$\surd$
SB 395	sdB	$00^h59^m11^s.7$	$-18°18'00''$	12.4	7a, 7b	– (l)
PHL 932	sdOB	$00^h59^m56^s.7$	$+15°44'14''$	12.0	2, 7a	– (s+i+l)
Feige 11	sdB	$01^h04^m21^s.8$	$+04°13'37''$	12.1	3	$\surd$
PG 0116+242	sdB+x	$01^h19^m29^s.1$	$+24°25'32''$	11.1	7a	– (i)
PG 0133+114	sdB	$01^h36^m26^s.3$	$+11°39'32''$	10.7	3, 5	$\surd$
CD−24° 731	sdOB	$01^h43^m48^s.6$	$-24°05'10''$	11.6	4, 6	– (s)
PG 0342+026	sdB	$03^h45^m34^s.6$	$+02°47'52''$	11.1	1, 3, 7a	– (s+i+l)
UVO 0512−08	sdOB	$05^h14^m44^s.0$	$-08°48'04''$	11.3	3, 7b	– (s+i+l)
PG 0909+276	sdOB	$09^h12^m51^s.7$	$+27°20'31''$	10.7	3	– (s+i)
PG 1047+003	sdB	$10^h50^m02^s.9$	$-00°00'35''$	13.5	3	– (s+i)
Feige 65	sdB	$12^h35^m51^s.1$	$+42°22'40''$	12.0	3	– (i)
Feige 86	HBB	$13^h38^m24^s.9$	$+29°21'56''$	10.0	3	– (s)
PG 1336−018	sdB	$13^h38^m48^s.2$	$-02°01'49''$	12.9	3	– (i)
PG 1505+074	sdOB	$15^h08^m20^s.9$	$+07°13'16''$	12.2	7a	– (i)
PG 1519+640	sdB	$15^h20^m31^s.3$	$+63°52'08''$	12.1	7a	$\surd$
PG 1524+611	sdB+x	$15^h25^m13^s.4$	$+60°53'21''$	11.6	7a	– (i)
PG 1530+212	B	$15^h32^m49^s.1$	$+21°03'35''$	10.0	7a	– (i)
PG 1607+174	sdB+x	$16^h09^m55^s.1$	$+17°14'57''$	10.2	7a	– (i)
LS IV−12 1	sdO	$16^h23^m44^s.1$	$-12°12'32''$	11.2	6	– (s+i)
HD 149382	sdOB	$16^h34^m23^s.4$	$-04°00'51''$	8.9	6, 7a	– (s+i)
PG 1654+138	sdB	$16^h57^m00^s.9$	$+13°43'59''$	11.8	7a	– (i)
PG 1705+537	HBB	$17^h06^m14^s.7$	$+53°35'29''$	12.0	7a	– (i)
PG 1710+490	sdB	$17^h12^m18^s.8$	$+48°58'36''$	12.1	7a	– (i)
UVO 1735+22	sdOB	$17^h37^m26^s.5$	$+22°08'58''$	11.8	2, 5	$\surd$
UVO 1758+36	sdB	$18^h00^m18^s.9$	$+36°28'59''$	11.4	1, 7a	– (s+i+l)
BD+48° 2721	sdB	$18^h34^m09^s.3$	$+48°27'38''$	10.7	1, 7a	– (s+i+l)
HD 171858	sdB	$18^h37^m56^s.7$	$-23°11'34''$	9.9	4, 6, 7a	$\surd$
HD 188112	sdB	$19^h54^m31^s.4$	$-28°20'21''$	10.2	4, 6, 7a	$\surd$
PHL 25	sdB	$21^h32^m04^s.6$	$-17°18'40''$	11.5	7a	– (i)
HD 205805	sdB	$21^h39^m10^s.6$	$-46°05'51''$	10.2	4, 6	– (s+i+l)
PG 2151+100	sdB	$21^h53^m57^s.5$	$+10°17'35''$	12.9	7a, 7b	$\surd$
PG 2159+051	sdB	$22^h01^m58^s.7$	$+05°24'28''$	11.5	7a	– (i)
HS 2224+2618	sdB	$22^h27^m17^s.5$	$+26°33'30''$	12.8	7a	– (i)
PHL 382	sdB	$22^h43^m06^s.0$	$-14°50'37''$	11.3	7a	– (i)
PB 7352	sdB	$22^h55^m43^s.2$	$-06°59'39''$	12.0	4, 6, 7a	$\surd$
LB 1516	sdB	$23^h01^m56^s.0$	$-48°03'48''$	12.7	4, 6	$\surd$
PG 2301+259	sdB	$23^h04^m17^s.3$	$+26°12'03''$	13.0	7a, 7b	– (l)
Feige 108	sdB	$23^h16^m12^s.5$	$-01°50'35''$	12.6	7a	$\surd$
PB 5333	sdB	$23^h19^m55^s.4$	$+04°52'35''$	12.9	7a	$\surd$
CD−35° 15910	sdB	$23^h44^m22^s.0$	$-34°27'00''$	11.0	4, 6	– (s+i+l)
PG 2351+198	sdB	$23^h53^m44^s.9$	$+20°06'05''$	12.0	7a	– (i)

Appendix B

Analyses results

B.1 Hamburg Quasar Survey

Table B.1: Effective temperatures, gravities, and helium abundances, the B magnitudes and extinctions, the radial velocities, the absolute visual magnitudes, the distances from earth and from the galactic plane, and the references are given for all program HQS stars.

sdB stars:

star	$T_{\rm eff}$ 1 000K	$\log(g)$ (cgs)	$\log(n_{\rm He}/n_{\rm H})$	B mag	E(B-V) mag	$v_{\rm rad}$ km/s	M_V mag	d kpc	$\|z\|$ kpc
HS 0016+0044	28.5 ± 1.0	5.15 ± 0.2	-2.9 ± 0.3	14.6	0.03	-	3.1	2.2	1.9
HS 0023+3049	30.8 ± 0.8	5.80 ± 0.1	-3.8 ± 0.5	14.6	0.09	-	4.6	1.0	0.0
HS 0039+4302	32.3 ± 0.8	5.70 ± 0.1	-2.3 ± 0.2	15.1	0.08	-	4.2	1.6	0.5
HS 0040+4417	31.0 ± 1.2	5.60 ± 0.2	-1.7 ± 0.3	15.6	0.08	-	4.1	2.2	0.7
HS 0055+0138	33.0 ± 0.9	5.60 ± 0.1	-1.9 ± 0.2	15.1	0.02	-	3.9	1.9	1.7
HS 0209+0141	30.9 ± 0.8	5.65 ± 0.1	-2.7 ± 0.2	13.6	0.04	-	4.2	0.8	0.7
HS 0212+1446	30.6 ± 0.8	5.90 ± 0.1	-2.8 ± 0.2	14.6	0.09	-	4.9	1.0	0.7
HS 0233+3037	27.5 ± 0.7	5.60 ± 0.1	-2.7 ± 0.2	14.1	0.16	-129	4.3	1.0	0.4
HS 0338+2946	29.9 ± 0.8	5.60 ± 0.1	-2.4 ± 0.2	15.1	0.26	-	4.2	1.6	0.5
HS 0349+0700	28.0 ± 1.5	5.70 ± 0.4	-2.6 ± 0.4	14.4	0.21	-	4.5	1.0	0.5
HS 0352+1019	24.9 ± 0.6	5.35 ± 0.1	-2.7 ± 0.2	13.9	0.20	-	3.9	1.0	0.5
HS 0357+0133	30.0 ± 0.8	5.70 ± 0.1	-2.1 ± 0.2	14.9	0.30	$+22$	4.4	1.2	0.7
HS 0430+7712	26.8 ± 0.7	5.40 ± 0.1	-3.0 ± 0.2	13.7	0.13	-	3.9	1.0	0.3
HS 0444+0458	33.8 ± 0.8	5.60 ± 0.1	-1.9 ± 0.2	15.2	0.08	-	3.9	2.0	0.8
HS 0445+7503	31.5 ± 0.8	5.70 ± 0.1	-2.1 ± 0.2	14.2	0.18	-	4.3	1.0	0.3
HS 0447+7545	30.0 ± 1.3	5.40 ± 0.2	-2.2 ± 0.2	15.7	0.16	-	3.7	2.7	0.9
HS 0702+6043	28.4 ± 0.7	5.35 ± 0.1	-2.7 ± 0.2	14.8	0.07	-	3.6	1.9	0.8
HS 0705+6700	30.2 ± 1.0	5.70 ± 0.2	-2.6 ± 0.3	14.2	0.05	-	4.4	1.0	0.5
HS 0707+8225	27.8 ± 1.0	5.30 ± 0.2	-3.8 ± 0.5	14.9	0.04	-	3.6	2.1	1.0
HS 0740+3734	20.4 ± 0.9	5.00 ± 0.2	-2.1 ± 0.4	14.4	0.06	-	3.4	1.7	0.8
HS 0741+3818	31.7 ± 1.1	5.35 ± 0.1	-1.6 ± 0.3	14.4	0.05	-	3.4	1.8	0.8
HS 0941+4649	34.7 ± 1.5	5.80 ± 0.2	-2.0 ± 0.4	16.7	0.01	-	4.3	3.4	2.5

continued on next page

(continued from last page

sdB stars:

star	$T_{\rm eff}$ 1 000K	$\log(g)$ (cgs)	$\log(n_{\rm He}/n_{\rm H})$	B mag	E(B-V) mag	$v_{\rm rad}$ km/s	M_V mag	d kpc	$\|z\|$ kpc
HS 1236+4754	28.4 ± 0.8	5.55 ± 0.1	-2.5 ± 0.2	15.5	0.02	-	4.1	2.1	2.0
HS 1320+2622	29.2 ± 0.8	5.55 ± 0.1	-2.7 ± 0.2	16.5	0.02	-110	4.1	3.4	3.4
HS 1547+6312	31.3 ± 0.8	5.75 ± 0.1	-3.2 ± 0.5	14.8	0.01	-	4.4	1.3	0.9
HS 1552+6333	34.1 ± 0.8	5.55 ± 0.1	-1.8 ± 0.2	16.4	0.02	-	3.8	3.8	2.6
HS 1641+4601	30.7 ± 0.8	5.65 ± 0.2	-1.7 ± 0.2	14.6	0.02	-	4.2	1.3	0.9
HS 1717+6042	29.6 ± 0.7	5.50 ± 0.1	-2.4 ± 0.2	14.4	0.03	-	3.8	1.4	0.8
HS 1736+8001	30.3 ± 0.8	4.90 ± 0.1	< -4.0	14.8	0.08	-	2.4	3.3	1.7
HS 1739+5244	36.0 ± 0.9	5.50 ± 0.1	-2.9 ± 0.4	14.6	0.03	-28	3.5	1.8	1.0
HS 1747+6924	27.5 ± 1.2	5.35 ± 0.2	-2.9 ± 0.3	15.1	0.03	-	3.7	2.1	1.1
HS 1747+8014	32.8 ± 1.0	5.75 ± 0.3	-2.1 ± 0.4	16.2	0.09	-	4.3	2.6	1.3
HS 1756+7056	29.5 ± 1.0	5.70 ± 0.2	-3.6 ± 0.5	15.6	0.03	-	4.4	1.9	1.0
HS 1813+7247	27.7 ± 1.3	5.20 ± 0.2	-2.7 ± 0.4	15.2	0.06	-	3.3	2.6	1.3
HS 1831+7647	23.3 ± 0.6	5.40 ± 0.1	-3.0 ± 0.2	14.4	0.08	-	4.2	1.2	0.6
HS 1832+7009	29.8 ± 0.8	5.50 ± 0.1	-1.5 ± 0.3	14.4	0.09	-	3.9	1.3	0.6
HS 1839+7951	27.5 ± 1.4	5.70 ± 0.5	-2.1 ± 0.5	17.6	0.06	-	4.6	4.5	2.0
HS 1842+6557	35.5 ± 1.5	6.65 ± 0.5	-1.0 ± 0.4	15.2	0.05	-	6.4	0.6	0.3
HS 1843+6953	38.0 ± 1.9	5.60 ± 0.2	-2.9 ± 0.4	15.0	0.06	-	3.7	2.0	0.9
HS 1846+8149	26.3 ± 0.7	5.40 ± 0.1	-2.8 ± 0.2	14.4	0.05	-	3.9	1.4	0.6
HS 1859+6219	29.0 ± 1.3	5.50 ± 0.2	-2.4 ± 0.3	14.9	0.08	-	4.0	1.7	0.7
HS 2126+8320	28.1 ± 0.7	5.40 ± 0.2	-3.0 ± 0.2	13.9	0.12	-	3.8	1.1	0.4
	28.2 ± 0.7	5.40 ± 0.2	-2.8 ± 0.2			-	3.8	1.1	0.4
HS 2143+8157	25.6 ± 0.7	5.10 ± 0.2	-3.1 ± 0.4	15.4	0.12	-	3.2	2.9	1.1
HS 2149+1428	36.0 ± 1.0	5.75 ± 0.2	< -4.0	14.4	0.10	-	4.2	1.2	0.6
HS 2151+0214	30.4 ± 0.8	5.60 ± 0.1	-2.3 ± 0.2	16.5	0.06	-	4.1	3.3	2.0
HS 2156+2517	34.7 ± 0.9	6.10 ± 0.1	-3.1 ± 0.5	14.1	0.06	-	5.1	0.7	0.3
HS 2158+2137	32.0 ± 0.8	5.80 ± 0.1	-2.2 ± 0.2	14.1	0.10	-	4.5	0.9	0.4
HS 2201+2610	29.3 ± 0.7	5.50 ± 0.1	-3.0 ± 0.2	13.6	0.07	-31	4.0	0.9	0.4
HS 2206+2847	32.2 ± 0.8	5.75 ± 0.1	-1.7 ± 0.2	14.2	0.09	0	4.4	1.0	0.4
HS 2208+2718	29.5 ± 0.8	5.50 ± 0.1	-3.8 ± 0.2	14.1	0.08	$+124$	3.9	1.2	0.5
HS 2209+2840	31.3 ± 0.8	5.80 ± 0.1	-1.7 ± 0.2	14.7	0.09	$+2$	4.6	1.2	0.4
HS 2213+1336	20.3 ± 1.0	4.75 ± 0.2	-2.3 ± 0.2	15.8	0.07	-	2.8	4.4	2.5
HS 2218+0201	24.7 ± 0.9	5.20 ± 0.1	-2.8 ± 0.2	13.9	0.08	-	3.5	1.3	0.9
HS 2224+2618	20.5 ± 0.5	4.70 ± 0.1	-1.7 ± 0.2	12.8	0.05	-	2.6	1.2	0.5
HS 2225+2220	31.5 ± 0.8	5.85 ± 0.1	-1.6 ± 0.2	15.5	0.05	$+4$	4.7	1.6	0.8
HS 2231+2441	27.4 ± 0.7	5.30 ± 0.1	-3.1 ± 0.2	14.1	0.05	-	3.6	1.4	0.7
HS 2233+2332	26.5 ± 0.7	5.30 ± 0.1	-2.7 ± 0.2	14.3	0.04	$+12$	3.7	1.5	0.7
	26.8 ± 0.7	5.35 ± 0.1	-2.9 ± 0.2			$+25$	3.8	1.4	0.7
HS 2240+0136	31.3 ± 0.8	6.00 ± 0.1	-2.4 ± 0.2	14.4	0.08	-36	5.1	0.8	0.6
HS 2242+3206	29.3 ± 0.7	5.65 ± 0.1	-2.8 ± 0.2	14.7	0.11	-168	4.3	1.3	0.5
HS 2246+0158	33.6 ± 1.0	5.85 ± 0.2	-1.6 ± 0.2	15.6	0.08	-	4.5	1.8	1.3

(continued on next page

(continued from last page

sdOB stars:

star	$T_{\rm eff}$ 1 000K	$\log(g)$ (cgs)	$\log(n_{\rm He}/n_{\rm H})$	B mag	E(B-V) mag	$v_{\rm rad}$ km/s	M_V mag	d kpc	$\|z\|$ kpc
HS 0025+3423	33.1 ± 0.8	6.25 ± 0.1	-0.9 ± 0.3	15.4	0.09	-37	5.6	1.0	0.5
HS 0035+3034	36.9 ± 0.9	5.75 ± 0.1	-1.6 ± 0.2	15.8	0.06	-17	4.1	2.4	1.3
HS 0048+0026	36.5 ± 1.8	5.45 ± 0.2	-1.0 ± 0.3	15.6	0.02	-	3.4	3.1	2.7
HS 0213+2329	32.4 ± 0.9	5.50 ± 0.1	-1.5 ± 0.2	14.6	0.09	-8	3.7	1.6	0.9
HS 0232+3155	34.3 ± 0.8	5.70 ± 0.1	-3.3 ± 0.5	15.1	0.11	-11	4.1	1.7	0.7
HS 0457+0907	35.4 ± 0.9	5.80 ± 0.1	-1.4 ± 0.2	14.1	0.16	-	4.3	1.0	0.3
HS 0546+8009	34.0 ± 0.8	5.75 ± 0.1	-2.0 ± 0.2	13.9	0.10	$+7$	4.1	1.0	0.4
HS 0600+6602	36.0 ± 1.5	6.30 ± 0.2	-1.5 ± 0.2	16.1	0.10	-	5.4	1.4	0.5
HS 0815+4243	33.8 ± 0.8	5.90 ± 0.1	-2.0 ± 0.2	16.4	0.06	$+41$	4.6	2.5	1.4
HS 1051+2933	36.3 ± 0.9	5.95 ± 0.1	-0.6 ± 0.2	16.1	0.02	-130	4.7	2.2	2.0
HS 1741+2133	35.6 ± 0.8	5.30 ± 0.1	-2.5 ± 0.2	14.1	0.11	-84	3.1	1.8	0.7
HS 1806+5024	36.4 ± 0.9	5.50 ± 0.1	-1.4 ± 0.2	16.8	0.05	-	3.5	5.0	2.3
HS 1824+5745	33.1 ± 0.8	6.00 ± 0.2	-1.6 ± 0.2	15.6	0.04	-	4.9	1.5	0.7
HS 1831+6432	36.0 ± 0.9	5.85 ± 0.1	-1.6 ± 0.2	14.9	0.04	-	4.4	1.4	0.6
HS 2100+1710	34.1 ± 0.9	6.05 ± 0.1	-1.3 ± 0.2	14.9	0.08	-30	5.0	1.0	0.3
	35.4 ± 0.9	5.85 ± 0.1	-1.4 ± 0.2			-3	4.4	1.4	0.4
HS 2149+0847	35.6 ± 0.9	5.90 ± 0.2	-1.8 ± 0.2	16.5	0.05	-	4.6	2.7	1.5
HS 2151+0857	34.5 ± 0.8	6.10 ± 0.3	-1.4 ± 0.2	16.5	0.05	-	5.1	2.1	1.2
HS 2156+2215	33.4 ± 1.0	5.25 ± 0.2	-3.1 ± 0.2	15.1	0.08	-22	3.0	2.8	1.2
HS 2229+0910	38.5 ± 0.9	6.20 ± 0.1	-1.9 ± 0.2	15.9	0.10	-	5.2	1.5	1.0
HS 2233+1418	37.0 ± 0.9	5.60 ± 0.1	-2.4 ± 0.2	13.8	0.07	-	3.8	1.1	0.7
HS 2240+1031	34.4 ± 0.8	5.70 ± 0.1	-1.5 ± 0.2	14.8	0.06	-	4.1	1.5	1.0
HS 2333+3927	37.6 ± 0.9	5.75 ± 0.1	-2.2 ± 0.2	14.6	0.09	$+68$	4.1	1.3	0.5
	39.0 ± 1.0	5.80 ± 0.1	-2.3 ± 0.2			-27	4.2	1.3	0.5

HBB stars:

HS 2229+2628	18.0 ± 0.5	4.25 ± 0.2	-1.8 ± 0.5	13.9	0.04	-	1.8	3.0	1.3

B stars:

HS 0231+8019	16.0 ± 0.6	3.85 ± 0.1	-1.0 ± 0.2	15.1	0.27	-	see text		
HS 1556+6032	13.1 ± 0.8	3.80 ± 0.1	-1.5 ± 0.5	15.9	0.01	-	see text		
HS 2131+0349	13.3 ± 0.4	3.50 ± 0.1	-1.1 ± 0.3	14.3	0.05	-	see text		

B.2 Hamburg ESO Survey

Table B.2: Effective temperatures, gravities, and helium abundances, the V magnitudes and extinctions, the absolute visual magnitudes, and the distances from earth and from the galactic plane are given for all program HES stars.

sdB stars:

star	$T_{\rm eff}$ 1 000K	$\log(g)$ (cgs)	$\log(n_{\rm He}/n_{\rm H})$	V mag	E(B-V) mag	M_V mag	d kpc	$\|z\|$ kpc
HE 2135−3749	29.6 ± 0.2	5.8 ± 0.1	-2.5 ± 0.2	13.926	0.035	4.7	0.71	0.53
HE 2154−4143	30.7 ± 0.2	5.7 ± 0.1	-2.7 ± 0.2	15.173	0.019	4.3	1.47	1.15
HE 2155−1724	30.2 ± 0.4	5.8 ± 0.1	-2.5 ± 0.2	15.042	0.046	4.7	1.16	0.87
HE 2156−1732	29.3 ± 0.4	5.7 ± 0.1	-2.5 ± 0.3	15.064	0.041	4.4	1.33	1.01
HE 2156−3927	28.1 ± 0.3	5.4 ± 0.1	-2.3 ± 0.1	14.448	0.019	3.8	1.36	1.08
HE 2200−4047	26.2 ± 0.4	5.3 ± 0.1	-2.7 ± 0.2	16.47	0.018	3.6	3.66	2.93
HE 2201−2113	30.4 ± 0.4	5.8 ± 0.1	-3.0 ± 0.3	15.903	0.037	4.7	1.75	1.37
HE 2205−1952	32.2 ± 0.4	5.9 ± 0.1	-1.6 ± 0.2	14.591	0.024	4.6	0.97	0.76
HE 2211−2021	29.0 ± 0.4	5.6 ± 0.1	-2.9 ± 0.4	14.54	0.029	4.2	1.17	0.94
HE 2213−4158	38.0 ± 0.6	5.4 ± 0.1	-2.5 ± 0.4	16.153	0.012	3.2	3.82	3.13
HE 2222−3738	30.4 ± 0.2	5.6 ± 0.1	-2.8 ± 0.2	14.889	0.016	4.0	1.45	1.22
HE 2316−0909	26.0 ± 0.3	5.2 ± 0.1	-2.4 ± 0.1	13.14	0.031	3.6	0.80	0.71
HE 2337−2944	35.6 ± 0.3	5.9 ± 0.1	-1.6 ± 0.1	14.452	0.019	4.5	0.96	0.92
HE 2340−2806	30.8 ± 0.3	5.7 ± 0.1	-3.9 ± 0.9	14.996	0.017	4.2	1.41	1.36
HE 2341−3443	28.0 ± 0.4	5.4 ± 0.1	-2.9 ± 0.2	10.89	0.013	3.8	0.27	0.26
HE 2343−2944	28.2 ± 0.6	5.7 ± 0.1	-2.5 ± 0.2	15.041	0.018	4.6	1.22	1.18
HE 2349−3135	29.1 ± 0.6	5.6 ± 0.2	-3.1 ± 1.0	15.908	0.015	4.3	2.08	2.02
HE 2355−3221	26.3 ± 0.7	5.4 ± 0.1	-2.5 ± 0.3	15.181	0.012	4.0	1.70	1.66
HE 0000−2355	25.5 ± 0.4	5.4 ± 0.1	-2.7 ± 0.2	13.293	0.020	4.0	0.74	0.73
HE 0002−2648	28.5 ± 0.5	5.5 ± 0.1	-2.3 ± 0.2	14.31	0.016	4.0	1.14	1.12
HE 0021−2326	33.5 ± 1.3	5.6 ± 0.3	-3.8 ± 2.0	15.942	0.018	3.8	2.60	2.58
HE 0049−2928	29.3 ± 0.8	5.5 ± 0.2	-2.5 ± 0.7	15.781	0.015	4.1	2.18	2.18
HE 0049−3059	30.2 ± 0.3	5.6 ± 0.1	-3.3 ± 0.8	14.413	0.017	4.0	1.17	1.17
HE 0123−2808	30.0 ± 0.5	5.5 ± 0.1	-3.4 ± 1.1	16.089	0.016	4.0	2.55	2.53
HE 0127−4325	26.6 ± 0.3	5.2 ± 0.1	-2.9 ± 0.2	14.597	0.017	3.5	1.63	1.55
HE 0136−2758	30.4 ± 1.2	5.8 ± 0.4	-2.3 ± 0.7	16.173	0.021	4.5	2.12	2.08
HE 0151−3919	20.2 ± 0.3	4.8 ± 0.1	-1.9 ± 0.1	14.311	0.014	1.5	0.92	0.88
HE 0218−3437	25.3 ± 0.3	5.4 ± 0.1	-3.4 ± 0.4	13.391	0.018	2.0	0.38	0.36
HE 0221−3250	24.8 ± 0.3	5.3 ± 0.1	-1.7 ± 0.1	14.700	0.016	1.9	0.79	0.74

continued on next page

continued from last page

sdB stars:

star	$T_{\rm eff}$ 1 000K	$\log(g)$ (cgs)	$\log(n_{\rm He}/n_{\rm H})$	V mag	E(B-V) mag	M_V mag	d kpc	$\|z\|$ kpc
HE 0230−4323	30.6 ± 0.3	5.5 ± 0.1	−2.7 ± 0.2	13.779	0.023	4.0	0.90	0.81
HE 0231−3441	34.1 ± 0.3	5.9 ± 0.1	−0.6 ± 0.1	14.828	0.022	4.7	1.06	0.97
HE 0258−2158	22.9 ± 0.7	5.1 ± 0.1	−2.3 ± 0.3	14.645	0.021	1.7	0.89	0.78
HE 0307−4554	29.8 ± 0.3	5.9 ± 0.1	−2.8 ± 0.2	15.063	0.023	4.9	1.06	0.89
HE 0315−4244	29.0 ± 0.7	5.3 ± 0.2	−4.0 ± 1.1	16.918	0.016	3.4	5.08	4.24
HE 0324−2529	30.6 ± 0.6	5.7 ± 0.2	−3.8 ± 1.1	14.624	0.017	4.3	1.13	0.93
HE 0340−3820	31.7 ± 0.3	5.7 ± 0.1	−1.8 ± 0.1	14.771	0.010	4.2	1.27	1.01
HE 0343−4748	21.0 ± 0.2	4.7 ± 0.1	−2.3 ± 0.9	14.193	0.010	1.3	1.05	0.81
HE 0351−3536	27.6 ± 0.4	5.7 ± 0.1	−4.0 ± 1.5	14.107	0.009	4.5	0.84	0.65
HE 0405−3859	24.6 ± 0.3	5.3 ± 0.1	−2.4 ± 0.1	14.392	0.007	1.9	0.67	0.50
HE 0407−1956	34.7 ± 0.2	5.6 ± 0.1	−1.7 ± 0.1	13.610	0.030	3.8	0.89	0.62
HE 0410−4901	30.6 ± 0.3	5.4 ± 0.1	−2.9 ± 0.4	14.508	0.017	3.5	1.53	1.10
HE 0419−2538	25.9 ± 0.3	5.1 ± 0.1	−2.5 ± 0.1	13.666	0.044	3.2	1.17	0.80
HE 0444−4945	31.0 ± 0.2	5.7 ± 0.1	−2.2 ± 0.1	15.113	0.011	4.2	1.49	0.96
HE 0447−3654	31.3 ± 0.3	5.7 ± 0.1	−3.0 ± 0.3	14.552	0.012	4.3	1.09	0.69
HE 0452−3654	28.0 ± 0.3	5.5 ± 0.1	−2.9 ± 0.2	13.836	0.011	4.2	0.85	0.53
HE 0500−3518	26.9 ± 0.7	5.7 ± 0.1	−2.7 ± 0.4	15.044	0.012	4.5	1.27	0.76
HE 0504−2041	26.9 ± 0.5	5.6 ± 0.1	−2.4 ± 0.2	14.959	0.033	4.3	1.34	0.71
HE 0505−2228	27.0 ± 1.1	6.0 ± 0.2	−2.9 ± 1.0	15.547	0.034	5.2	1.14	0.61
HE 0505−3833	28.4 ± 0.3	5.6 ± 0.1	−2.5 ± 0.3	14.185	0.024	4.4	0.91	0.54
HE 0510−4023	29.4 ± 0.5	5.6 ± 0.1	−3.2 ± 0.8	14.837	0.048	4.1	1.38	0.80
HE 0516−2311	30.1 ± 0.3	5.5 ± 0.1	−2.0 ± 0.1	15.57	0.037	4.0	2.08	1.04
HE 0521−3914	31.1 ± 0.2	5.6 ± 0.1	−4.0 ± 1.5	15.550	0.026	4.1	1.90	1.04
HE 0523−1831	33.9 ± 0.3	5.4 ± 0.1	−2.7 ± 0.3	14.307	0.058	3.3	1.57	0.71
HE 0532−4503	25.3 ± 0.3	5.4 ± 0.1	−4.0 ± 1.5	16.056	0.038	2.0	1.25	0.67
HE 0539−4246	23.5 ± 0.4	5.5 ± 0.1	−4.0 ± 1.5	14.804	0.046	2.2	0.59	0.30

sdOB stars:

HE 2350−3026	37.5 ± 0.4	5.8 ± 0.1	−0.8 ± 0.1	12.10	0.020	4.3	0.35	0.34
HE 2359−2844	38.3 ± 0.9	6.1 ± 0.3	−0.0 ± 0.2	16.440	0.019	5.0	1.92	1.88
HE 0004−2737	37.2 ± 0.5	6.0 ± 0.1	−1.8 ± 0.1	13.967	0.020	4.8	0.67	0.66
HE 0031−2724	36.3 ± 0.2	5.8 ± 0.1	−1.4 ± 0.1	14.229	0.014	4.4	0.93	0.92
HE 0341−2449	33.8 ± 0.4	5.9 ± 0.1	−1.8 ± 0.2	14.889	0.011	4.7	1.10	0.86
HE 0405−1719	33.9 ± 0.2	5.8 ± 0.1	−1.8 ± 0.1	14.003	0.025	4.3	0.86	0.60
HE 0429−2448	35.1 ± 0.4	6.1 ± 0.1	−1.6 ± 0.1	15.301	0.048	5.0	1.11	0.73
HE 0442−1746	34.0 ± 0.4	6.0 ± 0.1	−1.6 ± 0.2	15.150	0.043	4.8	1.17	0.68

He-sdB stars:

HE 0001−2443	39.7 ± 2.0	5.9 ± 0.2	+2.00 ± 0.5	-	-	-	-	-

continued on next page

continued from last page

HBB stars:

star	$T_{\rm eff}$ 1 000K	$\log(g)$ (cgs)	$\log(n_{\rm He}/n_{\rm H})$	V mag	E(B-V) mag	M_V mag	d kpc	$\|z\|$ kpc
HE 2134−4119	18.2 ± 0.5	4.4 ± 0.1	-1.7 ± 0.2	-	-	-	-	-
HE 2137−4221	18.5 ± 0.5	4.5 ± 0.1	-2.1 ± 0.2	-	-	-	-	-
HE 2204−2136	11.9 ± 0.3	3.7 ± 0.1	-1.5 ± 0.2	-	-	-	-	-
HE 0023−2317	14.1 ± 0.4	4.0 ± 0.2	-2.1 ± 0.2	-	-	-	-	-
HE 0128−4311	18.9 ± 0.5	4.6 ± 0.1	-2.0 ± 0.2	-	-	-	-	-
HE 0225−4007	13.3 ± 0.4	3.9 ± 0.1	-1.7 ± 0.2	-	-	-	-	-
HE 0238−1912	17.9 ± 0.5	4.6 ± 0.1	-3.0 ± 0.3	-	-	-	-	-
HE 0255−1814	15.7 ± 0.4	4.1 ± 0.1	-1.7 ± 0.2	-	-	-	-	-
HE 0319−5105	19.7 ± 0.5	4.0 ± 0.1	-1.6 ± 0.5	-	-	-	-	-
HE 0407−2122	15.7 ± 0.4	4.2 ± 0.1	-1.8 ± 0.2	-	-	-	-	-
HE 0420−1806	12.6 ± 0.3	3.7 ± 0.1	-2.0 ± 0.2	-	-	-	-	-
HE 0430−5341	14.6 ± 0.4	4.0 ± 0.1	-1.7 ± 0.2	-	-	-	-	-
HE 0519−3512	18.3 ± 0.5	4.9 ± 0.1	-1.7 ± 0.2	-	-	-	-	-

B stars:

HE 2203−3740	14.6 ± 0.4	4.0 ± 0.1	-0.7 ± 0.2	-	-	-	-	-
HE 2357−3940	15.9 ± 0.4	3.4 ± 0.2	-0.2 ± 0.3	-	-	-	-	-
HE 0437−5439	19.8 ± 0.5	3.6 ± 0.2	-0.9 ± 0.2	-	-	-	-	-
HE 0442−1908	14.2 ± 0.4	3.4 ± 0.1	-1.1 ± 0.2	-	-	-	-	-
HE 0528−5431	16.0 ± 0.4	3.8 ± 0.1	-0.9 ± 0.2	-	-	-	-	-

sdO stars:

HE 2151−2844	45.3 ± 1.1	6.1 ± 0.1	-1.7 ± 0.3	-	-	-	-	-
HE 2200−2154	54.5 ± 1.4	6.0 ± 0.1	-1.7 ± 0.2	-	-	-	-	-
HE 2210−1801	46.7 ± 1.2	6.2 ± 0.2	$+0.4 \pm 0.4$	-	-	-	-	-
HE 0019−2441	59.2 ± 1.5	5.8 ± 0.1	-1.0 ± 0.2	-	-	-	-	-
HE 0218−4447	44.5 ± 1.1	5.8 ± 0.1	-3.3 ± 0.2	-	-	-	-	-
HE 0222−3641	41.5 ± 1.0	6.0 ± 0.1	-1.7 ± 0.2	-	-	-	-	-

He-sd0 stars:

HE 2203−2210	47.6 ± 2.4	6.0 ± 0.2	$+0.4 \pm 0.4$	-	-	-	-	-
HE 2213−1734	46.7 ± 1.2	6.2 ± 0.2	$+0.4 \pm 0.4$	-	-	-	-	-
HE 2326−1022	45.7 ± 1.2	6.0 ± 0.2	$+0.5 \pm 0.4$	-	-	-	-	-
HE 0016−3212	42.4 ± 1.1	5.8 ± 0.2	$+1.5 \pm 0.2$	-	-	-	-	-
HE 0414−5429	46.3 ± 1.2	6.0 ± 0.2	$+3.5 \pm 0.5$	-	-	-	-	-
HE 0421−5415	45.3 ± 1.2	6.3 ± 0.2	$+0.8 \pm 0.4$	-	-	-	-	-
HE 0439−1826	46.2 ± 2.3	6.2 ± 0.1	$+0.7 \pm 0.2$	-	-	-	-	-
HE 0440−3211	46.9 ± 2.3	6.2 ± 0.1	$+0.5 \pm 0.2$	-	-	-	-	-
HE 0451−3706	43.2 ± 1.1	6.7 ± 0.2	$+1.5 \pm 0.4$	-	-	-	-	-

continued on next page

continued from last page

DA stars:

star	$T_{\rm eff}$ 1 000K	$\log(g)$ (cgs)	$\log(n_{\rm He}/n_{\rm H})$	V mag	E(B-V) mag	M_V mag	d kpc	$\|z\|$ kpc
HE 2151−3043	28.6 ± 0.7	8.3 ± 0.1	−6.0	-	-	-	-	-
HE 2350−2448	28.8 ± 0.7	8.3 ± 0.1	−6.0	-	-	-	-	-
HE 0308−2305	23.3 ± 0.6	8.5 ± 0.1	−6.0	-	-	-	-	-
HE 0343−4933	60.5 ± 1.5	7.9 ± 0.1	−6.0	-	-	-	-	-
HE 0511−2302	61.5 ± 1.5	7.9 ± 0.1	−6.0	-	-	-	-	-
post-AGB stars:								
HE 2159−1747	22.9 ± 0.6	3.33 ± 0.3	-1.4 ± 0.2	-	-	-	-	-

B.3 Bright sdB stars

Table B.3: Stellar parameters of our bright program stars.

name	$T_{\rm eff}$ (1 000 K)	$\log(g)$ (cgs)	$\log[n({\rm He})/n({\rm H}]$	spectrum	Ref.
PG 0001+275	25.4 ± 0.7	5.3 ± 0.1	-2.8 ± 0.2	low-res	here
HD 4539	23.0 ± 0.7	5.2 ± 0.1	-2.3 ± 0.2	low-res	here
PHL 932	34.6 ± 1.5	5.8 ± 0.2	-1.7 ± 0.2	high-res	here
PG 0133+114	29.6	5.7	−2.7	low-res	Mor03
PG 0342+026	25.3 ± 0.7	5.4 ± 0.1	-2.7 ± 0.2	low-res	here
UVO 0512−08	38.8 ± 1.0	5.5 ± 0.1	-0.8 ± 0.2	low-res	here
PG 0909+276	36.9 ± 0.9	5.9 ± 0.1	-0.8 ± 0.2	low-res	here
Feige 65	23.9 ± 0.7	5.3 ± 0.1	-2.7 ± 0.2	low-res	here
UVO 1735+22	40.5 ± 1.0	5.4 ± 0.1	-3.8 ± 0.2	low-res	here
UVO 1758+36	32.0 ± 0.8	5.8 ± 0.1	-1.6 ± 0.2	low-res	here
BD+48° 2721	20.7 ± 0.5	4.8 ± 0.1	-2.2 ± 0.2	low-res	here
HD 171858	27.7	5.3	−2.9	low-res	Mor03
HD 205805	25.6 ± 1.5	5.3 ± 0.2	-2.0 ± 0.2	high-res	here
LB 1516	26.1 ± 1.5	5.4 ± 0.2	-2.7 ± 0.2	high-res	here
PB 7352	23.4 ± 1.5	5.1 ± 0.2	-2.5 ± 0.2	high-res	here
CD−35° 15910	27.5 ± 1.5	5.3 ± 0.2	-3.0 ± 0.2	high-res	here

Ref.: Mor03 = Morales-Rueda et al. (2003)

Appendix C

Equivalent widths measurements

Table C.1: Metal line data and equivalent widths measured for all 'normal' program stars: 01 = PG 0001+275; 02 = HD 4539; 03 = PHL 932; 04 = PG 0133+114; 05 = PG 0342+026; 06 = Feige 65; 07 = UVO 1735+22; 08 = BD+48° 2721; 09 = HD 171858; 10 = HD 205805; 11 = LB 1516; 12 = PB 7352; 13 = CD−35° 15910

Ion	Ref.		W_λ/mA												
Mult.	λ/Å	$\log(gf)$	01	02	03	04	05	06	07	08	09	10	11	12	13
C II	Wie96														
53	6578.050	−0.026	-	83	-	-	25	-	-	8	-	102	-	-	-
53	6582.880	−0.340	-	72	-	-	21	-	-	6	-	93	-	-	-
61	3920.693	−0.232	-	58	-	-	-	22	-	9	-	82	-	-	-
74	4267.003	0.562	-	158	-	60	90	91	-	11	17	180	16	-	35
74	4267.258	−0.584	-	158	-	60	90	91	-	26	17	180	37	-	35
74	4267.261	0.717	-	158	-	60	90	91	-	26	17	180	37	-	35
99	6779.930	0.024	-	13	-	-	-	-	-	-	-	31	-	-	-
99	6783.900	0.304	-	-	-	-	-	-	-	-	-	47	-	-	-
99	6787.220	−0.378	-	26	-	-	-	-	-	-	-	13	-	-	-
99	6791.470	−0.271	-	10	-	-	-	-	-	-	-	15	-	-	-
100	5648.070	−0.424	-	9	-	-	-	-	-	-	-	15	-	-	-
100	5662.470	−0.249	-	14	-	-	5	6	-	-	-	23	-	-	-
101	5132.940	−0.211	-	16	-	-	-	-	-	-	-	29	-	-	-
101	5133.280	−0.178	-	14	-	-	-	5	-	-	-	29	-	-	-
101	5139.170	−0.740	-	4	-	-	-	-	-	-	-	11	-	-	-
101	5143.490	−0.212	-	16	-	-	-	6	-	-	-	30	-	-	-
101	5145.160	0.189	-	33	-	10	11	17	-	-	-	54	-	-	-
101	5151.090	−0.179	-	17	-	-	-	-	-	-	-	34	-	-	-
142	6098.510	0.226	-	-	-	9	5	-	-	-	-	26	-	-	-

continued on next page

continued from last page

Ion	Ref.		W_λ/mA												
Mult.	λ/Å	$\log(gf)$	01	02	03	04	05	06	07	08	09	10	11	12	13
C III	Wie96														
74	4647.420	0.070	-	12	-	-	-	-	-	4	-	29	-	-	-
74	4650.250	−0.152	-	-	-	-	-	-	-	-	-	23	-	-	-
74	4651.470	−0.629	-	-	-	-	-	-	-	-	-	10	-	-	-
193	4067.940	0.719	-	-	-	-	-	-	-	-	-	5	-	-	-
222	4056.062	0.265	-	-	-	-	-	-	-	-	-	2	-	-	-
N II	Wie96														
38	4035.080	0.600	-	34	-	-	-	47	-	-	21	41	-	-	-
38	4082.270	−0.410	-	-	-	9	-	-	-	-	-	18	-	-	-
39	4039.345	−0.890	-	-	-	-	-	-	-	-	-	5	-	-	-
39	4041.311	0.830	-	56	-	-	52	49	-	26	35	58	-	-	24
39	4043.529	0.710	-	28	-	-	-	-	-	-	-	40	-	-	7
39	4044.777	−0.460	-	-	-	-	-	-	-	-	-	8	-	-	-
39	4056.900	−0.460	-	17	-	-	-	6	-	-	-	11	-	-	-
43	4176.161	0.600	-	25	-	-	19	-	-	-	-	33	-	-	-
43	4171.607	0.280	-	16	-	-	10	20	-	8	-	19	-	-	11
48	4241.784	0.210	-	50	-	-	35	47	-	-	31	55	-	-	20
48	4241.784	0.730	-	50	-	-	35	47	-	-	31	55	-	-	20
48	4236.910	0.400	-	48	-	43	40	42	-	-	29	63	-	-	20
48	4237.050	0.570	-	48	-	43	40	42	-	-	29	63	-	-	20
49	4195.974	−0.290	-	6	-	-	-	-	-	-	-	9	-	-	-
49	4199.980	0.030	-	-	-	17	-	-	-	-	-	19	-	-	-
50	4173.572	−0.460	-	-	-	-	-	-	-	-	-	8	-	-	-
50	4179.674	−0.200	-	14	-	8	7	8	-	3	-	19	-	-	-
55	4427.236	−0.010	-	13	-	40	-	17	-	3	-	15	-	-	-
55	4427.964	−0.150	-	-	-	40	-	-	-	-	7	14	-	-	-
55	4432.735	0.600	-	28	-	27	30	24	-	-	16	38	-	-	-
55	4433.475	−0.030	-	9	-	8	9	12	-	-	6	15	-	-	-
57	4608.085	−0.250	-	-	-	-	-	-	-	-	-	9	-	-	-
57	4601.686	−0.710	-	-	-	-	-	-	-	-	-	4	-	-	-
58	4530.410	0.800	-	31	-	-	27	34	-	-	25	42	-	-	18
61	4694.637	0.100	-	19	-	11	11	18	-	4	-	22	-	-	-
67	4895.111	−1.338	-	-	-	-	-	-	-	-	-	12	-	-	-
73	5666.627	−0.045	28	52	-	43	42	44	-	16	32	68	-	47	31
73	5676.019	−0.368	-	33	-	28	29	30	-	10	20	51	-	-	-
73	5679.562	0.250	49	66	13	59	61	59	-	29	47	87	38	64	36
73	5686.213	−0.549	-	24	-	26	24	29	-	7	20	38	-	-	-
73	5710.766	−0.518	-	26	-	25	24	27	-	9	13	41	-	-	-
74	5002.703	−1.021	-	14	-	16	11	18	-	4	5	21	-	-	-
74	5010.620	−0.606	15	28	-	25	26	32	-	8	16	41	-	-	10
74	5045.100	−0.407	-	32	-	32	30	28	-	11	24	53	-	-	15
75	4601.480	−0.428	-	41	-	34	35	43	-	18	23	54	-	33	14
75	4607.157	−0.507	-	41	-	33	34	32	-	15	19	50	-	27	14

continued on next page

continued from last page

Ion	Ref.		W_λ/mA												
Mult.	λ/Å	$\log(gf)$	01	02	03	04	05	06	07	08	09	10	11	12	13
N II	Wie96														
75	4613.866	−0.665	-	30	-	26	27	25	-	8	10	39	-	21	8
75	4621.394	−0.514	-	32	-	29	28	27	-	8	16	50	14	-	15
75	4630.543	0.094	36	70	22	63	63	62	-	31	48	86	33	-	36
75	4643.085	−0.359	-	46	-	37	38	42	-	16	26	58	15	35	18
85	6482.053	−0.245	-	-	-	-	-	-	-	-	17	52	-	-	-
86	5747.296	−1.075	-	-	-	-	-	-	-	-	-	14	-	-	-
86	5767.440	−1.437	-	-	-	-	-	-	-	-	-	6	-	-	-
87	5073.590	−1.523	-	-	-	-	-	-	-	-	-	8	-	-	-
88	4654.532	−1.404	-	6	-	-	7	10	-	-	-	11	-	-	-
88	4667.206	−1.533	-	-	-	-	-	-	-	-	-	8	-	-	-
88	4674.909	−1.464	-	5	-	-	17	4	-	-	-	12	-	-	-
89	3994.988	0.208	43	70	-	57	65	-	-	47	10	94	46	-	53
104	4447.033	0.230	26	52	-	45	42	48	-	-	30	61	26	-	27
114	5001.136	0.263	68	41	-	93	43	52	-	15	79	58	13	87	68
114	5001.477	0.439	68	49	-	93	47	54	-	21	79	67	26	87	68
114	5005.149	0.592	37	56	24	60	58	63	-	26	40	73	34	-	45
114	5016.387	−0.515	-	14	-	7	13	-	-	-	7	20	-	-	13
114	5025.662	−0.546	-	9	-	13	11	12	-	-	-	16	-	-	-
116	4779.722	−0.587	-	14	-	11	12	8	-	-	6	15	-	-	-
116	4781.190	−1.307	-	-	-	-	-	-	-	-	-	5	-	-	-
116	4788.131	−0.363	-	23	-	16	15	14	-	-	8	27	-	-	-
116	4793.650	−1.095	-	-	-	-	-	-	-	-	-	7	-	-	-
116	4803.289	−0.113	-	24	-	23	23	28	-	8	15	36	-	-	-
116	4810.306	−1.084	-	-	-	-	-	-	-	-	-	8	-	-	-
117	4477.691	−1.098	-	-	-	-	-	-	-	-	-	8	-	-	-
117	4507.557	−0.817	-	7	-	-	-	-	-	-	-	13	-	-	-
127	4987.367	−0.555	-	11	-	14	6	-	-	-	-	14	-	-	-
127	4994.363	−0.069	-	23	-	25	25	22	-	6	21	34	-	-	10
127	5007.325	0.171	25	34	-	29	31	38	-	9	20	45	16	-	21
142	5927.811	−0.293	-	-	-	-	-	-	-	-	7	20	-	-	12
142	5931.779	0.052	-	-	-	24	-	-	-	-	16	25	-	-	19
142	5940.240	−0.445	-	-	-	15	-	-	-	-	7	10	-	-	-
142	5941.653	0.313	-	-	-	43	-	-	-	-	26	44	-	-	-
142	5952.388	−0.471	-	-	-	12	-	-	-	-	5	10	-	-	-
143	5452.083	−0.925	-	-	-	-	-	-	-	-	-	5	-	-	-
143	5462.592	−0.872	-	-	-	-	-	-	-	-	-	7	-	-	-
143	5478.096	−0.971	-	-	-	-	-	-	-	-	-	6	-	-	-
143	5480.062	−0.756	-	6	-	-	4	-	-	-	-	7	-	-	-
143	5495.666	−0.266	-	15	-	11	13	10	-	-	-	17	-	-	-
156	6610.565	0.464	-	20	-	-	21	28	-	-	19	29	-	-	-
159	4227.742	−0.060	-	20	-	20	26	24	-	6	8	31	-	-	11
175	6167.755	0.025	-	5	-	-	11	-	-	-	-	13	-	-	-
175	6170.166	−0.311	-	-	-	-	-	-	-	-	-	7	-	-	-

continued on next page

continued from last page

Ion	Ref.		W_λ/mA												
Mult.	λ/Å	$\log(gf)$	01	02	03	04	05	06	07	08	09	10	11	12	13
N II	Wie96														
175	6173.313	−0.126	-	-	-	-	-	-	-	-	-	12	-	-	-
194	6242.412	−0.052	-	-	-	-	-	-	-	-	-	10	-	-	-
233	5011.300	−0.181	-	-	-	-	-	-	-	-	-	4	-	-	-
233	5012.029	0.136	-	-	-	-	-	-	-	-	6	9	-	-	7
234	4133.672	−0.168	-	-	-	-	-	-	-	-	-	5	-	-	-
234	4145.776	−0.023	-	-	-	-	-	-	-	-	-	6	-	-	-
N III	Wie96														
102	4634.140	−0.087	-	-	23	-	-	-	-	-	-	6	-	-	-
102	4640.640	0.168	-	-	37	-	-	-	-	-	-	9	-	-	-
O II	Wie96														
64	4638.855	−0.332	-	6	-	17	11	14	-	4	20	18	15	-	13
64	4641.810	0.054	-	6	-	26	23	27	-	9	39	18	39	-	32
64	4649.135	0.308	-	8	-	39	29	34	-	12	52	28	42	-	40
64	4650.839	−0.361	-	3	-	13	9	-	-	4	18	6	-	-	14
64	4661.633	−0.278	-	-	-	13	12	-	-	-	22	7	-	-	15
64	4676.235	−0.395	-	-	-	15	-	-	-	-	19	8	-	-	-
65	4319.628	−0.380	-	-	-	-	-	-	-	-	12	5	-	-	18
65	4366.888	−0.348	-	-	-	12	-	-	-	-	16	6	-	-	-
67	4275.551	0.760	-	-	-	-	-	-	-	-	10	4	-	-	-
72	4414.901	0.172	-	8	-	27	28	30	-	9	30	15	51	-	28
72	4452.374	−0.789	-	-	-	-	-	-	-	-	8	4	-	-	-
73	3954.362	−0.396	-	-	-	-	-	-	-	-	20	11	-	-	-
90	4069.623	0.150	-	-	-	-	-	-	-	-	47	9	-	-	40
90	4069.886	0.344	-	-	-	16	-	-	-	-	47	9	-	-	40
90	4072.157	0.552	-	10	-	-	24	27	-	12	31	15	-	-	35
90	4075.862	0.692	-	-	-	-	-	-	-	-	43	49	-	-	20
93	4602.128	0.560	-	-	-	-	6	-	-	-	6	-	-	-	-
99	4590.972	0.350	-	4	-	20	11	17	-	5	24	8	29	-	9
99	4596.176	0.200	-	2	-	17	12	10	-	-	21	6	11	-	14
101	4253.895	0.920	-	-	-	-	10	-	-	-	-	-	-	-	-
107	4132.800	−0.065	-	-	-	-	-	-	-	-	8	5	-	-	-
107	4153.298	0.053	-	4	-	15	9	-	-	-	17	10	-	-	10
108	4119.215	0.451	-	-	-	23	-	-	-	-	19	9	-	-	20
109	4112.022	−0.561	-	-	-	-	-	-	-	-	7	-	-	-	-
118	4699.220	0.270	-	-	-	18	-	-	-	-	-	4	-	-	14
118	4705.350	0.476	-	-	-	16	11	15	-	-	20	10	-	-	17
130	4906.833	−0.160	-	-	-	-	-	-	-	-	10	-	-	-	-
130	4924.531	0.074	-	-	-	-	-	-	-	-	14	-	-	-	-
148	4941.069	−0.054	-	-	-	-	-	-	-	-	5	-	-	-	-
148	4942.999	0.239	-	-	-	12	-	-	-	-	14	4	-	-	13
160	4448.186	0.083	-	-	-	-	-	-	-	-	6	-	-	-	-
161	4185.449	0.604	-	-	-	-	-	-	-	-	13	-	-	-	10

continued on next page

continued from last page

Ion	Ref.		W_λ/mA												
Mult.	λ/Å	log(gf)	01	02	03	04	05	06	07	08	09	10	11	12	13
O II	Wie96														
161	4189.789	0.716	-	-	-	-	-	-	-	-	15	9	-	-	-
172	4703.163	0.262	-	-	-	-	6	-	-	-	4	-	-	-	-
Mg II	Hir95														
4	4481.129	−0.560	34	50	-	44	60	61	-	94	73	52	60	34	39
4	4481.130	0.740	34	50	-	44	60	61	-	94	73	52	60	34	39
4	4481.327	0.590	34	50	-	44	60	61	-	94	73	52	60	34	39
Al III	Hir95														
2	5696.603	0.235	-	15	-	-	12	11	-	20	17	27	-	-	-
2	5722.728	−0.069	-	11	-	8	6	14	-	24	11	11	-	-	-
3	4512.564	0.410	-	10	-	12	6	-	-	-	7	14	-	-	-
3	4528.942	−0.290	-	18	-	14	15	22	-	7	11	20	-	-	-
3	4529.194	0.660	-	18	-	14	15	22	-	7	11	20	-	-	-
8	4479.892	0.900	-	-	-	17	-	-	-	-	-	13	-	-	-
8	4479.973	1.020	-	-	-	17	-	-	-	-	-	13	-	-	-
8	4480.011	−0.530	-	-	-	17	-	-	-	-	-	13	-	-	-
Si II	Hir95														
3	4128.067	0.380	-	-	-	-	-	-	-	20	-	6	-	-	-
3	4130.873	−0.770	-	-	-	-	-	-	-	24	-	8	-	-	-
5	5055.981	0.510	-	-	-	-	-	10	-	11	-	-	-	-	-
Si III	Hir95														
2	4552.616	0.290	41	59	-	125	75	77	-	51	62	83	62	67	55
2	4567.823	0.070	36	41	-	103	53	52	-	35	50	60	39	52	38
2	4574.759	−0.406	12	22	-	75	31	29	-	13	24	34	36	-	22
4	5739.734	−0.110	-	-	-	87	-	-	-	-	-	-	-	-	-
9	4813.330	0.850	-	7	-	-	-	15	-	5	-	7	-	-	-
9	4819.718	0.750	-	8	-	-	14	12	-	-	-	17	-	-	-
9	4828.968	1.090	-	18	-	-	-	18	-	-	-	9	-	-	-
Si IV	Hir95														
1	4088.854	0.195	-	-	-	-	-	-	-	-	11	7	-	-	16
P III	Hir95														
1	4059.312	−0.050	-	-	-	-	-	-	-	-	-	5	-	-	-
S II	Hir95														
6	5428.667	−0.130	-	-	-	-	5	-	-	5	-	7	-	-	-
6	5432.815	0.260	-	13	-	7	13	14	-	8	-	13	-	-	-
6	5453.828	0.480	-	23	-	19	14	12	-	10	-	-	-	-	-
6	5473.620	−0.180	-	7	-	-	3	6	-	4	-	5	-	-	-
6	5509.718	−0.140	-	8	-	-	-	3	-	5	-	5	-	-	-
7	5009.564	−0.280	-	7	-	-	8	-	-	-	-	3	-	-	-
7	5032.447	0.270	-	15	-	17	12	12	-	10	-	10	-	-	-
8	4716.267	−0.410	-	4	-	-	-	8	-	-	-	4	-	-	-
9	4815.549	0.090	-	14	-	9	8	13	-	6	-	7	-	-	-

continued on next page

continued from last page

Ion	Ref.		W_λ/mA												
Mult.	λ/Å	log(gf)	01	02	03	04	05	06	07	08	09	10	11	12	13
S II	Hir95														
11	5606.151	0.310	-	10	-	-	6	6	-	3	-	7	-	-	-
11	5659.985	−0.050	-	7	-	-	5	-	-	-	-	-	-	-	-
14	5639.972	0.280	-	26	-	39	21	21	-	9	16	25	31	-	11
14	5647.033	0.040	-	17	-	25	15	19	-	5	12	20	17	-	8
15	4917.212	−0.320	-	-	-	14	-	-	-	-	-	10	-	-	-
15	5014.069	0.100	-	21	-	23	15	10	-	9	8	18	-	-	-
38	5320.732	0.490	-	12	-	-	11	-	-	7	-	-	-	-	-
38	5345.721	0.350	-	8	-	-	5	-	-	8	-	4	-	-	-
39	5212.620	0.320	-	9	-	-	6	-	-	3	-	4	-	-	-
39	5212.623	−0.620	-	9	-	-	6	-	-	3	-	4	-	-	-
40	4524.947	0.170	-	7	-	-	8	-	-	-	-	4	-	-	-
44	4153.064	0.620	-	16	-	-	9	-	-	11	-	11	-	-	-
44	4162.665	0.780	-	17	-	-	15	14	-	14	-	14	-	-	-
49	4294.398	0.560	-	8	-	-	6	-	-	5	-	6	-	-	-
55	3923.460	0.440	-	-	-	-	-	-	-	-	-	6	-	-	-
S III	Hir95														
4	4253.593	0.360	-	25	39	42	24	27	-	9	20	34	-	-	22
4	4284.991	0.090	-	11	30	24	20	26	-	6	8	24	-	-	15
4	4361.527	−0.350	-	-	13	-	-	-	-	-	4	-	-	-	-
7	4364.730	−0.710	-	4	8	-	-	-	-	-	2	6	-	-	-
Ar II	Hir95														
1	4400.986	−0.330	-	13	-	-	5	12	-	10	-	6	-	-	-
6	4735.906	−0.120	-	13	-	7	9	11	-	12	-	9	-	-	-
6	4806.021	0.210	-	22	-	13	16	17	-	18	-	18	-	-	-
6	5009.334	−0.460	-	6	-	-	2	-	-	7	-	-	-	-	-
7	4331.200	−0.220	-	-	-	-	-	-	-	-	-	8	-	-	-
7	4426.001	0.170	-	24	-	13	14	13	-	18	-	16	-	-	-
7	4430.189	−0.170	-	11	-	6	-	4	-	13	-	8	-	-	-
15	4657.901	−0.280	-	8	-	-	-	10	-	6	-	4	-	-	-
15	4764.865	−0.110	-	-	-	-	-	-	-	-	-	6	-	-	-
17	4579.349	−0.300	-	8	-	-	-	-	-	6	-	4	-	-	-
31	4589.898	0.080	-	11	-	-	-	-	-	-	-	6	-	-	-
31	4609.567	0.290	-	14	-	-	-	17	-	12	-	10	-	-	-
32	4277.528	0.000	-	-	-	-	-	-	-	-	-	4	-	-	-
39	4481.811	−0.050	-	-	-	-	-	-	-	-	-	4	-	-	-
Ar III	Hir95														
4	4361.530	−0.390	-	-	-	13	-	-	-	-	-	9	-	-	-

continued on next page

continued from last page

Ion	Ref.		W_λ/mA												
Mult.	λ/Å	$\log(gf)$	01	02	03	04	05	06	07	08	09	10	11	12	13
Fe III	Ekb93,Kur92														
4	4382.502	−3.092	-	-	-	-	-	-	-	-	7	4	-	7	-
4	4395.751	−2.703	-	-	-	8	10	26	-	-	15	14	23	-	-
4	4419.599	−2.335	-	19	-	9	19	20	-	7	24	22	22	-	23
4	4431.001	−2.710	-	-	-	12	16	10	-	6	13	11	-	-	14
5	5063.459	−3.139	-	-	-	-	-	-	-	-	-	3	-	-	6
5	5073.896	−2.741	-	7	-	-	14	11	-	-	12	12	-	-	11
5	5086.718	−2.767	-	11	-	6	8	9	-	-	12	10	8	-	14
5	5127.352	−2.404	28	18	-	15	10	6	-	-	40	17	14	59	34
5	5156.111	−2.018	33	-	-	13	22	19	-	-	34	23	20	38	27
5	5193.883	−3.084	-	-	-	-	-	14	-	-	-	6	-	-	22
45	4005.022	−1.755	-	-	-	-	-	-	-	-	-	10	-	-	13
53	4025.000	−2.454	-	-	-	-	-	-	-	-	-	5	-	-	-
68	5460.808	−1.741	-	-	-	-	-	-	-	-	-	5	-	-	8
68	5573.464	−1.613	-	-	-	-	8	-	-	-	-	6	-	-	-
113	5235.658	−0.107	27	-	-	-	-	9	-	-	15	-	-	-	16
113	5243.306	0.405	24	-	-	20	24	20	-	-	32	22	21	-	34
113	5272.369	−0.421	-	-	-	-	-	-	-	-	-	6	-	-	9
113	5276.476	−0.001	-	-	-	8	-	-	-	-	-	11	-	-	-
113	5282.297	0.108	-	-	-	10	-	-	-	-	-	13	-	-	-
113	5299.926	−0.166	-	-	-	6	7	11	-	-	12	11	-	18	10
113	5302.602	−0.120	-	-	-	7	-	-	-	-	-	10	15	-	12
113	5306.757	−0.341	-	-	-	7	7	-	-	-	9	7	-	-	11
114	5833.938	0.616	30	-	-	20	25	-	-	-	32	20	-	-	38
114	5929.685	0.351	-	-	-	10	-	-	-	-	30	13	-	-	25
117	5999.543	0.355	-	-	-	-	-	-	-	-	-	11	-	-	21
117	6032.604	0.497	-	-	-	-	-	16	-	-	-	9	-	-	-
118	4137.764	0.630	-	-	-	12	-	-	-	-	-	-	-	-	-
118	4139.350	0.520	-	-	-	9	17	5	-	-	21	14	-	-	21
118	4164.731	0.923	28	-	-	27	45	35	-	-	-	27	-	-	50
118	4166.840	0.409	-	-	-	-	13	14	-	12	15	12	-	-	19
118	4168.449	−0.323	-	-	-	-	-	-	-	-	5	6	-	-	-
119	4053.112	0.261	-	-	-	-	-	-	-	-	-	8	-	-	15
121	4286.091	−0.512	-	-	-	-	-	-	-	-	-	9	-	-	-
121	4286.164	0.705	-	-	-	-	-	-	-	-	-	9	-	-	-
121	4304.767	1.027	-	-	-	-	-	-	-	-	-	11	-	-	-
-	4154.963	0.891	-	-	-	-	-	-	-	-	-	4	-	-	-
-	4174.260	1.113	-	-	-	10	17	15	-	-	14	10	-	-	16
-	4222.271	0.272	-	-	-	-	-	-	-	-	13	15	12	-	-
-	5272.975	0.598	-	-	-	-	-	-	-	-	-	4	-	-	11
-	5363.764	−0.127	-	-	-	-	-	-	-	-	7	5	-	-	-
-	5363.764	0.286	-	-	-	-	-	-	-	-	7	5	-	-	-
-	5854.622	0.801	-	-	-	-	-	-	-	-	17	5	-	-	14
-	6036.549	0.790	-	-	-	-	-	-	-	-	10	8	-	-	-
-	6048.708	0.659	-	-	-	-	-	-	-	-	10	5	-	-	-

Table C.2: Metal line data and equivalent widths measured of the peculiar program stars: 01 = PG 0909+276, and 02 = UVO 0512−08.

Ion	Ref.		W_λ/mA	
Mult.	λ/Å	$\log(gf)$	01	02
C II	Wie96			
53	6582.880	−0.340	14	17
74	4267.003	−0.562	10	26
74	4267.258	−0.584	143	94
93	5125.200	−0.597	24	6
99	6783.900	−0.304	30	12
100	5662.470	−0.249	16	10
101	5143.490	−0.212	12	10
101	5145.160	−0.189	31	20
101	5151.090	−0.179	28	14
132	6731.070	−0.861	11	14
142	6095.290	−0.029	24	9
142	6098.510	−0.226	35	18
C III	Wie96			
74	4647.420	−0.070	158	147
74	4650.250	−0.152	126	122
74	4651.470	−0.629	95	85
88	5695.920	−0.016	79	88
136	6727.390	−0.644	22	13
136	6744.380	−0.021	18	28
137	5272.530	−0.487	22	22
138	4659.060	−0.654	20	29
138	4663.640	−0.530	21	20
138	4665.860	−0.044	41	43
138	4673.950	−0.434	39	25
150	4325.560	−0.759	33	21
168	4515.780	−0.280	21	24
186	5353.120	−0.674	22	5
192	4257.894	−0.267	8	15
193	4067.940	−0.719	48	58
193	4068.912	−0.837	88	93
193	4070.261	−0.340	64	87
193	4070.261	−2.157	64	87
198	6205.560	−3.227	13	22
200	4121.843	−0.036	21	-
207	4186.900	−0.918	71	84
215	4156.490	−0.058	8	39
215	4156.760	−0.844	35	11
215	4162.860	−0.218	52	56
215	4163.260	−0.844	5	-
219	5826.420	−0.416	29	38
220	5249.110	−0.316	7	20
222	4056.062	−0.265	38	51

Ion	Ref.		W_λ/mA	
Mult.	λ/Å	$\log(gf)$	01	02
C IV	Wie96			
29	5801.330	−0.194	27	30
29	5811.980	−0.495	-	13
N II	Wie96			
73	5666.627	−0.045	8	6
73	5679.562	−0.250	9	10
73	5710.766	−0.518	-	9
74	5045.100	−0.407	16	5
75	4630.543	−0.094	12	20
89	3994.988	−0.208	38	11
114	5001.136	−0.263	14	4
114	5001.477	−0.439	16	15
114	5005.149	−0.592	25	12
N III	Wie96			
102	4640.640	−0.168	34	-
128	4518.150	−0.461	18	20
139	4200.100	−0.250	35	27
175	4544.850	−0.152	10	20
Si IV	Hir95			
1	4088.854	−0.195	22	20
1	4116.104	−0.110	12	-
5	4950.111	−0.370	26	18
5	4950.111	−0.530	26	18
5	4950.111	−0.670	26	18
P II	Hir95			
10	5253.479	−0.280	11	-
S II	Hir95			
7	4991.974	−0.650	28	39
11	5640.333	−0.400	8	-
14	5639.972	−0.280	7	-
S III	Hir95			
4	4253.593	−0.360	74	72
4	4284.991	−0.090	59	49
4	4332.692	−0.240	24	18
4	4361.527	−0.350	35	26
4	4418.836	−0.520	13	10
7	4354.560	−0.610	29	18
7	4364.730	−0.710	37	16
7	4439.844	−0.520	28	20
7	4467.756	−0.060	6	13
7	4478.480	−0.620	7	-
7	4499.245	−0.480	9	-

continued on next page

continued from last page

Ion Mult.	Ref. λ/Å	$\log(gf)$	W_λ/mA 01	02
S III	Hir95			
8	3961.559	−0.810	76	-
8	3983.770	−0.440	36	29
8	3985.970	−0.790	24	16
10	4677.657	−0.760	27	14
Ar II	Hir95			
6	4735.906	−0.120	3	-
6	4806.021	−0.210	11	-
7	4426.001	−0.170	7	5
14	4879.864	−0.220	5	-
-	5036.229	−0.760	20	-
Ar III	Hir95			
-	4891.960	−0.220	11	-
-	4895.740	−2.640	4	-
-	5238.180	−4.570	9	6
-	6693.380	−0.690	9	-
Ca III	Hir95			
-	4184.200	−0.045	4	10
-	4233.713	−0.092	20	34
-	4233.736	−0.717	20	34
-	4240.742	−0.637	26	38
-	4271.891	−0.512	10	29
-	4279.722	−0.545	8	19
-	4284.388	−0.645	18	26
-	4296.004	−0.578	21	17
-	4302.803	−0.587	19	31
-	4399.584	−0.404	11	16
-	4406.285	−0.335	10	26
-	4431.290	−0.273	7	-
-	4499.885	−0.472	12	20
-	4516.586	−0.287	35	36
-	4572.125	−0.389	20	24
-	5231.814	−0.501	5	14
-	5270.309	−0.702	3	19
-	5321.287	−0.594	5	14
-	5328.057	−0.454	11	12
Sc III	Hir95			
-	4061.210	−0.296	18	15
-	4309.493	−0.971	21	18
-	4309.493	−0.573	21	18
-	5032.072	−0.635	30	14

Ion Mult.	Ref. λ/Å	$\log(gf)$	W_λ/mA 01	02
Ti II	Hir95			
-	3915.266	−0.057	-	25
-	3915.471	−0.415	-	14
-	4119.146	−0.387	6	12
-	4191.088	−0.060	15	18
-	4213.247	−0.850	15	18
-	4215.525	−0.917	40	26
-	4247.143	−0.702	12	16
-	4248.542	−0.715	6	13
-	4258.460	−0.792	9	5
-	4261.891	−0.579	14	15
-	4262.434	−0.179	4	4
-	4269.833	−0.823	24	13
-	4281.555	−0.128	13	4
-	4284.083	−0.604	20	12
-	4285.610	1.163	36	33
-	4286.504	−0.339	6	14
-	4288.672	−0.982	20	15
-	4295.432	−0.613	22	25
-	4296.693	1.040	28	28
-	4348.035	−0.787	17	6
-	4378.074	−0.867	3	7
-	4411.127	−0.471	35	17
-	4424.402	−0.609	11	7
-	4433.923	−0.978	26	17
-	4480.359	−0.184	4	10
-	4555.445	−0.074	10	6
-	4581.731	−0.077	14	14
-	4586.104	−3.684	5	22
-	4609.507	−0.328	14	30
-	4610.478	−0.008	5	8
-	4634.167	−0.120	25	23
-	4649.456	−0.366	12	8
-	4652.856	−0.829	27	21
-	4767.357	−2.334	9	29
-	4791.031	−0.028	5	10
-	4873.995	−0.587	12	11
-	4900.038	−0.397	16	-
-	4914.312	−0.017	6	5
-	4932.675	−0.260	8	6
-	4971.194	−0.976	29	24

continued on next page

continued from last page

Ion Mult.	Ref. λ/Å	log(gf)	W_λ/mA 01	02
Ti II	Hir95			
-	5020.425	−0.527	10	-
-	5083.801	−0.078	7	10
-	5147.313	−0.006	11	12
-	5157.167	−0.097	35	20
-	5247.489	−0.040	12	22
-	5278.120	−0.414	31	19
-	5301.213	−0.112	28	30
-	5306.889	−0.023	21	13
-	5533.012	−0.205	8	6
-	5566.581	−0.895	10	-
-	6667.996	−0.312	25	6
-	6862.278	−0.118	10	10
Ti III	Hir95			
1	5398.930	−0.161	59	62
1	5492.512	−0.148	53	52
3	4397.312	−0.116	22	35
3	4403.430	−0.272	20	29
4	4618.043	−0.277	33	80
4	4618.171	−0.366	33	80
-	5517.740	−0.303	5	14
-	5877.774	−0.552	5	14
-	5885.965	−2.882	16	32
-	6246.659	−0.355	-	23
V III	Hir95			
-	4204.942	−0.227	-	12
-	4497.733	−0.214	-	21
-	4508.853	−0.885	-	26
-	4534.882	−3.264	-	18
-	4763.693	−3.007	-	20
-	5133.392	−0.134	-	6
-	6404.884	−3.025	-	6
-	6449.331	−2.581	-	10
-	6712.747	−3.805	-	17
-	4304.420	−2.485	-	5
-	4762.910	−1.544	-	7
-	4845.087	−4.159	-	32
-	4878.400	−1.198	-	6
-	4887.024	−2.197	-	11
-	4906.292	−0.271	-	9
-	4985.643	−0.468	-	19

Ion Mult.	Ref. λ/Å	log(gf)	W_λ/mA 01	02
V III	Hir95			
-	5146.518	−0.392	-	16
-	5173.337	−1.664	-	20
-	5227.822	−0.227	-	6
-	5262.192	−0.024	-	13
-	5310.777	−0.183	-	6
-	5352.232	−0.404	-	13
-	5353.120	−0.007	-	5
-	5439.214	−0.552	-	7
-	5509.204	−0.063	-	7
Mn III	Hir95			
-	4431.303	−1.981	-	14
-	4916.223	−3.090	15	28
-	5175.951	−0.679	34	20
-	5189.401	−0.962	6	6
-	5365.612	−0.257	4	11
-	5869.230	−2.619	19	16
Ni III	Hir95			
-	4486.522	−3.955	7	6
-	4608.028	−2.735	9	18
-	4964.627	−2.320	31	45
-	5095.802	−0.973	13	19
-	5137.803	−0.960	4	11
-	5213.720	−0.665	3	8
-	5225.260	−2.920	22	28
-	5332.140	−0.743	17	-
-	5428.636	−2.001	12	-
-	5430.174	−0.330	18	-
-	5436.847	−0.485	8	-
-	5474.420	−3.211	10	9
-	5482.300	−0.638	17	5
-	5487.940	−0.101	10	-
-	5524.118	−0.169	14	-
-	5569.716	−0.596	8	-
-	5582.710	−0.408	16	6
-	5659.902	−0.198	36	20
-	6660.053	−3.210	10	12

Appendix D

Radial velocity measurements

Table D.1: Observing log, time of mid-exposure barycentric Julian dates (BJD_{mid}) and radial velocity measurements for all bright programme stars.

star	date y/m/d	start UT	dur. [s]	BJD_{mid} −2,450,000	v_{rad} [km/s]
SB 7	2002/08/18	02:37	3000	2505.63159	-4 ± 2
	2002/08/19	02:25	3000	2506.62295	-6 ± 3
PG 0011+283	1999/07/22	01:11	1800	1381.5605	$+1 \pm 2$
	1999/07/22	01:51	1800	1381.5879	$+1 \pm 2$
	1999/07/22	02:30	1800	1381.6151	$+1 \pm 2$
	2002/08/15	03:59	2400	2502.68352	$+2 \pm 2$
	2002/08/16	02:35	1031	2503.61715	$+5 \pm 4$
	2002/08/21	04:19	1800	2508.69396	-2 ± 2
CD−38° 222	2002/08/09	03:39	900	2495.66123	-35 ± 3
	2002/08/09	04:44	1200	2495.70811	-34 ± 3
	2002/08/11	10:39	800	2497.95176	$? \pm ?$
HD 4539	1998/09/11	01:29	1800	1067.57775	-4 ± 2
	1998/09/11	02:05	1800	1067.60228	-4 ± 2
	1998/09/11	02:40	1800	1067.62685	-4 ± 2
	2002/08/09	05:08	1200	2495.72384	-4 ± 3
	2002/08/09	06:58	900	2495.79854	-2 ± 3
PHL 6783	2002/08/14	04:28	1212	2501.69695	-7 ± 3
	2002/08/17	02:38	1500	2504.62235	-1 ± 2
	2002/08/18	03:31	1500	2505.65984	-12 ± 2
	2002/08/21	03:51	1500	2508.67355	-11 ± 2
	2002/11/26	22:45	1500	2604.45994	$+22 \pm 2$
SB 395	2002/08/16	02:56	2700	2503.64179	$+22 \pm 4$
	2002/11/26	21:56	2700	2604.43238	$+20 \pm 4$

continued on next page

continued from previous page

star	date y/m/d	start UT	dur. [s]	BJD_{mid} −2,450,000	v_{rad} [km/s]
PHL 932	1999/07/21	03:14	1800	1380.6445	$+18 \pm 2$
	1999/07/22	03:10	2000	1381.6439	$+18 \pm 2$
	1999/07/24	02:52	1800	1383.6305	$+18 \pm 2$
	1999/07/24	03:28	1800	1383.6557	$+18 \pm 2$
	2002/08/19	03:18	2700	2506.65645	$+17 \pm 2$
Feige 11	2000/01/30	18:22	1800	1574.2729	-23 ± 3
	2000/01/30	18:53	1800	1574.2946	-58 ± 3
	2000/01/30	19:26	1800	1574.3171	-75 ± 3
PG 0116+242	2002/08/14	02:53	1800	2501.63265	-104 ± 2
	2002/08/18	03:59	1800	2505.67882	-105 ± 2
	2002/08/19	04:04	1800	2506.68298	-104 ± 2
CD−24° 731	2000/09/08	08:23	1800	1795.86376	$+68 \pm 5$
	2000/09/08	08:58	1800	1795.88786	$+70 \pm 5$
	2002/08/11	09:53	2400	2497.92858	$? \pm 3$
PG 0342+026	1998/09/11	03:29	1800	1067.65786	$+14 \pm 2$
	1998/09/11	04:04	1800	1067.68250	$+14 \pm 2$
	1998/09/11	04:40	1800	1067.70699	$+14 \pm 2$
	2000/01/30	20:47	1800	1574.3779	$+14 \pm 2$
	2000/01/30	21:05	1800	1574.3995	$+14 \pm 2$
	2000/01/30	21:50	1800	1574.4212	$+14 \pm 2$
	2002/08/17	04:18	1200	2504.68615	$+12 \pm 2$
UVO 0512−08	2000/01/31	22:13	3600	1575.4487	$+11 \pm 2$
	2000/02/01	21:15	3600	1576.4081	$+11 \pm 2$
	2000/02/01	22:18	3600	1576.4523	$+11 \pm 2$
	2002/11/27	00:22	1500	2604.5289	$+10 \pm 2$
PG 0909+276	2000/01/29	23:44	1800	1573.5043	$+20 \pm 2$
	2000/01/30	00:15	1800	1573.5265	$+20 \pm 2$
	2000/01/30	00:48	1800	1573.5489	$+20 \pm 2$
	2000/02/02	01:55	1800	1576.5952	$+19 \pm 2$
	2000/02/02	02:27	1800	1576.6181	$+19 \pm 2$
PG 1047+003	2000/01/30	01:26	3600	1573.5844	-10 ± 3
	2000/01/30	02:30	3600	1573.6282	-10 ± 3
	2000/01/31	02:26	3600	1574.6265	-10 ± 3
Feige 65	2000/01/30	05:46	2400	1573.7574	$+54 \pm 2$
	2000/01/31	05:37	1700	1574.7473	$+53 \pm 2$
Feige 86	2000/01/29	03:52	1800	1572.6736	-28 ± 2
	2000/01/29	04:33	1800	1572.7019	-28 ± 2
PG 1336−018	2000/01/30	04:43	3600	1573.7183	$+38 \pm 5$
	2000/01/31	04:33	3600	1574.7117	$+38 \pm 5$
	2000/02/02	05:20	2700	1576.7395	$+38 \pm 5$

continued on next page

continued from previous page

star	date y/m/d	start UT	dur. [s]	BJD_{mid} −2,450,000	v_{rad} [km/s]
	2002/08/19	19:37	3000	2506.33325	-4 ± 3
PG 1505+074	2002/08/20	19:39	3000	2507.33509	-1 ± 2
	2002/08/21	20:50	3000	2508.38373	$+2 \pm 5$
	2002/08/16	20:44	2400	2503.37661	$+33 \pm 2$
	2002/08/18	19:46	2700	2505.33796	-2 ± 2
PG 1519+640	2002/08/18	23:14	2700	2505.48244	$+39 \pm 2$
	2002/08/19	20:29	2700	2506.36772	-26 ± 2
	2002/08/20	20:33	2700	2507.37015	-38 ± 2
PG 1524+611	2002/08/17	19:41	2100	2504.33114	-8 ± 4
	2002/08/18	00:02	2100	2505.51226	-8 ± 3
	2002/08/17	20:19	1200	2504.35281	-21 ± 5
PG 1530+212	2002/08/20	21:42	1200	2507.41046	-17 ± 5
	2002/08/21	21:42	1200	2508.41012	-25 ± 5
	2002/08/16	22:53	1200	2503.46049	$+25 \pm 2$
PG 1607+174	2002/08/17	20:41	1200	2504.36924	$+24 \pm 4$
	2002/08/19	21:18	1200	2506.39475	$+22 \pm 2$
	2002/08/07	23:56	1200	2494.50657	-179 ± 2
LS IV−12 1	2002/08/10	00:02	1200	2496.51013	-178 ± 2
	2002/08/10	01:21	1020	2496.56375	-180 ± 2
	2002/08/10	23:40	600	2497.49150	$+25 \pm 3$
HD 149382	2002/08/11	00:12	600	2497.51327	$+24 \pm 3$
	2002/08/11	01:27	600	2497.56524	$+24 \pm 3$
	2002/08/15	20:47	900	2502.37276	$+22 \pm 2$
	2002/08/15	21:48	1800	2502.42013	-197 ± 2
PG 1654+138	2002/08/17	22:03	2100	2504.43242	-192 ± 2
	2002/08/21	22:05	1800	2508.43159	-194 ± 2
	2002/08/19	22:12	2700	2506.44094	-159 ± 2
PG 1705+537	2002/08/20	22:06	3000	2507.43806	-157 ± 2
	2002/08/21	22:37	3000	2508.45995	-156 ± 2
	2002/08/14	21:27	3000	2501.41149	-58 ± 2
PG 1710+490	2002/08/18	00:43	2700	2505.54589	-52 ± 2
	2002/08/20	23:17	3600	2507.49121	-53 ± 2
	1998/09/12	18:59	1800	1069.30655	-31 ± 2
UVO 1758+36	1998/09/12	19:34	1800	1069.33125	-31 ± 2
	1998/09/12	20:11	1800	1069.35615	-31 ± 2
	2002/08/14	19:56	1800	2501.34259	-31 ± 2
	1998/09/09	20:39	1800	1066.37151	-188 ± 2
BD+48° 2721	1998/09/09	21:10	1800	1066.39346	-188 ± 2
	2002/08/14	20:29	1800	2501.36540	-188 ± 2
PHL 25	2002/08/19	23:27	2100	2506.49494	$+71 \pm 2$
	2002/08/20	00:24	2100	2507.53455	$+72 \pm 2$

continued on next page

continued from previous page

star	date y/m/d	start UT	dur. [s]	$\mathrm{BJD_{mid}}$ −2,450,000	v_{rad} [km/s]
HD 205805	2000/09/08	01:00	1800	1795.55600	-69 ± 2
	2000/09/08	01:34	1800	1795.57930	-69 ± 2
	2000/09/09	02:40	1800	1796.62537	-76 ± 10
	2002/08/09	05:54	720	2495.75481	-70 ± 2
PG 2151+100	2002/08/15	23:09	3600	2502.49111	-31 ± 2
	2002/08/17	23:54	3600	2504.52243	-25 ± 5
	2002/08/18	01:32	3600	2505.59009	-20 ± 2
	2002/08/21	00:02	2958	2508.52429	$+1 \pm 3$
	2002/11/26	17:50	3600	2604.26367	-25 ± 2
PG 2159+051	2002/08/15	00:12	1800	2502.52426	-1 ± 8
	2002/08/20	02:21	2400	2507.61750	$+7 \pm 3$
	2002/08/21	01:35	2400	2508.58551	$+8 \pm 3$
HS 2224+2618	2002/08/20	01:17	3600	2507.57887	-306 ± 2
	2002/08/21	02:24	3600	2508.62542	-305 ± 2
PHL 382	2002/08/14	02:17	1800	2501.61130	-13 ± 2
	2002/08/14	03:26	1200	2501.65602	-18 ± 2
	2002/08/15	01:34	1200	2502.57783	-15 ± 2
	2002/08/15	02:47	1200	2502.62884	-15 ± 2
	2002/08/17	03:07	1200	2504.64235	-15 ± 2
	2002/08/21	03:28	1200	2508.65720	-15 ± 2
LB 1516	2000/09/08	02:44	1800	1795.62809	-23 ± 2
	2000/09/08	03:21	1800	1795.65378	-22 ± 2
	2002/08/09	08:34	2700	2495.87673	$+39 \pm 3$
	2002/08/11	08:24	2400	2497.86693	-21 ± 3
PG 2301+259	2002/08/16	01:33	3600	2503.58970	-121 ± 4
	2002/11/26	23:18	3600	2604.49340	-119 ± 4
Feige 108	2002/08/17	00:58	2400	2504.55937	$+3 \pm 5$
	2002/08/18	22:30	2400	2505.45693	$+27 \pm 5$
	2002/08/19	01:41	2400	2506.58965	$+63 \pm 5$
	2002/08/20	03:03	2400	2507.64650	$+91 \pm 5$
PB 5333	2002/08/17	01:42	3000	2504.59312	-99 ± 10
CD−35° 15910	2000/09/07	05:08	1800	1794.72926	$+21 \pm 2$
	2000/09/07	05:42	1800	1794.75267	$+20 \pm 2$
	2000/09/08	04:33	1800	1795.70453	$+21 \pm 2$
	2002/08/09	06:20	900	2495.77354	$+22 \pm 2$
PG 2351+198	2002/08/19	00:54	2700	2506.55726	-278 ± 5
	2002/08/20	03:46	3600	2507.68207	-280 ± 5

continued on next page

continued from previous page

star	date y/m/d	start UT	dur. [s]	BJD_{mid} −2,450,000	v_{rad} [km/s]
UVO 1735+22	1999/07/17	20:50	300	1377.3730	-31 ± 15
	1999/07/19	22:28	1800	1379.4497	$+12 \pm 3$
	1999/07/19	23:08	1800	1379.4776	-3 ± 3
	1999/07/20	23:08	1800	1380.4773	$+112 \pm 3$
	2001/08/27	21:18	1800	2149.3985	-72 ± 3
	2001/08/27	22:15	1800	2149.4627	-48 ± 3
	2001/08/28	19:35	3600	2150.3373	-27 ± 3
	2001/08/28	20:37	3600	2150.3817	-50 ± 3
	2001/08/28	21:43	3600	2150.4262	-62 ± 3
	2001/08/28	22:44	3600	2150.4690	-74 ± 3
	2001/08/28	23:46	3600	2150.5117	-75 ± 3
	2001/08/29	19:28	3600	2151.3324	$+103 \pm 3$
	2001/08/29	20:34	3600	2151.3760	$+93 \pm 3$
	2001/08/29	21:34	3600	2152.4176	$+69 \pm 3$
	2001/08/29	22:35	3600	2151.4620	$+50 \pm 3$
	2001/08/29	23:35	3600	2151.5048	$+25 \pm 3$
	2001/08/30	19:27	3600	2152.3321	$+94 \pm 3$
	2001/08/30	20:28	3600	2152.3748	$+107 \pm 3$
	2001/08/30	21:31	3600	2152.4176	$+116 \pm 3$
	2001/08/30	22:32	3600	2152.4604	$+124 \pm 3$
	2001/08/30	23:34	3600	2152.5033	$+124 \pm 3$
	2001/08/31	21:45	3600	2153.4272	$+12 \pm 3$
PB 7352	2000/09/08	03:58	1800	1795.68084	-53 ± 2
	2000/09/08	05:09	1800	1795.73024	-51 ± 2
	2002/08/09	07:49	1800	2495.84110	$+47 \pm 3$
	2002/08/09	09:22	2700	2495.91108	$+55 \pm 3$
	2002/08/10	04:16	1500	2496.69189	$+35 \pm 3$
	2002/08/11	05:30	1800	2497.74566	-61 ± 3
	2002/08/11	06:23	1800	2497.78151	-62 ± 3
	2002/08/11	07:48	1800	2497.84114	-63 ± 3
	2002/08/11	09:05	2700	2497.89938	-62 ± 3
	2002/08/14	01:23	3000	2501.58075	-63 ± 2
	2002/08/15	00:44	2700	2502.55206	$+2 \pm 2$
	2002/08/15	03:12	2700	2502.65459	$+19 \pm 2$
	2002/08/16	21:32	2700	2503.41838	$+57 \pm 3$
	2002/08/16	23:47	2700	2503.51247	$+58 \pm 2$
	2002/08/16	03:43	2700	2503.67637	$+54 \pm 2$
	2002/08/17	21:13	2700	2504.40495	-14 ± 2
	2002/08/17	03:30	2700	2504.66725	-43 ± 2
	2002/08/18	21:42	2700	2505.42575	-58 ± 2
	2002/08/19	00:04	2700	2506.52414	$+37 \pm 2$
	2002/11/26	18:58	2700	2604.30646	$+35 \pm 2$

continued on next page

continued from previous page

star	date y/m/d	start UT	dur. [s]	BJD_{mid} −2,450,000	v_{rad} [km/s]
HD 171858	2000/09/06	23:13	900	1794.47450	$+146 \pm 2$
	2000/09/06	23:36	1800	1794.49581	$+147 \pm 2$
	2002/08/07	23:35	900	2494.49275	$+21 \pm 2$
	2002/08/08	00:45	1200	2494.54221	$+35 \pm 2$
	2002/08/08	01:30	1200	2494.57459	$+46 \pm 2$
	2002/08/08	02:19	1200	2494.60798	$+54 \pm 2$
	2002/08/08	03:06	1200	2494.64069	$+68 \pm 2$
	2002/08/08	03:54	1200	2494.67399	$+78 \pm 2$
	2002/08/08	04:43	900	2494.70653	$+89 \pm 2$
	2002/08/08	23:24	900	2495.48526	$+50 \pm 2$
	2002/08/09	00:01	900	2495.51070	$+41 \pm 2$
	2002/08/09	00:38	900	2495.53620	$+31 \pm 2$
	2002/08/09	01:14	600	2495.55970	$+26 \pm 2$
	2002/08/09	01:43	600	2495.57948	$+20 \pm 2$
	2002/08/09	02:11	600	2495.59941	$+13 \pm 2$
	2002/08/09	02:41	600	2495.61952	$+9 \pm 2$
	2002/08/09	03:09	600	2495.63962	$+3 \pm 2$
	2002/08/09	04:14	720	2495.68514	-8 ± 2
	2002/08/09	05:33	900	2495.74126	-16 ± 2
	2002/08/09	06:40	900	2495.78708	-22 ± 2
	2002/08/09	07:19	1200	2495.81617	-24 ± 2
	2002/08/09	22:47	1200	2496.46053	$+125 \pm 2$
	2002/08/09	23:11	900	2496.47488	$+128 \pm 2$
	2002/08/09	23:46	720	2496.49914	$+135 \pm 2$
	2002/08/10	00:46	720	2496.54079	$+142 \pm 2$
	2002/08/10	01:56	600	2496.58885	$+148 \pm 2$
	2002/08/10	02:40	600	2496.61899	$+147 \pm 2$
	2002/08/10	03:06	600	2496.63730	$+149 \pm 2$
	2002/08/10	03:32	720	2496.65624	$+149 \pm 2$
	2002/08/10	04:03	600	2496.67679	$+148 \pm 2$
	2002/08/10	04:45	720	2496.70622	$+148 \pm 2$
	2002/08/10	22:55	1200	2497.46650	-26 ± 2
	2002/08/10	23:19	900	2497.48082	-24 ± 2
	2002/08/10	23:53	900	2497.50508	-26 ± 2
	2002/08/11	00:24	900	2497.52682	-25 ± 2
	2002/08/11	01:06	900	2497.55556	-22 ± 2
	2002/08/11	01:39	900	2497.57878	-20 ± 2
	2002/08/11	06:05	900	2497.76281	$+21 \pm 2$
	2002/08/11	07:27	900	2497.82223	$+38 \pm 2$
	2002/08/15	21:13	1200	2502.39554	-26 ± 2

continued on next page

continued from previous page

star	date y/m/d	start UT	dur. [s]	BJD_{mid} −2,450,000	v_{rad} [km/s]
HD 171858	2002/08/16	20:21	1200	2503.35904	$+134 \pm 2$
	2002/08/16	22:21	1200	2503.44214	$+114 \pm 2$
	2002/08/16	23:26	1057	2503.48638	$+101 \pm 2$
	2002/08/16	00:37	900	2503.53540	$+87 \pm 2$
	2002/08/17	23:07	900	2504.47240	$+73 \pm 2$
	2002/08/20	21:25	900	2507.40147	-18 ± 2
	2002/08/20	22:59	900	2507.46662	-3 ± 2
	2002/08/21	23:31	900	2508.48859	$+63 \pm 2$
HD 188112	2000/09/07	00:19	1800	1794.52710	-156 ± 2
	2000/09/07	00:56	1800	1794.55250	-140 ± 2
	2000/09/08	02:08	1800	1795.60255	-41 ± 2
	2000/09/09	02:55	1800	1796.63537	$+208 \pm 3$
	2002/08/07	23:16	900	2494.47970	-156 ± 2
	2002/08/08	00:20	1200	2494.52651	-157 ± 2
	2002/08/08	01:07	1200	2494.55911	-133 ± 2
	2002/08/08	01:56	1200	2494.59250	-90 ± 2
	2002/08/08	02:43	1200	2494.62506	-34 ± 2
	2002/08/08	03:29	1200	2494.65755	$+30 \pm 2$
	2002/08/08	04:17	1200	2494.69110	$+93 \pm 2$
	2002/08/08	05:01	900	2494.72009	$+142 \pm 2$
	2002/08/08	05:38	900	2494.74550	$+178 \pm 2$
	2002/08/08	23:06	900	2495.47338	$+182 \pm 2$
	2002/08/08	23:42	900	2495.49868	$+147 \pm 2$
	2002/08/09	00:20	900	2495.52430	$+105 \pm 2$
	2002/08/09	00:56	720	2495.54855	$+61 \pm 2$
	2002/08/09	01:27	720	2495.57029	$+20 \pm 2$
	2002/08/09	01:55	720	2495.59009	-20 ± 2
	2002/08/09	02:25	720	2495.61000	-56 ± 2
	2002/08/09	02:54	720	2495.63033	-89 ± 2
	2002/08/09	03:23	600	2495.64967	-117 ± 2
	2002/08/09	03:58	720	2495.67480	-143 ± 2
	2002/08/09	04:29	720	2495.69649	-158 ± 2
	2002/08/09	23:28	900	2496.48832	$+50 \pm 2$
	2002/08/10	00:28	900	2496.52997	$+127 \pm 2$
	2002/08/10	01:01	900	2496.55321	$+162 \pm 2$
	2002/08/10	01:41	720	2496.57976	$+192 \pm 2$
	2002/08/10	02:10	720	2496.59947	$+207 \pm 2$
	2002/08/10	02:25	720	2496.60998	$+212 \pm 2$
	2002/08/10	02:53	600	2496.62900	$+215 \pm 2$
	2002/08/10	03:19	600	2496.64721	$+212 \pm 2$
	2002/08/10	03:48	720	2496.66755	$+200 \pm 2$
	2002/08/10	00:43	1200	2497.54200	-162 ± 2
	2002/08/15	22:22	1200	2502.44384	-133 ± 2
	2002/08/17	22:42	1200	2504.45810	$+184 \pm 2$

continued on next page

continued from previous page

star	y/m/d	start UT	dur. [s]	BJD_{mid} −2,450,000	v_{rad} [km/s]
PG 0133+114	1999/07/17	20:50	300	1377.3730	-31 ± 15
	1999/07/19	22:28	1800	1379.4497	$+12 \pm 3$
	1999/07/19	23:08	1800	1379.4776	-3 ± 3
	1999/07/20	23:08	1800	1380.4773	$+112 \pm 3$
	2001/08/27	21:18	1800	2149.3985	-72 ± 3
	2001/08/27	22:15	1800	2149.4627	-48 ± 3
	2001/08/28	19:35	3600	2150.3373	-27 ± 3
	2001/08/28	20:37	3600	2150.3817	-50 ± 3
	2001/08/28	21:43	3600	2150.4262	-62 ± 3
	2001/08/28	22:44	3600	2150.4690	-74 ± 3
	2001/08/28	23:46	3600	2150.5117	-75 ± 3
	2001/08/29	19:28	3600	2151.3324	$+103 \pm 3$
	2001/08/29	20:34	3600	2151.3760	$+93 \pm 3$
	2001/08/29	21:34	3600	2152.4176	$+69 \pm 3$
	2001/08/29	22:35	3600	2151.4620	$+50 \pm 3$
	2001/08/29	23:35	3600	2151.5048	$+25 \pm 3$
	2001/08/30	19:27	3600	2152.3321	$+94 \pm 3$
	2001/08/30	20:28	3600	2152.3748	$+107 \pm 3$
	2001/08/30	21:31	3600	2152.4176	$+116 \pm 3$
	2001/08/30	22:32	3600	2152.4604	$+124 \pm 3$
	2001/08/30	23:34	3600	2152.5033	$+124 \pm 3$
	2001/08/31	21:45	3600	2153.4272	$+12 \pm 3$
PG 0001+275	1999/07/23	01:51	1800	1382.5891	-27 ± 3
	1999/07/23	02:31	1800	1382.6161	-51 ± 3
	1999/07/23	03:07	2700	1382.6481	-89 ± 3
	2001/07/08	03:00	600	2098.6657	-67 ± 8
	2001/08/27	23:25	1800	2149.4901	-105 ± 3
	2001/08/30	01:18	3600	2151.5779	-128 ± 3
	2001/08/30	02:53	3600	2151.6444	-76 ± 3
	2001/08/31	01:12	3600	2152.5745	-134 ± 3
	2001/08/31	02:48	3600	2152.6417	-125 ± 3
	2001/08/31	20:51	3000	2153.3900	$+49 \pm 3$
	2001/08/31	22:49	2700	2153.4702	$+12 \pm 3$
	2001/08/31	23:36	2700	2153.5024	-20 ± 3
	2001/09/01	00:21	2700	2153.5346	-54 ± 3
	2001/09/01	01:43	2700	2153.5912	-104 ± 3
	2001/09/01	02:29	2700	2153.6234	-125 ± 3
	2001/09/01	04:20	2580	2153.6998	-129 ± 3

Appendix E

List of abbreviations

$\odot$	Solar
γ_0	Systemic velocity
λ	Wavelength
ξ	Microturbulent velocity
$^\circ$	Degree
’	Arc-Minute
”	Arc-Second
Å	Ångström
AGB	Asymptotic Giant Branch
Al	Aluminum
Am	magnetic main-sequence A
ALI	Accelerated Lambda Iteration
Ap	peculiar main-sequence A
Apr	April
Ar	Argon
Aug	August
B&C	Boller & Chivens
BB	Balloon-Born
BC	Bary-Centric
BD	Bonner Durchmusterung
BPS	Beers, Preston, & Shectman
C	Carbon
Ca	Calcium
CA	Calar Alto
CAFOS	Calar Alto Faint Object Spectrograph
CCD	Charged Coupled Device
CD	Cordoba Duchmusterung
CE	Common Envelope
cgs	centimeter-gram-second system
CNO	Carbon, Nitrogen, & Oxygen
CSO	Case low-dispersion northern sky survey of Stellar-like Objects
CV	Cataclysmic Variable

d	day
DA	hydrogen-rich white dwarf (Degenerate type A)
DAO	very hot hydrogen-rich white dwarf (Degenerate type AO)
DAZ	cool hydrogen-rich white dwarf (Degenerate type AZ)
DB	helium-rich white dwarf (Degenerate type B)
DBA	helium-rich white dwarf with traces of hydrogen (Degenerate type BA)
Dec	December
DFG	Deutsche Forschungsgemeinschaft
DFOSC	Danish Faint Object Spectrograph and Camera
DO	very hot helium-rich white dwarf (Degenerate type O)
DSAZ	Deutsch-Spanisches Astronomisches-Zentrum
EC	Edinburgh-Cape
ECS	Edinburgh-Cape Survey
EG	Eggen+Greenstein
EHB	Extended (Extreme) Horizontal Branch
emis	Emission
ESO	European Southern Observatory
f_m	Mass-Function
FBS	First Byurakan Sky
Fe	iron (Ferrum)
Feb	February
FEROS	Fiber-fed Extended Range Optical Spectrograph
Fig	Figure
FOCES	Fiber-Optics Cassegrain Echelle Spectrograph
FR	Focal Reductor
FWHM	Full Width Half Maximum
g	gravity
G	Gravitational Constant $G = 6.673 \cdot 10^{-8}\mathrm{dyne\,cm^{-2}\,g^{-}2}$
GD	Giclas Dwarfs
h	Hour
H	Hydrogen
HBB	Horizontal Branch B
HD	Henry Draper
He	Helium
HE	Hamburg ESO
HeMS	Helium-Main-Sequence
He-sdB	Helium-rich subdwarf B
He-sdO	Helium-rich subdwarf O
HES	Hamburg ESO Survey
Hg	Mercury (Hydrargyrum)
HQS	Hamburg Quasar Survey
HR	Hertzsprung-Russell
HRD	Hertzsprung-Russell-Diagram
HS	Hamburg Schmidt
HZ	Humason & Zwicky

i	Inclination
IUE	International Ultraviolet Explorer
Jan	January
JD	Julian Date
Jun	June
Jul	July
K	Radial Velocity Semi-Amplitude
K	Kelvin
km	Kilometer
KPD	Kitt-Peak-Downes
KUV	Kiso UV
L	Luminosity
L_e	Eddington luminosity
LB	Luyten Blue
LINFOR	LINLTE.FOR
LS	Luminous Stars
LTE	Local ThermoEquilibrium
LTT	Luyten Two Tenths
m	meter
M	Mass
M	Metal
Mar	March
MCT	Montreal-Cambridge-Tololo
Mg	Magnesium
MIDAS	Munich Image Data Analysis System
Mn	Manganese
MS	Main Sequence
n	by number
N	Nitrogen
Ni	Nickel
NLTE	Non-Local ThermoEquilibrium
nois	Noisy
Nov	November
Oct	October
O	Oxygen
ovl	OVerLap
P	Period
P	Phosphorus
PB	Palomar Berger
PG	Palomar Green
PGS	Palomar Green Survey
PHL	Palomar Haro Luyten
Rb	Rubidium
RLOF	Roche Lobe Overflow
prep	Preparation
RV	Radial Velocity
RVV	Radial Velocity Variable

s	Second
S	Sulfur
S/N	Signal to Noise
SA	Durchmusterung of Selected Areas
sat	Saturated
SB	Slettebak & Brundage
SBSS	Second Biurakan Spectral Sky
sdB	subdwarf B
sdB+x	subdwarf B + unknown companion
sdBV	subdwarf B Variable
sdO	subdwarf O
sdOB	subdwarf OB
Sep	September
Si	Silicon
SN	Supernova
SPY	Sn Ia Progenitor surveY
SVD	Singular Value Decomposition
$t_{\rm evol}$	Time of Evolution
$T_{\rm eff}$	effective temperature
TAEHB	Terminal Age Extended (Extreme) Horizontal Branch
Ti	Titanium
TON	Tonantzintla
unid	Unidentified
US	Usher Survey
UV	Ultra Violet
UVO	Ultra Violet Object
v	Velocity
$v_{\rm rad}$	Radial Velocity
V	Vanadium
VLT	Very Large Telescope
WD	White Dwarf
y	Year
ZAEHB	Zero Age Extreme (Extreme) Horizontal Branch

References

Abrahamian H. V., Lipovetsky V. A., Mickaelian A. M., Stepanian D. A., 1990, Afz 33, 345

Abrahamian H. V., Mickaelian A. M., 1996, Astrophysics 39, 315

Allard F., Wesemael F., Fontaine G., Bergeron P., Lamontagne R., 1994, AJ 107, 1565

Altmann M., de Boer K. S., 2000, A&A 353, 135

Altmann M., Edelmann H., de Boer K. S., 2003, A&A in prep.

Aznar Cuadrado R., Jeffery C. S., 2001, A&A 368, 994

Aznar Cuadrado R., Jeffery C. S., 2002, A&A 385, 131

Barnard A. J., Cooper J., Smith E. W., 1974, JQSRT 14, 1025

Baschek B., Sargent W. L. W., Searle L., 1972, AJ 173, 611

Baschek B., Norris J., 1975, ApJ 199, 694

Bauer F., Husfeld D., 1995, A&A 300, 481

Beers T. C., Preston G. W., Shectman S. A., Doinidis S. P., Griffin K. E, 1992, AJ 103, 267

Beers T. C., Rossi S., O'Donoghue D., Kilkenny D., Stobie R. S., Koen C., Wilhelm R., 2001, MNRAS 320, 451

Berger J., Fringant A. M., 1977, A&AS 28, 123

Bergeron P., Wesemael F., Michaud G., Fontaine G., 1988, ApJ 332, 964

Bergeron P., Saffer R. A., Liebert J., 1992, ApJ 394, 228

Billéres M., Fontaine G., Brassard P., Charpinet S., Liebert J., Saffer R. A., Vauclair G., 1997, ApJ 487, L81

Bixler J. V., Bowyer S., Laget M., 1991, A&A 250, 370

de Boer K. S., Aguilar Sanchez Y., Altmann M., Geffert M., Odenkirchen M., Schmidt J. H. K., Colin J., 1997, A&A 327, 577

Brown T. M., Ferguson H. C., Davidsen A. F., Dorman, B., 1997, ApJ 482, 685

Brown T. M., Bowers C. W., Kimble R. A., 2000a, ApJ 529, L89

Brown T. M., Bowers C. W., Kimble R. A., Sweigart A. V., Ferguson H. C., 2000b ApJ 532, 308

Castellani V., Chieffi A., Tornambe A., Pulone L., 1985, ApJ 296, 204

Charpinet S., Fontaine G., Brassard P., Dorman B., 1996, ApJ 471, L103

Charpinet S., Fontaine G., Brassard P., Chayer P., Rogers F. J., Iglesias C. A., Dorman B., 1997, ApJ 483, L123

Charpinet S., 2001, Astron. Nachr. 322, 387

Christlieb N., Graßhoff G., Nelke A., Schlemminger A., Wisotzki L., 1998, *Linné, a software system for automatic classification*, in 'Astronomical Data Analysis and Software Systems VII', Vol. 145 of ASP Conf. Ser., eds. R. Albrecht, R. Hook, & H. Bushouse, p. 457

Christlieb N., Wisotzki L., Reimers D., Homeier D., Koester D., Heber U., 2002, A&A 366, 898

D'Cruz N. L., Dorman B., Rood R. T., O'Connell R. W., 1996, ApJ466, 359

Demers S., Wesemael F., Irwin, M. J., Fontaine G., Lamontagne R., Kepler S. O., Holberg J. B., 1990, ApJ 351, 271

Dorman B., Rood R. T., O'Connell R. W., 1993, ApJ 419, 596

Drechsel H., Heber U., Napiwotzki R., Østensen R., Solheim J.-E., Johannessen F., Schuh S. L., Deetjen J., Zola S., 2001, A&A 379, 893

Dreizler S., Heber U., Werner K., Moehler S., de Boer K. S., 1990, A&A 235, 234

Dreizler S., Heber U., Jordan S., Engels D., 1994, Proc. of the IAU Colloq. 180, eds. Adelman S. J., Upgren A. R., Adelman C. J., Cambridge Univ. Press, "Hot stars in the Galactic Halo", 228

Dreizler S., Schuh S., Deetjen J. L., Edelmann H., Heber U., 2002, A&A 386, 249

Driebe T., Schönberner D., Blöcker T., Herwig F., 1998, A&A 339, 123

Edelmann H., Heber U., Napiwotzki R., Reid I. N., Saffer R. A., 1999, Proc. of the 11$^{\rm th}$ European Workshop on White Dwarfs, Eds. S.-E. Solheim and E. G. Meistas., ASP Conf. Series 169, 546

Ekberg J. O., 1993 A&AS 101, 1

Feige J., 1958, ApJ 128, 267

Ferguson D. H., Green R. F., Liebert J., 1984, ApJ 287, 320

Fontaine G., Chayer P., 1997, Conference on Faint Blue Stars, eds. A. G. D. Philip, J. Liebert, R. Saffer and D. S. Hayes, Published by L. Davis Press, 169

François, P., FEROS User's Manual, Version 1.1, Doc. No. LSO-MAN-ESO-22200-000001

Fred M., Tomkins F. S., Brody J. K., Hamermesh M., 1951, Phys. Rev. 82, 406

Giclas H. L., Burnham R., Thomas N. G., 1980, Lowell Obs. Bull. 8, 157

Green E. M., Liebert J., Saffer R. A., 2001, Proc. of the 12$^{\rm th}$ European Workshop on White Dwarfs, eds. J. L. Provencal, H. L. Shipman, J. MacDonald & S. Goodchild, ASP Conf. Series 226, 192

Green R. F., Schmidt M., Liebert J., 1986, ApJS 61, 305

Greenstein J. L., 1954, AJ 59, 322

Greenstein J. L., Truran J. W., Cameron A. G. W., 1967, Nature 213, 871

Greggio L., Renzini A., 1990, ApJ 364, 35

Griem H. R., 1974, Spectral line broadening by plasmas, Pure and Applied Physics, Academic Press, New York

Hagen H.-J., Groote D., Engels D., Reimers D., 1995, A&AS 111, 195

Hagen H.-J., Engels D., Reimers D., 1999, A&AS 134, 483

Han Z., Podsiadlowski P., Maxted P. F. L., Marsh T. R., Ivanova N., 2002, MNRAS 336, 449

Han Z., Podsiadlowski P., Maxted P. F. L., Marsh T. R., 2003, MNRAS in press (astro-ph/0301380)

Haro G., Luyten W. J., 1962 Bol. Inst. Tonantzintla 3, 37

Heber U., Hunger K., Jonas G., Kudritzki R. P., 1984, A&A 130, 119

Heber U. 1986, A&A 155, 33

Heber U., Jordan S., Weidemann V., 1989, Proc. of the Astron. Gesellschaft, Abstract Ser., 3, 94

Heber U., Jordan S., Weidemann V., 1991a, Proc. of the 7$^{\rm th}$ European Workshop on White Dwarfs, eds. G. Vauclair and E. Sion., NATO Advanced Science Institutes (ASI) Series C, 336, 109

Heber U., 1991b, Proc. of the 145$^{\rm th}$ Symposium of the IAU, eds. G. Michaud and A. V. Tutukov, Kluwer Academic Publishers, Dordrecht, 363

Heber U., Dreizler S., Hagen H.-J., 1996, A&A 311, L17

Heber U., Reid I. N., Werner K., 1999 A&A 348, L25

Heber U., Reid I. N., Werner K., 2000, A&A 363, 198

Heber U., Moehler S., Napiwotzki R., Thejll P., Green E.M., 2002, A&A 383, 938

Hirata R., Horaguchi T., 1995, Atomic spectral line list, Department of Astronomy, Faculty of Science, Kyoto University, and National Science Museum, 3-23-1 Hyakunin-cho, Shinjuku-ku, Tokyo

Homeier D., Koester D., Hagen H.-J., Jordan S., Heber U., Engels D., Reimers D., Dreizler S., 1999b, A&A 338, 563

Homeier D., Koester D., Jordan S., Hagen H.-J., Engels D., Heber U., Dreizler S., 1999, Proc. of the 11th European Workshop on White Dwarfs, eds. J.-E. Solheim & E. G. Meištas, ASP Conf. Series 169, 37

Humason M. L., Zwicky F., 1947, ApJ 105, 85

Hunger K., Gruschinske J., Kudritzki R. P., Simon K. P., 1981, A&A 95, 244

Iben I. Jr., Tutukov A. V., 1986b, ApJ311, 753

Iriarte B., Chavira E., 1957, Bol. Obs. Tonantz. Tacub., 2, part no 16, 3

Jeffery C. S., Drilling J. S., Harrison P. M., Heber U., Moehler S., 1997, A&AS 125, 501

Jeffery, C. S., Pollacco D. L., 1998, MNRAS 298, 179

Kilkenny D., 1984, MNRAS 211, 969

Kilkenny D., Heber U., Drilling J. S., 1988, SAAO Circular 12, 1

Kilkenny D., Muller S., 1989, SAAO Circular 13, 69

Kilkenny D., O'Donoghue D., Stobie R. S., 1990, MNRAS 248, 664

Kilkenny D., Koen C., O'Donoghue D., Stobie R. S., 1997, MNRAS 285, 640

Koen C., Kilkenny D., O'Donoghue D., Stobie R. S., 1998, IAU Symp. 185, 361

Koen C., O'Donoghue D., Kilkenny D., Stobie R. S., Saffer R. A., 1999, MNRAS 306, 213

Koester D., Napiwotzki R., Christlieb N., Drechsel H., Hagen H.-J., Heber U., Homeier D., Karl C., Leibundgut B., Moehler S., Nelemans G., Pauli E.-M., Reimers D., Renzini A., Yungelson L, 2001, A&A 378, 556

Kurucz R. L., 1979, ApJS 40, 1

Kurucz R.L., 1992, Proc. of the 149th Symposium of the IAU, Eds. B. Barbuy and A. Renzini, Kluwer Academic Publishers, Dordrecht, 225

Lamontagne R., Wesemael F., Fontaine G., Sion E.M., 1985, ApJ 299, 496

Lamontagne R., Wesemael F., Fontaine G., 1987, ApJ 318, 844

Lamontagne R., Demers S., Wesemael F., Fontaine G., Irwin M. J., 2000, AJ 119, 241

Lemke M., Heber U., Napiwotzki R., Dreizler S., Engels D., 1997a, Proc. of the 3rd Conference on Faint Blue Stars, eds. A. G. D. Philip, J. Liebert, R. Saffer and D. S. Hayes, Published by L. Davis Press, 375

Lemke M., 1997b, A&AS 122,285

Lorenz L. Mayer P., Drechsel H., 1998, A&A 332, 909

Marietta E., Burrows A., Fryxell B., 2000, ApJS 128, 615

Markarian B. E., Stepanian J. A., 1983, Afz 19, 639

de Marchi G., Paresce F., 1996, ApJ 467, 658

Maxted P. F. L., Marsh T. R., North R. C., 2000, MNRAS 317, L41

Maxted P. F. L., Heber U., Marsh T. R., North R. C., 2001 MNRAS 326, 1391

Mengel J. G., Norris, J., Gross P. G., 1976, ApJ 204, 488

Michaud G., Vauclair G., Vauclair S., 1983, ApJ 267, 256

Michaud G., Bergeron P., Heber U., Wesemael F., 1989, ApJ 338, 417

Mitchell K. J., 1998, ApJ 494, 256

Moehler S., de Boer K. S., Heber U., 1990a, A&A 239, 265

Moehler S., Richtler T., de Boer K. S., Dettmar R. J., Heber U, 1990b, A&AS 86, 53

Morales-Rueda L., Marsh T. R., North R. C., Maxted P. F. L., 2002, Proceedings of the 13th European Meeting on White Dwarfs, in press

Morales-Rueda L., Maxted P. F. L., Marsh T. R., North R. C., Heber U., 2003, MNRAS 338, 752

Moran C., Maxted P., Marsh T. R., Saffer R. A., Livio M., 1999, MNRAS 304, 535

Napiwotzki R., Schönberner D., Wenske V., 1993, A&A 268, 653

Napiwotzki R., 1997, A&A 322, 256

Napiwotzki R., 1999, A&A 350, 101

Napiwotzki R., Christlieb N., Drechsel H., Hagen H.-J., Heber U., Homeier D., Karl C., Koester D., Leibundgut B., Marsh T. R., Moehler S., Nelemans G., Pauli E.-M., Reimers D., Renzini A., Yungelson L., 2001a, Astron. Nachr. 322, 411

Napiwotzki R., Edelmann H., Heber U., Karl C., Drechsel H., Pauli E.-M., Christlieb N. 2001b, A&A 378, L17

Napiwotzki R., Koester D., Nelemans G., Yungelson L., Christlieb N., et al., 2002, A&A 386, 957

Noguchi T., Maehara H., Kondo M., 1980, Tokyo, University, Tokyo Astronomical Observatory, Annals, Second Series, vol. 18, no. 1, 55

O'Donoghue D., Koen C., Kilkenny D., Stobie R. S., 1999, Proc. of the 11$^{\rm th}$ European Workshop on White Dwarfs, eds. J.-E. Solheim & E. G. Meištas, ASP Conf. Series 169, 149

Ohl R. G., Chayer P., Moos H. W., 2000, ApJ 538, L95

Oke J. B., 1990 AJ 99, 1621

Østensen R., Solheim J.-E., Heber U., Silvotti R., Dreizler S., Edelmann H., 2001a, A&A 368, 175

Østensen R., Heber U., Silvotti R., Solheim J.-E., Dreizler S., Edelmann H., 2001b, A&A 378, 466

Paczyński B., 1971, Acta Astron. 21, 1

Pesch P., Sanduleak N., 1983, ApJS 51, 171

Pauldrach A., Puls J., Kudritzki R. P., Mendez R. H., Heap S. R., 1988, A&A 207, 123

Pickering E. C., Kapteyn J. C., 1918, Ann. Astron. Obs. Harvard Coll. 101

Pfeiffer M., Frank C., Baumüller D., Fuhrmann K., Gehren T., 1998, A&AS 130, 381

Ramspeck M., Heber U., Moehler S., 2001, A&A 378, 907

Ramspeck M., Heber U., Edelmann H., 2001, A&A 379, 235

Rodgers A. W., Roberts W. H., Walker, I., 1993, AJ 106, 591

Rolleston W. R. J., Hambly N. C., Keenan F. P., Dufton P. L., Saffer R. A., 1999, A&A 347, 69

Saffer R. A., Bergeron P., Koester D., Liebert J. 1994, ApJ 432, 351

Saffer R. A., Livio M., Yungelson L. R., 1998, ApJ 502, 394

Sargent W. L. W., Searle L., 1966, ApJ 145, 652

Schaller G., Schaerer D., Meynet G., Maeder A., 1992, A&AS 96, 269

Schlegel D. J., Finkbeiner D. P., Davis M., 1998, ApJ 500, 525

Schöning T., Butler K., 1989, A&AS 78, 51

Shamey Louis J., 1969, PhD thesis, Loyola Univerity of Los Angeles

Silvotti R., Østensen R., Heber U., Solheim J.-E., Dreizler S., Altmann M., 2002, A&A 383, 239

Slettebak A. & Brundage R. K., 1971, AJ 76, 338

Strittmatter P. A., Norris J., 1971, A&A 15, 239

Sweigart A. V., 1997, ApJ 474, L23

Theissen A., Moehler S., Heber U., de Boer K. S., 1993, A&A 273, 524

Theissen A., Moehler S., Heber U., Schmidt J. H. K., de Boer K. S, 1995, A&A 298, 577

Thejll P., Theissen A., Jimenez R., 1994 A&A 292, 457

Tüg H., 1977, ESO Messenger 11, 7

Ulla A., Thejll P., 1998, A&AS132, 1

Unglaub K., Bues I., 2001, A&A 374, 570

Usher P. D., 1981, ApJS 46, 117

Vidal C. R., Cooper J., Smith E. W., 1973, ApJS 25, 37

Vauclair S., 1975, A&A 45, 233

Vauclair S., Vauclair G., 1982, Ann. Rev. Astron. Astrophys. 20, 37

Wade R. A., 2001 Proc. of the 12$^{\rm th}$ European Workshop on White Dwarfs, eds. J. L. Provencal, H. L. Shipman, J. MacDonald & S. Goodchild, ASP Conf. Series 226, 199

Wegner G., Swanson S. R., 1990, AJ 100, 1274

Werner K., Husfeld D., 1985, A&A 148, 417

Werner K., 1986, A&A 161, 177

Wiese W. L., Fuhr J. R., Deters T. M., 1996, Atomic transition probabilities of carbon, nitrogen, and oxygen: a critical data compilation. Eds. W. L. Wiese, J. R. Fuhr, and T. M. Deters. Washington, DC : American Chemical Society ... for the National Institute of Standards and Technology (NIST), QC 453 .W53

Wisotzki L., Reimers D., Wamsteker W., 1991, A&A 247, L17

Wisotzki L., Koehler T., Groote D., Reimers D. 1996, A&AS 115, 227

Acknowledgements

This dissertation is dedicated to my parents, Wolfgang and Dora Edelmann. Without their faith, patience and support for all this years, in particular when I decided not to learn the trade of a craftsmen but spent years and years in schools and universities to become a scientist, this work would not have been possible. I am happy and proud to have such parents. Thank you!

I wish to acknowledge and thank next my PhD supervisor, referee of my work, and colleague Ulrich Heber for entrusting me with the exploration of the *'wonderful world of sdB stars'*. Uli has given unstintingly of his time, talent, knowledge, and resources over the last years. He has given me every opportunity to pursue my own interests, and he has unselfishly allowed me to present results to the international astronomical community by making it possible for me to attend several meetings and workshops.

The research presented in this dissertation would not have been possible without the help and collaboration of

Ralf Napiwotzki who provided me with his NLTE models, spectra, programs, routines, advice of any kind. Lots of discussions with him were very fruitful to me.

the colleages from the Hamburg group, especially Norbert Christlieb, Hans-Jürgen Hagen, and Dieter Engels, for providing me with the data of the HES and HQS,

Betsy Green for generously sharing radial velocity data of several stars,

Martin Altmann who provided me with the photometric data for the HES sdB stars,

Klaus Fuhrmann from the Munich group for providing me with the IDL routines to reduce the FOCES spectra, and teaching me how to use them,

and to all colleagues who participated in the observing campaigns presented in this dissertation (Christian Karl, Thorsten Lisker, Zorica Pavković, Stefan Dreizler, Michael Lemke, Stefan Haas, Stefan Jordan, Rolf Möller, and Holger Marten).

I am also grateful to Klaus Werner for being a referee of this thesis, and to Irmela Bues for her interest in my work and for the proofreading of this dissertation.

Many thanks go also to all colleagues of the Dr. Karl Remeis Sternwarte, Bamberg, for valuable discussions, their support and help concerning any kind of problems.

I appreciate the help, support, and valuable assistance provided by the staff of the Calar Alto observatory, Spain, and the La Silla observatory, Chile, during my visits.

I made extensive use of NASAs Astrophysics Data System Abstract Service (ADS), the SIMBAD database, operated at CDS, Strasbourg, France, the Digital Sky Survey (DSS), and the LEO English/German Dictionary (`http://dict.leo.org`). In addition, thanks go to all developers of DEBIAN Linux, for the best Linux distribution available.

This work was supported by the Deutsche Forschungs Gemeinschaft (DFG) under grant He 1354/30–1. In addition, I gratefully acknowledge several travel grants to the Calar Alto observatory.

Last but not least, I would like to thank all people who are supported the accomplishment of this thesis in one way or another, but were forgotten to be mentioned here.

Lebenslauf

Name	Heinz Wolfgang Edelmann	
Geburtsdatum/-ort	23.04.1968 in Nürnberg	
Nationalität	deutsch	
Schulbildung	Aug.1974 – Jul.1983 abgeschlossen mit	Grund- und Hauptschule Roßtal Qual. Hauptschulabschluß
	Aug.1983 – Jul.1985 abgeschlossen mit	Staatliche Realschule Oberasbach Realschulabschluß
	Aug.1985 – Jul.1986 abgeschlossen mit	D. Bonhoeffer-Gymnasium Oberasbach Oberstufenreife
	Aug.1986 – Jun.1988 abgeschlossen mit	Staatliche Fachoberschule Fürth Fachhochschulreife
Grundwehrdienst	Jun.1988 – Aug.1989	in Regensburg, als Kraftfahrer F, Beobachtungspanzer
Studium	Okt.1989 – Feb.1991	Grundstudium der Feinwerktechnik an der Fachhochschule Nürnberg
	14.Feb.1991	Vordiplom
	Nov.1991 – Okt.1998	Studium der Physik an der Friedrich-Alexander-Universität (FAU) Erlangen-Nürnberg
	Okt.1997 – Okt.1998	Diplomarbeit bei Prof. Dr. Ulrich Heber an der Dr. Remeis-Sternwarte Bamberg Astronomisches Institut der FAU Erl.-Nbg.
		Thema: "Spektralanalyse von heliumarmen unterleuchtkräftigen B- und O-Sternen"
Studienabschluß	12.Okt.1998	**Dipl.-Phys. Univ.** (Note: 1,73)
Promotion	Nov.1998 – Mai 2003	Doktorarbeit bei Prof. Dr. Ulrich Heber an der Dr. Remeis-Sternwarte Bamberg Astronomisches Institut der FAU Erl.-Nbg.
Beschäftigung:	seit Apr.2003	Entwicklungsingenieur bei GIWS, Nürnberg

Curriculum Vitae

Name:	Heinz Wolfgang Edelmann	
Date of Birth:	April 23rd 1968, Nuremberg, Germany	
Citizenship:	German	
University:	Nov.1998 – May 2003	PhD student at the Dr. Remeis-Observatory, Bamberg, Germany Supervisor: Prof. Dr. Ulrich Heber
	Oct. 12th 1998	Degree: Dipl.-Phys. Univ. (1,73)
	Oct.1997 – Oct.1998	Diploma student at the Dr. Remeis-Observatory, Bamberg, Germany Thesis topic: "Spektralanalyse von heliumarmen unterleuchtkräftigen B- und O-Sternen" Supervisor: Prof. Dr. Ulrich Heber
	Nov.1991 – Oct.1998	Student at the Friedrich-Alexander-University of Erlangen-Nbg., Germany Field of Study: Physics
	Oct.1989 – Feb.1991	Student at Georg-Simon-Ohm University of Applied Sciences of Nuremberg, Germany Field of study: Precision Engineering
Secondary School:	Aug.1986 – Jun.1988	Student at the Fachhochschule Fuerth
	Aug.1985 – Jul.1986	Student at the D. Bonhoeffer-Gymnasium Oberasbach
Primary School:	Aug.1983 – Jul.1985	Student at the Realschule Oberasbach
	Aug.1974 – Jul.1983	Student at the Grund- and Hauptschule Rosstal
Military Service:	Jun.1988 – Aug.1989	Regensburg, Germany
Employment History:	since Apr.2003	Designing engineer at the GIWS, Nuremberg, Germany
	Feb.1999 – Feb.2003	Scientific coworker at the Dr. Remeis-Observatory, Bamberg, Germany
	Sep.1996 – Jan.1999	Undergraduate auxiliary worker at the Dr. Remeis-Observatory, Bamberg, Germany